# Freshwater variability in the Arctic Ocean and subarctic North Atlantic

**Myriel Horn**

Universität Bremen, 2018

# Freshwater variability in the Arctic Ocean and subarctic North Atlantic

Vom Fachbereich für Physik und Elektrotechnik
der Universität Bremen
zur Erlangung des akademischen Grades einer
**Doktorin der Naturwissenschaften (Dr. rer. nat.)**
genehmigte Dissertation

von

**M.Sc. Myriel Horn**
aus Braunschweig

| | |
|---|---|
| Erstgutachter: | Prof. Dr. Torsten Kanzow |
| Zweitgutachterin: | Dr. Maren Walter |
| Eingereicht am: | 05. Juli 2018 |
| Verteidigt am: | 15. Oktober 2018 |

# Abstract

In the past decades, observations in the upper Arctic Ocean and subpolar North Atlantic have shown significant freshwater changes that were in each region mainly attributed to independent processes. Both regions are sensitive to changes in the density stratification with possible implications for the ocean–atmsophere heat exchange and the deep convection. Thus changes in the freshwater content of the Arctic Ocean and subpolar North Atlantic have the potential to impact the climate locally and globally.

The objectives of the present study are to investigate the freshwater content (co)variability of the upper Arctic Ocean and subpolar North Atlantic, to identify the processes causing the observed changes in freshwater content and to analyse possible drivers of these processes.

To investigate the freshwater content variability I used objectively mapped salinity fields for the subpolar North Atlantic and Nordic Seas, and objectively mapped liquid freshwater inventories and sea ice volume estimates from the Pan-Arctic Ice Ocean Modeling and Assimilation product for the upper Arctic Ocean. To explore possible links, I compared the liquid freshwater content of the subarctic North Atlantic (SANA; combination of subpolar North Atlantic and Nordic Seas) with the sum of liquid and solid freshwater content of the upper Arctic Ocean from the observational and assimilation products. I found a distinct anti-correlation of the freshwater anomalies in these two regions between 1992 and 2013 with anomalies of the same magnitude.

An analysis of freshwater fluxes from the global Finite Element Sea ice Ocean Model and the Common Ocean-ice Reference Experiment version 2 atmospheric forcing data set suggested that the observed freshwater variations resulted from changing freshwater transports. Variations in the Arctic freshwater export to the North Atlantic are found to be most important for the total freshwater content variability of the upper Arctic Ocean and for the liquid freshwater content variability of the western SANA. The eastern SANA freshwater content seems to be mainly influenced by the exchange with the subtropical North Atlantic.

Furthermore, this study reveals that the observed freshwater changes are correlated with the Arctic and North Atlantic Oscillation indices. Therefore I suggest that a changing freshwater export from the Arctic Ocean to the SANA responds to decadal alternations of the dominant large-scale atmospheric variability. Thereby the export through the Canadian Arctic Archipelago is associated to different patterns of the atmospheric and oceanic pressure and circulation than the export through the Fram Strait and Barents Sea Opening. I propose, that the recently observed rapid changes in the SANA and upper Arctic Ocean freshwater content resulted from an interplay of these different driving patterns causing parallel changes in the freshwater export on both sides of Greenland.

According to the present phase of the decadal alternations of the atmospheric variability and the final years in my freshwater content time series, the fresh water accumulated in the Arctic Ocean during the previous decades started to be released into the SANA. This release might continue in the following years and could have the potential to impact the Atlantic Meridional Overturning Circulation and the oceanic heat release to the Arctic atmosphere and sea ice.

# Zusammenfassung

In den letzten Jahrzehnten wurden signifikante Süßwassergehaltsänderungen in der oberen Arktis und dem subpolaren Nord Atlantik beobachtet, die in beiden Regionen jeweils unabhängigen Prozessen zugeschrieben wurden. Beide Regionen sind empfindlich gegenüber Dichteveränderungen, die zur Beeinflussung des Wärmeaustausches zwischen Ozean und Atmosphäre und der Tiefenkonvektion führen können. Somit haben Änderungen im Süßwassergehalt der oberen Arktis und des subpolaren Nordatlantiks das Potential, das Klima lokal und global zu beeinflussen.

Gegenstand dieser Arbeit ist es, die (Ko-)Variabilität der Süßwassergehalte der oberen Arktis und des subpolaren Nordatlantiks zu untersuchen, die verantwortlichen Prozesse für die beobachteten Süßwasseränderungen zu identifizieren und die möglichen Treiber dieser Prozesse zu analysieren.

Um die Süßwassergehaltsvariabilität zu untersuchen, habe ich objektiv kartierte Salzgehaltsfelder für den subpolaren Nordatlantik und das Europäische Nordmeer verwendet, sowie objektiv kartierte Süßwasserinventare und Meereisvolumenabschätzungen vom Pan-Arktischen Eis Ozean Modellierungs- und Assimilationsprodukts für die obere Arktis genutzt. Um mögliche Verbindungen zu erforschen, habe ich den flüssigen Süßwassergehalt des subarktischen Nordatlantiks (SANA; Kombination aus subpolarem Nordatlantik und Europäischem Nordmeer) und die Summe des flüssigen und festen Süßwassergehalts der oberen Arktis aus Beobachtungs- und Assimilationsdaten miteinander verglichen. Dabei habe ich eine eindeutige Anti-Korrelation der Süßwasseranomalien der beiden Regionen zwischen 1992 und 2013 gefunden mit Anomalien der gleichen Größenordnung.

Eine Analyse der Süßwasserflüsse im globalen Finite-Elemente Meereis Ozean Model und dem atmosphärischen Antriebs-Datensatz des Gemeinschaftlichen Ozean-Eis Referenz Experiments - Version 2 deutet darauf hin, dass die beobachteten Süßwasservariationen von veränderten Süßwassertransporten herrühren. Variationen im Arktischen Süßwasserexport in den Nordatlantik wurden als wichtigster Beitrag zur Variabilität des totalen Süßwassergehalts der oberen Arktis und des flüssigen Süßwassergehalts des westlichen SANAs identifiziert. Der Süßwassergehalt

des östlichen SANAs scheint hauptsächlich durch den Austausch mit dem subtropischen Nordatlantik beeinflusst zu sein.

Des weiteren zeigt diese Studie, dass die beobachteten Süßwasserschwankungen mit den Arktischen und Nordatlantischen Oszillations-Indices korreliert sind. Daraus schließe ich, dass die Süßwasserexporte aus der Arktis in den SANA auf dekadischen Schwankungen in der Variabilität der großskaligen atmosphärischen Zirkulation reagieren. Dabei ist der Export durch das Kanadisch-Arktische Archipel mit anderen Mustern in den atmosphärischen und ozeanischen Druck- und Zirkulationsfeldern verknüpft als der Export durch die Framstraße und die Barentssee-Öffnung. Ich vermute, dass die kürzlich beobachteten rapiden Änderungen in dem Süßwassergehalt des SANAs und der oberen Arktis von einem Zusammenspiel dieser unterschiedlichen Antriebsmuster resultierten, welches parallele Veränderungen im Süßwasserexport auf beiden Seiten Grönlands verursachte.

Entsprechend der momentanen Phase der dekadischen Schwankungen in der atmosphärischen Variabilität und den letzten Jahren meiner Süßwassergehaltszeitreihen hat eine Entlassung des Süßwassers, das in dem vorangegangenen Jahrzehnt in der Arktis angesammelt wurde, in den SANA bereits begonnen. Diese Entlassung wird sich möglicherweise in den folgenden Jahren fortsetzen, welches das Potential haben könnte, sich auf die Atlantische Umwälzbewegung sowie die ozeanische Wärmeabgabe an die Arktische Atmosphäre und das Meereis auszuwirken.

# Contents

# Chapter 1

# Introduction

The Arctic Ocean is undergoing remarkable environmental changes due to global warming (e.g., Serreze and Francis, 2006). The rise in the Arctic near-surface air temperature in the past decades is twice as high as the global average (Fig. 1.1), a phenomenon that is known as the Arctic amplification (e.g., Serreze and Francis, 2006; Miller et al., 2010). These non-linear changes in the Arctic atmosphere have largely been related to the so-called sea ice-albedo feedback (e.g., Winton, 2008; Screen and Simmonds, 2010; Serreze and Barry, 2011).

Albedo $\alpha$ is a measure of the reflectivity of a surface and is given as the fraction of incident radiation that is reflected. Sea ice is highly reflective ($\alpha$ = 0.5-0.7; Fig. 1.1d), and a sea ice cover with a thick snow cover can result in the reflection of up to 90 % of the solar radiation (Fig. 1.1e; Miller et al., 2010). In contrast, the open ocean has a significantly lower albedo and absorbs almost 94 % of the solar energy (Fig. 1.1c).

The warming atmosphere supports sea ice melt in summer time and inhibits sea ice formation in winter time leading to a reduced sea ice cover and a decrease of the overall albedo of the Arctic Ocean (e.g., Pistone et al., 2014). Thus more solar radiation is absorbed providing extra heat to the ocean that in turn can initiate increased sea ice melt from below. As the sea ice acts as an insulator between the ocean and the atmosphere, a decreased sea ice cover allows enhanced heat flux from the ocean back to the atmosphere, which closes the feedback loop. As a consequence the Arctic summer sea ice extent has decreased by more than 40 % in recent decades (e.g., Comiso et al., 2008; Overland and Wang, 2013), and moreover a year-round sea ice loss in extent and thickness was recorded (Fig. 1.2; e.g., Rothrock et al., 2008; Lindsay and Schweiger, 2015). Furthermore, increased freshwater and sea ice export to the North Atlantic associated with the decreasing Arctic sea ice cover are projected to affect the deep convection in the Labrador Sea, Irminger Sea and Nordic Seas due to surface freshening (Jahn and Holland, 2013).

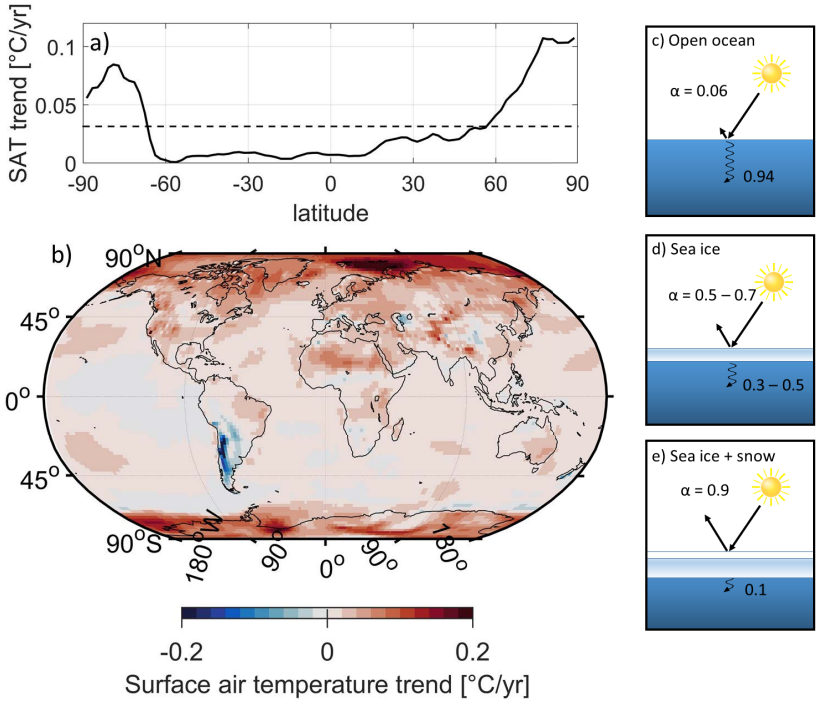


***Figure 1.1:*** *Arctic amplification and albedo feedbacks. Linear trends in annual mean surface air temperature for the period 1979-2017 obtained from NCEP-DOE Reanalysis 2 data: a) Zonal averaged trends (solid line) and global average trend (dashed line), b) global map of trends. Albedo feedbacks (based on Miller et al. (2010)): c) the open ocean has a very low albedo and absorbs almost 94 % of the incident solar energy, d) bare sea ice can reflect 50 to 70 % of the solar radiation, e) a snow cover on top of sea ice has a reflectance of ∼90 %.*

The subpolar North Atlantic and the Nordic Seas are known to be of great importance for global climate (e.g., Rhein et al., 2011; Xu et al., 2013). They are the main regions in the northern hemisphere where deep water formation takes place and where warm and saline water masses of subtropical origin are advected towards higher latitudes than in the Pacific Ocean providing heat to moderate the winters in Western Europe. One of the regional impacts of the atmospheric warming (supported by the warming ocean) is the enhanced melting of land ice (glaciers and Greenland Ice Sheet) and the associated freshwater flux to the ocean (e.g., IPCC, 2014). The accelerating mass loss of the Greenland Ice Sheet is most evident in the west and south-east of Greenland, thereby mostly releasing meltwater and ice to the Irminger Sea, Labrador Sea and Baffin Bay (Fig. 1.3; Bamber et al., 2012).

The recent study by Bamber et al. (2018) used satellite observations of ice discharge and simulated melt water runoff to estimate the total freshwater flux from the Greenland Ice Sheet and Arctic glaciers and ice caps to the Arctic Ocean and North Atlantic. They found a total freshwater flux of about 1,300 $km^3$/yr since

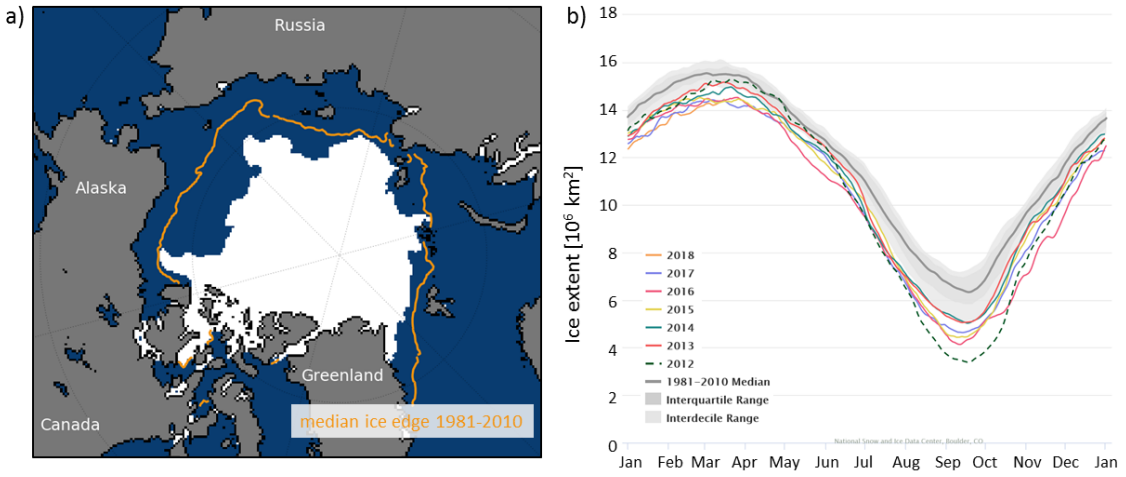


***Figure 1.2:*** *Arctic sea ice decline. a) satellite-derived sea ice extent of September 13, 2017 (white shading) compared to the median ice edge of September 13 of the period 1981-2010 (orange contour). b) Seasonal cycle of sea ice extent in the years 2012 to 2017 (coloured lines) compared to the median of the period 1981-2010 (grey line) and the interquartile and interdecile range (grey shadings). Image courtesy of the National Snow and Ice Data Center, University of Colorado, Boulder, USA.*

2010, which is an approximate increase of 50 % of the total freshwater flux compared to the average flux prior to 1990. This additional freshwater input to the oceans does not only change the oceans freshwater budget, but also affects the regional ocean stratification, impacts the local ecosystem and contributes to global sea level rise (e.g., Rahmstorf, 2007; IPCC, 2014; Dutton et al., 2015; Prowse et al., 2015; Carmack et al., 2016).

Moreover, global warming due to the increase of anthropogenic greenhouse gases does not only comprise a warming atmosphere but even more a warming ocean. About 90 % of the extra energy from the radiation imbalance forced by the anthropogenic greenhouse gases is absorbed by the oceans (Fig. 1.4; Levitus et al., 2012; IPCC, 2014). Due to thermal expansion the extra heat stored in the oceans is one major contributor to the global sea level rise (e.g., Rahmstorf, 2007; Kuhlbrodt and Gregory, 2012; Levitus et al., 2012; IPCC, 2014). Additionally it has the potential to enhance land and sea ice melt as well as impact deep water formation (e.g., Holland et al., 2008; Straneo and Heimbach, 2013; Marshall and Zanna, 2014; Carmack et al., 2015; Timmermans, 2015).

In these times of a changing climate, significant changes in the freshwater content of the Arctic Ocean and North Atlantic have been observed. The liquid freshwater content of the upper Arctic Ocean increased rapidly in the past two decades (Fig. 1.5a; McPhee et al., 2009; Rabe et al., 2011, 2014; Giles et al., 2012; Mori-

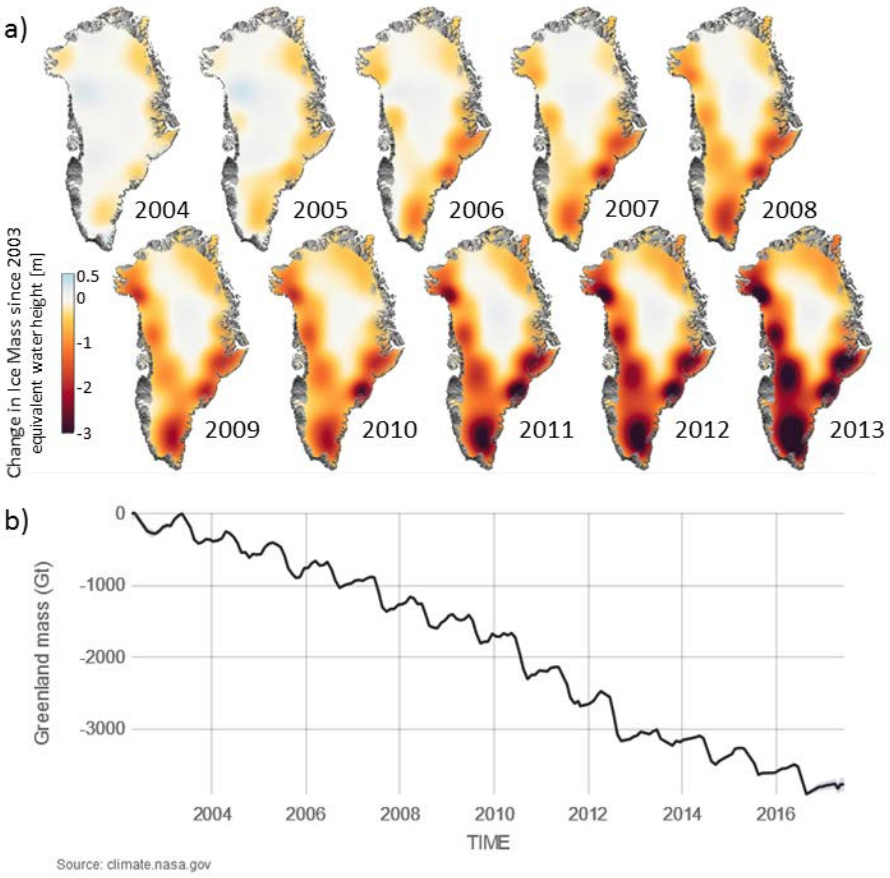


***Figure 1.3:*** *Greenland Ice Sheet mass loss. a) Satellite-derived spatial change in ice mass relative to 2003. b) Time series of Greenland Ice Sheet mass relative to 2003 based on satellite measurements. Courtesy NASA/JPL-Caltech (downloaded at http://svs.gsfc.nasa.gov/30478 in March 2018).*

son et al., 2012), while the Arctic sea ice volume has been shrinking significantly (e.g., Lindsay and Schweiger, 2015). In contrast, the subpolar North Atlantic and the Nordic Seas became more saline after a freshening from the 1960s to 1990s (Fig. 1.5b; Curry and Mauritzen, 2005; Boyer et al., 2007; Mauritzen et al., 2012).

Both regions are sensitive to freshwater changes. The deep convection in the subpolar North Atlantic and Nordic Seas is part of the Atlantic meridional overturning circulation, which is an important component of the global thermohaline ocean circulation. Freshwater changes may decrease deep convection due to higher stratification (e.g., Aagaard and Carmack, 1989; Haak et al., 2003; Häkkinen, 1999; Yang et al., 2016) and thereby have a profound impact on our climate (e.g., Koenigk et al., 2007; Rennermalm et al., 2007). In the Arctic Ocean, fresh water has an impact on the warming of the atmosphere as well as sea ice formation and melting because the density stratification, which regulates the upward heat transport from the warm water of Atlantic origin at intermediate depths, is mostly set by salinity

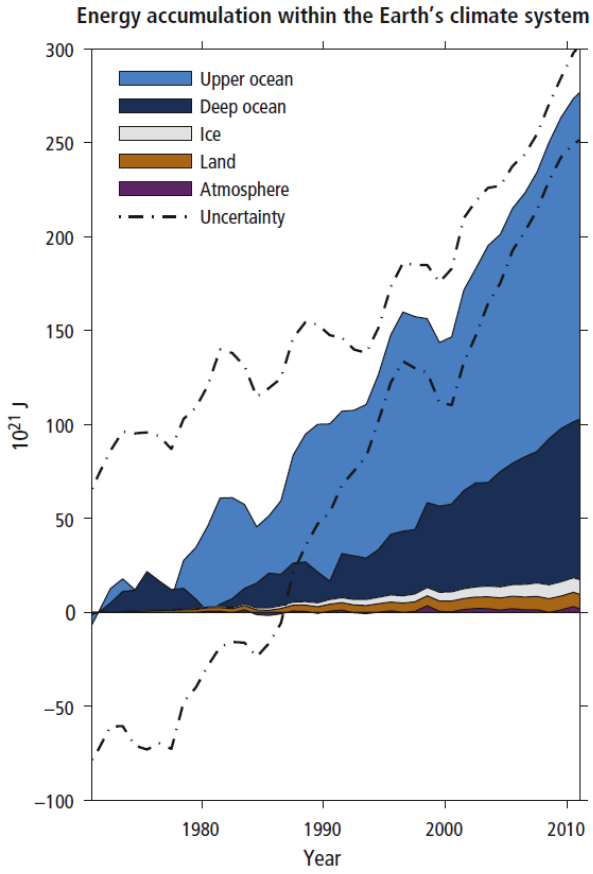


***Figure 1.4:*** *Energy accumulation within the Earths climate system (IPCC, 2014). Estimates are in* $10^{21}$ *J, and are given relative to 1971 and from 1971 to 2010, unless otherwise indicated. Components included are upper ocean (above 700 m), deep ocean (below 700 m; including below 2,000 m estimates starting from 1992), ice melt (for glaciers and ice caps, Greenland and Antarctic ice sheet estimates starting from 1992, and Arctic sea ice estimate from 1979 to 2008), continental (land) warming, and atmospheric warming (estimate starting from 1979). Uncertainty is estimated as error from all five components at 90 % confidence intervals.*

(e.g., Rudels, 2009; Toole et al., 2010). Consequently, a decrease in fresh water might intensify the Arctic amplification.

Observational and model studies addressing the freshwater variability of the two regions have mainly proposed independent processes to be responsible for the observed changes. Giles et al. (2012), for example, related the increased liquid freshwater content in sub regions of the Arctic Ocean since the 1990s to a strengthening of the atmospheric Beaufort High causing a convergence of fresh surface water in the accelerated Beaufort Gyre. However, Rabe et al. (2011, 2014) observed that the freshwater content increase in the upper Arctic Ocean from the 1990s to the period 2006-2008 is mainly due to a mean decrease in the upper ocean salinity rather

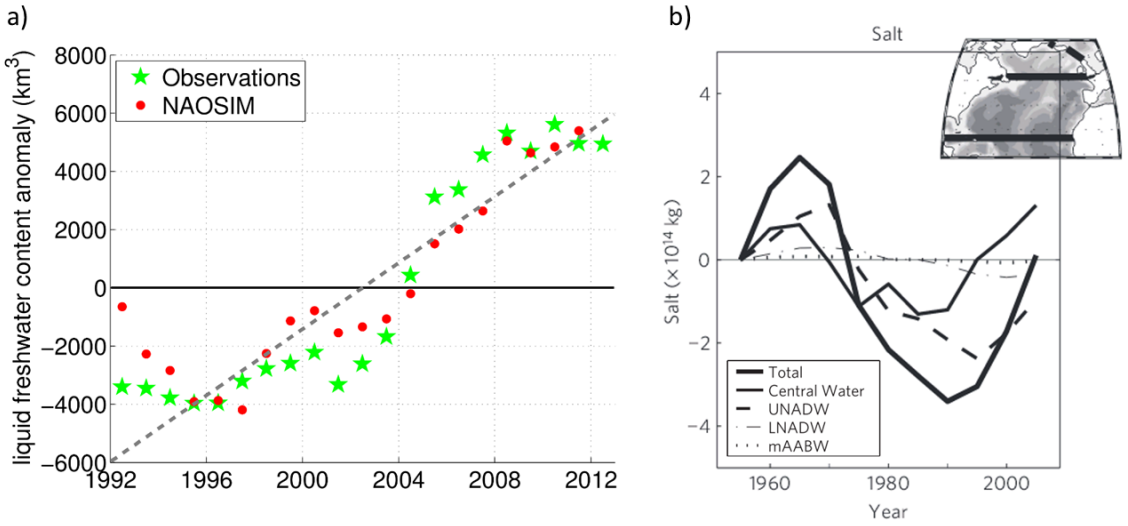


***Figure 1.5:*** *Freshwater and salt content changes of the Arctic Ocean and subpolar North Atlantic. a) Liquid freshwater content anomaly of the central upper Arctic Ocean above the 34-isohaline relative to a reference salinity of 35 (figure from Rabe et al., 2014 with permission): Observational estimates (green stars) and estimates from the sea ice ocean model NAOSIM (red dots). b) Pentadal means of salt content anomalies within different water masses of the subpolar North Atlantic (figure from Mauritzen et al., 2012 with permission): total salt content changes (thick line), thermocline waters or Central Waters ($\sigma_\theta$ < 32.15; thin line), Upper North Atlantic Deep Water originating in the Subpolar Gyre (UNADW, 32.15 < $\sigma_\theta$ < 37.0; dashed line), Lower North Atlantic Deep Water originating north of the Greenland-Scotland Ridge (LNADW, 37.0 < $\sigma_\theta$ < 45.9; dot-dashed line), and modified Antarctic Bottom Water (mAABW, $\sigma_\theta$ > 45.9; dotted line).*

than a deepening of the lower halocline forced by regional Ekman pumping. They suggested the mean freshening of the upper Arctic Ocean to be associated with increased net sea ice melt and the advection of increased amounts of Siberian river waters. Similarly, other studies discussed a re-routing of Eurasian river runoff as a response to the large-scale atmospheric circulation or local winds and the effect on the Arctic freshwater content (Bourgain et al., 2013; Jahn et al., 2010b; Morison et al., 2012; Niederdrenk et al., 2016). Further, there is evidence of an increase in continental runoff and net precipitation in the past decades (Peterson et al., 2002; Overeem and Syvitski, 2010; Haine et al., 2015).

The increased salinity of the subpolar North Atlanic and Nordic Seas since the 1990s has been related to a transport of more saline waters from the subtropical North Atlantic, where net evaporation has been anomalously high (Curry et al., 2003; Mauritzen et al., 2012). Similarly, Glessmer et al. (2014) attributed a freshening of the Nordic Seas prior to the 1990s to an inflow of less saline waters from the subpolar North Atlantic. Further, Holliday et al. (2008) tracked increased salinities of the Atlantic Water from the Subpolar Gyre to the Fram Strait explaining the

reversed salinity trend after the freshening of the 1960s to 1990s in the eastern subpolar North Atlantic and Nordic Seas. Hátún et al. (2005) related these changes in the salinity of the Atlantic inflow to the Nordic Seas to changing contributions from the subtropical and the subpolar gyre. Moreover, Josey and Marsh (2005) related the freshening of the eastern subpolar gyre from the 1960s to 1990s to an increase in net precipitation driven by changes in the local sea level pressure pattern.

While fresh water is added to the Arctic Ocean by continental runoff, net precipitation, and the inflow of Pacific Water, it can only be removed by advection to the North Atlantic (e.g., Lique et al., 2009). In the past decades, so called Great Salinity Anomalies (GSA), which are patches of anomalously low salinity travelling in a cyclonic pattern through the northern North Atlantic, have been observed (e.g., Dickson et al., 1988). They were found to originate in anomalous freshwater exports from the Arctic Ocean (Belkin et al., 1998; Haak et al., 2003; Belkin, 2004) and/or weakened transport of saline waters to the region (Häkkinen, 2002). In fact, Peterson et al. (2006) described that the freshwater content increase in the North Atlantic between 1965 and 1995 can be partly explained by anomalous local net precipitation but the largest amount results from anomalously high freshwater export from the Arctic Ocean. Moreover, Karcher et al. (2005) found from a simulation with a regional sea-ice ocean model and from salinity observations of the East Greenland Current a strong link between Arctic Ocean large-scale changes of the thermohaline structure and the freshwater export to the North Atlantic in the 1990s.

Most studies focus on independent processes when investigating the freshwater content changes in the Arctic Ocean or in the North Atlantic. Hypothesizing that the observed freshwater/salinity changes in the subarctic North Atlantic (SANA, combination of subpolar North Atlantic and Nordic Seas) and Arctic Ocean are related to each other, I compare the freshwater contents of both regions using observational salinity data from 1990 to 2013 and sea ice volume estimates from a model assimilation product. As observational transport time series at the gateways of the Arctic Ocean and SANA are either too short or do not exist, I use a global ocean sea-ice model and its forcing to identify the drivers of the freshwater variability in the upper Arctic Ocean and SANA. Thus I address the following main research questions:

- Are the recent freshwater content changes in the upper Arctic Ocean and the SANA linked?
- What drives the freshwater variability of the two regions?
- Which processes/physical mechanisms have led to the observed changes in the freshwater content?

After providing background information on the geographical setting, as well as on the ocean circulation and hydrography of the research site (Chap. 2), I will present the various observational, reanalysis and model data and the methods that I have used to answer my research questions (Chap. 3). The results from the analysis of the observed and simulated freshwater content variability of the Arctic Ocean and SANA, including a comparison of both and the discussion of the results, are given in Chap. 4. Furthermore, I have analysed the different freshwater sources and sinks of the two regions and show the mean freshwater budget as well as the temporal freshwater flux variability in Chap. 5. This is followed by the analysis of atmospheric parameters and associated changes in the sea surface height and sea ice/ocean circulation that could explain the observed freshwater variability of the Arctic Ocean and SANA (Chap. 6). After the detailed discussions in Chap. 4-6, a final discussion of the major results of my study will be provided in Chap. 7. Finally I will give the conclusions and an outlook in Chap. 8. The appendix includes tables of abbreviations and symbols as well as supplementary information about a simple box model used for testing different reference salinities for the calculation of the freshwater transport. Moreover, I show the volume budget of the study area in the model and compare the simulated freshwater transports to observational data.

# Chapter 2

# The Arctic – subarctic ocean system

*In this chapter the main components of the circulation and hydrography of the subpolar North Atlantic, Nordic Seas and Arctic Ocean are presented. At first the bathymetry is shown and the main topographic characteristics of the research area are introduced. This provides the background for the geographical setting of this study. The paragraphs marked with an asterisk (*) are taken from Campos and Horn (2018) and are based on information from Rudels (2009).*

---

## 2.1 Geographical setting

The Arctic Mediterranean consists of two major parts: the Arctic Ocean and the Nordic Seas. The Arctic Ocean is the northernmost part of the Arctic Mediterranean which is enclosed by North America, the Eurasian continent, Svalbard, and Greenland (Fig. 2.1). The Nordic Seas are enclosed by Svalbard, Norway, Scotland, Iceland and Greenland and include the Greenland Sea, Norwegian Sea, and Iceland Sea (also called the GIN Seas).*

The Arctic Ocean connects to the Nordic Seas via the Fram Strait (between Greenland and Svalbard, ∼2,600 m deep) and the Barents Sea Opening (between Svalbard and Norway, ∼200 m deep). Other Arctic gateways are the narrow channels through the Canadian Arctic Archipelago (CAA, islands northwest of Greenland, ∼150 - 230 m deep) and the Bering Strait (∼45 m deep and only 50 km wide), which is the only connection to the Pacific Ocean. Towards the Eurasian continent the Arctic Ocean consists of wide, shallow shelves (<50 - 300 m deep), which make up almost half of the entire Arctic Ocean and comprise five marginal seas: Barents Sea,

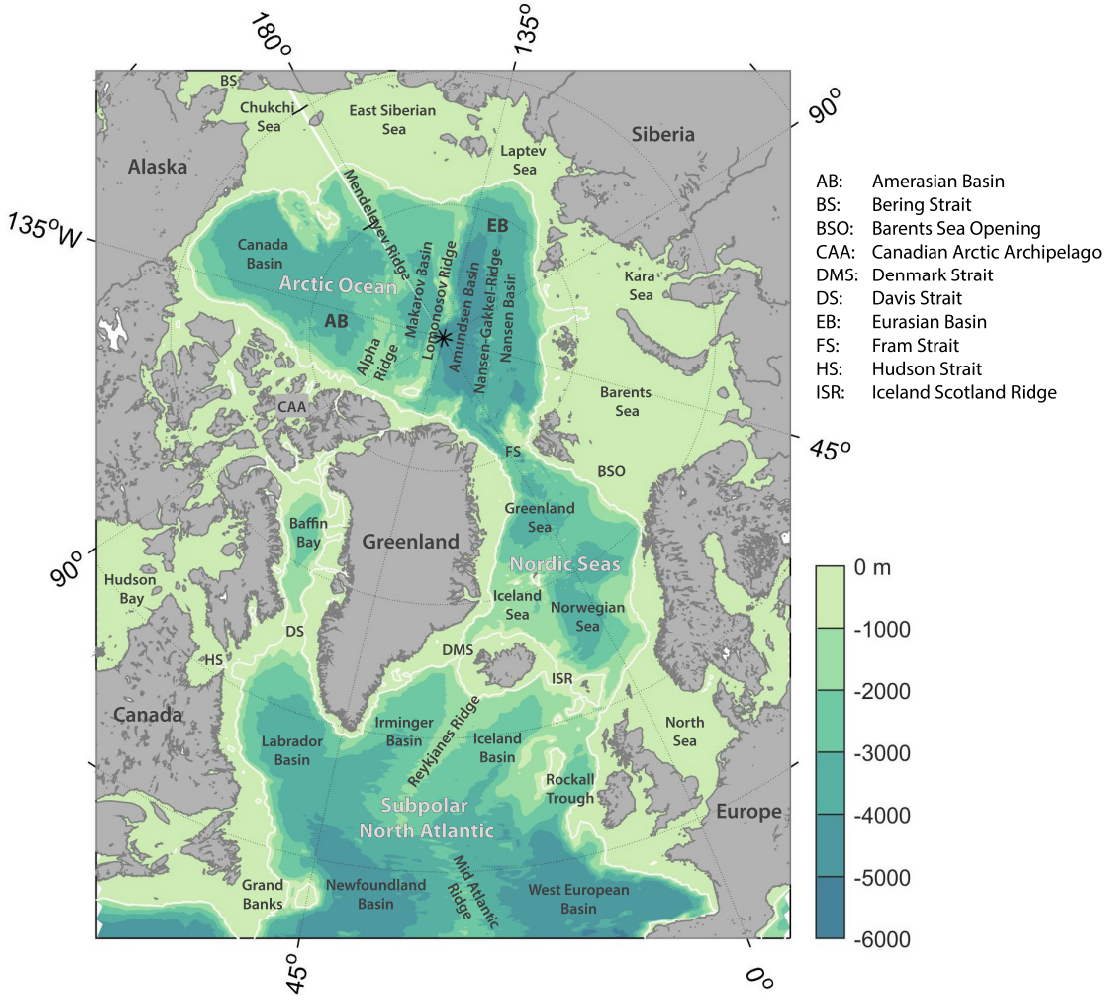


***Figure 2.1:*** *Bathymetry of the Arctic Mediterranean Sea and the subpolar North Atlantic derived from the ETOPO2 database in 2-minute resolution. The white contour indicates the 500 m isobath.*

Kara Sea, Laptev Sea, East Siberian Sea and Chukchi Sea. At the coasts of North America and Greenland the shelves are much narrower. The deep basins in the center of the Arctic Ocean are divided into two major parts, the Amerasian Basin and the Eurasian Basin. They are separated by the Lomonosov Ridge, which reaches until 1,600 m below the sea surface. The Eurasian Basin consists of the Nansen Basin and the Amundsen Basin, which are separated by the Gakkel Ridge. The Mendeleyev Ridge and Alpha Ridge divide the Amerasian Basin into the Makarov Basin and the Canada Basin. With approximately 4,500 m depth, the Amundsen Basin is the deepest, while the Canada Basin is by far the largest (Fig. 2.1). The boundary of the Nordic Seas to the North Atlantic is the Denmark Strait (∼500 - 700 m sill depth) and the Iceland-Scotland-Ridge (∼300 - 850 m sill depth). The shelves along the Greenland coast are wide and shallow with a steep shelf break.*

The subpolar North Atlantic is framed by Canada, Greenland and Europe and has its southern boundary to the subtropical North Atlantic at approximately 45 °N. In the west it connects to the Baffin Bay via the Davis Strait (∼650 m sill depth) and to the Hudson Bay via the Hudson Strait (∼950 m sill depth). The western part of the subpolar North Atlantic comprises the Newfoundland, Labrador and Irminger Basins and is separated from the eastern basins by the Mid Atlantic Ridge (∼1,700 - 3,600 m crest height) and its northern extension, the Reykjanes Ridge (∼1,000 - 1,500 m crest height). The wide shelf on the western side of the Newfoundland Basin is called the Grand Banks of Newfoundland. In the east the subpolar North Atlantic connects to the Nordic Seas and the North Sea. The eastern deep subpolar North Atlantic consists of the West European Basin in the south and Iceland Basin and Rockall Trough further north (Fig. 2.1). The Newfoundland and West European basins are the deepest reaching down to 5,000 m water depth, while the basins further north are shallower with depths of approximately 2,000 to 4,000 m.

## 2.2 Circulation and Hydrography

Since the Arctic Ocean is a largely enclosed ocean, there are only two water masses that enter the basin from other oceans: Pacific Water (PW) and Atlantic Water (AW). The relatively fresh PW is transported through the Bering Strait (Fig. 2.3) and is mainly advected at the surface into the Canadian Basin and adjacent shelf regions. In addition to continental runoff and precipitation, the low salinity PW is an important Arctic freshwater source. Due to relatively small differences in temperature throughout the water column of the Arctic Ocean, the stratification is mainly determined by salinity changes (Fig. 2.2; e.g., Rudels, 2009; Toole et al., 2010). Thus, the fresh (light) waters stay in the upper ocean and form the so called Polar Mixed Layer (Fig. 2.2). Large parts of the Arctic Ocean are covered by sea ice which is formed from these fresh surface waters at near-freezing temperatures. By sea ice formation and melt, fresh water is concentrated at the surface.*

The AW is warmer and saltier than PW and meteoric waters from continental run-off and precipitation. Thereby, it is denser and can be found deeper in the water column of the central Arctic Ocean (Fig. 2.4). The significant difference in salinity creates a strong halocline between the Polar Mixed Layer and the AW layer establishing a strong permanent stratification in the deep basins (Fig. 2.2). The halocline, which is defined by high vertical salinity gradients ($32.5 < S < 34.5$), is thickest in the Canada Basin (200 - 250 m) and thinnest in the Amundsen Basin (50 - 100 m). In the Nansen Basin there is no halocline present (Rudels, 2009). The temperatures of the halocline remain close to the freezing point. Due to heat loss

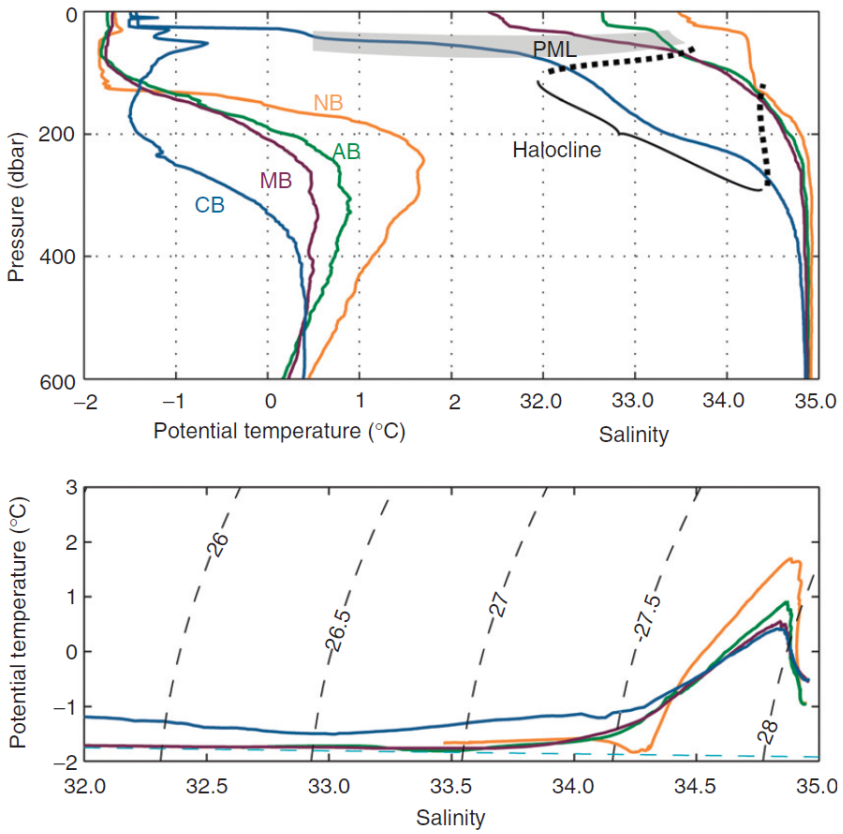


***Figure 2.2:*** *Upper Arctic Ocean hydrography (figure from Rudels, 2009 with permission). Potential temperature and salinity profiles (upper panel) and potential temperature-salinity curves (lower panel) of the upper Nansen Basin (NB, orange), Amundsen Basin (AB, green), Makarov Basin (MB, purple), and Canada Basin (CB, blue). The Polar Mixed Layer (PML) and the halocline are indicated in the salinity profiles (upper panel). The dashed black lines indicate isopycnals [kg/m$^3$] and the dashed blue line indicates the freezing temperature (lower panel).*

and mixing with shelf waters there are many modifications of AW at intermediate depths. Just below the halocline, temperatures are the highest (Fig. 2.2). The temperature of the AW layer is highest in the Nansen Basin and decreases towards the Canada Basin (Fig. 2.2). The densest waters are formed on the shelves of the Barents Sea, where the AW subsequently releases heat to the atmosphere and is mixed with brine rejected from newly formed sea ice before it sinks down the shelf break into the Nansen Basin (Fig. 2.3-2.4). This Arctic bottom water is the densest water of the world ocean and can only be found in the Arctic region (Tomczak and Godfrey, 1994). Only a small part is able to flow over the sill of the Fram Strait into the Nordic Seas balancing the bottom/deep water formation on the Arctic shelves (e.g., Bönisch and Schlosser, 1995). There it mixes with other lighter waters at the bottom.*

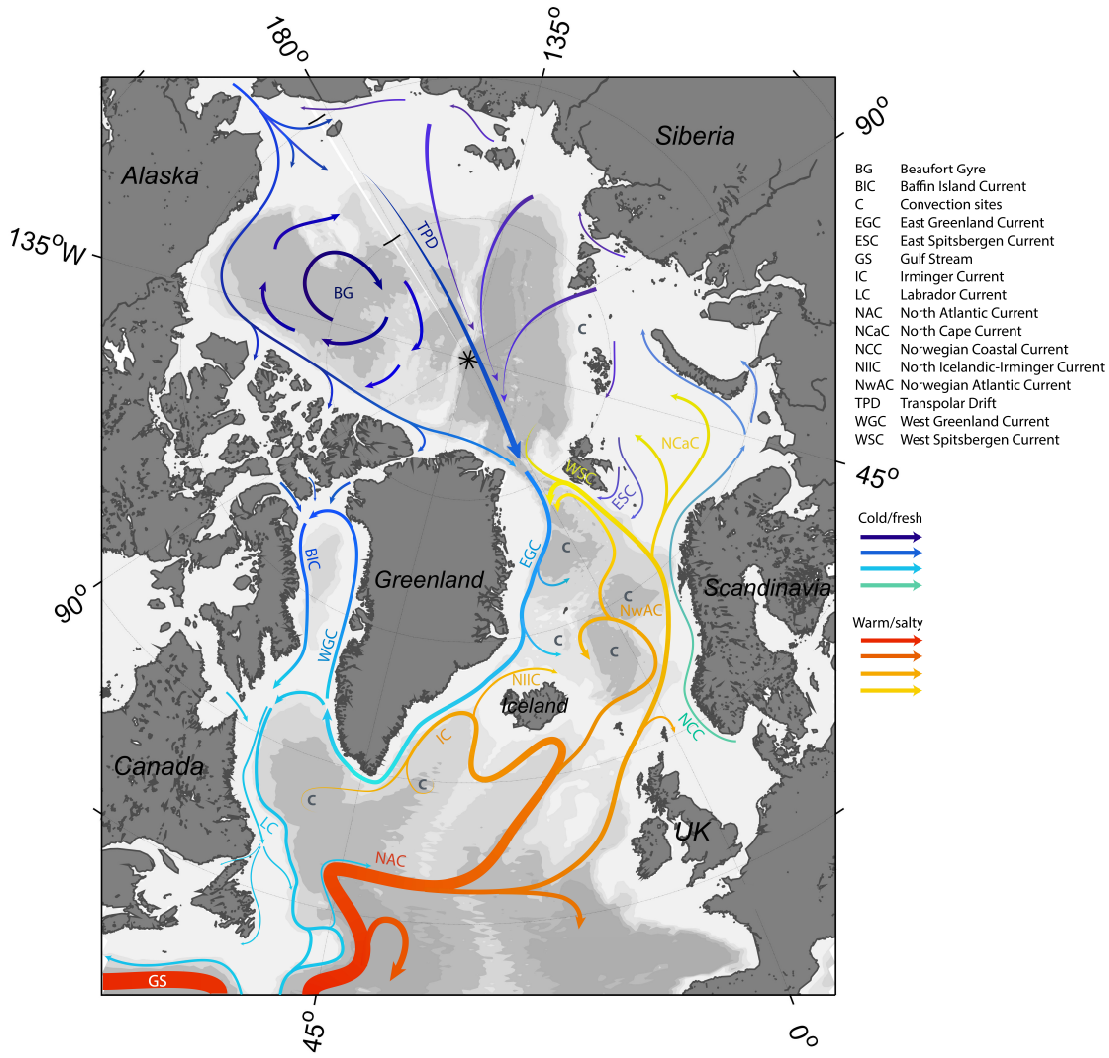


***Figure 2.3:*** *Surface circulation sketch of the Arctic Mediterranean and subpolar North Atlantic. The main convection cites are marked with C. Cold and fresh currents are indicated by blue/green arrows; warm and salty currents by red/yellow arrows. The schematic is based on Fischer and Schott (2002); Rudels (2009); Rhein et al. (2011); Mertens et al. (2014); Yashayaev et al. (2015); Carmack et al. (2016); Latarius and Quadfasel (2016).*

Warm and salty water masses of tropical/subtropical origin transported by the Gulf Stream enter the subpolar North Atlantic from the southwest (Fig. 2.3). These water masses then propagate further north with the North Atlantic Current, which flows northward along the shelf break of the Grand Banks, partly recirculating at ∼50 °N, and sharply turns east at ∼52 °N(e.g., Mertens et al., 2014). After passing the Mid Atlantic Ridge it splits into several branches. One branch turns south towards subtropical latitudes. Two branches flow via the Rockall Trough and the

Iceland Basin into the Nordic Seas crossing the Iceland-Scotland Ridge. Another branch performs a cyclonic turn into the Irminger and Labrador Sea becoming the Irminger Current. The small branch from the Irminger Current on the western side of Iceland is called the North Icelandic-Irminger Current (Fig. 2.3). As the waters transported by the North Atlantic Current and the Irminger Current subsequently release heat to the atmosphere, they get colder and denser. The increased buoyancy loss in winter time leads to deep convection in the central Irminger and Labrador Seas causing vertical homogenisation of the water column down to a depth of 200 - 2000 m (Kieke et al., 2007). The formed water mass is called Labrador Sea Water and following Stramma et al. (2004) is defined as water in the density range $\sigma_\theta$ = 27.68 - 27.80 kg/m$^3$. The Labrador Sea Water spreads at mid-depths almost all over the subpolar North Atlantic partly following the Deep Western Boundary Current and leaving it again, crossing the Mid Atlantic Ridge turning north into the Rockall Trough and the Iceland Basin and turning south on both sides of the Mid Atlantic Ridge (e.g., Rhein et al., 2011; Fig. 2.4).

The relatively warm and saline AW, which is the main water source of the entire Arctic Ocean, enters the Nordic Seas from the south via the different branches of the North Atlantic Current. The Norwegian Atlantic Current carries the AW through the Nordic Seas at the surface and splits into two main branches. One branch enters the Arctic Ocean through the Barents Sea Opening, the North Cape Current, the other, which then is called West Spitsbergen Current, flows through the Fram Strait. Only a part of the West Spitsbergen Current propagates further north into the Arctic Ocean, the other part recirculates close to the Fram Strait and joins the East Greenland Current. The AW dives underneath the sea ice when reaching it north of Fram Strait and later meets the other cooled AW branch, which flows down the continental slope of the Barents Sea shelf into the Nansen Basin. Steered by the topography, the AW flows along the shelf breaks and spreads all over the Arctic Ocean forming counterclockwise circulations in all deep basins (Fig. 2.4).*

These denser AW modes at intermediate to greater depths can only exit the Arctic Ocean via the Fram Strait (Fig. 2.4). They are transported southward in the deeper part of the East Greenland Current along the Greenland shelf partly being deflected into the Greenland and Iceland Sea. Other dense water masses formed by winter convection in the deep basins of the Nordic Seas partly flow northward into the Arctic Ocean, join the deep East Greenland Current or flow over the Iceland Scotland Ridge or Denmark Strait. The deep waters flowing over the sills east and west of Iceland are termed Iceland Scotland Overflow Water and Denmark Strait Overflow Water and have a density of $\sigma_\theta = 27.80 - 27.88\ kg/m^3$ or $\sigma_\theta > 27.88\ kg/m^3$, respectively (Fischer and Schott, 2002). The Iceland Scotland Ridge Overflow Water flows into the Iceland Basin and partly propagates further

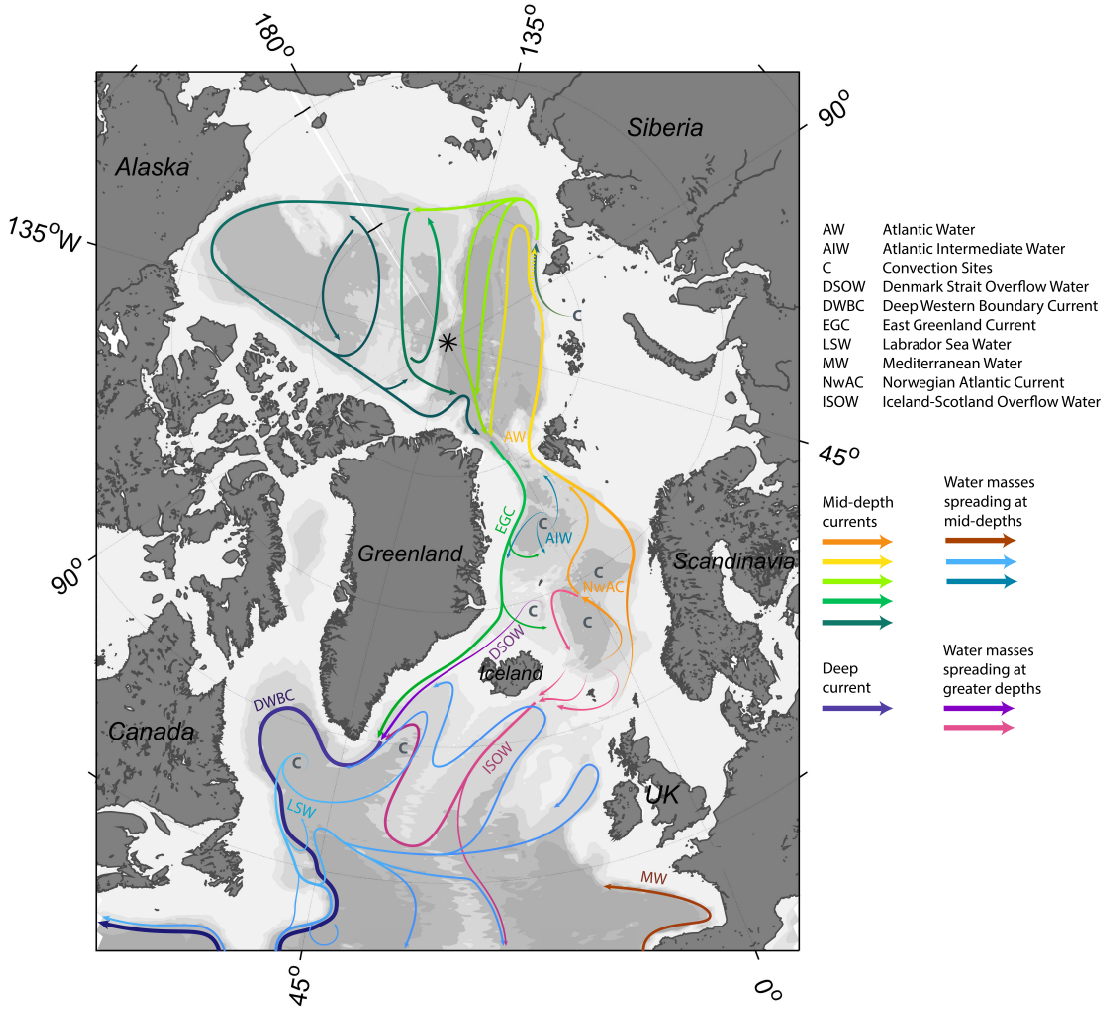


***Figure 2.4:*** *Sketch of the Arctic Mediterranean and subpolar North Atlantic circulation at intermediate and greater depths. The main convection cites are marked with C. The legend on the right summarizes which currents and water mass spreading paths are at intermediate depths and which are at greater depths. The schematic is based on Rudels (2009); Rhein et al. (2011); Mertens et al. (2014); Yashayaev et al. (2015); Carmack et al. (2016); Latarius and Quadfasel (2016).*

south towards subtropical latitudes and partly crosses the Mid Atlantic Ridge at the deeper fracture zones joining the Denmark Strait Overflow Water in the Irminger Sea and feeding into the Deep Western Boundary Current. This current flows along the Labrador Shelf and Grand Banks approximately following the 3,000 m isobath (Fig. 2.4).

The surface circulation in the central Arctic Ocean mainly comprises two features: the Beaufort Gyre and the Transpolar Drift (Fig. 2.3). The Beaufort Gyre is an anticyclonic circulation in the Canada Basin that is forced by a high pressure system in the lower atmosphere, the so called Beaufort High. Fresh surface waters

from the shelves and from the Pacific accumulate in the interior of the gyre and leave the Arctic through the CAA or the Fram Strait. The Transpolar Drift is a wind-driven current that directs sea ice and waters from the Siberian shelves and the Bering Strait to the Fram Strait, where it exits the Arctic Ocean into the Nordic Seas and subpolar North Atlantic.*

The fresh and cold waters of Arctic origin are then transported by the East and West Greenland Current along the Greenland shelf break (Fig. 2.3). In the Davis Strait one branch of the West Greenland Current turns west towards the western Labrador Shelf. The other branch flows further north along the eastern shelf of the Baffin Bay until it reaches the CAA (Fig. 2.3). There the waters return south along the western shelf of the Baffin Bay with the Baffin Island Current also carrying the Arctic surface waters flowing through the CAA. In the Davis Strait the Baffin Island Current is joined by the other branch of the West Greenland Current and flows further south along the western Labrador shelf now termed Labrador Current. The Labrador Current, partly flowing over the Labrador Shelf, further propagates south at the shelf break of the Grand Banks encountering the North Atlantic Current and partly been trapped by it back towards the north (Fischer and Schott, 2002). The anti-clockwise surface circulation in the western subpolar North Atlantic performed by the North Atlantic, Irminger, West Greenland and Labrador Currents is called the subpolar gyre and is mainly driven by changes in surface heat flux and wind stress curl associated with the North Atlantic Oscillation (e.g. Curry and McCartney, 2001; Böning et al., 2006).

The above given information provides the background to the connection of the Arctic Ocean, the Nordic Seas and the subpolar North Atlantic, which is crucial to understand possible links of their freshwater contents. Further it highlights the importance of fresh water in both regions. In the Arctic Ocean fresh water is the major determiner of the ocean stratification and limits the upward heat transfer from the AW to the sea ice and atmosphere. In the subpolar North Atlantic and Nordic Seas relatively fresh polar waters are transported close to the deep convections sites where it has the potential to change the ocean stratification and thereby influence the deep water formation. Therefore I investigate the freshwater content variability of the Arctic Ocean and North Atlantic and aim to understand the drivers. In the following the data and the methods used to tackle the objectives of my study are presented.

# Chapter 3

# Data and methods

*This chapter deals with the data used in this study and the methods used to analyse these data. To answer my research questions, I used a variety of observational, reanalysis, model and assimilation data, which I will describe in the first two sections. This is followed by a detailed description of the used methods applied to analyse the freshwater variability of the Arctic Ocean and North Atlantic and their relationship to atmospheric variability.*

---

To answer my first research question, if the recent freshwater changes in the Arctic Ocean and SANA are linked, I calculated the freshwater content for these regions from observational and assimilation datasets and from a model simulation. The calculation is described in Chap. 3.3.

For the SANA, I used the COriolis Re-Analysis salinity product (Chap. 3.1.1) to calculate the observational liquid freshwater content from 1990 to 2013. By SANA I mean the combined region of subpolar North Atlantic (45 - 67 °N, 0 - 65 °W) and Nordic Seas (63 - 77 °N, 35 °W - 20 °E) (Fig. 3.5). For the upper Arctic Ocean, I calculated the observational total freshwater content from 1992 to 2013, considering both the liquid and solid components, from objectively mapped liquid freshwater inventories from Rabe et al. (2011, 2014) (Chap. 3.1.2) and from the Pan-Arctic Ice Ocean Modeling and Assimilation product (Chap. 3.2.2), respectively.

As observational transport time series are too short, I used data from a model simulation with AWIs global finite-element sea ice ocean model (FESOM; Chap. 3.2.1) to identify the drivers of the freshwater content variability of the Arctic Ocean and the SANA. For comparison to the observations, I calculated the freshwater contents of the Arctic Ocean and the SANA from the model data the same way as I did from the observational data. As the time series compare well, I used the FESOM data and the models forcing (Chap. 3.1.3, 3.1.6) for analysing the

freshwater fluxes to the Arctic Ocean and the SANA as I assume that fresh water is conserved in the model and freshwater content changes need to be explained by changing freshwater fluxes (Chap. 3.4). Additionally I used freshwater flux estimates from the Greenland Ice Sheet and Arctic glaciers and ice caps (3.1.7) for comparison, as it is not included in the models forcing. Whereas fluxes from precipitation, evaporation, river runoff and land ice are pure fresh water, fluxes from oceanic transport are not. Therefore an equivalent freshwater transport needs to be calculated to compare to the other fluxes. The calculation and a critical examination of the method are given in Chap. 3.5. Moreover, I calculated the effective salinity of the transported waters, which is a transported weighted salinity, to quantify changes in the oceanic freshwater transports caused by salinity variations (Chap. 3.6). The benefit of the effective salinity is that the values are independent of a reference value.

The time series analysis that I used to describe the (co)variability of freshwater contents and freshwater fluxes and to identify the atmospheric and oceanic patterns that are assocaited with the freshwater variability, are presented in Chap. 3.7. For this analysis I used additionally indices of the dominant modes of the large-scale atmospheirc circulation variability in the Arctic-North Atlantic region (Chap. 3.1.5) and atmospheric reanalysis data (Chap. 3.1.4).

## 3.1 Observational and reanalysis data

### 3.1.1 The Coriolis Re-analysis dataset

For the calculation of the SANA liquid freshwater content I used gridded salinity data from the COriolis Re-Analysis (CORA) dataset – version 4.0 (Cabanes et al., 2013). CORA is an in-situ global temperature and salinity dataset consisting of data from the Coriolis database. It is available as profile data interpolated on standard depths and as gridded data using objective mapping. The product I used is the gridded CORA data product called INSITU_GLO_TS_REP_OBSERVATIONS_013_001_b and is available through the Copernicus Marine environment monitoring service (http://marine.copernicus.eu/, download 1st July, 2015; user manual: Pouliquen and Grouazel, 2013). The CORA data products are provided by the Coriolis team in Brest, France, and updated once a year. The gridded CORA data are available at 158 depth levels between the sea surface and 2,000 m depth (3 m steps between the surface and 5 m depths, 5 m steps between 5 m and 100 m depths, 10 m steps between 100 m and 800 m depths, and 20 m steps between 800 m and 2,000 m depths), with a spatial resolution of 1/3 ° latitude and 1/2 ° longitude and a temporal resolution of one month.

The data used for the CORA product comes from measurements with different types of instruments: mainly Argo floats, expendable bathythermographs, Conductivity Temperature Depth probes (CTD), expendable CTDs, and moorings (Pouliquen and Grouazel, 2013). The profile positions in the SANA region for every year are shown in Fig. 3.1, and the number of profiles for every year separated by the instrument type and the monthly distribution of profile data are shown in Fig. 3.2. The amount of profiles increased over time, especially when profiling floats became available in 1999/2000 (Fig. 3.1; Fig. 3.2a). However, the salinity profiles from floats are largely limited to the deeper basins, resulting in a lack of data on the shelves. Especially on the Greenland shelf data coverage is very sparse and in the central Baffin Bay there is almost no data at all (Fig. 3.1). Moreover, the monthly distribution of profile numbers reveal that there are almost twice as many profiles in summer than in winter (Fig. 3.2b).

I used delayed-time data for 1990 to 2012 and near real-time data for 2013 since the data were not yet available in delayed-time mode. The data in the near real-time and delayed-time modes differ in the used data sources and the level of processing (Cabanes et al., 2013; Pouliquen and Grouazel, 2013). The data of the Coriolis database undergoes automatic checks and objective analysis within the database before being extracted for the CORA dataset (Pouliquen and Grouazel, 2013). The automatic checks include impossible dates, locations and speeds tests, checking that pressure and density increases with depth, global and regional range tests of the values, spike and gradient tests in profiles, checking for identical measurements within a profile and tests only applied to Argo float data described in Wong et al. (2012) (Cabanes et al., 2013).

The near real-time processing further includes checks for duplicates and a visual check of suspicious profiles (Cabanes et al., 2013). The data for the delayed-time mode additionally goes through a series of further validation which is summarised in Tab. 3.1. In contrast to other reanalysis products, CORA is not processed with a numerical model. It only uses a model to identify measurements that have a too strong innovation value when assimilated in the model.

The uncertainties given in the CORA product are confidence values of the analysis estimate from the optimum interpolation method. The confidence value is the ratio of the observations variance (i.e. the spread of the observations selected in the optimum interpolation analysis) to a priori variance (i.e. the variance associated to the climatological background field). It thereby indicates the amount of data used in the estimates and the statistical robustness of the analysed value (Jèrôme Gourrion, French National Centre for Scientific Research, Paris, France, pers. comm.). The resulting uncertainties of the calculated freshwater content for the subpolar North Atlantic and the Nordic Seas are shown in Chap. 4.2.

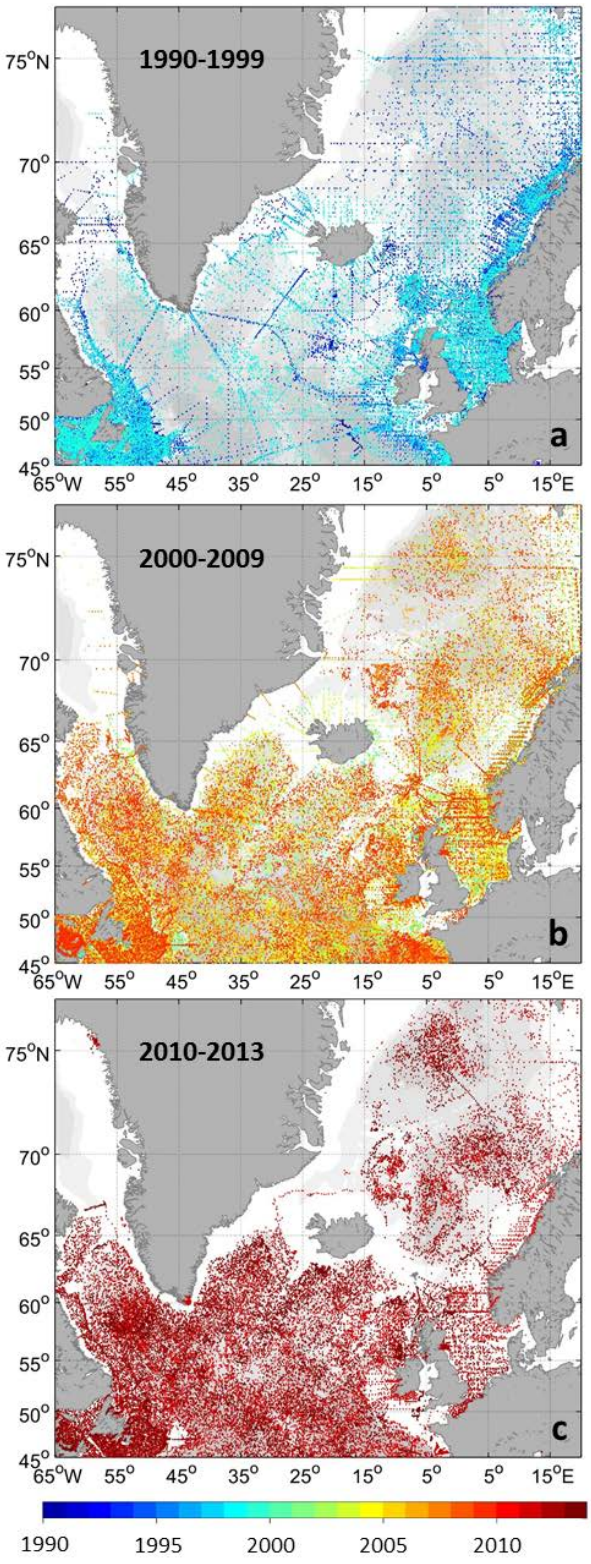


***Figure 3.1:*** *Profile positions of CORA 4.1 data in the SANA region for the periods 1990-1999 (a), 2000-2010 (b) and 2010-2013 (c). Colours indicate the years in which the profiles were obtained.*

***Table 3.1:*** *Validation process of the CORA 4.0 delayed-time data. Table adapted from Pouliquen and Grouazel (2013)*

| Name of validation | Description |
|---|---|
| Measure on Earth | Compare position of bathymetry, to reject bad positions |
| Date check | Checks that the date corresponds to the name of the file |
| Parameter range check | Checks that temperature, practical salinity, pressure and depth have acceptable values |
| Constant check | Check that temperature, practical salinity, pressure and depth have different values along the vertical |
| Ascending immersion check | Check that pressure and/or depth are increasing |
| Duplicate levels check | Check that immersion level are not duplicated |
| Climatological | V_temperature=max(clim+9xSigma, clim+9*0.1) V_salinity=max(clim+9xSigma,clim+9*0.025) |
| Spike check | Semi-automatic (need a visual control) check that spot spikes on profiles |
| Quality flag relevance | Control that a given QC is relevant with the associated measure |
| Depth wrote in pressure field | Check that depth measurements are not written in the pressure field (especially for XBT and XCTD) |
| Duplicate profile | Detect duplicate profile and delete the one having a worse quality or less meta-data |
| XBT correction | Empirical correction of depth bias and temperature offset on XBTs. Method of Hamon et al. (2012) based on co-localisation with CTD profiles. |
| Assimilation feedback | Alerst on profiles raised by a too strong innovation value when assimilated in a model. |
| Ultimate objective analysis | Last step of the process that guarantee a global (spatial and temporal) consistency of the dataset by computing a residual value between each measure and the background given by the climatology and the other measurements. |

*Abbreviations: CTD – Conductivity Temperature Depth probe, QC – Quality Control, XBT – Expendable Bathythermograph, XCTD – Expendable Conductivity Temperature Depth probe.*

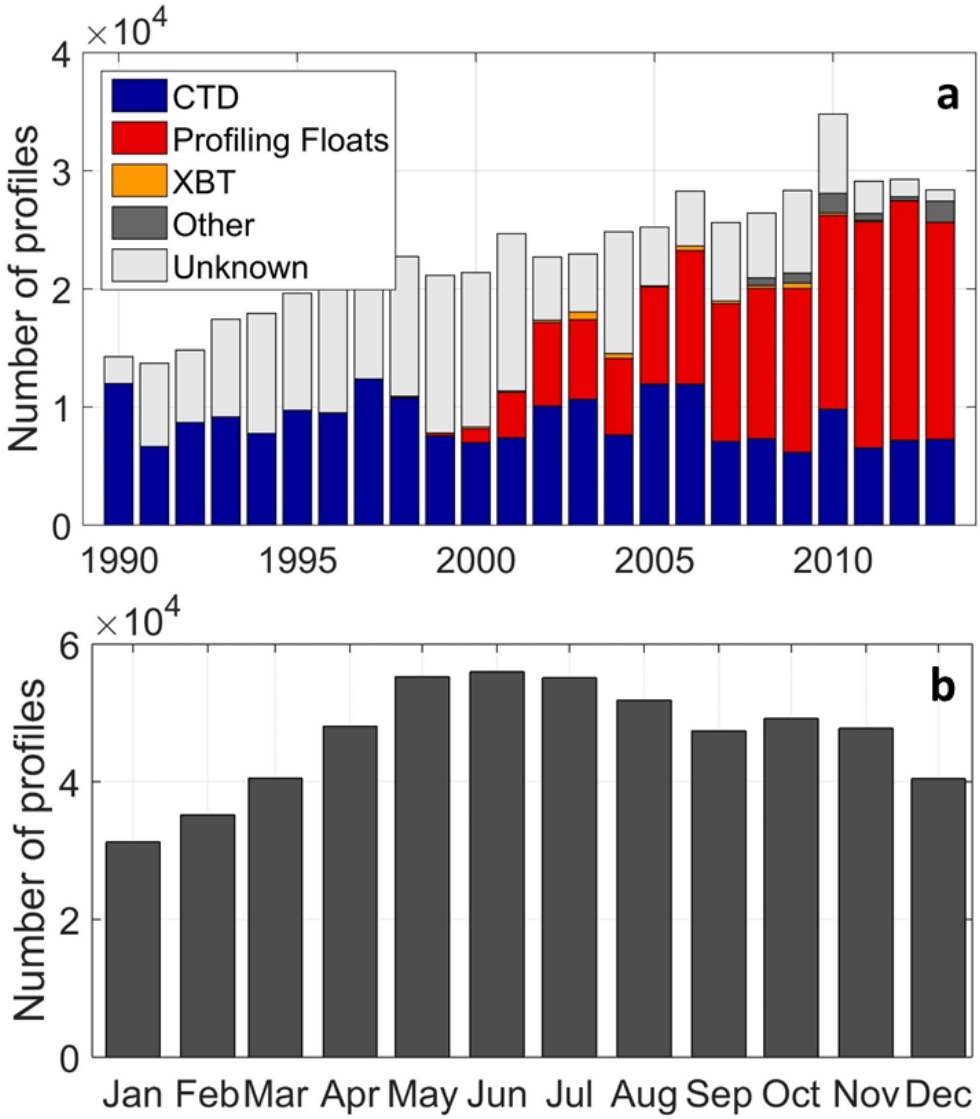


***Figure 3.2:*** *Number of CORA 4.1 salinity profiles by instrument type for the SANA region from 1990 to 2013: Conductivity Temperature Depth probes (CTD; blue), profiling floats (red), Expendable Bathythermographs (XBT; orange), other instruments (e.g., attached to gliders, sea mammals or moorings; dark grey) and unknown instruments (light grey). The information of the instrument type is directly given in the CORA profile data product.*

### 3.1.2 Objectively mapped freshwater inventories of the Arctic Ocean

For the liquid freshwater content of the upper Arctic Ocean I used an update of the observationally based time series by Rabe et al. (2014), calculated from objectively mapped liquid freshwater inventories of the Polar Mixed Layer and the Upper Halocline (between the surface and the lower halocline, represented by the 34 isohaline)

of the deep basins (seafloor depth >500 m, area shown in Fig. 3.5) relative to a reference salinity of 35. The update comprises an extension of the time series to 2013 and was provided by Benjamin Rabe, Alfred Wegener Institute for Polar and Marine Research, Bremerhaven, Germany. The freshwater inventories are calculated from in-situ salinity measurements from CTD devices on various platforms between 1992 and 2013 (calculation described in Chap. 3.3); the data sources used in addition to the ones described in Rabe et al. (2014) and published in Rabe et al. (2014) are listed in Tab. 3.2. The profile positions for 1992 to 2012 are shown in Fig. 3.3 (Rabe et al., 2014). After calculating the liquid freshwater inventories, they were objectively mapped in space and time resulting in a monthly liquid freshwater inventory field on a regular horizontal grid. The objective mapping method is described in detail in the supporting information of Rabe et al. (2014).

***Table 3.2:*** *Data sources for salinity data of the Arctic Ocean. The listed data sources are for the data used in addition to the data described in Rabe et al. (2014) and published in Rabe et al. (2014).*

| Expedition, Project, Institute | Year(s) | Platform | Source URL or contact |
|---|---|---|---|
| Beaufort Gyre Project | 2012-2013 | various ships | http://www.whoi.edu/beaufortgyre/ |
| NPEO | 2012-2014 | Airborne and ice-based | ftp://psc.apl.washington.edu/NPEO Data Archive/NPEO Aerial CTDs/ |
| WHOI | 2012-2014 | ITP | http://www.whoi.edu/itp |
| PS86 | 2014 | RV Polarstern | http://doi.pangaea.de/10.1594/PANGAEA.853768 (Vogt et al., 2015) |
| PS87 | 2014 | RV Polarstern | http://doi.pangaea.de/10.1594/PANGAEA.853770 (Roloff et al., 2015) |

*Abbreviations: ITP – Ice-Tethered Profiler, NPEO – North Pole Environmental Observatory, WHOI – Woods Hole Oceanographic Institution.*

### 3.1.3 Atmospheric forcing data set

The atmospheric data used to force FESOM in the used setup (Chap. 3.2.1) and used for the analysis of the atmospheric freshwater fluxes (Chap. 5) and atmospheric drivers (Chap. 6) is taken from the Common Ocean-ice Reference Experiment version 2 data set (CORE-II; Large and Yeager, 2009). The CORE-II data set contains globally computed air-sea fluxes of momentum, heat and fresh water from 1948 to 2009 on the T62 grid with a zonal resolution of ∼1.875 ° longitude. It is freely

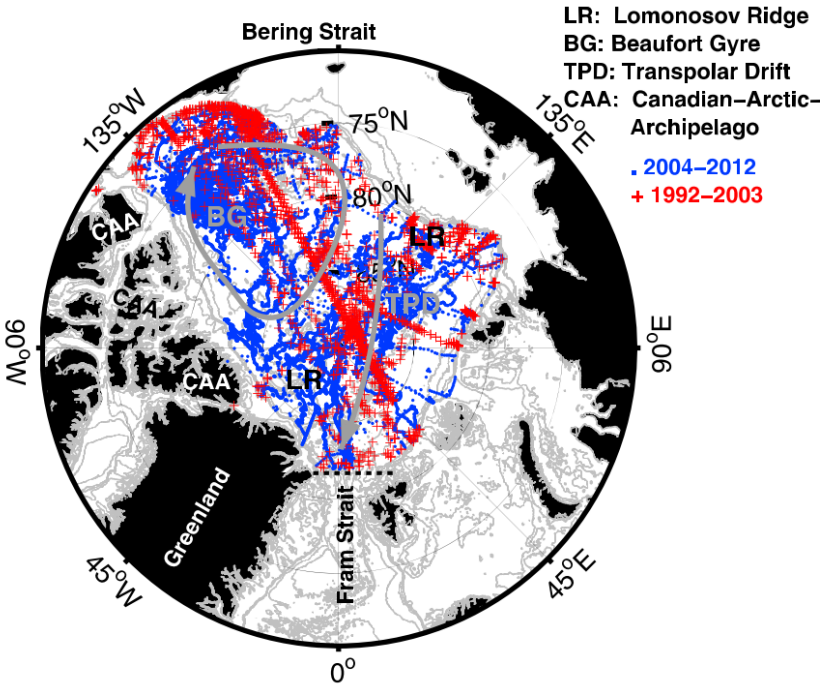


***Figure 3.3:*** *Positions of the salinity profiles used for the Arctic Ocean basin liquid freshwater inventory calculations (figure from Rabe et al., 2014 with permission). Profiles from 1992 to 2003 are indicated by red crosses and profiles from 2004 to 2012 are indicated by blue dots. Abbreviations: BG – Beaufort Gyre, CAA – Canadian Arctic Archipelago, LR – Lomonosov Ridge, TPD – Transpolar Drift.*

available from the Research Data Archive of the National Centers of Atmospheric Research (NCAR) at https://rda.ucar.edu/datasets/ds260.2/. The data set is based on the National Centers for Environmental Prediction (NCEP)/NCAR reanalysis data for the near surface winds, air temperature, specific humidity and density, and based on various satellite data including radiation, sea surface temperature, sea ice concentration and precipitation (Large and Yeager, 2009). These data are adjusted based on comparisons with other satellite and in-situ observations that are more reliable but have a too small coverage in space or in time for the data product itself (Large and Yeager, 2009). The data used for the forcing of FESOM in the used configuration is listed in Tab. 3.3. In addition to these listed atmospheric fields, I use the 6-hourly sea level pressure [Pa] from the CORE-II data set for the analysis of the atmospheric drivers (Chap. 6).

### 3.1.4 Atmospheric reanalysis data set

The NCEP-Department of Energy (DOE) Atmospheric Model Intercomparison Project Reanalysis (NCEP-DOE Reanalysis 2; Kanamitsu et al., 2002) is a follow-

***Table 3.3:*** *CORE-II atmospheric forcing fields used in the FESOM model configuration. Table adapted from Wekerle (2013).*

| variable | unit | resolution in time |
|---|---|---|
| 10 m zonal wind | m/s | 6-hourly |
| 10 m meridional wind | m/s | 6-hourly |
| 10 m air temperature | K | 6-hourly |
| 10 m specific humidity | kg/kg | 6-hourly |
| precipitation | mm/s | monthly |
| downward shortwave radiation | m/s | daily |
| downward longwave radiation | m/s | daily |

on to the NCEP/NCAR Reanalysis project (Kalnay et al., 1996). The NCEP-DOE Reanalysis 2 data comprises global atmospheric fields using a state-of-the-art global data assimilation system and a database as complete as possible (Kalnay et al., 1996). The data are taken from observations from land, ship and aircraft and from satellite retrieval.

The reanalysis data fields are given on the T62 grid (∼1.875 ° longitude zonal resolution) from January 1979 to May 2018 and are provided by the National Ocean and Atmosphere Administration/Earth System Research Laboratory's Physical Science Divison, Boulder, Colorado, USA, from their website at https://www.esrl.noaa.gov/psd/data/gridded/data.ncep.reanalysis2.html (last accessed March 15, 2018).

### 3.1.5 Arctic and North Atlantic Oscillation indices

The Arctic Oscillation (AO) is the leading natural mode of variability in the atmosphere of the middle and high northern latitudes (e.g., Thompson and Wallace, 1998). The AO is characterized by low sea level pressure anomalies over the central Arctic Ocean ("polar vortex") and high sea level pressure anomalies over the mid-latitudes strongly influencing the jet stream (e.g., Talley et al., 2011). The AO index is the amplitude of the dominant empirical orthogonal function of winter sea level pressure north of 20 °N.

The North Atlantic Oscialltion (NAO), which is closely related to the AO, is a natural climate mode of the North Atlantic characterized by a north–south dipole pattern of sea level pressure anomalies (e.g., Talley et al., 2011). One center is located over the subpolar North Atlantic and the other center with the opposite sign in sea level pressure is located over the subtropical North Atlantic. The NAO

is associated with changes in the strength and location of the North Atlantic jet streams (e.g., Talley et al., 2011). Indices of the NAO are either computed from the difference between the Iceland Low and the Azores High or from the leading modes of empirical orthogonal function analysis. The NAO index used in this study is based on the latter approach.

Both indices were provided by the National Ocean and Atmosphere Administration/National Weather Service and are freely available from their website at http://www.cpc.ncep.noaa.gov/data/teledoc/telecontents.shtml.

### 3.1.6 Continental runoff

The river runoff [Sv] used for the freshwater flux analysis and for forcing FESOM in the used configuration is a dataset described by Dai et al. (2009). It consists of monthly streamflow data at the farthest downstream gauge stations of the worlds 925 largest ocean reaching rivers from 1948-2004 (Dai et al., 2009). The assembled gauge data covers approx. 80 % of the global ocean-draining land areas and the time record is fairly complete for most of the large rivers (Dai et al., 2009). Data gaps in the stream flow of single rivers are filled on the basis of known relations of the individual rivers to the precipitation and other atmospheric forcing due to a linear regression analysis using a land surface model (Dai et al., 2009). The dataset is freely available from the Climate Analysis Section from NCARs Climate and Global Dynamics Laboratory at http://www.cgd.ucar.edu/cas/catalog/surface/dai-runoff/ with a resolution of 1 ° latitude and 1 ° longitude or 4 ° latitude and 5 ° longitude.

### 3.1.7 Freshwater flux estimates from the Greenland Ice Sheet and Arctic glaciers and ice caps

The freshwater flux estimates from the Greenland Ice Sheet and Arctic glaciers and ice caps by Bamber et al. (2018) include melt water runoff as well as ice discharge. The runoff is derived from 1958 to 2016 using a regional climate model coupled to a snow diagenesis model. The ice discharge of the Greenland Ice Sheet is estimated from satellite-based measurements. It is the product of surface velocity and ice thickness across the flux gate (Bamber et al., 2018). The surface velocities are based on observational time series for 1958, 1964, 1992-2010 (annual values) and 2000-2016 (sub-annual values). For the time periods when no observations were available a correlation of time-mean runoff and ice discharge is used to estimate the surface velocities (Bamber et al., 2018). The data is provided through the British Oceanographic Data Centre at https://www.bodc.ac.uk/resources/inventories/edmed/report/6778/.

## 3.2 Model and assimilation data

### 3.2.1 The Finite Element Sea ice Ocean Model

For calculating the freshwater fluxes and the simulated freshwater contents I used data from a simulation with the global unstructured-mesh Finite Element Sea ice Ocean Model (FESOM; Danilov et al., 2004) of the Alfred Wegener Institute for Polar and Marine Research in Bremerhaven, Germany. The FESOM ocean general circulation model (Wang et al., 2014) using unstructured triangular meshes in the horizontal and tetrahedra in the vertical (Fig. 3.4a) is coupled to a dynamic-thermodynamic sea ice model operating on the same surface mesh as the ocean model (Timmermann et al., 2009; Danilov et al., 2015). The sea ice model is based on the ice thermodynamics by Parkinson and Washington (1979) and the ice dynamics by Hunke and Dukowicz (2002). Using an unstructured mesh (Fig. 3.4a) to model the ocean allows to resolve small topographic features like narrow straits, islands and steep continental slopes and at the same time keep the overall resolution to an affordable level (Danilov et al., 2004)

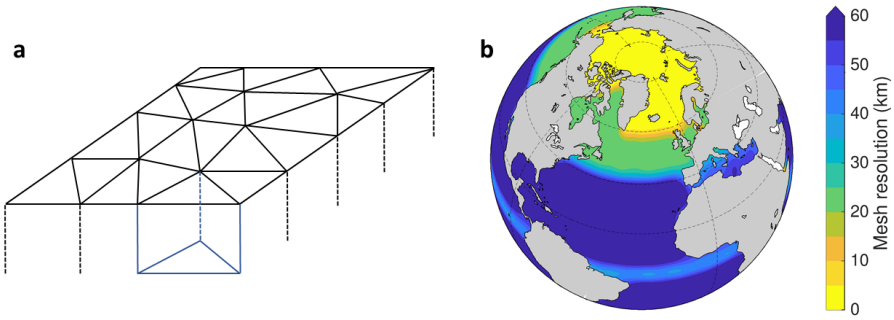


***Figure 3.4:*** *The FESOM mesh: a) schematic of the finite-element mesh, which is triangular at the surface (black lines) and consist of prisms below each triangle (blue lines) which are then divided into three tetrahedra. b) mesh resolution of the used setup.*

The used FESOM setup has an increased horizontal resolution of approximately 5 km in the Arctic Ocean and Nordic Seas and approximately 24 km in the Baffin Bay and subpolar North Atlantic (Wekerle et al., 2017; Fig. 3.4b). The model was forced with the CORE-II data set (Large and Yeager, 2009; Chap. 3.1.3), and interannual monthly mean river runoff is taken from Dai et al. (2009) (Chap. 3.1.6). Since the runoff data set only covers the time period 1948-2004, river runoff from the year 2004 was used for the last five years of the simulation. The model was integrated two times from 1969 to 2009. The first run was initialized with mean temperature and salinity fields from the Polar science center Hydrographic global ocean Climatology version 3 (PHC 3.0; Steele et al., 2001), which is provided by the Polar Science

Center at http://psc.apl.washington.edu. The second run started with the final conditions of the first run. Sea surface salinity restoring to the PHC 3.0 climatology was used. This is necessary in ocean models without a coupled atmospheric model to compensate for the missing ocean-atmosphere feedbacks and prevent local salinity trends e.g., caused by inaccurate precipitation (Wang et al., 2018b). The strength of the restoring (given in piston velocity) is 10 m per 60 days. The surface freshwater fluxes in the model are virtual salt fluxes and have no volume flux.

The studies by Wekerle et al. (2013, 2017) have shown that FESOM in a setup with increased resolution in the high-latitudes is able to simulate the transports through the gateways connecting the Arctic Ocean with the North Atlantic close to observations. Moreover, Wang et al. (2018b) just recently have shown a good representation of the observed Arctic Ocean freshwater content variability with FESOM.

### 3.2.2 The Pan-Arctic Ice Ocean Modeling and Assimilation Product

For the solid freshwater content of the Arctic Ocean I used a sea ice volume time series from Schweiger et al. (2011) from 1979 to 2016 calculated by using the Pan-Arctic Ice Ocean Modeling and Assimilation System (PIOMAS; Zhang and Rothrock, 2003). The time series is freely available through the Polar Science Center at psc.apl.uw.edu. PIOMAS is a global coupled ocean and sea ice model using a generalized orthogonal curvilinear coordinate system and a 12-category thickness and enthalpy distribution sea ice model which explicitly allows simulating sea ice ridging (Zhang and Rothrock, 2003). The sea ice thickness and volume results are validated by comparing with sea ice thickness data from moorings, submarines, satellite measurements and airborne electromagnetic induction measurements. Additionally model sensitivity studies are conducted. From this validation process, the uncertainty in sea ice thickness and volume is estimated (Schweiger et al., 2011), which I used to calculate the uncertainty in solid freshwater content shown in Chap. 4.1.

## 3.3 Equivalent freshwater content calculation

The liquid freshwater content is defined as an equivalent amount of fresh water that is required to dilute water with a reference salinity, $S_{ref}$, to obtain the observed salinity, $S$. The liquid freshwater content $C_{fw,liq}$ of an ocean region with the liquid freshwater inventory $h_{fw}$ between the surface and a depth $h$ is defined by

$$C_{fw,liq} = \int_{A_1}^{A_n} \underbrace{\int_{z=0\ m}^{h} \frac{S_{ref} - S}{S_{ref}}\, dz}_{h_{fw}}\, dA\ [km^3] \tag{3.1}$$

I calculated the liquid freshwater content of the subpolar North Atlantic and the Nordic Seas for the upper 2,000 m, which I expected to cover the part of the water column where the main salinity variations take place. The areas are shown in Fig. 3.5.

I chose a reference salinity $S_{ref} = 35$ (e.g., Rahmstorf, 1996), which is between the two oceanic inflows of the SANA, the salty waters of the North Atlantic Current originating from the tropics/subtropics and the relatively fresh waters of the East Greenland and Labrador Currents from polar origin. Calculations with different reference salinities showed no significant influence on the freshwater content anomalies (Fig. 3.6).

For the liquid freshwater content of the Arctic Ocean I used an update of the observationally based time series by Rabe et al. (2014), which is described in more detail in Chap. 3.1.2. The area used for the calculation is indicated in Fig. 3.5. A reference salinity of 35 was chosen (e.g., Rabe et al., 2011, 2014), which is approximately the salinity of the Atlantic Water inflow to the Arctic Ocean. There are no negative freshwater inventories, as the integration limit is the depth of the 34-isohaline.

For the calculation of the solid freshwater content of the Arctic Ocean I used the sea ice volume time series from Schweiger et al. (2011) from 1979 to 2016 for the entire Arctic Ocean region, obtained from the PIOMAS product (Zhang and Rothrock, 2003), which is described in Chap. 3.2.2. The solid freshwater content is calculated in an analogous way as the liquid freshwater content with the reference salinity 35, an assumed average sea ice salinity of 6 and the sea ice density 910 kg/m$^3$ (same values as used in the FESOM simulation). The uncertainties in the liquid and solid freshwater content of the Arctic Ocean are indicated in Fig. 4.2. I did not calculate the solid freshwater content of the SANA as I assume that the sea ice being transported into the SANA through the Barents Sea Opening, the Fram Strait and the Davis Strait melts before it can leave the SANA.

The simulated freshwater contents are calculated from the FESOM simulation described in Chap. 3.2.1. They are computed from 1979 to 2009 for the same areas and the same way as the observational time series.

Freshwater content and salt content time series have been derived for the subpolar North Atlantic and the Nordic Seas in other studies (Curry and Mauritzen, 2005; Mauritzen et al., 2012), which I use for comparison with my results. They

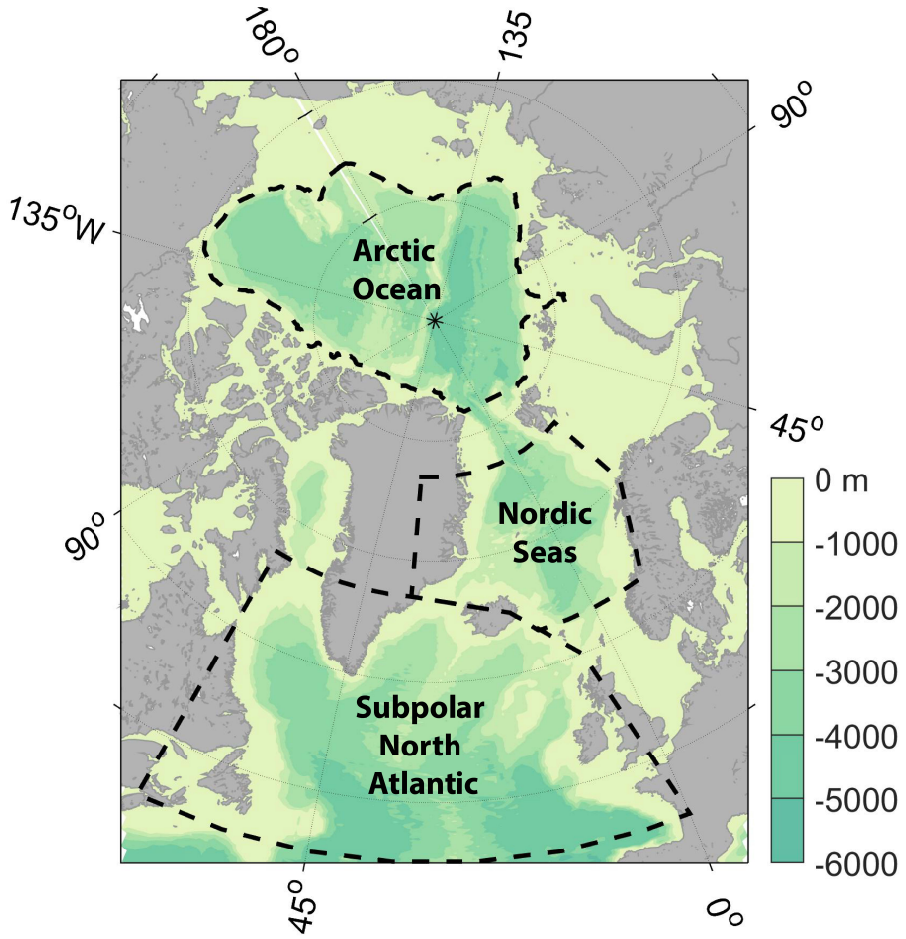


***Figure 3.5:*** *Bottom topography of the research area derived from the ETOPO2 database (2-minute resolution). Dashed black lines indicate the areas that were used to calculate the liquid freshwater content of the Arctic Ocean and the SANA. The gap between the Nordic Seas and the Arctic Ocean results from the lack of data in the CORA salinity fields north of 77 °N.*

have been calculated for longer time periods, but slightly different regions than the SANA defined for this study (Fig. 3.7), and a different set of data sources were used for the analysis. Curry and Mauritzen (2005) calculated pentadal means of liquid freshwater content from 1955 to 2000 for the subpolar North Atlantic and the Nordic Seas from a set of hydrographic data. The data are given in the supplementary information to their study. Mauritzen et al. (2012) presented pentadal means of salt content between 1955 and 2005 for the subpolar North Atlantic, which were calculated from an updated hydrographic data set. The time seris was provided by Arne Melsom, Norwegian Meteorological Institute, Oslo, Norway, and Rowan Sutton, National Center for Atmospheric Science, Reading, UK, after personal communication. I converted the pentadal salt content values of Mauritzen et al. (2012) into the freshwater content estimating the total ocean volume as $11.7 * 10^6\ km^3$

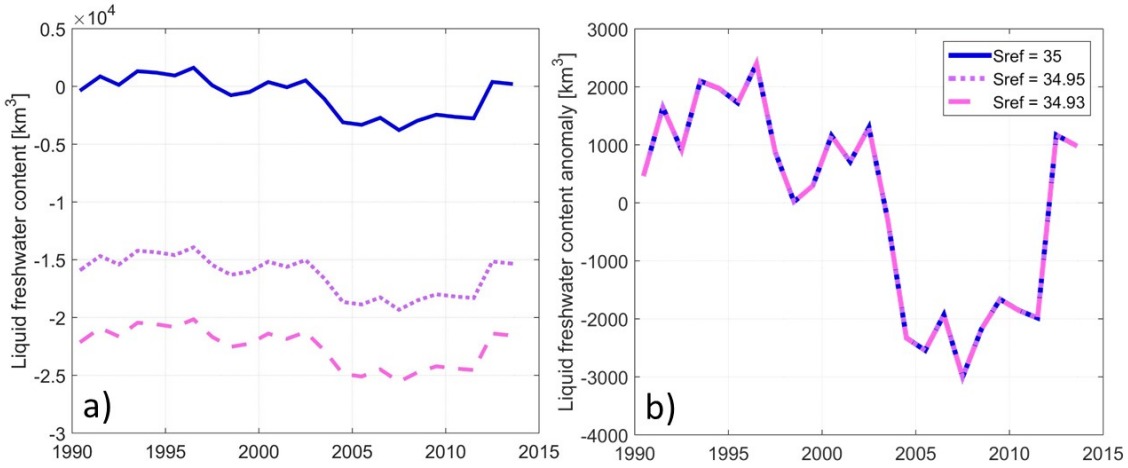


***Figure 3.6:*** *Liquid freshwater content (a) and liquid freshwater content anomaly (b) of the subpolar North Atlantic calculated with different reference salinities: $S_{ref}$ = 35 (blue solid line) according to Rahmstorf (1996), $S_{ref}$ = 34.95 (purple dotted line) according to Jungclaus et al. (2005) and $S_{ref}$ = 34.93 (pink dashed line) according to Aagaard and Carmack (1989).*

(following Curry and Mauritzen, 2005) and using the reference salinity $S_{ref} = 35$.

Comparison with these time series enables me (i) to examine the robustness of my results and (ii) to consider the nature of the changes on longer time scales. The subpolar North Atlantic area of these studies has the same extent to the North but extents less to the South (50 °N instead of 45 °N, Fig. 3.5) and the Nordic Seas area is extended northward to 80 °N (instead of 77 °N, Fig. 3.5). However, the slightly different study areas have only a small effect on the freshwater content (Fig. 3.7).

### 3.3.1 The uncertainty of the freshwater content estimates

The uncertainties of the SANA liquid freshwater content time series are calculated from the uncertainties given by the CORA product (description in Chap. 3.1.1). From the uncertainty of the salinity estimate given by the product $\sigma^2(S_i(z))$ at every grid point $i$ and depth $z$ I calculated the uncertainty of the freshwater content $\sigma^2(C_{fw,liq})$ as follows

$$\sigma^2(C_{fw,liq}) = \int_{A_1}^{A_n} \int_{z=0m}^{h} \frac{\sigma^2(S_i(z))}{S_{ref}} \, dzdA \; [km^3] \tag{3.2}$$

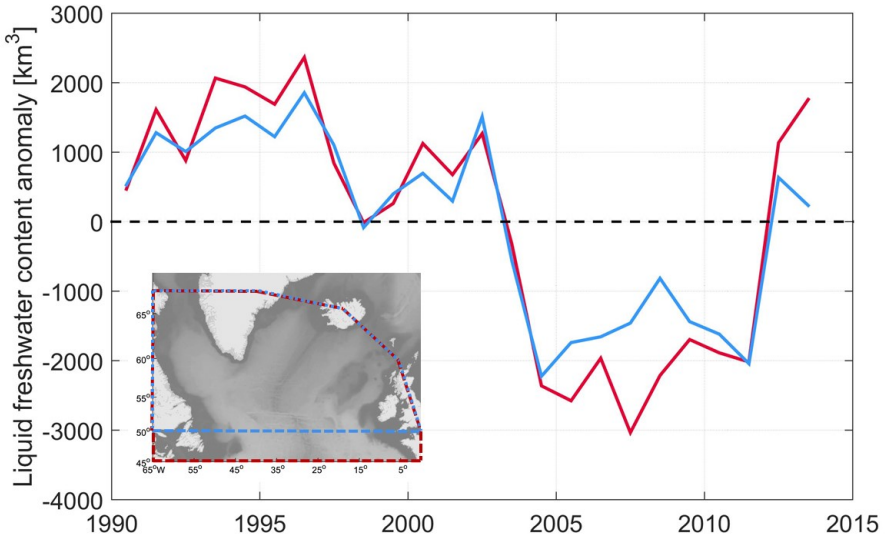


***Figure 3.7:*** *Liquid freshwater content anomaly of the subpolar North Atlantic calculated from CORA 4.0 salinity fields for 45 °N to 67 °N (red, study area of this paper) and for 50 °N to 67 °N (blue, study area of Curry and Mauritzen, 2005; Mauritzen et al., 2012.*

with the depth limit $h$ = 2,000 m and the reference salinity $S_{ref}$ = 35.

This way all uncertainties are summed up, although they might not be independent from each other. Thus the resulting uncertainty in the liquid freshwater content is the maximum uncertainty and is most probably overestimated.

The monthly uncertainties of the upper Arctic Ocean liquid freshwater content time series were calculated as the sum of the statistical mapping errors at each horizontal grid point, which were derived using typical spatial, potential vorticity decorrelation and time scales for the Arctic (Rabe et al., 2014, 2011). For the annual mean upper Arctic Ocean liquid freshwater content I plotted the annual means of monthly uncertainties (Fig. 4.2).

For the sea ice volume time series from the PIOMAS product, the uncertainty comes from various validation steps through comparison with observational ice thickness estimates and model sensitivity studies, which are described in more detail in Schweiger et al. (2011).

## 3.4 Conservation of fresh water in the model

Due to conservation, the simulated freshwater storage $dC_{fw}/dt$ needs to equal the sum of all freshwater fluxes in the model. These are river runoff $R$, precipitation $P$, evaporation $E$, oceanic advective transport $T_{fw}$, eddy diffusion $D_{eddy}$, numerical diffusion $D_{num}$ and surface salinity restoring $S_{rest}$:

$$\frac{dC_{fw}}{dt} = R + P - E + T_{fw} + D_{eddy} + D_{num} + S_{rest} \tag{3.3}$$

In the Arctic Ocean I consider both, the solid and liquid freshwater content, together and therefore do not need to quantify the freshwater flux between the sea ice and the ocean (sea ice melt and formation). In the SANA, however, I only consider the liquid freshwater content as I assume that the sea ice coming from the Arctic Ocean will melt before it can leave the SANA. Therefore I calculated the difference of the net solid freshwater transport (calculation see Chap. 3.5) and the net sea ice melt (sea ice melt minus sea ice formation) of the SANA region to get the freshwater flux from the net melt of sea ice that has not been advected from the Arctic Ocean (referred to as local sea ice melt in the following). For the SANA, this term needs to be added to Eq. 3.3.

The calculation of the freshwater transports is described in the following section. The surface fluxes (river runoff, net precipitation and damping) are virtual salt fluxes, meaning that they numerically change the ocean surface salinity without adding volume to the ocean. The eddy diffusion term was not available for the model run I used in this study and I expect the numerical diffusion to be irrelevant for the large freshwater budget I am analysing. That is why I only analysed the surface freshwater fluxes and the oceanic transport from the mean flow advection.

For the Arctic Ocean, the oceanic transport $T_{fw,AO}$ includes the freshwater transports (liquid + solid) through the Bering Strait $T_{fw,Beri}$, the CAA $T_{fw,CAA}$, the Fram Strait $T_{fw,Fram}$, and the Barents Sea Opening $T_{fw,BSO}$ (Fig. 3.8):

$$T_{fw,AO} = T_{fw,Beri} + T_{fw,CAA} + T_{fw,Fram} + T_{fw,BSO} \tag{3.4}$$

For the SANA, the oceanic transport $T_{fw,SANA}$ includes the freshwater transports (liquid + solid) through the Hudson Strait $T_{fw,Huds}$, the Davis Strait $T_{fw,Davi}$, the Fram Strait $T_{fw,Fram}$, the Barents Sea Opening $T_{fw,BSO}$, the gateways to the North Sea $T_{fw,NS}$, and across 45 °N $T_{fw,45N}$ (Fig. 3.8):

$$T_{fw,SANA} = T_{fw,Huds} + T_{fw,Davi} + T_{fw,Fram} + T_{fw,BSO} + T_{fw,NS} + T_{fw,45N} \tag{3.5}$$

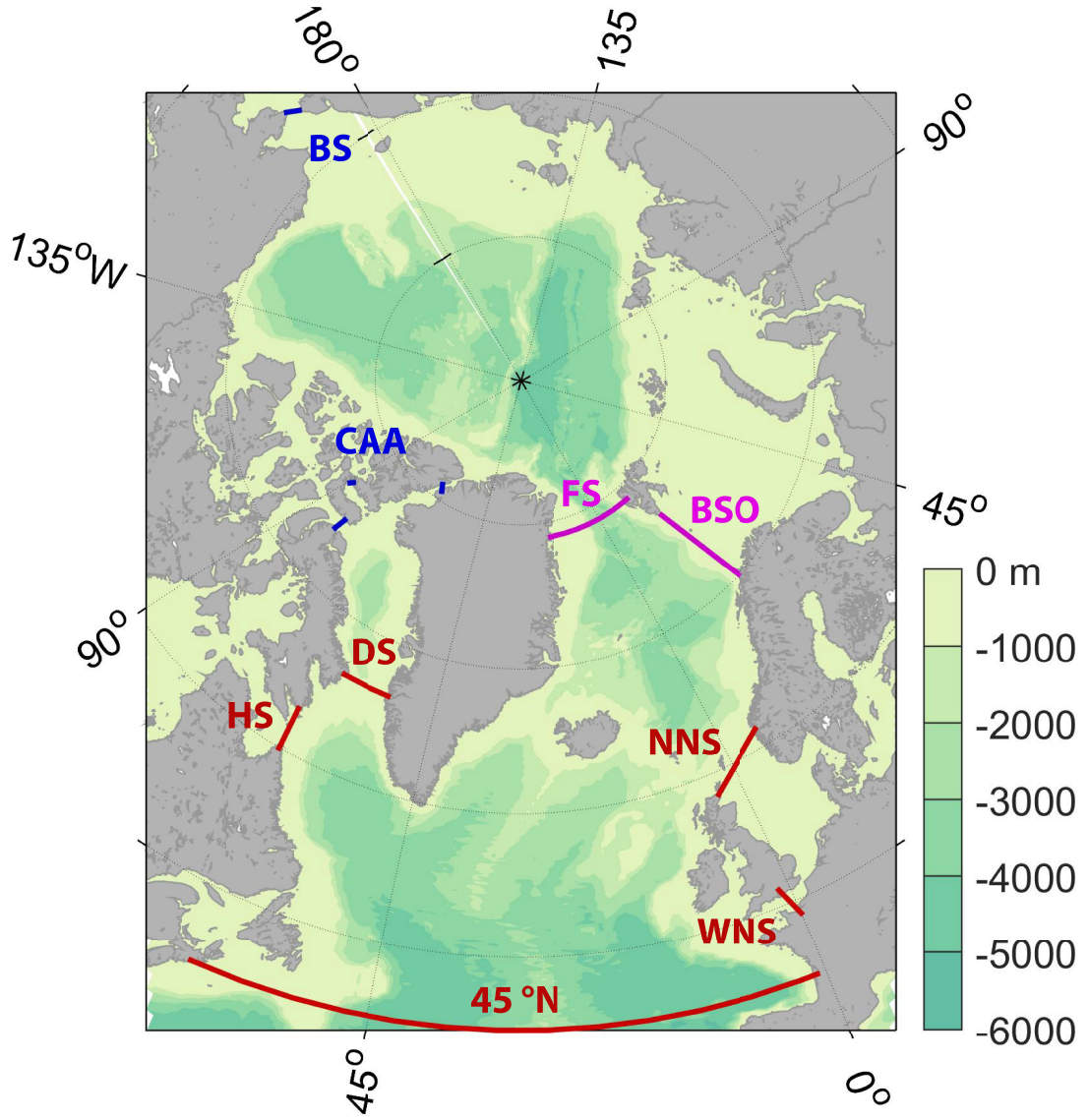


***Figure 3.8:*** *Geographic map of the Arctic Ocean and SANA showing the section positions used for the oceanic transport calculations: for the Arctic Ocean (blue), for the SANA (red) and for both (magenta). Bottom topography derived from the ETOPO2 database (2-minute resolution). BS: Bering Strait, BSO: Barents Sea Opening, CAA: Canadian Arctic Archipelago, DS: Davis Strait, FS: Fram Strait, HS: Hudson Strait, NNS: northern North Sea, WNS: western North Sea.*

## 3.5 Calculation of equivalent freshwater transport

By freshwater transport I understand (similar to the freshwater content) an equivalent amount of fresh water that is required to dilute the transported water with a reference salinity, $S_{ref}$, to obtain the observed salinity, $S$. The simulated liquid

freshwater transport is calculated by

$$T_{fw,liq} = \int_{x_1}^{x_n} \int_{z=0m}^{h} v_\perp \frac{S_{ref} - S}{S_{ref}} \, dzdx \; [m^3/s] \tag{3.6}$$

where $v_\perp$ is the velocity perpendicular to the cross-section, $h$ is the integration depth and $x_1$ and $x_n$ are the start and the end point of the section, respectively. The solid freshwater transport, meaning the advection of sea ice and snow across a transect, is computed in an analogous way with a salinity of 6 for sea ice and 0 for snow, as well as a density of 910 $kg/m^3$ for sea ice and 290 $kg/m^3$ for snow (same values as used in the FESOM simulation). The sections are shown in Fig. 3.8.

To calculate the transport across the sections, the velocity and salinity data need to be interpolated from the unstructured model mesh onto the sections. This may cause interpolation errors (Sidorenko et al., 2009).

Following Jahn et al. (2010a), the liquid freshwater transport can be divided in four different components using the time-mean ($\langle f \rangle$ and $\langle v_\perp \rangle$) and time-varying ($f^{'}$ and $v_\perp^{'}$) parts of the velocity $v_\perp$ and the freshwater fraction $f = (S_{ref} - S)/S_{ref}$. The overbar denotes spatial integrals:

(i) the mean freshwater flux $\overline{\langle f \rangle \langle v_\perp \rangle}$,

(ii) the freshwater flux due to the advection of water with the mean salinity by the volume flux anomaly (volume-driven) $\overline{\langle f \rangle v_\perp^{'}}$,

(iii) the freshwater flux due to the advection of salinity anomalies by the mean flow (salinity-driven) $\overline{f^{'} \langle v_\perp \rangle}$ and

(iv) the freshwater flux due to the advection of salinity anomalies by an anomalous volume flow (non-linear) $\overline{f^{'} v_\perp^{'}}$.

These components indicate which part of the freshwater transport variability through the different gateways is due to volume transport variations (volume-driven), which part is due to variations in the salinity of the transported waters (salinity driven) and which part is due to both, variations in the volume transport and related variations in the salinity (non-linear).

In Chap. 5 I also show cumulative freshwater transport anomalies to illustrate the effect of the freshwater transport on the freshwater content. The cumulative freshwater transport anomaly is calculated by

$$Y(x) = \int_{t=0}^{x} T_{fw}(t) - \overline{T_{fw}} \, dt \tag{3.7}$$

where $T_{fw}(t) - \overline{T_{fw}}$ is the freshwater transport anomaly at the time $t$.

The cumulative oscillation indices shown in Chap. 6 are calculated in an analogous way.

### 3.5.1 Choice of the reference salinity and integration depth

Similar to the freshwater content anomaly, the net freshwater transport across all boundaries of a defined region is not significantly affected by different choices of the reference salinity (Fig. 3.9 and Tsubouchi et al., 2012). However, the freshwater transports through the single gateways are sensitive to the choice of the reference salinity, although the differences are rather small when comparing reference salinities that are usually chosen for the Arctic Ocean and SANA region (Fig. 3.10). So one should carefully think about an appropriate reference salinity to address the research question and keep this in mind when interpreting the resulting freshwater transports.

There are mainly three different concepts for the choice of the reference salinity:

1. The most common concept is to choose the mean salinity of the region of interest to distinguish between freshwater sources and sinks for this region. Many studies use estimates of the mean ocean salinity assuming that it is approximately constant over time. Commonly used estimates are $S = 34.8$ (e.g., Aagaard and Carmack, 1989; Serreze et al., 2006; Haine et al., 2015)for the Arctic Ocean and $S = 34.93$ (e.g., Aagaard and Carmack, 1989), $S = 34.95$ (e.g., Jungclaus et al., 2005) or $S = 35$ (e.g., Rahmstorf, 1996) for the subpolar North Atlantic.

2. An alternative concept is to choose the salinity of the salt source of the ocean region and thereby define all other inputs as freshwater sources and all outputs as freshwater sinks. In the Arctic Ocean the salt source is the Atlantic Water import through Fram Strait and the Barents Sea with an estimated salinity of $S = 35$ (e.g., Köberle and Gerdes, 2006; Rabe et al., 2011, 2014). In the subpolar North Atlantic it would be the waters of tropical/subtropical origin carried by the North Atlantic Current.

3. Another approach is to use the mean salinity of the boundary of the research area. This could be all gateways of a certain ocean basin (e.g., Tsubouchi et al., 2012; Bacon et al., 2015), but also much smaller, the boundary of a single eddy (e.g., Müller et al., 2017). When investigating only parts of the water column, the boundary could be the isobar, isotherm, isopycnal or isohaline defining the investigated layer.

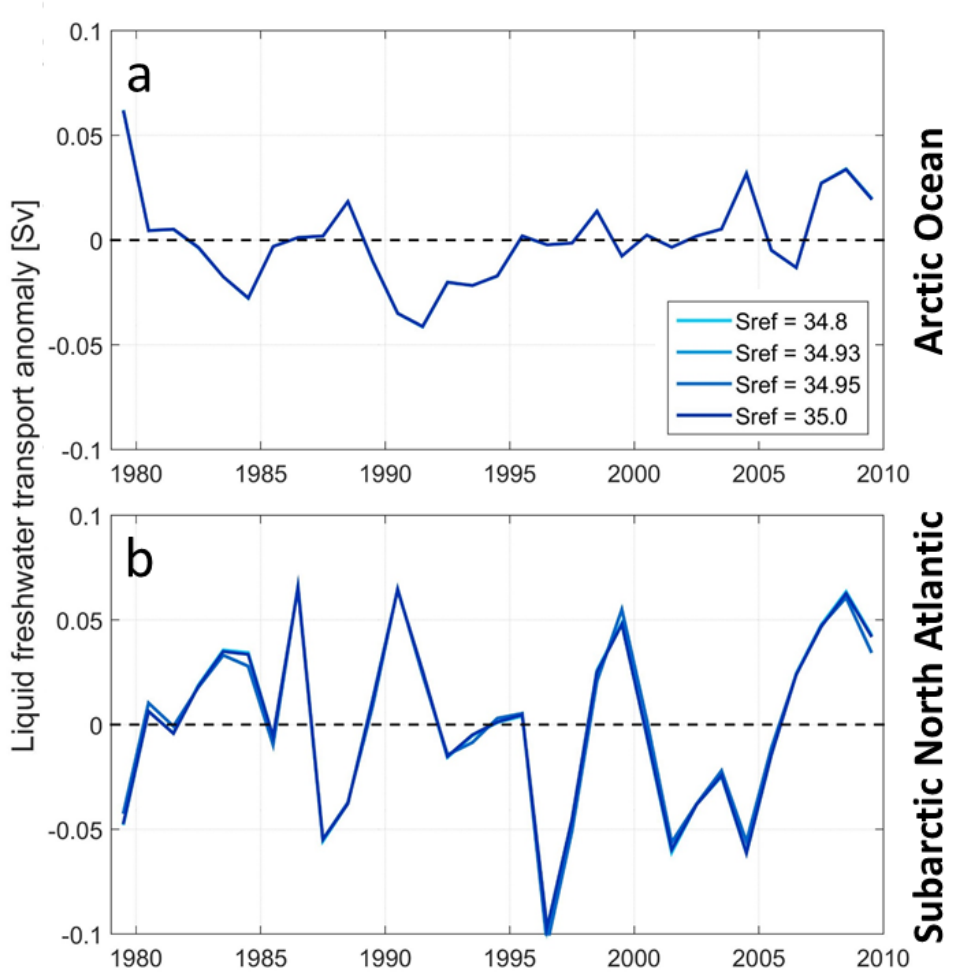


***Figure 3.9:*** *Simulated (FESOM) net liquid freshwater content anomaly of the Arctic Ocean (a) and SANA (b) for different reference salinities (full water column). Positive values indicate a net freshwater input to the region.*

Using a simple box model I found that choosing the mean salinity of the investigated region represents best the relative influence of each transport component on the salt/freshwater content of that region (full description in the appendix). As the mean salinity of the Arctic Ocean and the SANA is not constant (Fig. 3.11), I used the time-varying mean salinity as the reference salinity for the freshwater transport calculations for the entire Arctic Ocean and SANA.

The comparison of the simulated freshwater content for the upper 2,000 m of the SANA and the freshwater content of the full water column shows that the main variability occurs in the upper 2,000 m (Fig. 4.11). As it is difficult to quantify the portion of the waters being transported into the SANA, that stays within the upper 2,000 m of the basins, I decided to use the simulated mean top to bottom salinity for each month (Fig. 3.11) as a reference salinity and the bottom as the integration

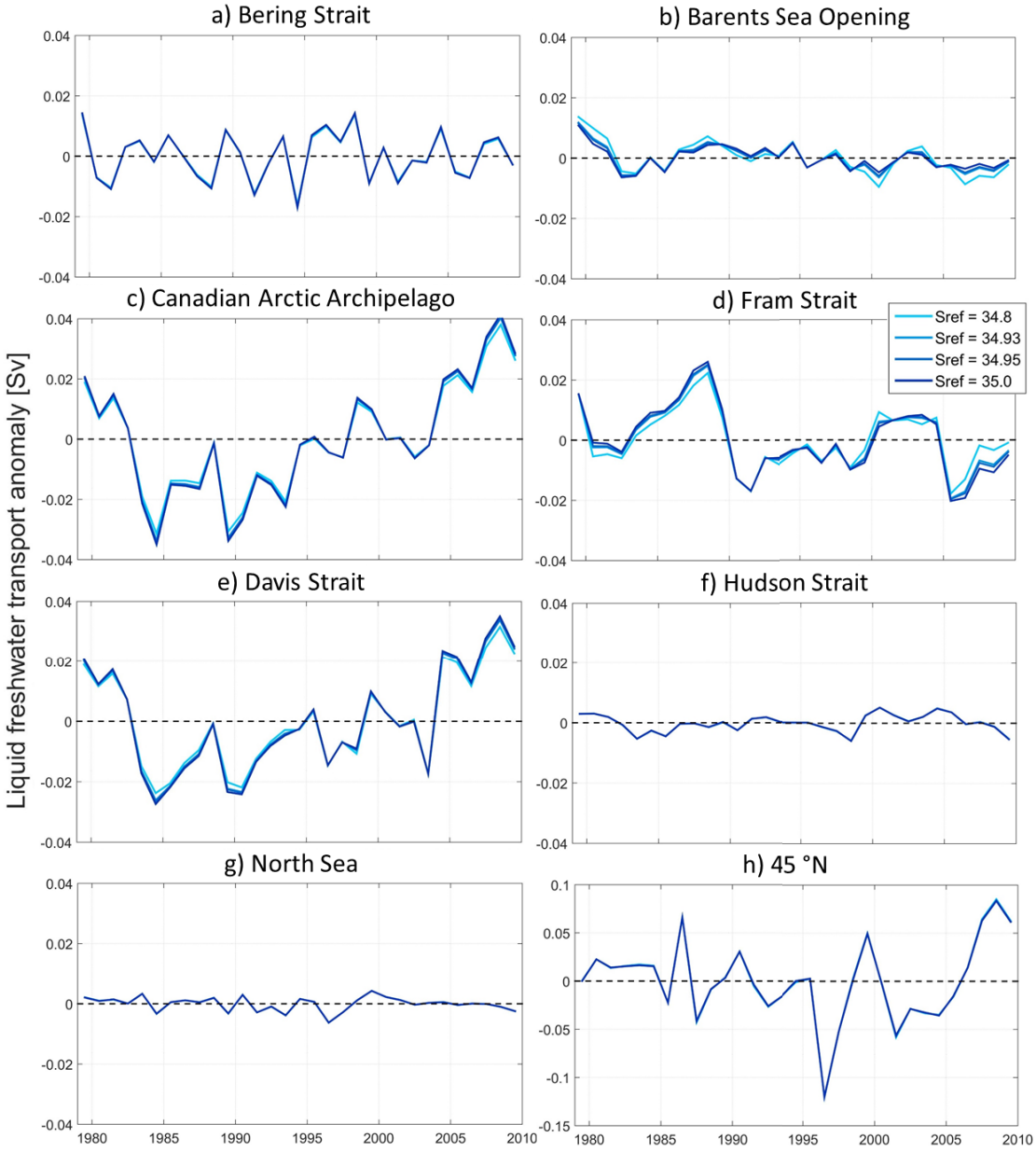


***Figure 3.10:*** *Simulated (FESOM) net liquid freshwater transport anomalies through the Bering Strait (a), the Barents Sea Opening (b), the CAA (c), the Fram Strait (d), the Davis Strait (e), the Hudson Strait (f), the North Sea openings (g), and across 45 °N (h) with different reference salinities. Positive values indicate an increased net northward/eastward freshwater transport (a, b, f, g) or a decreased net southward/westward freshwater transport (c, d, e, h). Please note that the transport across 45 °N has a different y-axis.*

depth for the transport calculation.

For the Arctic Ocean I differentiate between the freshwater fluxes of the "entire Arctic Ocean" and of the "upper Arctic Ocean" (above the 34-isohaline). To describe the freshwater fluxes for the entire Arctic Ocean, I used the same concept as for the SANA and calculated the transports from the surface to the bottom and relative to the simulated monthly mean top to bottom Arctic Ocean salinity.

For the upper Arctic Ocean the freshwater content anomalies are almost the same for the region covering only the deep basins and for the region including also the shelves (Fig. 4.4). Therefore I can use the same sections for the transport calculations and the same area for the surface fluxes as for the entire Arctic Ocean, to describe the freshwater content variability of the upper Arctic Ocean. However, for the freshwater transport calculation I used the concept of the boundary salinity (3rd concept) and choose 34 as the reference salinity as well as the 34-isohaline as the integration depth. Freshwater fluxes from river runoff, net precipitation or the surface salinity restoring (damping) are added/removed at the surface and the calculated transports only account for the advection within the investigated layer. But there will also be processes like entrainment, convection or salt intrusion from sea ice formation, that lead to an exchange of salt between the layer above the 34-isohaline and the saltier waters (S>34) of the adjacent layer. In the following I will refer to the freshwater flux associated with these processes by calling it the "entrainment term", although there might be more processes involved than only entrainment. To quantify the entrainment term $M$, I calculated the difference between the liquid freshwater storage of the entire upper Arctic Ocean (basins + shelves, surface to 34-isohaline) $dC_{fw,liq}/dt$ and the net liquid freshwater flux from river runoff $R$, net precipitation $P - E$, net local sea ice melt $I$, damping $S_{rest}$ and liquid freshwater transport above the 34-isohaline $T_{fw,liq}$:

$$M = \frac{dC_{fw,liq}}{dt} - R - P + E - I - S_{rest} - T_{fw,liq} \tag{3.8}$$

This way, however, the entrainment term does not only combine the freshwater fluxes associated with the above mentioned processes, but also includes the diffusive fluxes and the interpolation errors.

## 3.6 Effective salinity of transported waters

When calculating the mean salinity across a section, the parts of the section where the volume transport is low or zero are equally weighted as the parts with higher volume transport. For a better estimate of the salinity of the transported waters I

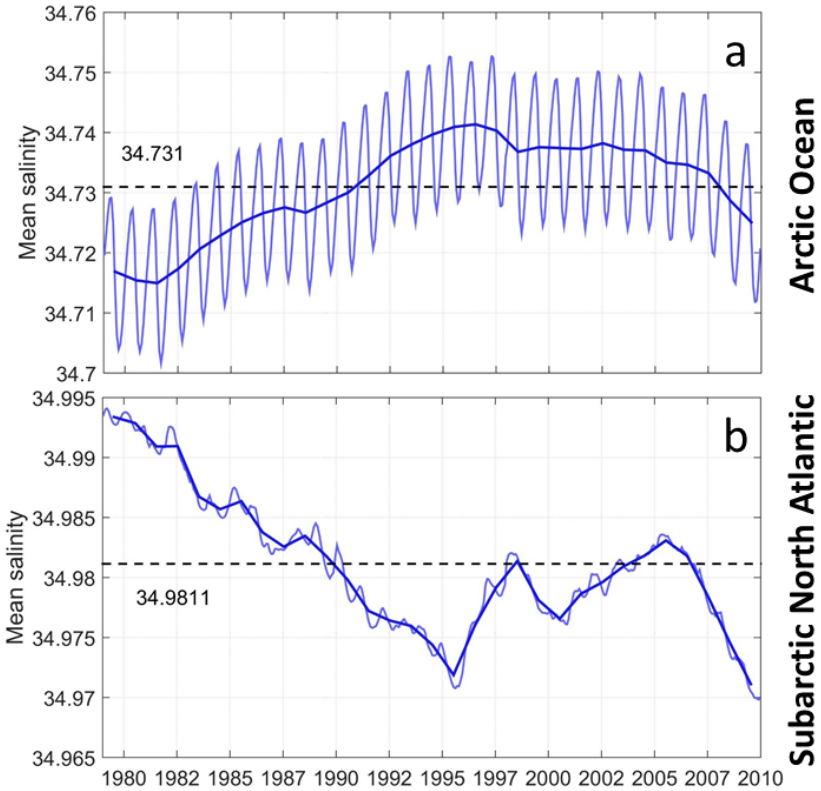


***Figure 3.11:*** *Simulated (FESOM) mean top to bottom salinity of the entire Arctic Ocean (a) and the SANA (b): monthly means (lighter blue) and annual means (darker blue). The dashed black lines indicate the time-mean salinity.*

therefore calculated the effective salinity $S_{eff}$ from the salinity $S$ and the velocity perpendicular to the cross-section $v_\perp$ by

$$S_{eff} = \frac{\int_{x_1}^{x_n} \int_{z=0m}^{h} S v_\perp \, dz dx}{\int_{x_1}^{x_n} \int_{z=0m}^{h} v_\perp \, dz dx} \tag{3.9}$$

This way not only salinity changes across the section are displayed but also changes in the volume transport in different locations of the section. Taking the Arctic outflow through Fram Strait as an example, the effective salinity will decrease when there is a stronger transport in the upper fresh surface layer although the mean salinity across the strait might not change.

## 3.7 Time series analysis

For this study, I mainly analysed time series of freshwater contents, freshwater fluxes and atmospheric conditions. Therefore I calculated standard deviations and stan-

dard errors (Chap. 3.7.1), percentage variances (Chap. 3.7.2) and correlations and regressions (Chap. 3.7.3). These calculations are described in the following.

### 3.7.1 Standard deviation and standard error of the mean

To quantify the variations or dispersion of data points in a time series, the standard deviation is calculated by

$$\sigma = \sqrt{\frac{\Sigma_{i=1}^{n}(x_i - \overline{x})^2}{n-1}} \tag{3.10}$$

with the data $x$ at each point $i$ and the number of data points $n$.

For estimating the robustness of a time series mean, I calculated the standard error of the mean by

$$\sigma_M = \frac{\sigma}{\sqrt{N^*}} \tag{3.11}$$

with the the effective degrees of freedom $N^*$ (see Chap. 3.7.3).

### 3.7.2 Percentage variance

The percentage variance $P_V$, used to quantify the proportion of variance of the time series $A$ that is explained by the variance of time series $B$, is calculated by

$$P_V = 1 - \frac{\sigma^2(B-A)}{\sigma^2(A)} \tag{3.12}$$

### 3.7.3 Cross-correlation and regression analysis

To identify spatial patterns in freshwater inventories, sea level pressure, wind stress, sea surface height and upper ocean circulation that are associated with transport changes or variations in the freshwater content, I performed cross-correlation and regression analyses. For the cross-correlation maps I calculated the correlation of a time series (e.g., freshwater transport) and the temporal variations at each grid point of a field (e.g., sea level pressure). The correlation coefficient $r$ of the time series $x$ and $y$ with $n$ data points is defined by

$$r = \frac{\Sigma_{i=1}^{n} x_i\, y_i - n\,\bar{x}\,\bar{y}}{\sqrt{(\Sigma_{i=1}^{n} x_i^2 - n\,\bar{x}^2)(\Sigma_{i=1}^{n} y_i^2 - n\,\bar{y}^2)}}\,,\ -1 <= r <= 1 \tag{3.13}$$

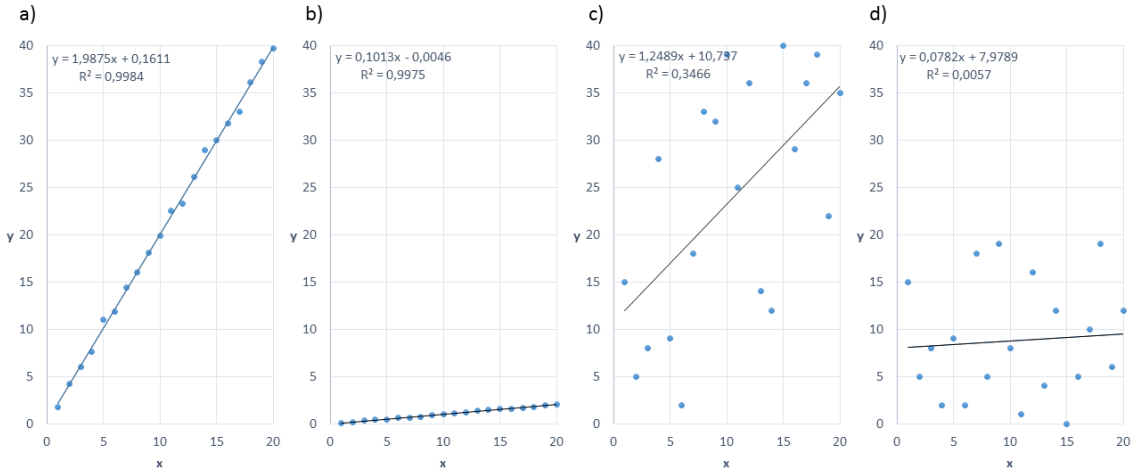


***Figure 3.12:*** *Examples for linear regressions and cross-correlations of two time series (x, y): a) high correlation and high regression, b) high correlation and low regression, c) low correlation and high regression, and d) low correlation and low regression.*

The regression analysis is based on a linear fit of the two variables, the so-called regression line $y = a\,x + b$, where the slope $a$ (also called regression coefficient) and the axis intercept $b$ are calculated by

$$a = \frac{n * \Sigma_{i=1}^{n} x_i\, y_i - (\Sigma_{i=1}^{n} x_i) * (\Sigma_{i=1}^{n} y_i)}{n * \Sigma_{i=1}^{n} x_i^2 - (\Sigma_{i=1}^{n} x_i)^2} \tag{3.14}$$

$$b = \frac{(\Sigma_{i=1}^{n} x_i^2) * (\Sigma_{i=1}^{n} y_i) - (\Sigma_{i=1}^{n} x_i) * (\Sigma_{i=1}^{n} x_i\, y_i)}{n * \Sigma_{i=1}^{n} x_i^2 - (\Sigma_{i=1}^{n} x_i)^2} \tag{3.15}$$

A high regression coefficient ($a > 1$) indicates that small changes in $x$ are related to larger changes in $y$. However, a high regression coefficient (Fig. 3.12a, c) does not always coincides with a significant correlation (Fig. 3.12c). The other way around, highly correlated time series (Fig. 3.12a, b) can also have a rather small regression coefficient (Fig. 3.12b). Therefore I considered both, the regression coefficient and the correlation coefficient, together to investigate the statistical relationship of two time series.

For the vector fields (wind stress, ocean velocity and ice velocity) I calculated the correlation and regression coefficients separately for the zonal and meridional components and plotted the arrows from these zonal and meridional coefficients.

### Effective degrees of freedom and significance of time series correlations

To determine the significance of the calculated correlation values, I calculated the effective degrees of freedom of the correlated time series. Following Talley et al. (2011) the effective degrees of freedom ($N^*$), meaning the number of independent samples, for a time series cross-correlation can be calculated by dividing the total length of the time series by the integral timescale, which is defined as the time integral of the autocorrelation. I estimated the integral timescale by the first zero crossing of the auto-correlation as described by Talley et al. (2011). The correlation is statistically significant if the $p$-value, which is calculated from the effective degrees of freedom and the correlation coefficient $r$, is smaller than 0.1 (90 % confidence level), smaller than 0.05 (95 % confidence level) or even smaller than 0.01 (99 % confidence level).

# Chapter 4

# Freshwater content variability

*This chapter deals with the freshwater content variability of the Arctic Ocean, Nordic Seas and subpolar North Atlantic. It starts with a short review of observed freshwater changes in these regions and the introduction of the related research questions. In the following the freshwater content variability of both regions is described separately using observational and model data, which are described in the former chapter. Finally, the freshwater content variability of the Arctic Ocean and the SANA are compared to investigate possible links. The results are discussed at the end of each section by answering the introduced research questions. Paragraphs which partly contain text by Campos and Horn (2018) are marked with an asterisk (*).*

---

A rapid increase in liquid freshwater content has been observed in the upper layers of the Arctic Ocean in the past two decades (McPhee et al., 2009; Rabe et al., 2011, 2014; Giles et al., 2012; Morison et al., 2012). At the same time a significant part of Arctic sea ice volume has been lost to melt (Lindsay and Schweiger, 2015). In contrast to the Arctic Ocean, the subpolar North Atlantic and the Nordic Seas have become more saline in recent years (Curry and Mauritzen, 2005; Boyer et al., 2007; Holliday et al., 2008; Mauritzen et al., 2012). As pointed out before, both regions are sensitive to freshwater changes with potential impact on our climate.

Therefore I adress the following questions:

- Is the increase in the liquid freshwater content of the Arctic Ocean due to the anomalous amount of net sea ice melt?
- Did the freshwater content changes take place all over the Arctic Ocean or only in parts of it?
- Where (horizontally and vertically) did the liquid freshwater content of the subpolar North Atlantic and the Nordic Seas vary the most?

- How do the freshwater content anomalies of the Arctic Ocean, the subpolar North Atlantic and the Nordic Seas compare?

To answer these questions I calculated the liquid freshwater contents (see Chap. 3.3) of the subpolar North Atlantic and the Nordic Seas from CORA salinity fields (see Chap. 3.1.1). For the upper Arctic Ocean (surface to 34-isohaline) I used an update of the objectively mapped liquid freshwater inventories of Rabe et al. (2014) (see Chap. 3.1.2) and the sea ice volume estimates from Schweiger et al. (2011), which are based on the PIOMAS assimilation product (see Chap. 3.2.2). The areas used for the liquid freshwater content calculations are shown in Fig. 3.5. For comparison with longer time series, I used the time series of pentadal freshwater content values of the subpolar North Atlantic and the Nordic Seas from Curry and Mauritzen (2005) as well as the pentadal salt content values of the subpolar North Atlantic from Mauritzen et al. (2012) (see Chap. 3.3).

## 4.1 The liquid and solid freshwater content of the upper Arctic Ocean

The liquid freshwater content of the upper Arctic Ocean has significantly increased since the 1990s, especially between 2003 and 2005 (Fig. 4.1a). The average freshwater content (relative to the reference salinity $S_{ref} = 35$) in the period 1992-2003 was about 38,800 km$^3$ and increased to an average of 46,700 km$^3$ in the period 2005-2013. The difference between the maximum and minimum annual mean liquid freshwater content is about 10,000 km$^3$ (Fig. 4.2).

Since 1979 about 50 % of the Arctic sea ice volume was lost to melt (Fig. 4.1b). The solid freshwater content of the Arctic Ocean was almost 20,000 km$^3$ in 1979 and constantly decreased to about 10,000 km$^3$ in 2016. Calculating the linear trend reveals a loss of fresh water stored in sea ice of about 230 km$^3$/yr.

Comparing the anomalies between 1992 and 2013 (Fig. 4.2) reveals, that the liquid freshwater content increase ($\sim$10,000 km$^3$) exceeded the decrease in solid freshwater content ($\sim$7,000 km$^3$). However, the uncertainties in the liquid freshwater content estimates are relatively high compared to the uncertainties in the solid freshwater content due to rare profile data in the Arctic Ocean and the different approach of calculating the uncertainty (see Chap. 3.3.1).

The sum of the liquid and solid freshwater content gives the total freshwater content (Fig. 4.3). In the following I will call the combination of the two time series displayed in Fig. 4.1 "observed" total freshwater content, although the solid freshwater content is derived from an assimilation product.

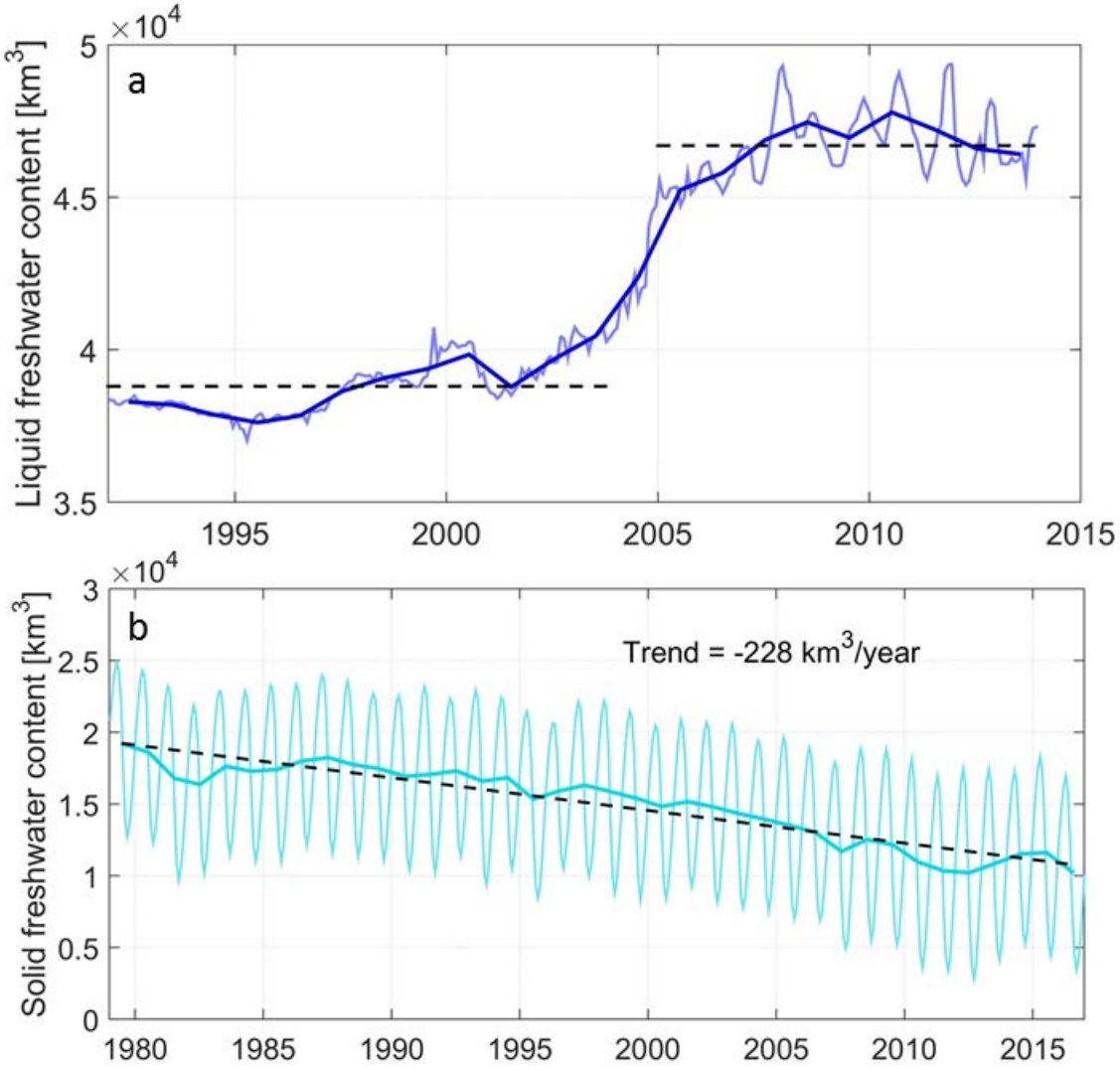


***Figure 4.1:*** *Monthly and annual means of the upper Arctic Ocean (surface to 34-isohaline) liquid freshwater content from observations (a; update of the time series in Rabe et al. (2014)) and solid freshwater content from the PIOMAS assimilation product (b; Schweiger et al., 2011). The two dashed lines in (a) indicate the mean for the periods 1992-2003 and 2005-2013. The dashed line in (b) indicates the linear trend from 1979 to 2016. The freshwater content values were calculated with the reference salinity* $S_{ref} = 35$.

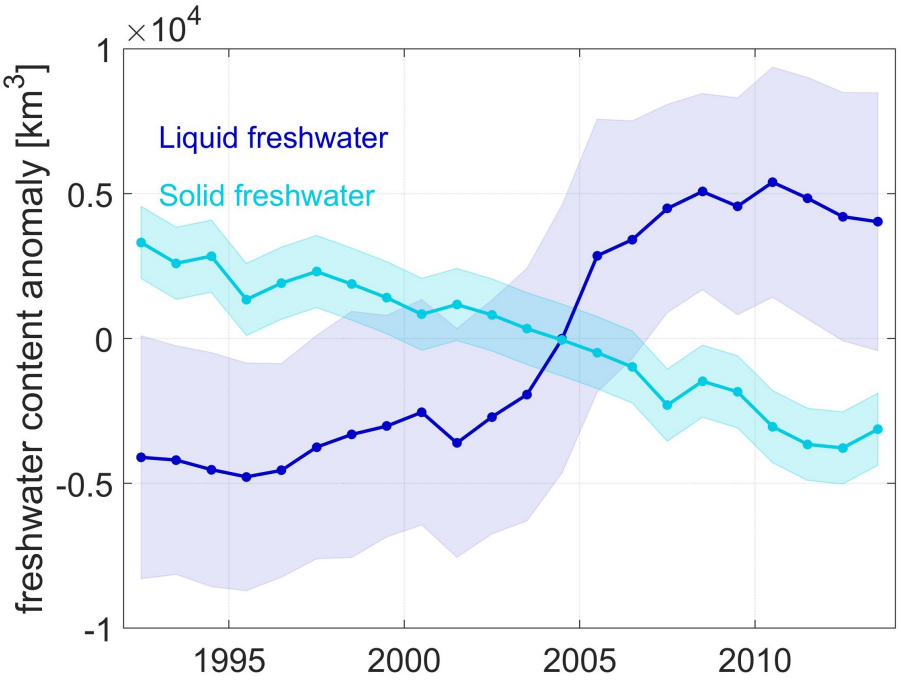


***Figure 4.2:*** *Anomalies of the annual mean liquid (blue) and solid (turquoise) freshwater content of the upper Arctic Ocean (surface to 34-isohaline) from 1992 to 2013. The shadings indicate the annual means of monthly uncertainties. The freshwater content values were calculated with the reference salinity* $S_{ref} = 35$.

The observed total freshwater content of the Arctic Ocean between 1992 and 2013 suggests an alternation between high and low phases (Fig. 4.3) rather than an increase seen in liquid freshwater content only (Fig. 4.1a). The observed total freshwater content is relatively low between 1992 and 2003 with a minimum of approx. 53,000 km$^3$ in 1995 and is relatively high between 2005 and 2013 with a maximum of approx. 60,000 km$^3$ in 2008 (Fig. 4.3). Hence, the total range is around 7,000 km$^3$.

The simulated total freshwater content was relatively high in the 1980s with about 75,000 km$^3$ and decreased towards the mid-1990s to a minimum of about 68,000 km$^3$ in 1995 (Fig. 4.3). It stayed quite low until the mid-2000s, when the freshwater content started to increase again reaching about 76,500 km$^3$ in 2009. The anomalies of the simulated and observed total freshwater content anomalies compare relatively well between 1992 and 2009, however the absolute values have an offset of about 15,000 km$^3$ with the simulated freshwater content being too high (Fig. 4.3).

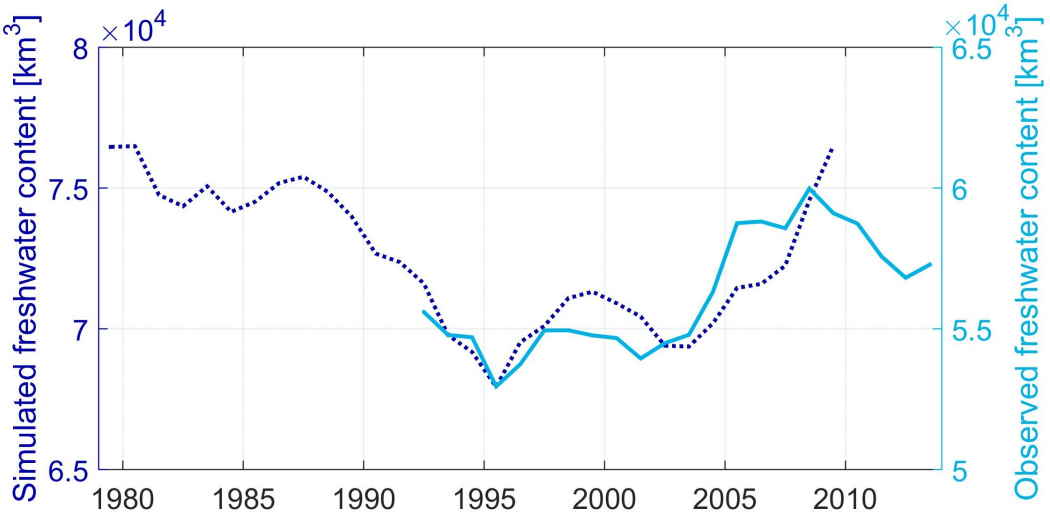


***Figure 4.3:*** *Comparison of the total freshwater content of the upper Arctic Ocean (surface to 34-isohaline) from observations (solid light blue line) and from the FESOM simulation (dotted dark blue line). Both time series have been calculated with the reference salinity* $S_{ref} = 35$.

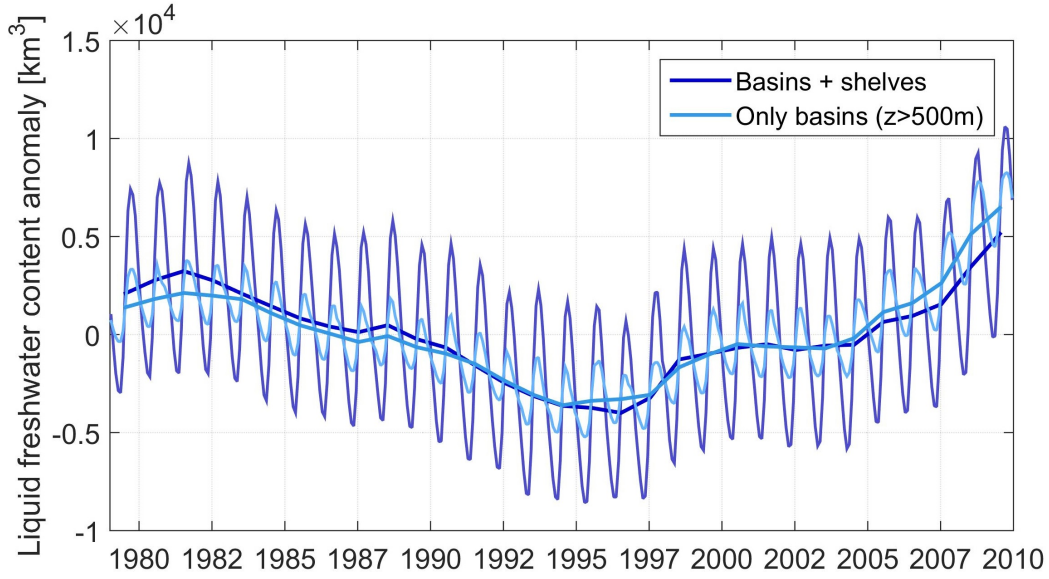


***Figure 4.4:*** *Comparison of the simulated (FESOM) liquid freshwater content anomaly of the Arctic Ocean region covering only the deep basins (> 500 m, light blue line) and of the Arctic Ocean region including also the shelves (dark blue line). Both time series have been calculated with the reference salinity* $S_{ref} = 35$ *and from the surface to the 34-isohaline. Thinner lines indicate the monthly means, thicker lines the annual means.*

Since the shelf region is not included in the observational Arctic Ocean freshwater content time series due to a lack of data, I used the model to determine the change in the freshwater content anomalies when including the shelf region. Although the seasonal variability and the absolute value of freshwater content is much higher when including the shelves, the interannual variability is almost the same in comparison to the liquid freshwater content anomaly of the only basins region (Fig. 4.4).

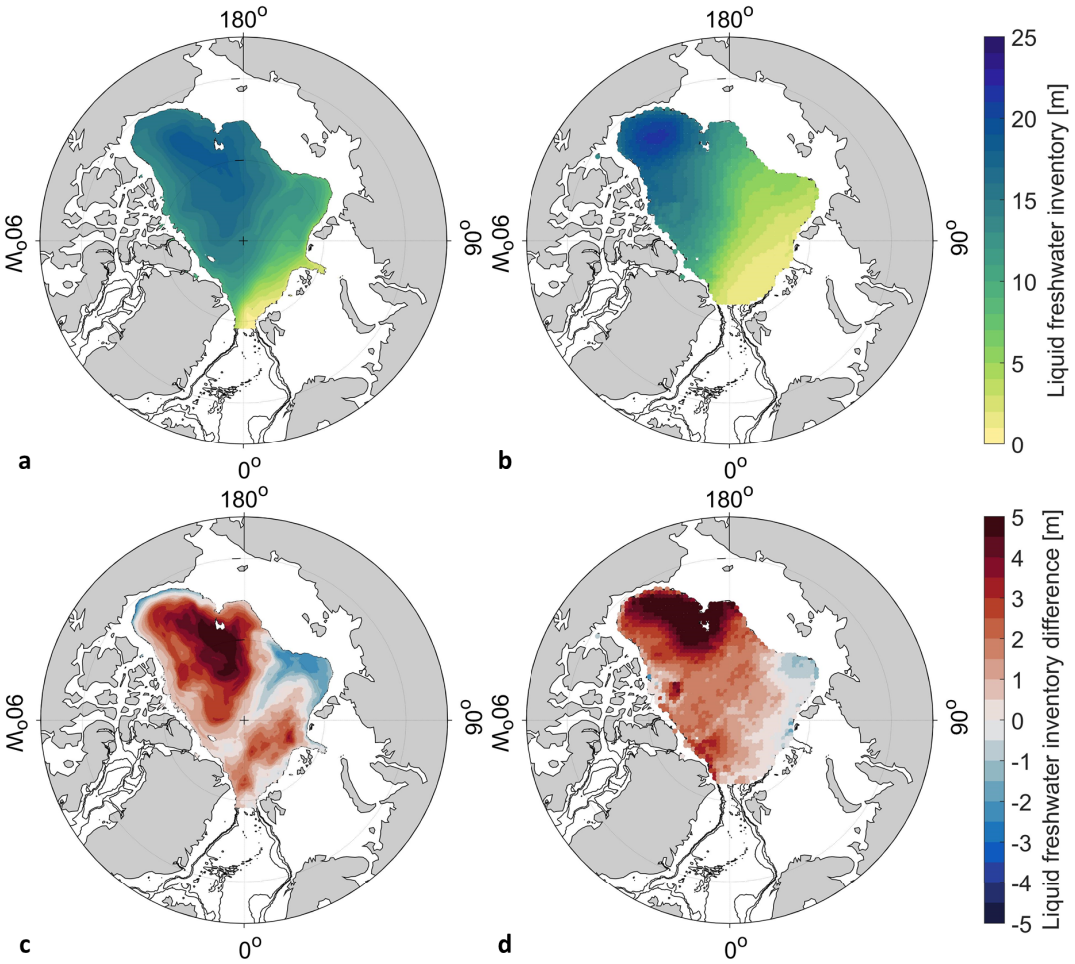


***Figure 4.5:*** *Liquid freshwater inventories of the Arctic Ocean above the 34-isohaline from the FESOM simulation (a, c) and observations (b, d) calculated with the reference salinity* $S_{ref} = 35$*. Mean for the period 1992-2009 (a, b), difference between the periods 1992-2003 and 2007-2009 (c), as well as the difference between the periods 1992-2003 and 2005-2013 (d). Positive freshwater inventory differences indicate an increase from the earlier to the later period. Black lines indicate the 500 m-, 1000 m-, and 2000 m-isobaths.*

Looking at the regional distribution of liquid fresh water in the Arctic Ocean, the highest freshwater inventories exist in the Canada Basin (Fig. 4.5a-b). The temporal mean (1992-2009) of the simulated liquid freshwater inventories (Fig. 4.5a) shows higher values in the Eurasian Basin and lower values in the Canada Basin than the temporal mean (1992-2009) of the observed liquid freshwater content (Fig. 4.5 b). The observed rapid increase in liquid freshwater content between the periods 1992-2003 and 2005-2013 happened almost all over the Arctic deep basins, but amplified in the Canada Basin (Fig. 4.5d). Between similar time periods (1992-2003 and 2007-2009) also the simulated freshwater inventories increased in most parts of the Arctic deep basins with an amplified signal in the Amerasian Basin (Fig. 4.5c). Compared to the observations (Fig. 4.5d), the increase is stronger in the northern part of the Amerasian Basin (Fig. 4.5c), where the mean freshwater inventories are also higher in the model (Fig. 4.5a) than in the observations (Fig. 4.5b). Moreover there is a more pronounced liquid freshwater content increase in the western Eurasian Basin and decrease in the eastern Eurasian Basin (Fig. 4.5c) compared to the observations (Fig. 4.5d).

Coming to the regional distribution of solid fresh water/sea ice in the Arctic Ocean, the highest values in the mean (1979-2009) solid freshwater inventories from the FESOM simulation can be found North of Greenland and the CAA (Fig. 4.6a). This is where the most multiyear sea ice is located, which means year round sea ice cover and ice thicknesses of typically two to five meters (e.g., Maslanik et al., 2007). From the first 10 years (1979-1989) to the last 10 years (1999-2009) of the model simulation the solid freshwater inventories decreased all over the Arctic Ocean (Fig. 4.6b). The highest decreases happened on the East Siberian shelf, north of Greenland and in the CAA (Fig. 4.6b).

Having presented the results from the analysis of the upper Arctic Ocean freshwater content variability, I now come to the research questions introduced in the beginning of this chapter that are related to the presented results. I will discuss the most important findings by answering these questions in the following.

**Is the increase in the liquid freshwater content of the upper Arctic Ocean due to the anomalous amount of net sea ice melt?**

The liquid freshwater content increased by about 10,000 $km^3$ between 1995 and 2010 while at the same time the average solid freshwater content decreased by about 7,000 $km^3$ (Fig. 4.1-4.2). This would mean that the increasing net sea ice melt cannot fully explain the increased liquid freshwater content of the upper Arctic Ocean, which is also indicated by the high variations of the total freshwater content of the upper Arctic Ocean (Fig. 4.3). However, the uncertainties in the liquid and

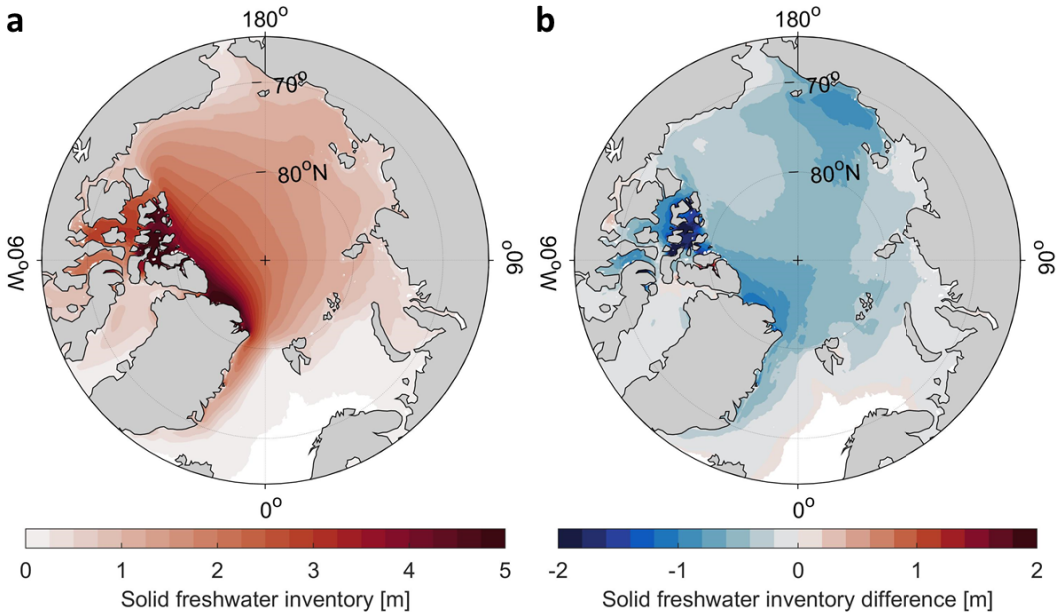


***Figure 4.6:*** *Simulated (FESOM) solid freshwater inventory of the Arctic Ocean: mean for the period 1979-2009 (a) and difference between the mean of 1979-1989 and the mean of 1999-2009 (b). Positive freshwater inventory differences indicate an increase from the earlier to the later period.*

solid freshwater content time series are relatively high and a balance of the trends would be possible within the range of uncertainties. Still, the model simulation with FESOM and results from many other studies (e.g., Yamamoto-Kawai et al., 2008; McPhee et al., 2009; Haine et al., 2015 show an increase in the total freshwater content of the upper Arctic Ocean in the past decades (Fig. 4.3). Thus it is likely that there has been an additional increase in liquid freshwater content (other than from net sea ice melt) that needs to result from another anomalously high freshwater input to the Arctic Ocean or an anomalously low freshwater output out of the Arctic Ocean.

### Did the freshwater content changes take place all over the Arctic Ocean or only in parts of it?

The liquid freshwater content of the Arctic Ocean increased between the periods 1992-2003 and 2005-2013 almost everywhere in the Arctic Ocean deep basins (Fig. 4.5d). However, the increase is highest in the western Canada Basin. This is where the Beaufort Gyre is situated, which is known to accumulate fresh water in its interior by Ekman Pumping when spinning up due to increased anticyclonic winds (e.g., Proshutinsky et al., 2002). Still, Rabe et al. (2011, 2014) observed that the

liquid freshwater content increase in the upper Arctic Ocean from the 1990s to the following decade is 2/3 due to a mean decrease in the upper ocean salinity and only 1/3 due to a deepening of the lower halocline forced by regional Ekman pumping. They suggested the mean freshening of the upper Arctic Ocean to be associated with increased net sea ice melt and the advection of increased amounts of Siberian river waters.*

In the period of the model simulation the solid freshwater inventories decreased all over the Arctic region (Fig. 4.6b). The highest decrease appeared in the region of multiyear ice (CAA and north of Greenland) due to decreasing sea ice thicknesses and in the East Siberian Sea due to both a decrease in the sea ice thickness as well as a decline in sea ice concentration (not shown). Maslanik et al. (2007) describe a decline in the Arctic sea ice extent by 42 % in summer 2007 compared to the 1980s and a shift in the perennial Arctic sea ice pack from predominantly old and thick multiyear ice (>5 years old, >2.5 m thick) to relatively young and thin sea ice (2-3 years old, 2.0-2.2 m thick). They argue that the reduced sea ice extent and the thinner sea ice, which is faster melted in summer and allows easier transport out of the Arctic Ocean, exposes more open water which accelerates the sea ice decline due to the ice-albedo-feedback.

## 4.2 The liquid freshwater content of the subpolar North Atlantic and the Nordic Seas

The liquid freshwater content of the subpolar North Atlantic has significantly decreased from the 1990s to the 2000s (Fig. 4.7a). The average freshwater content (relative to the reference salinity 35) was about 400 $km^3$ between 1990 and 2002 with an annual mean maximum of 1,600 $km^3$ in 1996. Thereafter it rapidly decreased to about -3,000 $km^3$ on average between 2004 and 2011 with an annual mean minimum of -3,800 $km^3$ in 2007 (a negative freshwater content results from salinities higher than the reference salinity). After 2011 the liquid freshwater content suddenly increased again to about 700 $km^3$ in the period 2012-2013 (Fig. 4.7a).

Furthermore, the liquid freshwater content of the Nordic Seas decreased significantly since 1990 (Fig. 4.7b). While the mean freshwater content of 1990 to 2002 (relative to the reference salinity 35) was about 8,700 $km^3$, it was only 7,400 $km^3$ on average in the last 10 years of the observed time period (2003-2013). The highest annual mean of the liquid freshwater content was 9,300 $km^3$ in 1997 and the lowest was about 6,700 $km^3$ in 2013 (Fig. 4.7b).

In both regions, the Nordic Seas and the subpolar North Atlantic, a decrease in liquid freshwater content can be observed from the mid-1990s to mid-2000s (Fig. 4.8).

However, variations in the subpolar North Atlantic are higher and changes are more rapid. The range of the annual mean liquid freshwater content anomalies is 5,400 km$^3$ in the subpolar North Atlantic and 2,600 km$^3$ in the Nordic Seas. The uncertainties in both freshwater content time series are almost the same for both regions with slightly higher uncertainties in the first half of the time period when no float data were yet available (Fig. 4.8).

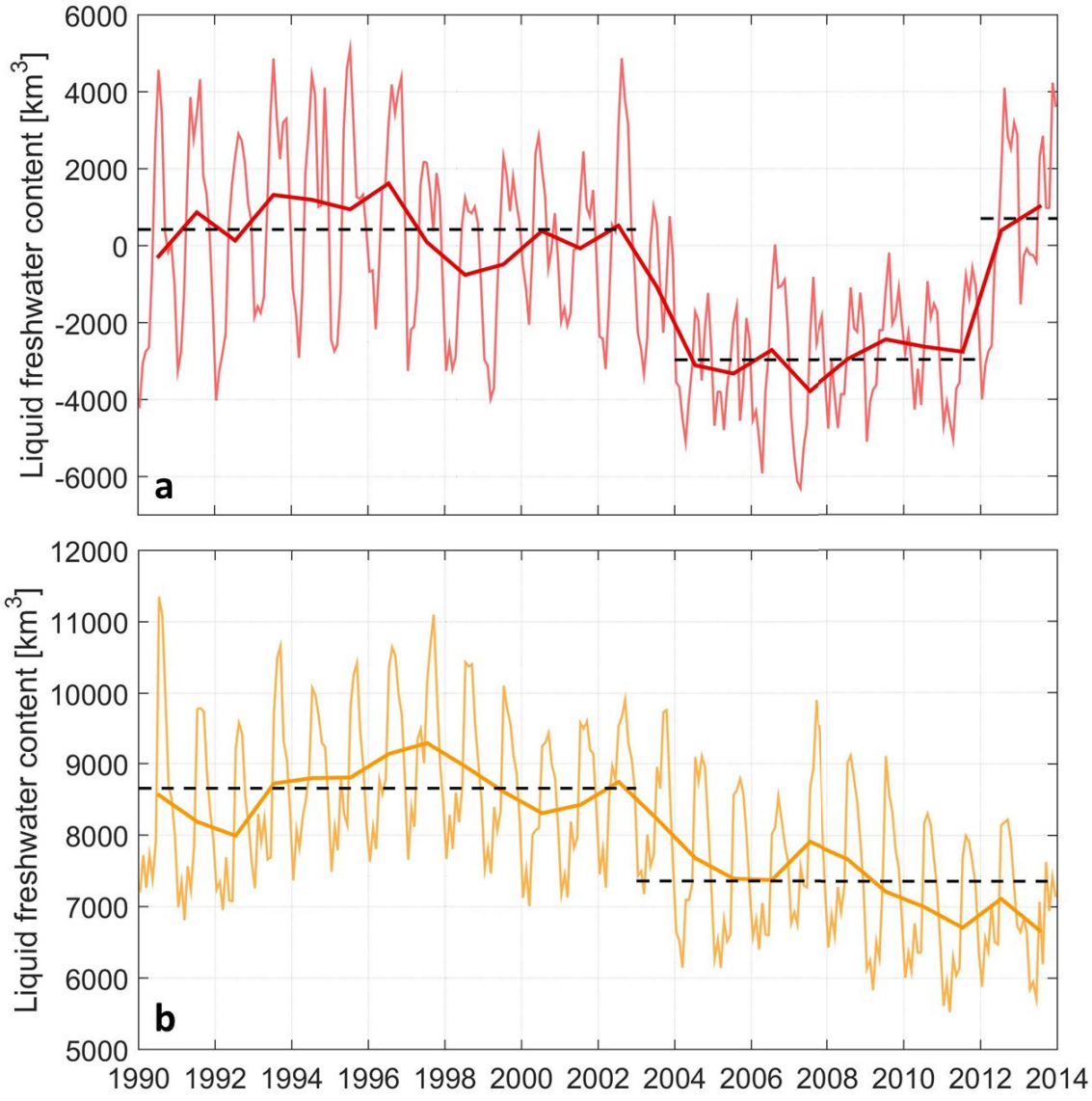


***Figure 4.7:*** *Monthly and annual means of the liquid freshwater content from observations: subpolar North Atlantic (a) and Nordic Seas (b). The three dashed lines in (a) indicate the mean for the periods 1992-2002, 2004-2011, and 2012-2013. The two dashed lines in (b) indicate the mean for the periods 1990-2002 and 2003-2013. The freshwater content values were calculated with the reference salinity* $S_{ref} = 35$.

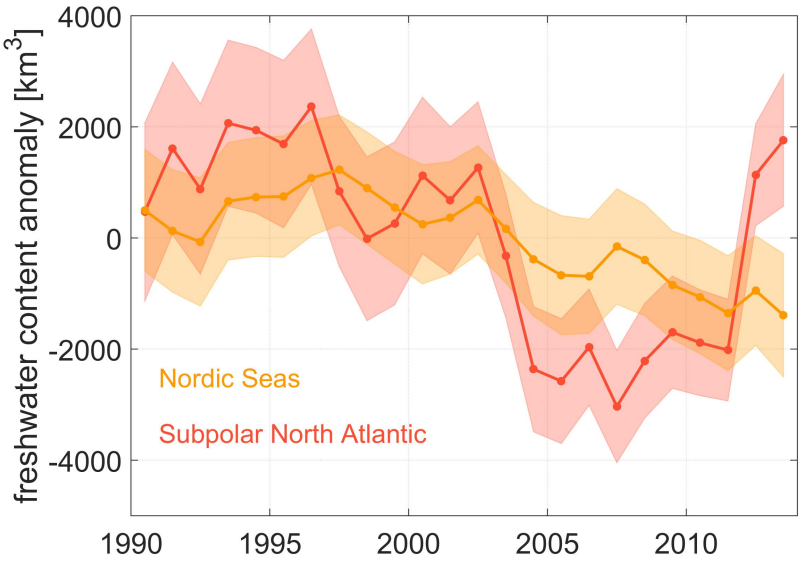


***Figure 4.8:*** *Annual averages of observed liquid freshwater content anomaly of the Nordic Seas (orange) and subpolar North Atlantic (red) from 1990 to 2013. The shadings indicate the annual means of monthly uncertainties. The freshwater contents were calculated with the reference salinity* $S_{ref} = 35$.

Analysing the liquid freshwater content variability in different depth layers of the Nordic Seas and the western and eastern subpolar North Atlantic (separated by the Mid Atlantic Ridge), the main variability can be observed in the upper 500 m with the highest variability in the upper 100 m (Fig. 4.9). In the Nordic Seas there is almost no variability deeper than 1,000 m (Fig. 4.9f). In western subpolar North Atlantic the liquid freshwater content decreased from 2002 to 2013 in the deeper layers, which can still be found in 1,500 m to 2,000 m depth (Fig. 4.9b). In the eastern subpolar North Atlantic the liquid freshwater content variability in the layers from 1,000 m to 2,000 m is similar to the variability in the layers above, but with significantly smaller anomalies (Fig. 4.9d). The rapid decrease in the western subpolar North Atlantic liquid freshwater content started in 2000 in the upper 100 m and is followed by a decrease in the layers from 200 m to 500 m with approximately two years lag (Fig. 4.9a). The same holds for the following increase in liquid freshwater content from 2007 onwards (Fig. 4.9a). In the eastern subpolar North Atlantic and in the Nordic Seas salinity changes seem to happen more simultaneously in the upper 500 m or the vertical propagation of the signal happens on shorter time scales than one year (Fig. 4.9c, e).

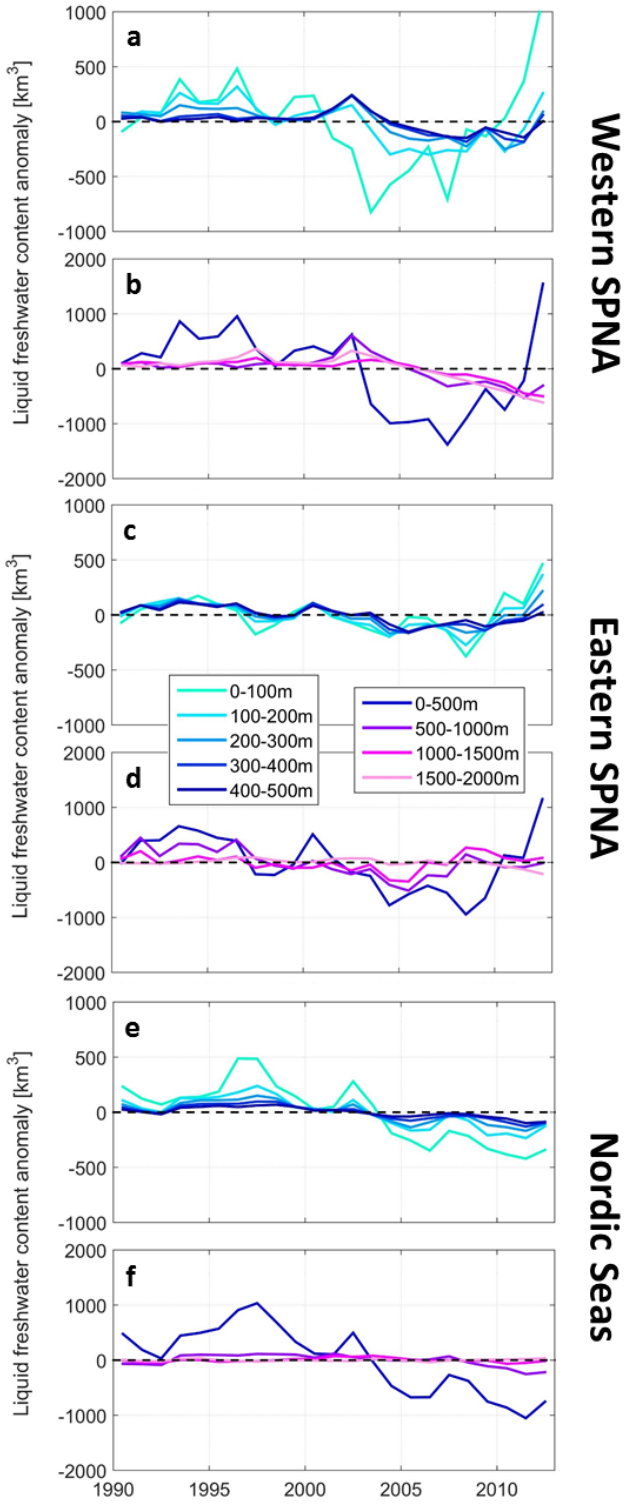


***Figure 4.9:*** *Observed liquid freshwater content anomalies of the western (a, b) and eastern (c, d) subpolar North Atlantic (SPNA) and the Nordic Seas (e, f) in the period 1992-2013 for different depth layers: 100 m thick layers in the upper 500 m (a, c, e) and 500 m tihck layers between the surface and 2,000 m depth (b, d, f). All freshwater contents have been calculated relative to the reference salinity* $S_{ref} = 35$.

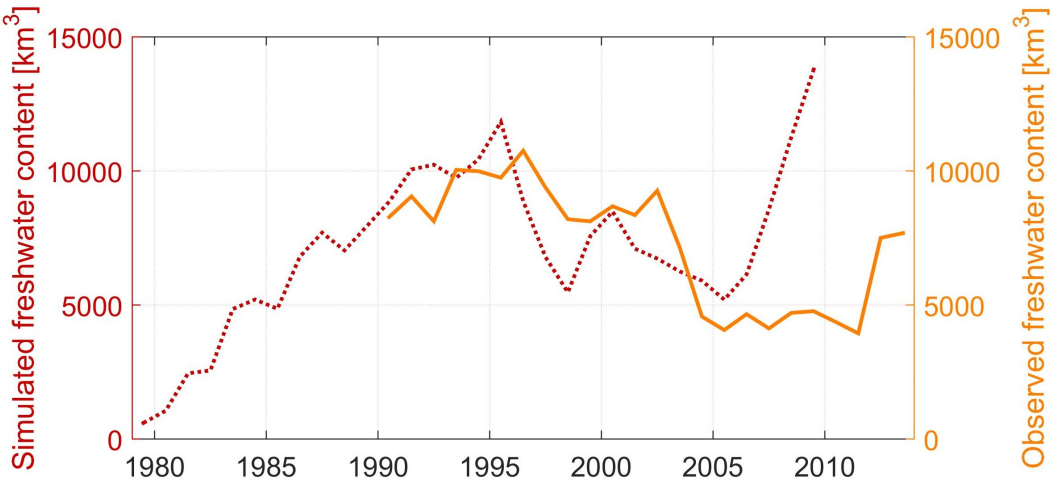


***Figure 4.10:*** *Comparison of the liquid freshwater content of the SANA from observations (solid orange line) and from the FESOM simulation (dotted red line). Both time series have been calculated with the reference salinity* $S_{ref} = 35$.

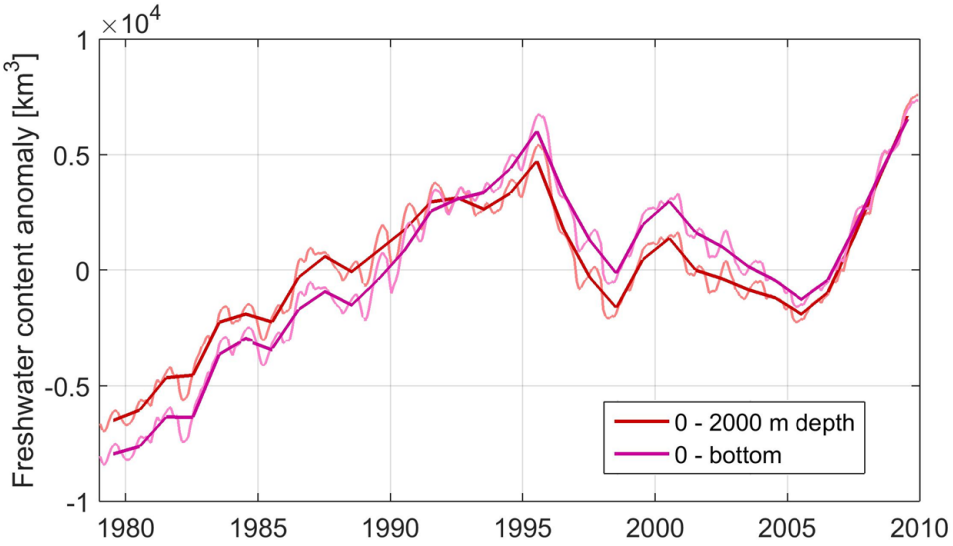


***Figure 4.11:*** *Comparison of the simulated (FESOM) liquid freshwater content anomaly of the SANA for the upper 2,000 m (red line) and for the full water column (magenta line). Both time series have been calculated with the reference salinity* $S_{ref} = 35$. *Thinner lines indicate the monthly means, thicker lines the annual means.*

As the liquid freshwater content of the subpolar North Atlantic and of the Nordic Seas both show similar variability, I use the liquid freshwater content for the combined region, SANA, to later compare to the total freshwater content of the upper Arctic Ocean. First, however, I compare the observational to the simulated freshwater content time series. The observed liquid freshwater content of the SANA varies between 10,800 $km^3$ in 1996 and 3,900 $km^3$ in 2011 (Fig. 4.10). The simulated liquid freshwater content was close to zero in 1979 and monotonously increased to 13,800 $km^3$ in 1995. After a sudden decrease in 1996 to 1998, the liquid freshwater content stayed between 5,000 $km^3$ and 8,000 $km^3$ until 2006, when it rapidly increased again, reaching almost 14,000 $km^3$ in 2009. Although the absolute values from the observations and the model simulation are on a similar level, the anomalies differ significantly at times. This is especially the case during 1996-1998, 2001-2002 and after 2006. Still, FESOM simulates a rapid drop in the SANA liquid freshwater content from the 1990s to 2000s, only happening earlier than in the observational time series.

As described in Chap. 3.3, I calculated the liquid freshwater content of the SANA from the surface to 2,000 m depth, as the CORA salinity data is only available for that depth range and as I assume that most of the variability is captured within the upper 2,000 m of the water column. This assumption is already supported by the analysis of the liquid freshwater content variability for the different depth layer (Fig. 4.9). Additionally, I used the FESOM simulation to quantify the difference in the SANA liquid freshwater content variability of the upper 2,000 m and the full water column (Fig. 4.11). This comparison reveals no significant differences in the frequency and sign of the freshwater content anomalies and only relatively small differences in the magnitude of the anomalies (Fig. 4.11). Consequently the main part of the SANA liquid freshwater content variability is covered by the observational SANA liquid freshwater content time series of the upper 2,000 m of the water column.

Looking at the regional distribution of the liquid freshwater inventories of the SANA, the highest values can be observed in the western deep basins of the Nordic Seas and the subpolar North Atlantic (Fig. 4.12b). These are the Greenland, Iceland, Irminger, and Labrador Seas, which are provided with cold and fresh polar waters by the East Greenland, West Greenland and Labrador currents. Further east the liquid freshwater inventories become negative as the salinity is on average higher than the reference salinity 35. This is where warm and salty water masses from the tropical/subtropical North Atlantic are transported by the North Atlantic, Irminger and Norwegian Atlantic currents into the SANA. The decrease in liquid freshwater content from the periods 1990-2002 to 2004-2011 (Fig. 4.10) mainly occurred due to decreasing freshwater inventories close to the shelves of the SANA (Fig. 4.12d).

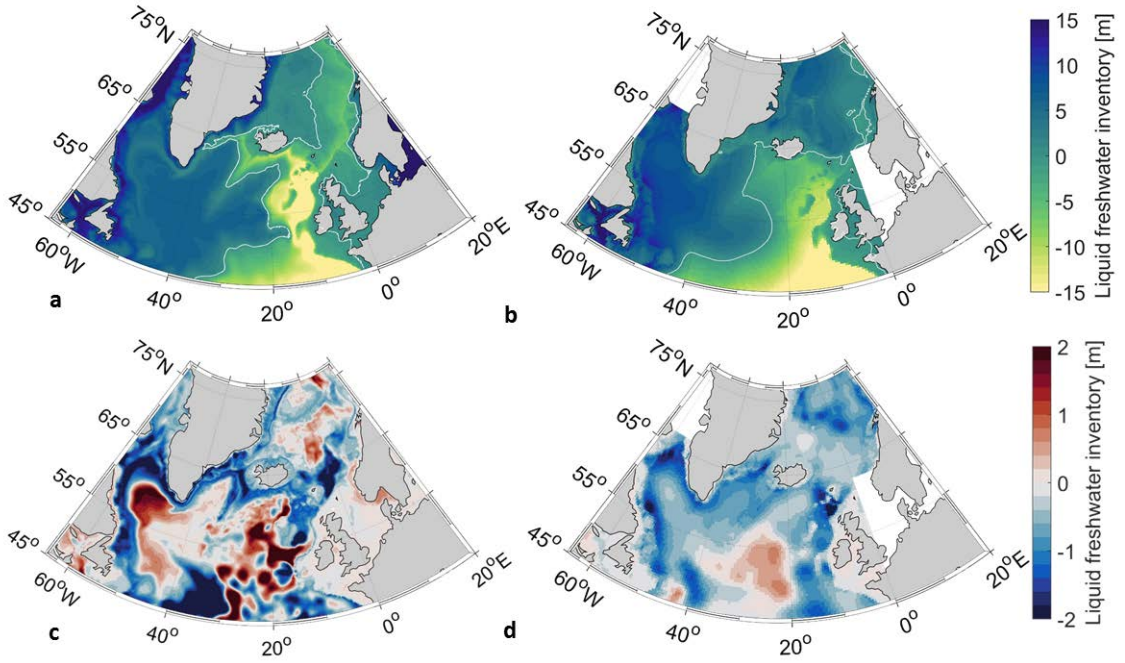


***Figure 4.12:*** *Map of liquid freshwater inventories of the SANA from the FESOM simulation (a, c) and from observations (b, d) relative to the reference salinity* $S_{ref} = 35$*. Mean for the period 1990-2009 (a, b), difference between the periods 1998-2005 and 2007-2009 (c), as well as the difference between the periods 1990-2002 and 2004-2011 (d). Positive freshwater inventory differences indicate an increase from the earlier to the later period. The white contour (a, b) indicates the zero liquid freshwater inventory isoline.*

In contrast, the liquid freshwater inventories increased in the Mid Atlantic Ridge region (Fig. 4.12d).

The mean simulated liquid freshwater inventories from 1990 to 2009 (Fig. 4.12a) show higher values on the western shelves, in the Newfoundland and Iceland Basins and at the Mid-Atlantic Ridge than in the mean observed freshwater inventories from 1990 to 2009 (Fig. 4.12b). However, the simulated values are lower in the Labrador, Greenland and Iceland Seas (Fig. 4.12a) than the observed ones (Fig. 4.12b). The liquid freshwater content decrease of the simulation from the period 1998-2005 to the period 2007-2009 (Fig. 4.10) results from a pronounced freshwater decrease on western shelves, in the Norwegian Sea, the Rockall Trough and the Newfoundland Basin (Fig. 4.12c). On the contrary, the salinity increased in the eastern subpolar North Atlantic, in the Labrador Sea and in parts of the Nordic Seas (Fig. 4.12c).

In the following I will discuss the results presented above by answering my research question concerning the freshwater variability of the subpolar North Atlantic and the Nordic Seas.

**Where (horizontally and vertically) did the liquid freshwater content of the subpolar North Atlantic and the Nordic Seas vary the most?**

The observed liquid freshwater decrease of the SANA between 2002 and 2004 appeared to be strongest north of the Rockall Trough, where one branch of the Norwegian Atlantic current is located, and along the western shelves, where the West Greenland, East Greenland and Labrador Currents transport cold and fresh waters from polar origin further south (Fig. 4.12d). Moreover the liquid freshwater inventories increased in the Mid Atlantic Ridge region at the same time (Fig. 4.12d). At these locations (north of the Rockall Trough, on the western shelves and in the Mid Atlantic Ridge region) the model simulation shows changes in the liquid freshwater inventories between 2005 and 2007 of the same sign (Fig. 4.12c) as in the observed change between 2002 and 2004 (Fig. 4.12d).

The main variability is observed in the upper 500 m of the water column with the highest variability near the surface (Fig. 4.9). This suggests that either changes in the continental runoff (including ice and meltwater from Greenland), the net precipitation or the lateral exchange with the adjacent seas at the surface have caused the observed freshwater content changes.

As the freshwater input from the Greenland Ice Sheet and the Arctic glaciers increased significantly during the past decades (e.g., Yang et al., 2016; Velicogna, 2009; Bamber et al., 2012, 2018) and an intensification of the global water cycle due to global warming suggests an increasing precipitation and river runoff (Huntington, 2006), these freshwater sources are unlikely to have caused the observed freshwater content decrease in the SANA. Decreasing freshwater transports from the Arctic Ocean, however, could not only explain the decrease in the western SANA freshwater content, but at the same time also the increase in the Arctic freshwater content. The liquid freshwater inventory increase in the central subpolar North Atlantic and decrease north of the Rockall trough could either result from local changes in the net precipitation or from changes in the subpolar gyre strength and extent which is proposed to be related to changes in the salt transport into the Nordic Seas (Hátún et al., 2005).

## 4.3 Comparison of Arctic and subarctic freshwater content

The Nordic Seas are located between the Arctic Ocean and the subpolar North Atlantic and influenced by both, the import of relatively saline waters from the subpolar North Atlantic and the import of relatively fresh waters from the Arctic

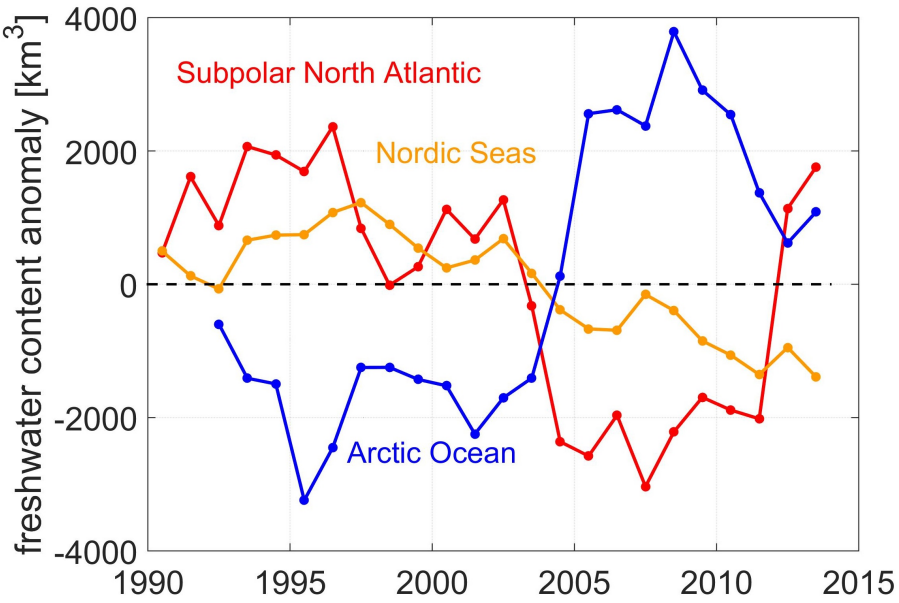


***Figure 4.13:*** *Observed freshwater content anomalies of the upper Arctic Ocean, subpolar North Atlantic and Nordic Seas. Annually averaged liquid freshwater content anomaly (1990-2013) of the subpolar North Atlantic (red) and Nordic Seas (orange) and the total freshwater content anomaly (1992-2013) of the upper Arctic Ocean above the 34-isohaline (blue). The freshwater contents were calculated with the reference salinity* $S_{ref} = 35$.

Ocean (see Chap. 2.2). Therefore I compared the liquid freshwater content of the Nordic Seas to the liquid freshwater content of the subpolar North Atlantic as well as the total freshwater content of the Arctic Ocean (Fig. 4.13). The comparison reveals that the Nordic Seas liquid freshwater content variability is more similar to the variability in the subpolar North Atlantic than in the Arctic Ocean. Therefore I combined the liquid freshwater content time series for the subpolar North Atlantic and the Nordic Seas and use this combined SANA time series in the following.

Comparing the observed total freshwater content of the upper Arctic Ocean and the observed liquid freshwater content of the SANA (Fig. 4.14) reveals a significant anti-correlation between 1992 and 2013 with a correlation coefficient of r = -0.878 at zero lag ($N^* = 3.14$, p = 0.047). The maximum correlation (r = -0.894, p = 0.039) is found at a one year lag of the Arctic freshwater content. However, I will not discuss this one year lag as the correlation is based on annual means and the uncertainties are relatively high due to limited observational data. In both regions a rapid change occurred between 2002 and 2005, resulting in a higher Arctic freshwater content and a lower SANA freshwater content than in the previous years. From 2010/11 onwards the freshwater content started to increase/decrease again in both regions.

In order to put my findings in the context of longer time scales, I compared them

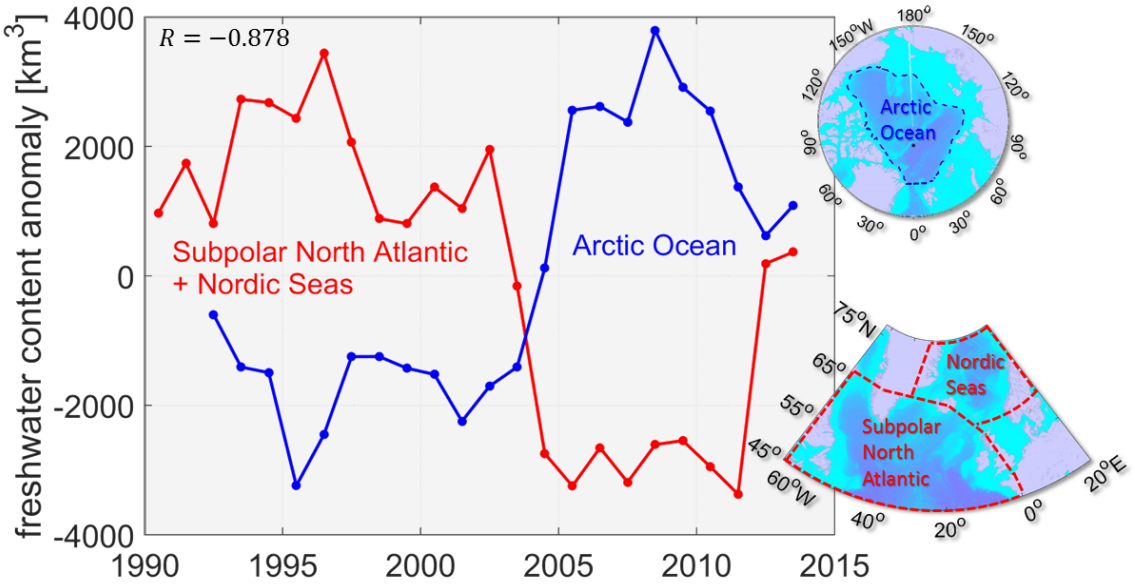


***Figure 4.14:*** *Freshwater content anomalies of the upper Arctic Ocean and the SANA. Annually averaged liquid freshwater content anomaly (1990-2013) of the SANA in red and the total freshwater content anomaly (1992-2013) of the Arctic Ocean in blue. The freshwater contents were calculated with the reference salinity $S_{ref} = 35$. The correlation coefficient, R, is -0.878 at zero lag, $N^* = 3.14$ and $p = 0.047$.*

to other observational syntheses in the subpolar North Atlantic and the Nordic Seas (see Chap. 3.3). The pentadal means of my relatively short time series, and those presented by Curry and Mauritzen (2005) and Mauritzen et al. (2012) compare relatively well so that I am confident that they capture a part of a longer-period process (Fig. 4.15).

The pentadally averaged observations of 50 years in the subpolar North Atlantic show a minimum in liquid freshwater content in the 1960s, followed by an increase until the 1990s, and then by a decrease until 2010. The increase in the 1970s, 1980s and 1990s (the latter only in the annual means) coincides with the repeated observations of GSAs (e.g., Dickson et al., 1988) in the subpolar North Atlantic. What is striking is the rapid increase in the liquid freshwater content of the subpolar North Atlantic from the mid-2000s to 2012/13 (Fig. 4.13-4.15).

To further investigate, how the freshwater variability of different regions of the SANA compares to the Arctic freshwater variability, I performed a cross-correlation and regression analysis (see Chap. 3.7.3) of the SANA liquid freshwater inventories and the total freshwater content of the upper Arctic Ocean (Fig. 4.16). This cross-correlation map shows the highest anti-correlation with the liquid freshwater inventories in the Greenland, Labrador and Irminger Seas as well as north of the Rockall Trough and in the West European Basin (Fig. 4.16a). East of the Mid

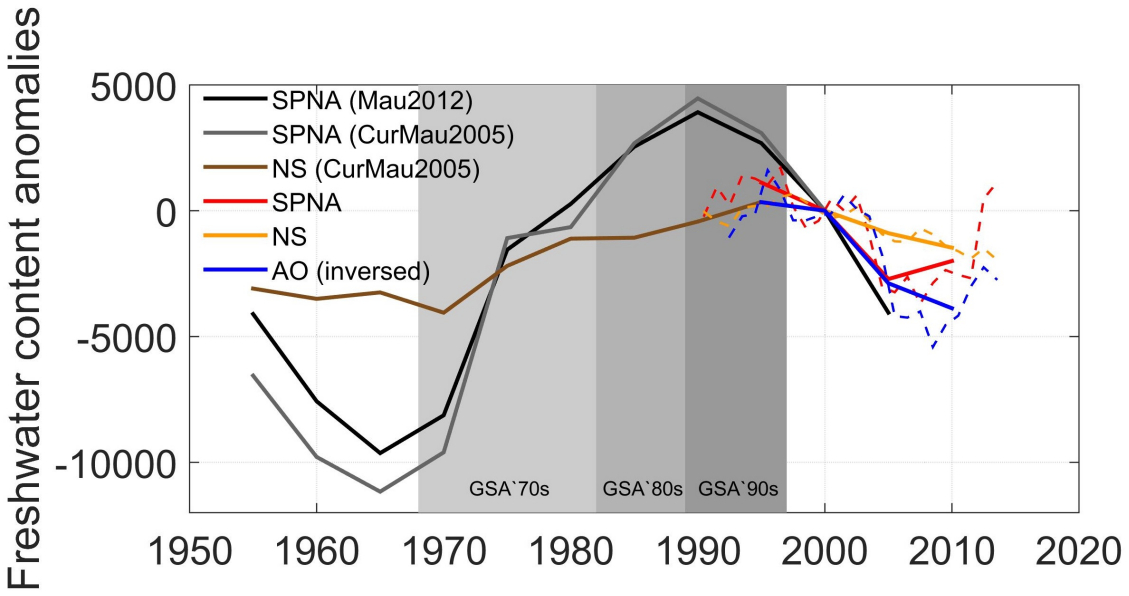


***Figure 4.15:*** *Decadal freshwater variability. The solid lines represent pentadal means, the dashed lines indicate annual means where available. All time series are anomalies to their pentadal mean of the year 2000. The colour coding refers to different regions, studies and data sets: liquid freshwater content of the subpolar North Atlantic from the present study (red), from Curry and Mauritzen (2005) (grey), and calculated from the salt content from Mauritzen et al. (2012) (black), of the Nordic Seas from the present study (orange) and from Curry and Mauritzen (2005) (brown), and the total freshwater content of the Arctic Ocean from the present study (blue; inversed). The gray shadings indicate the time periods of the Great Salinity Anomalies of the 1970s, 1980s and 1990s (Belkin et al., 1998; Belkin, 2004).*

Atlantic Ridge and towards the Iceland Sea the liquid freshwater inventories are positively correlated with the upper Arctic Ocean total freshwater content (Fig. 4.16a). Due to the small number of effective degrees of freedom ($N^* = 3.14$) only correlations with a correlation coefficient higher than $r = 0.8$ are statistically significant at the 90 % confidence level (white contours in Fig. 4.16a). The map of regression coefficients (Fig. 4.16b) shows a similar pattern with high negative regression coefficients in the central Nordic Seas and north of the Rockall Trough. In the western subpolar North Atlantic, however, the highest neagtive regression with the upper Arctic Ocean total freshwater content appears along the shelves (Fig. 4.16b), where the western boundary currents are located, rather than in the central basin regions, where the correlation is highest (Fig. 4.16a). In the following these results are discussed with regard to my last research question introduced in the beginning of this chapter.

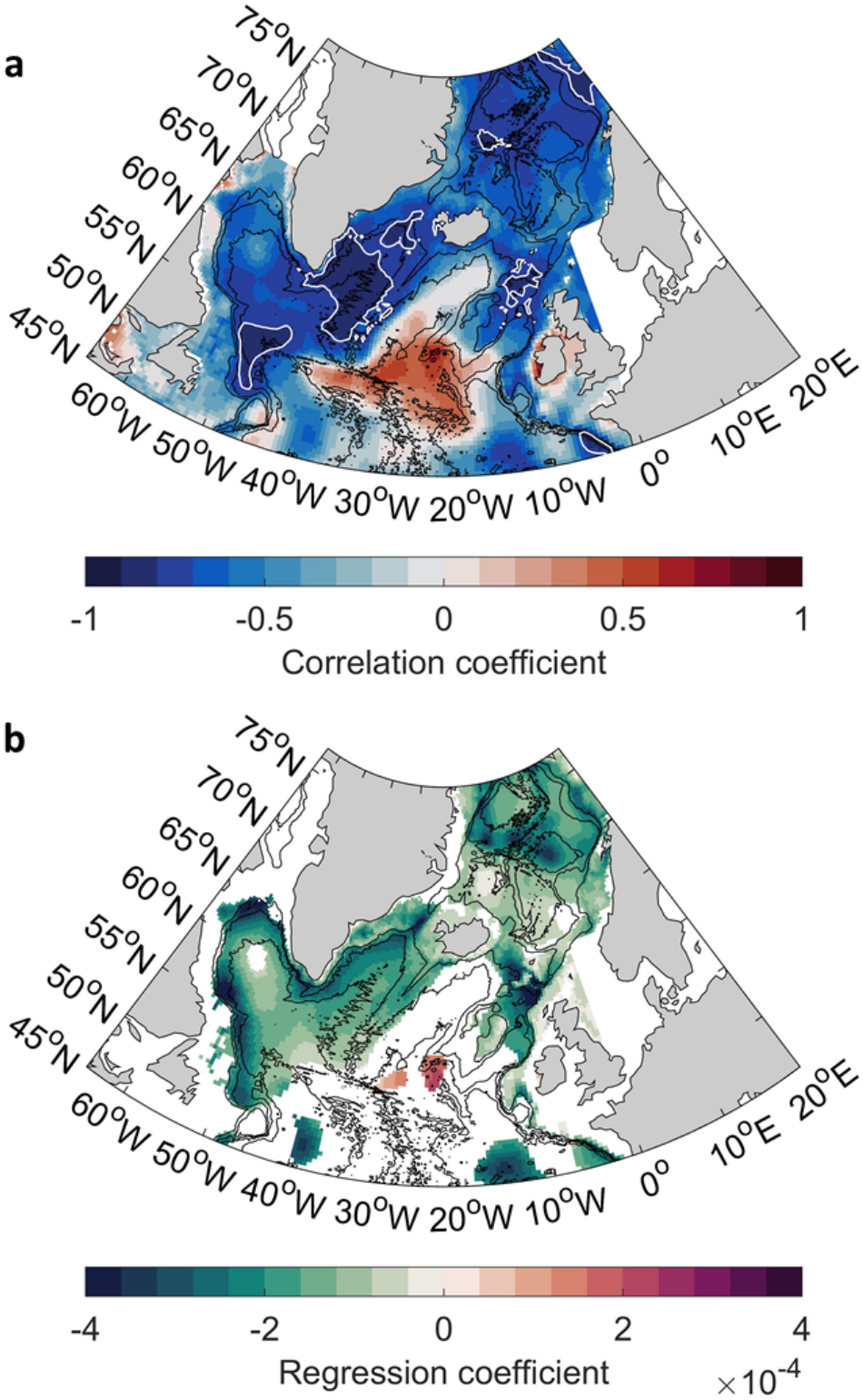


***Figure 4.16:*** *Zero-lag cross-correlation (a) and regression (b) of the observed SANA liquid freshwater inventories and the observed total freshwater content of the Arctic Ocean ($N^* = 3.14$). The white contours in the correlation map (a) enclose regions of significant correlations (90 % confidence). The regression coefficient (b) is only shown for correlations higher than 0.5.*

**How do the freshwater content anomalies of the Arctic Ocean, the subpolar North Atlantic and Nordic Seas compare?**

As the liquid freshwater content of the Nordic Seas decreased from the 1990s to late-2000s, it better compares to the decrease observed in the subpolar North Atlantic than the increase in the upper Arctic Ocean freshwater content (Fig. 4.13). This is also supported by findings of Curry and Mauritzen (2005). Therefore I combined the liquid freshwater contents of the subpolar North Atlantic and the Nordic Seas (SANA) to compare to the total freshwater content of the Arctic Ocean.

The liquid freshwater content of the SANA and the total freshwater content of the Arctic Ocean are significantly anti-correlated between 1992 and 2013 (Fig. 4.14). They vary in opposing sense alternating between high and low phases with anomalies of the same size. My results suggest a decadal link between the freshwater anomalies of the Arctic Ocean and the SANA in the time period of 22 years when observations were made in both regions. Only for the SANA, observations reach back to the 1950s, suggesting alternations with scales longer than a decade.

The GSAs in the 1970s (e.g., Dickson et al., 1988), the 1980s (e.g., Belkin et al., 1998) and the 1990s (e.g., Belkin, 2004) have been related to changing freshwater exports from the Arctic due to anomalous atmospheric conditions (e.g., Haak et al., 2003). The fact that the GSAs coincide with the phase of strong freshwater content increase in the SANA suggests that the latter results from accumulating a series of freshwater pulses released from the Arctic Ocean to the North Atlantic.

The idea of changing freshwater exports from the Arctic Ocean explaining the observed anti-correlation of the freshwater contents is supported by the spatial cross-correlation (Fig. 4.16), which shows that most of the strongest anti-correlations appear in the western basins of the SANA. These are the deep water formation sites of the SANA and the regions most influenced by the waters exported from the Arctic Ocean. In contrast, the regions more influenced by the waters transported from the subtropics are either less anti-correlated or even positively correlated. This is especially evident east of the Mid Atlantic Ridge and in the Iceland Basin. This positive correlation and the negative correlation north of the Rockall Trough could result from a changing strength and extent of the Subpolar Gyre, a parallel change in local net precipitation or a change in the salinity of the waters transported by the North Atlantic and Norwegian Atlantic Currents.

In order to find an explanation for the observed freshwater content changes in the upper Arctic Ocean and the SANA, and their anti-correlation, I focus on the variability of the different freshwater sources and sinks of both regions in the next chapter.

# Chapter 5

# Freshwater fluxes

*This chapter aims on identifying the processes that drive the freshwater content changes described in the former chapter. After a short introduction to the topic including the main research questions related to the freshwater fluxes, data from the FESOM simulation and its forcing are used to describe the time mean (Chap. 5.1) and temporal variations (Chap. 5.2) of the freshwater fluxes of the entire Arctic Ocean, the upper Arctic Ocean, and the SANA. The results are discussed by answering the different research questions at the end of each section. Some parts of text from Campos and Horn (2018) are used in the paragraphs marked with an asterisk (*).*

---

As salt is largely conserved in the oceans globally, the only way to change the ocean salinity is by adding or removing fresh water. Thus the strong observed freshwater content changes in the Arctic Ocean and SANA described in the previous chapter needs to be explained by changes in the freshwater fluxes to these regions. While fresh water is added to the Arctic Ocean by continental runoff, precipitation, and the inflow of low salinity Pacific Water, it can only be removed by evaporation and the exchange with the North Atlantic (e.g., Haine et al., 2015; Serreze et al., 2006; Lique et al., 2009). In the SANA an additional important freshwater source besides river runoff, precipitation and the inflow from the Arctic Ocean is the melt water runoff and ice discharge from Greenland (e.g., Peterson et al., 2006). The sinks are evaporation and the exchange with the subtropical North Atlantic.

To understand the observed freshwater content changes described in the previous chapter, I analysed the different freshwater sources and sinks of the Arctic Ocean and the SANA using the FESOM simulation and other reanalysis products and data sets listed below. I calculated for both regions from 1979 to 2009

— the evaporation and precipitation from the CORE-II atmospheric forcing data

set (see Chap. 3.1.3),

— the river runoff from the data set of Dai et al. (2009) (see Chap. 3.1.6),

— the liquid and solid oceanic freshwater transports from the FESOM simulation (see Chap. 3.2.1) for all sections displayed in Fig. 3.8, and

— the artificial freshwater flux due to surface salinity restoring in the model (Damping Term).

Moreover, I used estimates of the freshwater flux from the Greenland Ice Sheet and Arctic glaciers and ice caps from Bamber et al. (2018) (see Chap. 3.1.7).

In this chapter I differentiate between the upper Arctic Ocean, the entire Arctic Ocean and the SANA. The freshwater transports to/from the upper Arctic Ocean are calculated above the 34-ishaline and relative to the refrence salinity 34. Additionally the entrainment term is introduced, which is supposed to summarise the freshwater fluxes associated with the processes causing diahaline mixing across the 34-isohaline. The freshwater transports to/from the entire Arctic Ocean are calculated for the entire water column and with the monthly mean salinity of the entire Arctic Ocean as the reference salinity. Further the freshwater transports to/from the SANA are calculated for the entire water column and with the monthly mean salinity of the entire SANA. For more details see Chap. 3.5.1.

The analyses presented in this chapter are aimed at answering the following research questions:

- What are the largest time mean freshwater sources and sinks in the Arctic Ocean and SANA?
- How did the freshwater fluxes change in the past decades?
- Which freshwater flux component had the largest effect on the freshwater content changes of the upper Arctic Ocean and of the SANA in the model?
- Are the changes in the freshwater transport between the Arctic Ocean and the SANA rather driven by changes in volume flux or due to changes in the salinity of the transported waters?

## 5.1 Mean simulated freshwater budgets of the Arctic Ocean and SANA

Large amounts of fresh water are added to and removed from the Arctic Ocean (Fig. 5.1, Tab. 5.1). The three large freshwater sources of the Arctic Ocean are river

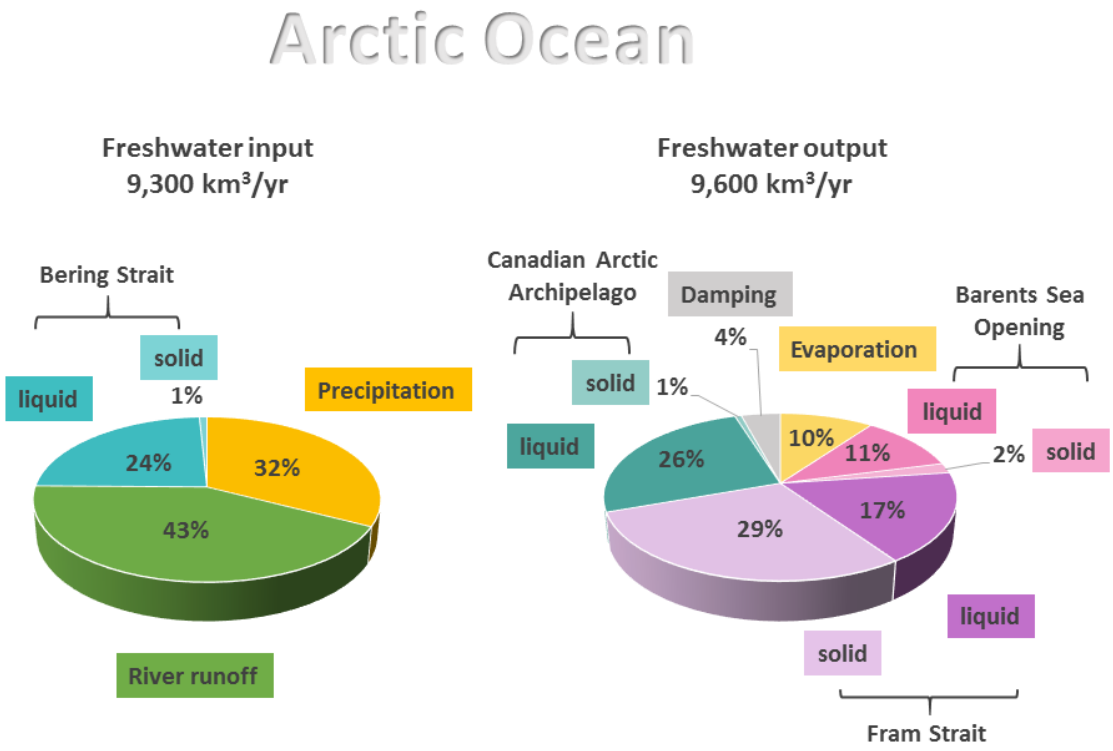


***Figure 5.1:*** *Mean simulated freshwater budget of the entire Arctic Ocean averaged from 1979 to 2009. The freshwater transports were calculated from the surface to the bottom and relative to the monthly mean Arctic Ocean salinity. The damping term is the freshwater flux from the surface salinity restoring in the model.*

runoff, the low salinity PW inflow through Bering Strait (S ≈ 32) and precipitation (Fig. 5.1, Tab. 5.1). With the mean Arctic Ocean salinity as the reference salinity for the freshwater trasnport calculation (see Chap. 3.5.1, Fig. 3.11a), river runoff is the largest freshwater source (∼43 %, Fig. 5.1).

The freshwater sinks are evaporation, AW import through both, the Fram Strait and the Barents Sea Opening (S ≈ 35), the export of low salinity water (S ≈ 33-34) and sea ice to the North Atlantic via the CAA, the Fram Strait and the Barents Sea Opening (Fig. 5.1, Tab. 5.1). The largest sinks are the sea ice export through Fram Strait (∼46 %) and the liquid freshwater export through the CAA (∼27 %, Fig. 5.1). Another mean freshwater sink in the model is the damping, which is on average relatively small (-400 km$^3$/yr) but is highly variable ($\sigma$ = 780 km$^3$/yr, Tab. 5.1).

The highest volume transports are the net inflow through the Barents Sea Opening (∼90,500 km$^3$/yr) and the net outflow through the Fram Strait (∼ -74,000 km$^3$/yr). As the surface fluxes and river runoff in the model are only virtual salt fluxes (see Chap. 3.4), they do not have a volume transport.

***Table 5.1:*** *Average simulated freshwater sources and sinks of the entire Arctic Ocean from 1979 to 2009 and their standard error of the mean (see Chap. 3.7.1) calculated from annual means. The top to bottom freshwater transports are computed relative to the monthly mean salinity of the entire Arctic Ocean. The damping term is the freshwater flux from the surface salinity restoring in the model. The solid volume transports are liquid water equivalents.*

| | Mean salinity | Volume transport [km$^3$/year] | Salt transport [10$^1$2 kg/year] | Freshwater transport [km$^3$/year] |
|---|---|---|---|---|
| *Freshwater sources* | | | | |
| River runoff | — | — | — | 3,990 ± 90 |
| Precipitation | — | —- | — | 3,050 ± 10 |
| Bering Strait (liq) | 32.20 ± 0.02 | 31,050 ± 440 | 1,000 ± 10 | 2,240 ± 40 |
| Bering Strait (sol) | 5.84 ± 0.01 | 90 ± 20 | 0 ± 0 | 70 ± 20 |
| **Total input** | | | | **9,350 ± 90** |
| *Freshwater sinks* | | | | |
| Fram Strait (liq) | 34.91 ± 0.01 | -73,970 ± 1,140 | -2,510 ± 400 | -1,680 ± 90 |
| Fram Strait (sol) | 5.83 ± 0.01 | -3,370 ± 200 | -20 ± 0 | -2,800 ± 170 |
| CAA (liq) | 33.63 ± 0.02 | -46,170 ± 5,290 | -1,520 ± 170 | -2,460 ± 300 |
| CAA (sol) | 5.93 ± 0.00 | -80 ± 10 | -0 ± 0 | -70 ± 10 |
| BSO (liq) | 35.08 ± 0.02 | 90,410 ± 4,280 | 3,180 ± 150 | -1,050 ± 60 |
| BSO (sol) | 5.61 ± 0.02 | -220 ± 40 | -0 ± 0 | -180 ± 30 |
| Evaporation | — | — | — | -960 ± 50 |
| Damping | — | — | — | -400 ± 310 |
| **Total output** | | | | **-9,610 ± 490** |
| **Residual** | | | | **-260** |

*Abbreviations: BSO – Barents Sea Opening, CAA – Canadian Arctic Archipelago, liq – liquid, sol – solid*

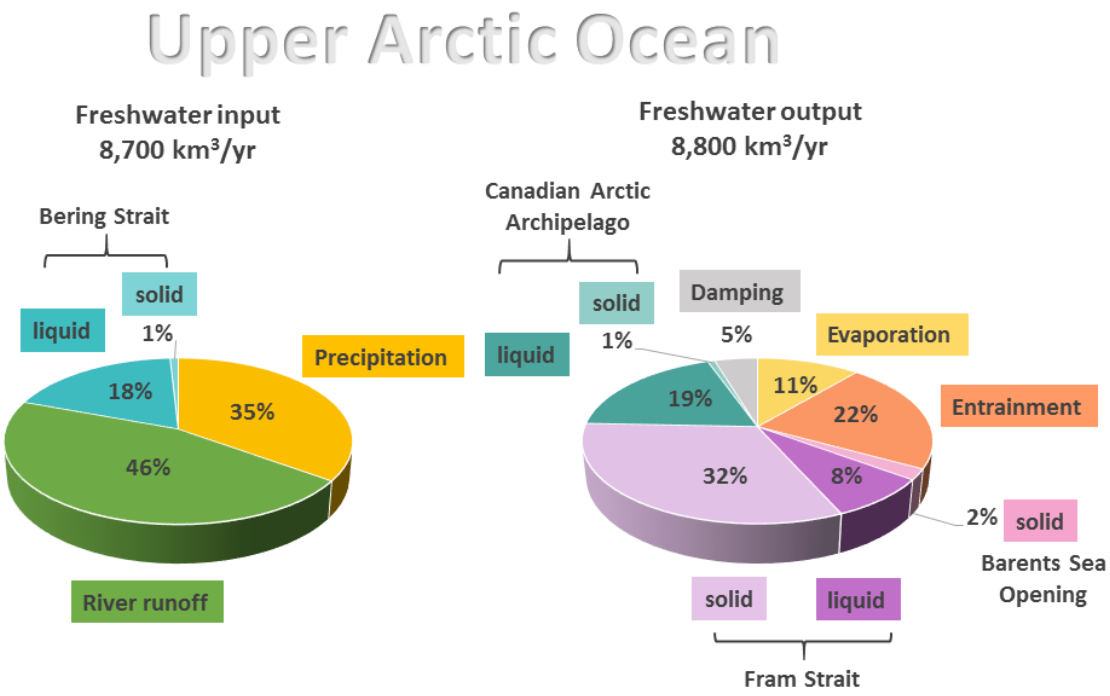


***Figure 5.2:*** *Mean simulated freshwater budget of the upper Arctic Ocean (surface to 34-isohaline) averaged from 1979 to 2009. The freshwater transports and content were calculated from the surface to the 34-isohaline and relative to $S_{ref} = 34$. The damping term is the freshwater flux from the surface salinity restoring in the model. The entrainment term is introduced in Chap. 3.5.1.*

Now we turn to the upper Arctic Ocean freshwater budget. The surface freshwater fluxes and solid volume transports for the upper Arctic Ocean are the same as for the entire Arctic Ocean (Tab. 5.2). However, the solid freshwater transports differ slightly ($< 20$ km$^3$/yr) due to the different reference salinity (entire Arctic Ocean: $S_{ref} \approx 34.70$-$34.75$, upper Arctic Ocean: $S_{ref} = 34$, see Chap. 3.5.1). The liquid freshwater transports are generally smaller due to the lower reference salinity and lower volume transports above the 34-isohaline (Fig. 5.2; Tab. 5.2).

The largest freshwater sources for the upper Arctic Ocean are the river runoff and the precipitation (Fig. 5.2; Tab. 5.2). Compared to the full water column estimate, the liquid freshwater transport through Bering Strait is 620 km$^3$/yr smaller rather due to the different reference salinity than due to the different integration depth as the volume transport is only reduced by 90 km$^3$/yr.

***Table 5.2:*** *Average simulated freshwater sources and sinks of the upper Arctic Ocean (surface to 34-isohaline) from 1979 to 2009 and their standard error of the mean (see Chap. 3.7.1) calculated from annual means. The freshwater transports are calculated between the surface and the 34-isohaline and relative to $S_{ref} = 34$. The damping term is the freshwater flux from the surface salinity restoring in the model. The entrainment term is introduced in Chap. 3.5.1. The solid volume transports are liquid water equivalents.*

| | Mean salinity | Volume transport [km$^3$/year] | Salt transport [10$^1$2 kg/year] | Freshwater transport [km$^3$/year] |
|---|---|---|---|---|
| *Freshwater sources* | | | | |
| River runoff | — | — | — | 3,990 ± 90 |
| Precipitation | — | —- | — | 3,050 ± 10 |
| Bering Strait (liq) | 32.20 ± 0.02 | 30,960 ± 440 | 1,000 ± 10 | 1,620 ± 40 |
| Bering Strait (sol) | 5.84 ± 0.01 | 90 ± 20 | 0 ± 0 | 80 ± 20 |
| **Total input** | | | | **8,730 ± 80** |
| *Freshwater sinks* | | | | |
| Fram Strait (liq) | 33.23 ± 0.02 | -35,240 ± 1,970 | -1,170 ± 70 | -710 ± 50 |
| Fram Strait (sol) | 5.83 ± 0.01 | -3,370 ± 200 | -20 ± 0 | -2,790 ± 170 |
| "Entrainment" | — | — | — | -1,890 ± 390 |
| CAA (liq) | 32.79 ± 0.02 | -38,640 ± 5,020 | -1,260 ± 160 | -1,630 ± 200 |
| CAA (sol) | 5.93 ± 0.00 | -80 ± 10 | -0 ± 0 | -70 ± 10 |
| Evaporation | — | — | — | -960 ± 50 |
| Damping | — | — | — | -400 ± 310 |
| BSO (liq) | 33.80 ± 0.03 | -510 ± 210 | -20 ± 10 | -0 ± 0 |
| BSO (sol) | 5.61 ± 0.02 | -220 ± 40 | -0 ± 0 | -180 ± 30 |
| **Total output** | | | | **-8,630 ± 260** |
| **Residual** | | | | **100** |

*Abbreviations: BSO – Barents Sea Opening, CAA – Canadian Arctic Archipelago, liq – liquid, sol – solid*

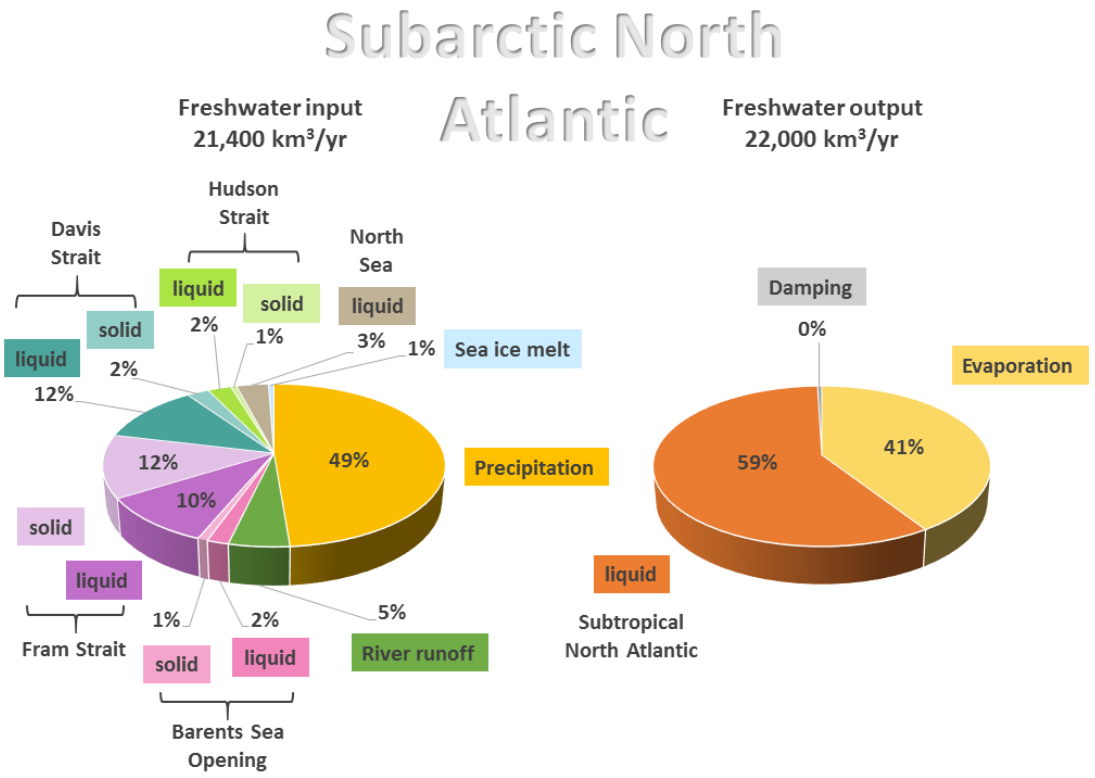


***Figure 5.3:*** *Mean simulated freshwater budget of the SANA averaged from 1979 to 2009. The freshwater transports and content were calculated from the surface to the bottom and relative to the monthly mean SANA salinity. Consequently the liquid freshwater content is zero.*

---

The largest freshwater sink for the upper Arctic Ocean is still the solid freshwater transport through the Fram Strait (Fig. 5.2). Another large freshwater sink is the entrainment term, which combines all processes that lead to the diahaline exchange of salt across the 34-isohaline (see Chap. 3.5.1). While in the CAA most of the transported waters are above the 34-isohaline, there is only a small part in the Fram Strait. Consequently, the volume transport and thereby the freshwater transport through Fram Strait is significantly lower for the upper ocean (Tab. 5.2) than for the entire water column (Tab. 5.1). In the Barents Sea Opening the volume transport above the 34-isohaline is close to zero as the waters are mostly saltier than 34. Hence, there is also no considerable freshwater transport.

***Table 5.3:*** *Average simulated freshwater sources and sinks of the SANA from 1979 to 2009 and their standard error of the mean (see Chap. 3.7.1) calculated from annual means. The top to bottom freshwater transports are relative to the monthly mean salinity of the SANA. The damping term is the freshwater flux from the surface salinity restoring in the model. The solid volume transports are liquid water equivalents.*

| | Mean salinity | Volume transport [km$^3$/year] | Salt transport [10$^1$2 kg/year] | Freshwater transport [km$^3$/year] |
|---|---|---|---|---|
| *Freshwater sources* | | | | |
| Precipitation | – | — | – | 10,880 ± 90 |
| Fram Strait (liq) | 34.91 ± 0.01 | 73,970 ± 1,140 | 2,510 ± 400 | 2,200 ± 110 |
| Fram Strait (sol) | 5.83 ± 0.01 | 3,370 ± 200 | 20 ± 0 | 2,800 ± 170 |
| Davis Strait (liq) | 34.07 ± 0.02 | 46,600 ± 5,260 | 1,540 ± 180 | 2,590 ± 270 |
| Davis Strait (sol) | 5.89 ± 0.00 | 640 ± 70 | 0 ± 0 | 530 ± 60 |
| River runoff | — | — | — | 1,110 ± 20 |
| North Sea | 35.01 ± 0.02 | 870 ± 40 | 10 ± 0 | 720 ± 10 |
| Hudson Strait (liq) | 32.99 ± 0.04 | 1,430 ± 70 | 30 ± 0 | 570 ± 30 |
| Hudson Strait (sol) | 5.84 ± 0.01 | 170 ± 20 | 0 ± 0 | 140 ± 10 |
| BSO (liq) | 35.08 ± 0.02 | -90,410 ± 4,280 | -3,180 ± 150 | 400 ± 40 |
| BSO (sol) | 5.61 ± 0.02 | 220 ± 40 | 0 ± 0 | 180 ± 30 |
| Local sea ice melt | – | – | – | 140 ± 50 |
| **Total input** | | | | **22,230 ± 420** |
| *Freshwater sinks* | | | | |
| Subtropical NA | 35.05 ± 0.00 | -24,570 ± 1,290 | 410 ± 50 | -12,920 ± 400 |
| Evaporation | – | – | – | -9,040 ± 60 |
| Damping | – | – | – | -430 ± 450 |
| **Total output** | | | | **-22,390 ± 640** |
| **Residual** | | | | **-160** |

*Abbreviations: BSO – Barents Sea Opening, liq – liquid, NA – North Atlantic, sol – solid*

In the SANA, both precipitation and evaporation are higher than in the Arctic Ocean, yet, the average net precipitation is much lower (Tab. 5.3). The freshwater flux of approximatley 10,900 $km^3$/yr from precipitation makes up almost half of the entire freshwater input to the region (Fig. 5.3). Other large freshwater sources are the liquid and solid transport from the Arctic Ocean through the Fram Strait ($\sim$5,000 $km^3$/yr) and the Davis Strait ($\sim$3,100 $km^3$/yr) as well as the river runoff ($\sim$1,100 $km^3$/yr). Moreover, fresh water is added to the SANA from the North Sea, the Hudson Bay, net melt of local sea ice (see Chap. 3.4) and the export of rather salty waters into the Barents Sea (Tab. 5.3).

Another important freshwater source of the SANA (missing in the model forcing and therefore not displayed in Fig. 5.3) is the freshwater input from the Greenland Ice Sheet ($\sim 990 \pm 110$ $km^3$ on average between 1979 and 2009, Bamber et al., 2012). Compared to the simulated freshwater import from the Arctic Ocean, it is almost 9 times smaller. However, the mass loss of the Greenland Ice Sheet is accelerating and expected to have a larger influence in the near future (e.g., Bamber et al., 2012; Velicogna, 2009).

The large freshwater sinks of the SANA are the exchange with the subtropical North Atlantic and the evaporation (Fig. 5.3). The average damping term is, in comparison, negligible (Tab. 5.3). Still, the variability of the damping is quite high ($\sigma \approx 700$ $km^3$/yr).

In the following I will review the mean freshwater budget of the Arctic Ocean and SANA from the FESOM simulation by comparison with other model and observational studies. In the section thereafter I will focus on the temporal variability of the introduced freshwater fluxes.

### What are the largest time mean freshwater sources and sinks in the Arctic Ocean and SANA?

In the model simulation, the largest freshwater source of the Arctic Ocean is the river runoff, followed by the precipitation and the transport through Bering Strait (Fig. 5.1-5.2, Tab. 5.1-5.2). The observational estimates by Serreze et al. (2006) suggest that precipitation is 100 $km^3$ larger than river runoff and 800 $km^3$ larger than the Bering Strait freshwater transport (relative to $S_{ref} = 34.8$). However, an update by Haine et al. (2015) supports the model results in suggesting that river runoff is the largest freshwater source of the Arctic Ocean. A more detailed comparison of the simulated freshwater fluxes to estimates from literature can be found in the appendix.

The largest freshwater sink of the Arctic Ocean in the FESOM model is the transport through the Fram Strait including the export of low-salinity water, sea

ice and snow as well as the import of high-salinity water. This agrees with the findings of Serreze et al. (2006) and Haine et al. (2015). The next largest sinks are the export of low-salinity water, sea ice and snow through the CAA and, for the upper Arctic Ocean, the processes summarised in the entrainment term (see Chap. 3.5.1). However, as this term is calculated from the difference between the liquid freshwater storage (derivative of the content) and the net liquid freshwater flux (net precipitation, river runoff, net sea ice melt, salinity restoring and liquid freshwater transport), it also includes uncertainties in the calculation.

The largest source of uncertainty is most probably the interpolation of the model data onto a section that is needed to calculate transports in a finite-element model with an unstructured mesh (Sidorenko et al., 2009). The resulting imbalances from the calculated volume transports are shown in the appendix (Fig. 5.9). Moreover, the oceanic transports only include advection by the ocean currents and neither eddy diffusive transport nor numerical diffusive transport across the section. In freshwater fluxes calculated for the upper Arctic Ocean the freshwater flux associated with these diffusive transports will be included in the entrainment term. In the freshwater fluxes calculated for the entire Arctic Ocean and the SANA the oceanic freshwater transport might be overestimated or underestimated due to the missing diffusive transports. Numerical diffusion will likely only have an effect at the section at 45 °N, where the mesh size and the section length is significantly larger than at the other sections (Fig. 3.4 and Fig. 3.8). If the resolution is high enough and the eddies are resolved or correctly parameterised, there should be a freshening effect from eddies carrying Labrador Current waters into the North Atlantic Current inflow branch to the SANA (Müller et al., 2017) and a pronounced eddy driven recirculation of AW in the Fram Strait (Hattermann et al., 2016).

The largest freshwater source of the SANA in the model simulation is by far the precipitation (Fig. 5.3, Tab. 5.3), followed by the transport from the Arctic Ocean. The largest freshwater sinks are the high-salinity transport from the subtropical North Atlantic and the evaporation. In both regions, the SANA and the Arctic Ocean, net precipitation is positive. This is consistent with results of other studies (e.g., Haine et al., 2015; Serreze et al., 2006; Curry et al., 2003; Josey and Marsh, 2005). Many studies investigate single freshwater sources or sinks like net precipitation (e.g., Curry et al., 2003; Josey and Marsh, 2005; Boyer et al., 2007) or the salt flux from lower latitudes (e.g., Holliday et al., 2008) to compare to freshwater/salinity changes in the North Atlantic, but do not compare several freshwater sources/sinks with each other.The only study I found analysing different freshwater sources of the SANA region is the study by Peterson et al. (2006). However, they only show freshwater flux anomalies and no absolute values or time means that I could compare with my results.

## 5.2 Temporal variability of the freshwater fluxes

For analysing the variability of the different freshwater flux contributions I display the time series of freshwater flux anomalies (relative to the time mean) and the cumulative freshwater flux anomalies (for calculation see Chap. 3.5) in Fig. 5.4. The latter illustrate the effect of the fluxes on the freshwater content of the Arctic Ocean and the SANA, if we assume that the sum of all freshwater fluxes equals the freshwater storage (see Chap. 3.4).

The comparison of the different freshwater sources and sinks reveals that the oceanic transport dominates the variations in the total freshwater flux in both regions, the Arctic Ocean (P-E: $\sigma$ ≈150 km$^3$/yr, R: $\sigma$ ≈160 km$^3$/yr, T: $\sigma$ ≈880 km$^3$/yr, Damping: $\sigma$ ≈780 km$^3$/yr; Fig. 5.4a) and the SANA (P-E: $\sigma$ ≈150 km$^3$/yr, R: $\sigma$ ≈160 km$^3$/yr, T: $\sigma$ ≈880 km$^3$/yr, Damping: $\sigma$ ≈78 km$^3$/yr; Fig. 5.4a). The predominantly negative transport anomalies for the Arctic Ocean sum up to a removal of about 10,000 km$^3$ fresh water until the mid-1990s (Fig. 5.4b, d). This fresh water ends up in the SANA (Fig. 5.4f). After 1995, the Arctic Ocean freshwater transport anomalies change sign (Fig. 5.4a) adding about 10,000 km$^3$ fresh water to the Arctic Ocean until 2009 (Fig. 5.4b, d). At the same time, the oceanic freshwater transport anomalies of the SANA become predominantly negative (Fig. 5.4e) causing a removal of about 12,000 km$^3$ fresh water until the mid-2000s (Fig. 5.4f).

In the Arctic Ocean, river runoff was increasing (9.32 km$^3$/yr$^2$; green lines in Fig. 5.4a, c), while net precipitation was decreasing (-10.15 km$^3$/yr$^2$; magenta lines in Fig. 5.4a, c). The surface salinity restoring shows high variability (Arctic Ocean: $\sigma$ ≈780 km$^3$/yr, SANA: $\sigma$ ≈780 km$^3$/yr; grey lines in Fig. 5.4a, c, e) mainly varying opposite to to the net freshwater flux, thus damping the freshwater content variability in the model. The variations in the entrainment term are relatively high ($\sigma$ ≈600 km$^3$/yr) and sum up to an addition of about 6,000 km$^3$ fresh water to the upper Arctic Ocean until the end of the 1990s (orange line in Fig. 5.4d) due to anomalously low salt flux into the layer above the 34-isohaline. The variability of the oceanic freshwater transport of the upper Arctic Ocean (blue line in Fig. 5.4c) is very similar to the variability of the transports of the entire Arctic Ocean (r=0.919; blue line in Fig. 5.4a).

For the SANA, variations in the oceanic transport are higher than for the Arctic Ocean (blue lines in Fig. 5.4a, c, e), still the cumulative flux anomalies vary in a comparable range (∼10,000 km$^3$ for the Arctic Ocean, ∼12,000 km$^3$ for the SANA, blue lines in Fig. 5.4b, d, f). The net precipitation and river runoff were both slightly decreasing during the 30 years of simulation (-11.31 km$^3$/yr$^2$ and -3.46 km$^3$/yr$^2$, respectively; magenta and green line in Fig. 5.4e), while the freshwater flux from

land ice increased (11.70 $km^3/yr^2$; yellow line in Fig. 5.4e). As in the Arctic Ocean, the surface salinity restoring shows high variability ($\sigma \approx 730$ $km^3/yr$; grey line in Fig. 5.4e) and damps the influence of the other freshwater flux variations on the oceans freshwater storage.

The results presented in this section indicate that the oceanic transport is the major contributor to freshwater content changes in the Arctic Ocean and the SANA. This will be further discussed at the end of this chapter. Due to the importance of the oceanic transport variability, I present results of further analyses of the freshwater transport components in the following section.

### 5.2.1 Oceanic freshwater transport components

As shown in the previous section, the oceanic freshwater transport is highly variable and seems to strongly influence the freshwater content of the respective region (inicated by the high cumulative freshwater transport anomalies). That is why I take a closer look on the different components of the net oceanic freshwater transport including the transports through the various gateways, the separation into the northward and southward transport components as well as considering the solid and liquid freshwater transports separately.

Considering the oceanic exchanges through the various passages (Fig. 5.5a), the dominant source of content variability in the Arctic Ocean (upper Arctic Ocean as well as entire Arctic Ocean) in the model simulation is the freshwater export to the Atlantic (explaining ∼89 % of the upper Arctic Ocean and ∼70 % of the entire Arctic Ocean net freshwater flux variability, calculation see Chap. 3.7.2). Again, I illustrate this by cumulative freshwater transport anomalies (Fig. 5.5b, c). The cumulative anomalies of the freshwater inflow from the Pacific Ocean (northward transport through Bering Strait; green lines in Fig. 5.5b, c) are about 10 times smaller than the cumulative freshwater outflow anomalies into the Arctic Ocean (southward transport through the CAA, the Fram Strait and the Barents Sea Opening; blue lines in Fig. 5.5b, c). The cumulative freshwater transport anomalies of the Atlantic inflow (northward transport through the Fram Strait and the Barents Sea Opening; purple line in Fig. 5.5b) varies in opposing sense to the outflow to the Atlantic (blue line in Fig. 5.5b). However, the influence of the former on the Arctic Ocean freshwater content variability, indicated by the cumulative freshwater transport anomalies, is significantly smaller. For the upper Arctic Ocean it is close to zero as only the transport above the 34-isohaline is considered (purple line in Fig. 5.5c).

In the SANA, cumulative transport anomalies of the freshwater exchange with both, the subtropical North Atlantic as well as the Arctic Ocean, are high (range

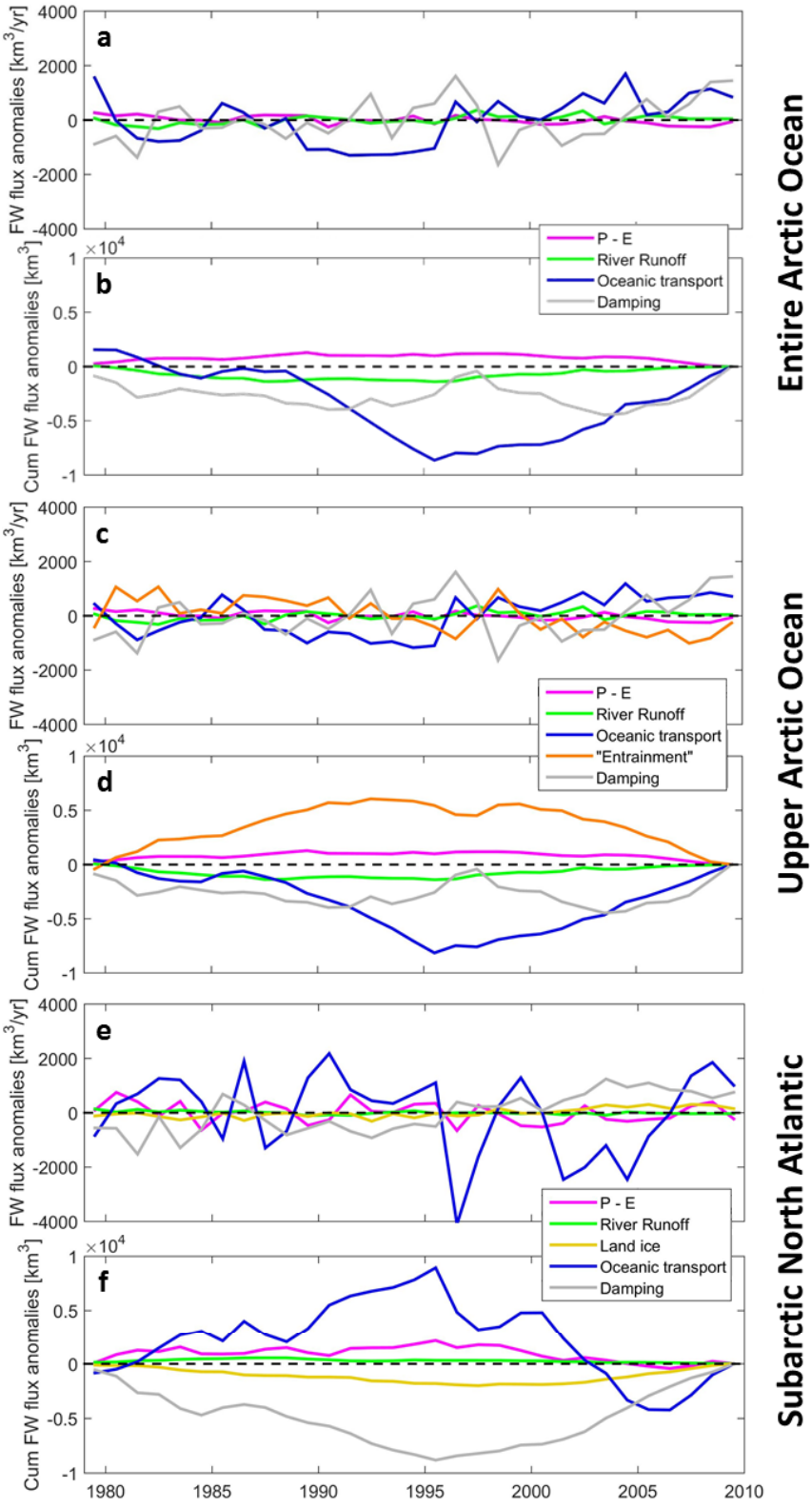


***Figure 5.4:*** *Freshwater flux variability. Anomalies relative to the 1979-2009 mean (a,c,e) and the cumulative anomalies (b,d,f) for the entire Arctic Ocean (a,b), the upper Arctic Ocean (c,d), and the SANA (e,f): net precipitation i.e. precipitation minus evaporation (P-E, magenta), river runoff (green), simulated net freshwater transport (solid + liquid; blue), the damping term from the model simulation (grey), the entrainment term (orange), and the freshwater flux from land ice (Bamber et al., 2018; yellow). Positive values indicate an anomalously freshwater input into the respective region.*

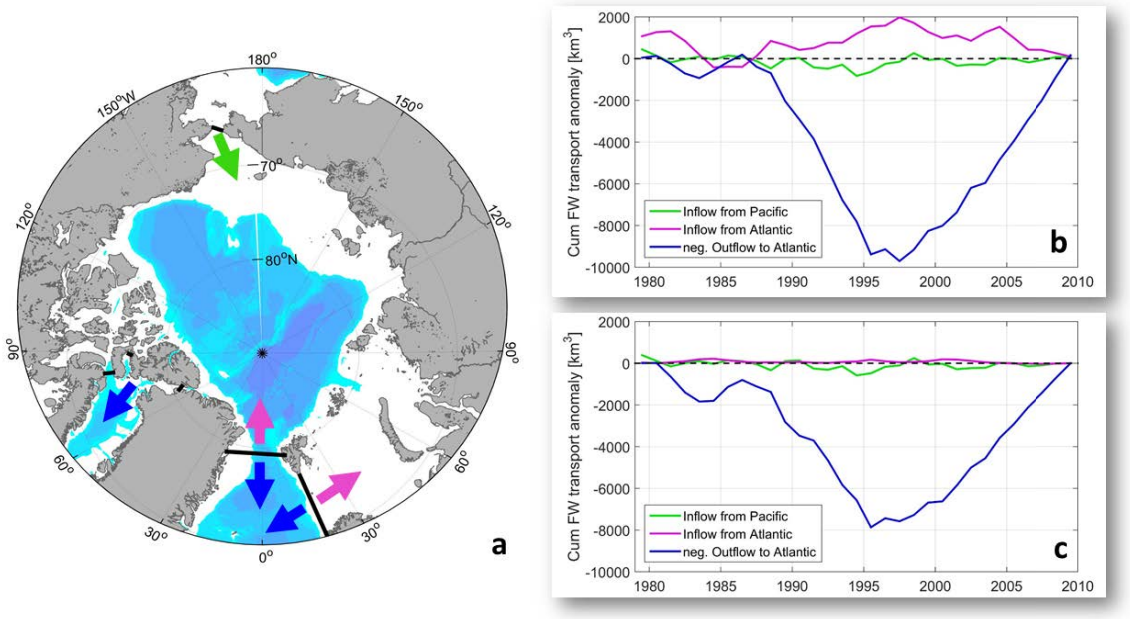


***Figure 5.5:*** *Arctic freshwater transport components. Simulated cumulative freshwater transport anomalies of the Arctic Ocean (b: full water column, $S_{ref}$ = monthly mean salinity of the entire Arctic Ocean, c: surface to 34-isohaline, $S_{ref}$ = 34): inflow from the Pacific Ocean (green) and the Atlantic (magenta), inverse outflow to the Atlantic (blue). Positive values indicate a net gain of fresh water for the region. The sections used for the transport calculations are indicated in the map (a).*

of cumulative anomalies > 9,000 km$^3$; yellow, red and dark blue lines in Fig. 5.6b). However, the transports from and to the Subtropics vary in a way that they largely balance each other, reducing the net influence on the freshwater content variability of the SANA (yellow and red lines in Fig. 5.6b). Still, the net oceanic transport in the model simulation (black line in Fig. 5.6c) is shaped by both, the oceanic exchange with the Arctic Ocean (range of cumulative anomalies ~10,000 km$^3$, ~19 % percentage variance; purple line in Fig. 5.6c) as well as with the subtropical North Atlantic (range of cumulative anomalies ~11,000 km$^3$, ~76 % percentage variance; orange line in Fig. 5.6c). When using the monthly mean salinity of the SANA as a reference ($S_{ref}$ ≈ 34.97-34.99; Fig. 3.11b), the cumulative freshwater transport anomalies are much higher for the outflow from the Arctic Ocean (dark blue line Fig. 5.6b) than for the inflow to the Arctic Ocean (magenta line Fig. 5.6b). The freshwater transports from the Hudson Bay and the North Sea have no significant effect on the freshwater content variability (light blue and green lines Fig. 5.6b).

Looking in more detail into the further transport components, the variability of southward freshwater transport from the Arctic Ocean displays a combination of southward freshwater transport variations in the Fram Strait and Barents Sea Opening (FB; liquid+solid) and in the CAA (liquid) (Fig. 5.7). The variability of

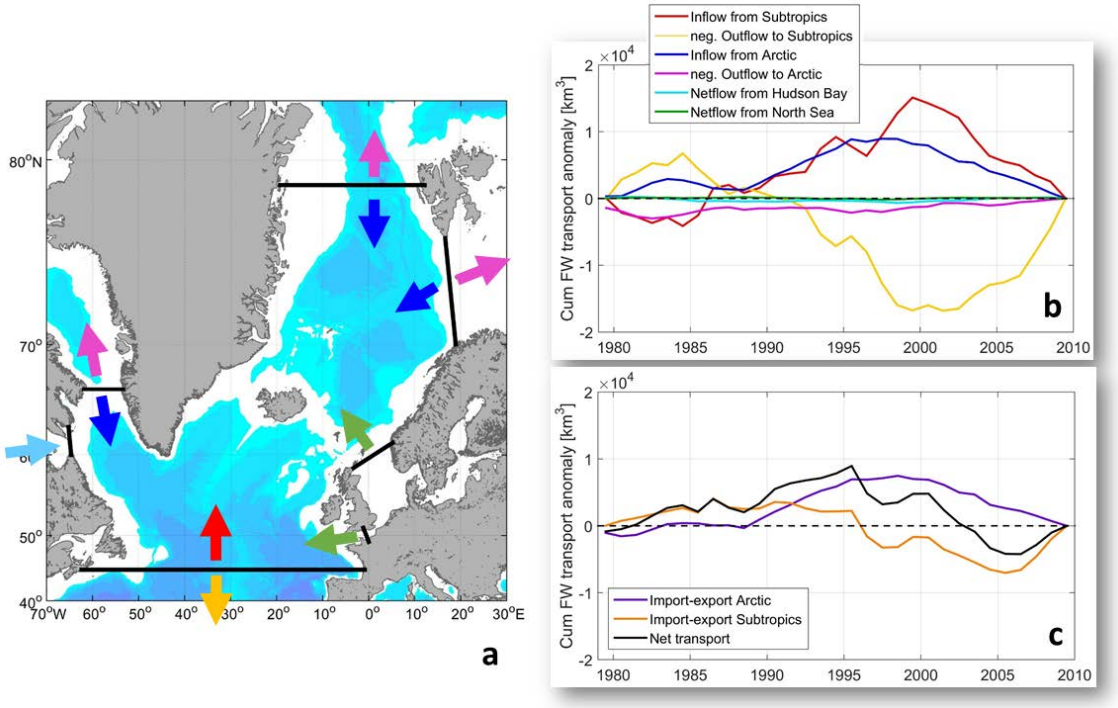


***Figure 5.6:*** *Subarctic freshwater transport components. Simulated cumulative freshwater transport anomalies of the SANA (full water column, $S_{ref}$ = monthly mean salinity of the SANA). a, b: inflow from the subtropical North Atlantic (yellow) and the Arctic Ocean (dark blue), inverse outflow from the subtropical North Atlantic (red) and Arctic Ocean (magenta), and net transport from the Hudson Bay (light blue) and from the North Sea (green). c: net transport from the Arctic Ocean (purple), net transport from the subtropical North Atlantic (orange) and net transport across all straits (black). Positive values indicate a net gain of fresh water for the region.*

the solid freshwater transport through the CAA is negligible (dashed purple lines in Fig. 5.7a, b). Although the transport anomalies are smaller for the upper Arctic Ocean (CAA: $\sigma$ ≈350 km$^3$/yr, FB: $\sigma$ ≈130 km$^3$/yr; Fig. 5.7b) than for the entire Arctic Ocean (CAA: $\sigma$ ≈530 km$^3$/yr, FB: $\sigma$ ≈320 km$^3$/yr; Fig. 5.7a), the temporal evolution is similar (CAA: r=0.998, FB: r=0.579).

The southward liquid freshwater transport through the CAA increased in the early 1980s and was anomalously high until the early 1990s (purple solid lines in Fig. 5.7a, b). Thereafter it decreased until the end of the 2000s. The liquid freshwater transport through the FB was anomalously low in the period 1983-1989 and anomalously high in the 1990s (green solid lines in Fig. 5.7a, b). After a short drop in the early 2000s, the anomalies stayed positive. The solid freshwater transport through the FB is highly variable in the first half of the time series with positive peaks in 1981/82, 1989 and 1995 and negative peaks in 1984/85 and 1996 (green dashed lines in Fig. 5.7a, b). From the late 1990s to the late 2000s the anomalies

stayed negative.

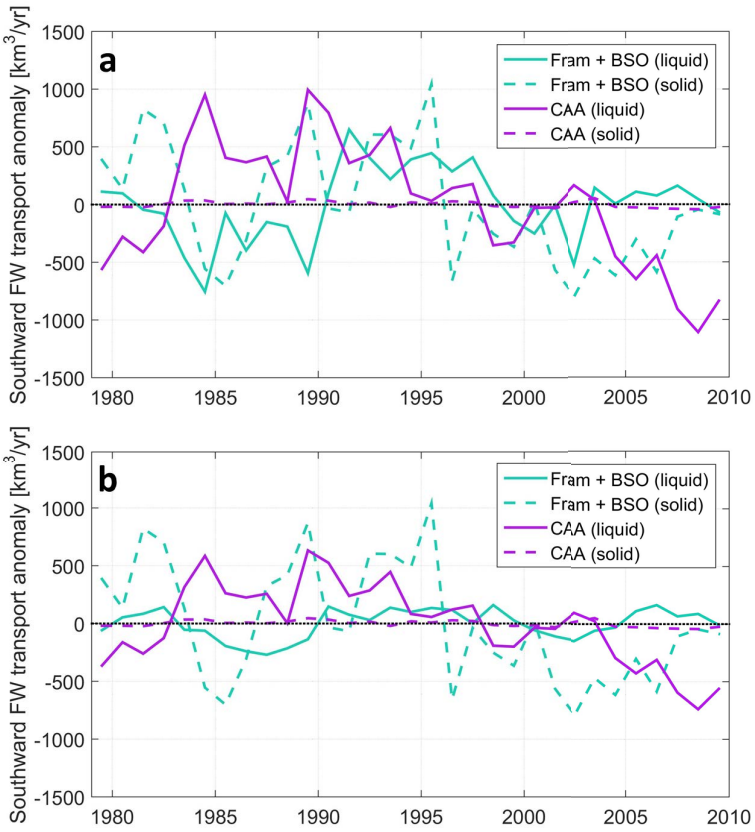


***Figure 5.7:*** *Simulated southward freshwater transport anomalies from the Arctic Ocean to the SANA (a: full water column, $S_{ref}$ = monthly mean salinity of the entire Arctic Ocean, b: Surface to 34-isohaline, $S_{ref}$ = 34): Fram Strait and Barents Sea Opening (BSO; green) and CAA (purple) liquid (solid lines) and solid (dashed lines) freshwater transport.*

Calculated for the SANA, the freshwater transport from the Arctic Ocean consists on the one hand of the southward freshwater transport through the FB and on the other hand of the southward freshwater transport through the Davis Strait (see Fig. 5.6a). Compared to the CAA (purple lines in Fig. 5.7a), the liquid freshwater transport anomalies through Davis Strait (solid purple line in Fig. 5.8a) are very similar (r=0.925), while the solid freshwater transport anomalies are about four times higher (r=0.567; dashed purple line in Fig. 5.8a). Although calculated with a different reference salinity, the liquid freshwater export anomalies through the FB (green solid line in Fig. 5.8a) show similar variability as calculated for the entire Arctic Ocean (r=0.666; green solid line in Fig. 5.7a).

The northward and southward freshwater transport across 45 °N are highly variable and co-varying (r = 0.806; Fig. 5.8b). Both transport anomalies show positive peaks in 1983, 1985/86, 1990, 1993 and 1997/98 and negative peaks in

1980, 1984, 1988, 1995/96 and 2003. In the last five years of the simulation both freshwater transport components decreased with a more pronounced decrease in the southward transport. I will come back to the covariability in the following discussion.

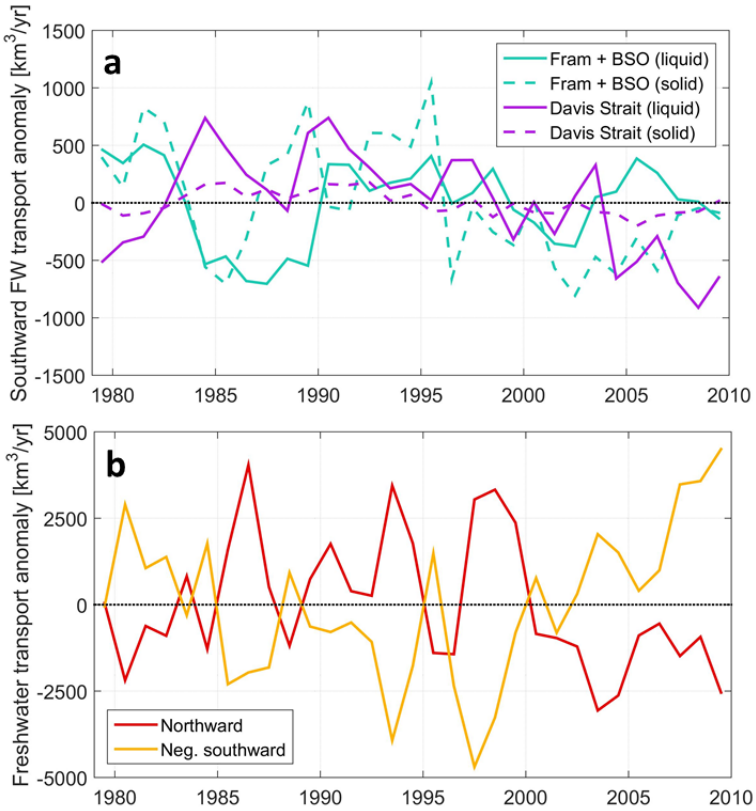


***Figure 5.8:*** *Simulated freshwater transport anomalies of the SANA (full water column, $S_{ref}$ = monthly mean salinity of the SANA). Southward freshwater transport from the Arctic Ocean to the SANA (a): Fram Strait and Barents Sea Opening (BSO; green) and Davis Strait (purple) liquid (solid lines) and solid (dashed lines) freshwater transport. Liquid freshwater transport across 45 °N (b): northward transport (red) and inverse southward transport (orange).*

Having analysed the different freshwater flux components, I will discuss their temporal variability and their effect on the freshwater content variability of the upper Arctic Ocean and the SANA. Therefore I will answer the second and third research question given in the beginning of this chapter.

### How did the freshwater fluxes change in the past decades?

In both regions, the net precipitation in the CORE-II forcing decreased over the 30 years of simulation (trend for both regions ≈ -10 km$^3$/yr$^2$; Fig. 5.4). As a consequence the artificial freshwater flux induced by the model from surface salinity restoring (damping) increased at the same time for compensation. However, in the

Arctic Ocean the positive linear trend in the damping term is 20 $km^3/yr^2$ larger than the negative trend in net precipitation and in the SANA it is even 50 $km^3/yr^2$ larger. As the negative trend in river runoff to the SANA of less than 5 $km^3/yr^2$ cannot explain this comparably strong increase, the damping needs to react to the upper ocean freshwater changes induced by advection from the adjacent oceans. The upper Arctic Ocean freshwater transport is positively correlated with the SANA damping term (r=-0.799) and explains ∼61 % of the variance.

River runoff shows a concise positive trend of ∼9 $km^3/yr^2$ in the Arctic Ocean, which agrees with findings of other studies: Syntheses of Arctic river discharge data revealed an increase of 7-10 % in the last 30 to 60 years correlated with the NAO and global mean surface air temperature (Peterson et al., 2002; Overeem and Syvitski, 2010). Niederdrenk et al. (2016) showed in a model study that a strong Icelandic low promoting warmer and wetter conditions over Eurasia leads to increased precipitation and thus enhanced river runoff to the Arctic Ocean. This mechanism is proposed to be responsible for the most of the Arctic river runoff variability. Although Déry and Wood (2005) found a 10 % decrease in annual river discharge from Canadian rivers into the Arctic Ocean and North Atlantic, the total river discharge into the Arctic Ocean increased by 5.6 $km^3/yr^2$ during the second half of the 20th century (McClelland et al., 2006).

Moreover, freshwater fluxes from land ice significantly increased in the last few decades (Fig. 5.4), which is mainly attributed to the warming atmosphere and ocean (e.g., Yang et al., 2016). The Greenland Ice Sheet mass-loss more than doubled from 2002 to 2009 (Velicogna, 2009). Yang et al. (2016) estimated the acceleration of the trend to 20 $Gt/yr^2$. Freshwater flux anomalies from surface meltwater and solid ice discharge from 1995 to 2010 sum up to about 3,000 $km^3$ (Bamber et al., 2012). Thereby the highest freshwater flux with an increase of about 50 % was released into the Irminger Sea and the Labrador Sea (Bamber et al., 2012).

Compared to variations in river runoff and net precipitation, the simulated oceanic freshwater transport clearly dominates the interannual to decadal freshwater flux variability (Fig. 5.4). In the Arctic Ocean, the highest variations appear in the freshwater export from the Arctic to the North Atlantic (Fig. 5.5). The liquid freshwater outflow through the CAA and the Fram Strait show large interannual variability, but no significant long-term trend, neither since the beginning of observational records (Haine et al., 2015) nor in my results from the model simulation. A new data record of Fram Strait area sea ice export, which was developed from satellite radar images and surface pressure observations across Fram Strait by Smedsrud et al. (2017), reveals a positive trend of about 5.9 % per decade from 1979 to 2014. However, this trend cannot be observed in the Fram Strait sea ice volume export from the FESOM simulation, which shows interannual variability ($\sigma$ ≈475 $km^3/yr$)

with a negative trend of ∼-20 $km^3/yr^2$. The increasing sea ice area export, but decreasing volume sea ice export would point to a decreased thickness of the sea ice. Observations presented by Woodgate et al. (2012) showed a slight increase in Bering Strait freshwater flux since 2001 due to increased volume fluxes which coincides with the results from the FESOM simulation.

Moreover, the freshwater exchange between the SANA and the subtropical North Atlantic shows high interannual variability (Fig. 5.8b) and no significant linear trend. Both, the northward and southward transport across 45 °N show parallel variations with a comparably high amplitude and rapid changes between positive and negative anomalies (r=0.806). In good agreement, observations and model results of the boundary currents at 47 °N by Mertens et al. (2014) show high interannual covariability of the northward and southward volume transport in the Newfoundland Basin. The volume import via the North Atlantic Current is compensated by the recirculation in the Newfoundland Basin, the Labrador Current as part of the subpolar gyre and the Deep Wester Boundary Current, which is the lower limb of the Atlantic meridional overturning circulation (Mertens et al., 2014). As the combined region of the Arctic Ocean and SANA is largely enclosed by landmasses and surface fluxes (including river runoff) do not add volume to the oceans in FESOM, the only difference between the northward and southward volume transports at 45 °N needs to result from the inflow through Bering Strait and ocean surface elevation changes. The variations in the simulated net volume transport across 45 °N explain less than 1 % of the variability of the net freshwater transport across 45 °N. Thus the net freshwater transport needs to largely result from variations in the salinity of the northward and southward transports across 45 °N. The recirculation of the North Atlantic Current will likely not experience large salinity changes between leaving the main branch of the North Atlantic and flowing back south across 45 °N. As the water masses of the Subpolar Gyre that later join the Deep Western Boundary Current travel a long distance at the surface before they reach the deep water formation sites and return south at depth, they are exposed to surface freshwater fluxes and can change their salinity by mixing with other water masses such as the fresh Greenland shelf waters. Precipitation is usually higher than evaporation in the SANA and adjacent water masses are mostly fresher than the subtropical waters of the North Atlantic Current. Therefore the outflow via the Deep Western Boundary Current is fresher (S≈34.8–34.9; e.g., Stramma et al., 2004) than the inflow via the North Atlantic Current (S>35.5 at the surface; e.g., Mertens et al., 2014). The Labrador Current is fed by fresh water from the Arctic Ocean via the East and West Greenland Currents and the Baffin Island Current. Thus the waters transported by the Labrador Current across 45 °N have the strongest contrast in salinity (S<34.8 at the surface; e.g., Mertens et al., 2014) to the northward flowing waters

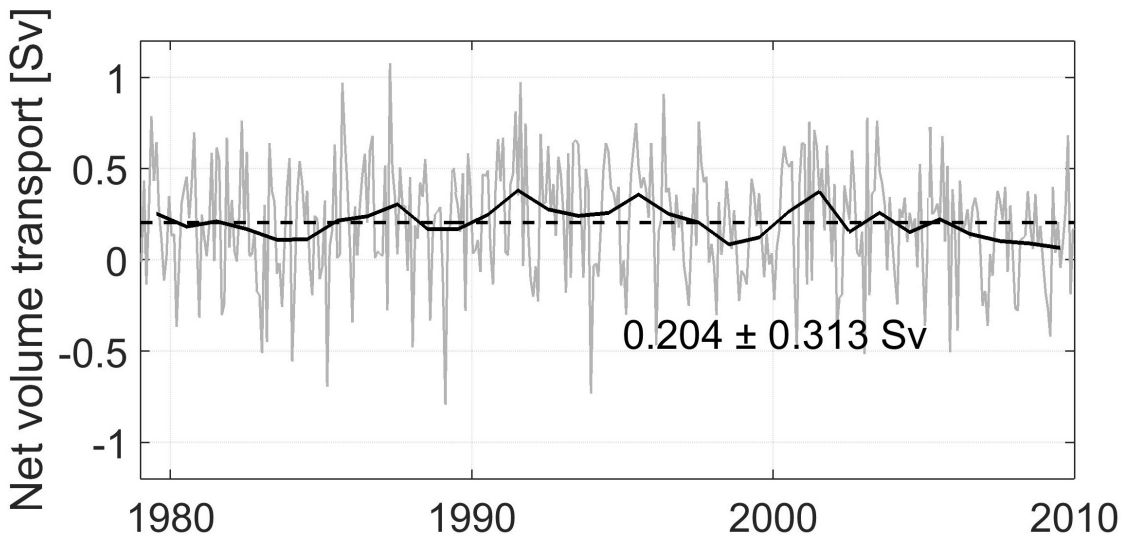


***Figure 5.9:*** *Simulated net volume transport across Bering Strait and 45 °N. Monthly means (gray solid line), annual means (black solid line) and the time mean (dashed black line) are shown. Positive values indicate a net volume input to the region. The mean volume imbalance is 0.204 Sv and the standard deviation is 0.313 Sv*

of the North Atlantic Current. Consequently, the net freshwater transport at 45 °N is also influenced by the freshwater export from the Arctic Ocean. The other way around,the Arctic freshwater export through the Fram Strait is influenced by the AW recirculation.

As described above, in the model the sum of ocean volume change (due to sea surface height changes) and all oceanic volume transports of a defined region needs to equal zero. However, the calculated volume transports across Bering Strait and the section at 45 °N are not balanced (Figure 49). The imbalance of ∼0.2 Sv cannot be explained by the sea surface height change in the Arctic Ocean and SANA (equivalent to a volume transport of <0.3 mSv). Therefore it needs to result from the interpolation errors. Due to the grid size and section length I expect the interpolation error to be significantly higher at 45 °N than in the Bering Strait. This implies that the calculated inflow from the subtropics is overestimated and thereby the salt inflow might be overestimated as well. Unfortunately, there are no observational transport data across the North Atlantic close to 45 °N for comparison.

**Which freshwater flux component had the largest effect on the freshwater content changes of the upper Arctic Ocean and of the SANA in the model?**

Due to conservation, the freshwater content changes of a defined region need to equal the sum of all freshwater fluxes to this region (see Chap. 3.4). However, I do not consider the diffusive transports in my study and be aware of interpolation errors in the calculated advective transports. Still, the net freshwater fluxes including the oceanic transport (advection only), net precipitation, river runoff and damping term (and local sea ice melt for the SANA) are able to represent most of the variability in the freshwater storage (derivative of freshwater content) in both, the Arctic Ocean ($P_V$=60.76 %, r=0.783; Fig. 5.10a) and the SANA ($P_V$=54.62 %, r=0.762; Fig. 5.10b). Therefore I will use the variability of the net freshwater flux (comprising the terms described above) as the representation of freshwater content changes in the following discussion.

The variability in the simulated upper Arctic Ocean freshwater content can be explained by the oceanic transport (r=0.721, $P_V$=51.25 %), the damping term (r=0.749, $P_V$=55.81 %) and the entrainment term (r=-0.652, $P_V$=41.14 %). The freshwater fluxes from the damping term and from the entrainment term covary in opposing sense (r=-0.468; Fig. 5.4c, d). The entrainment seems to compensate the damping and thereby is likely to be artificially high in the model. Moreover, surface salinity restoring induces an artificial freshwater flux in the model, that is needed to keep the salinity in the model close to observations, but is absent in the real world. Having this in mind, I propose that the observed freshwater content changes in the upper Arctic Ocean are largely due to variations in the oceanic freshwater transport. In the model, the variability of the upper Arctic Ocean net freshwater transport is clearly dominated by variations in the freshwater export to the North Atlantic ($P_V$=88.87 %). Thereby the largest part of the variance is explained by the sea ice export through FB ($P_V$=57.80 %), followed by the liquid freshwater export through the CAA ($P_V$=38.08 %), the liquid freshwater export through the FB ($P_V$=9.95 %) and the sea ice export through the CAA ($P_V$=2.93 %).

In the SANA, the simulated liquid freshwater storage variability is clearly best explained by variations in the oceanic freshwater transport (r=0.901, $P_V$=79.98 %), which is composed of the freshwater exchange with the Arctic Ocean (r=0.443, $P_V$=19.09 %) and the freshwater exchange with the subtropical North Atlantic (r=0.871, $P_V$=75.86 %). Thereby the exchange with the Arctic Ocean is dominated by the southward freshwater transport component, whereas the southward and northward freshwater transport components at 45 °N are equally important. This means that in the model the oceanic freshwater fluxes at the southern bound-

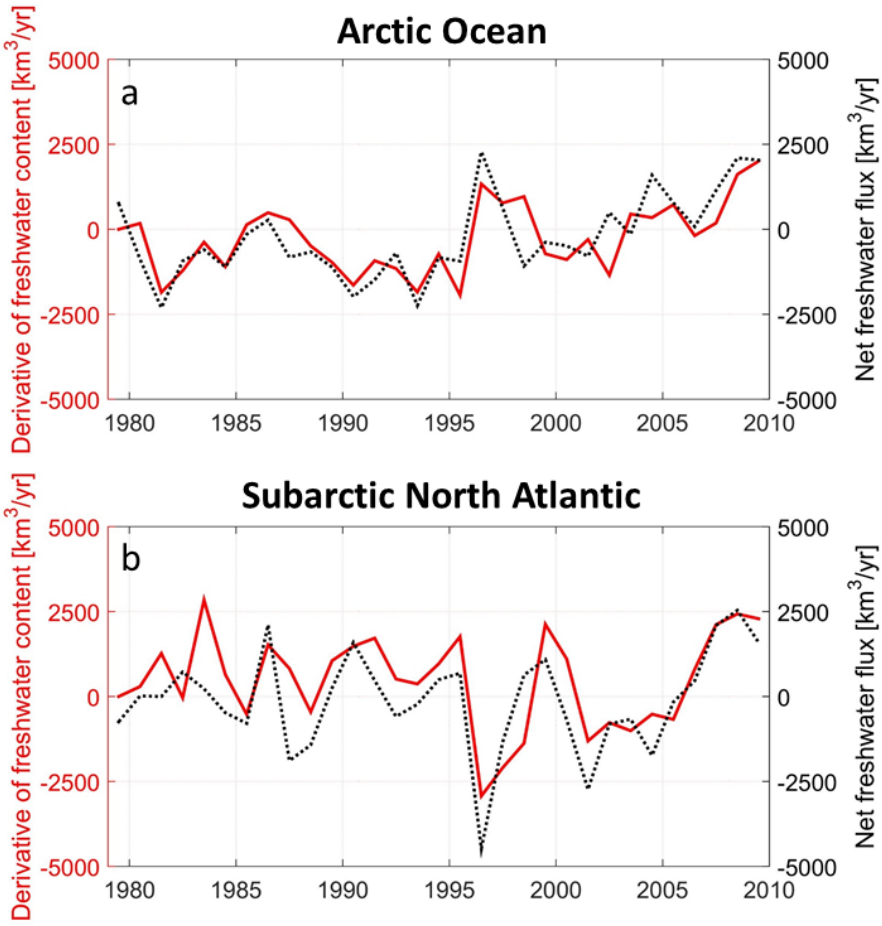


***Figure 5.10:*** *Comparison of simulated freshwater storage and net freshwater flux. a: derivative of total freshwater content for the entire Arctic Ocean ($S_{ref}$ = 35) and the net freshwater flux including net precipitation, river runoff, oceanic transport (full water column, $S_{ref}$ = monthly mean salinity of the Arctic Ocean) and the damping. b: derivative of liquid freshwater content of the SANA ($S_{ref}$ = 35) and the net freshwater flux including net precipitation, river runoff, oceanic transport (full water column, $S_{ref}$ = monthly mean salinity of the Arctic Ocean), local sea ice melt and the damping.*

ary of the SANA have a higher impact on the liquid freshwater content of the SANA than the oceanic freshwater fluxes at the northern boundary. In contrast to the Arctic Ocean however, the simulated freshwater content in the lower latitudes differs significantly from observations (Fig. 4.10). The used FESOM setup was optimised for the Arctic Ocean and Nordic Seas with an increased resolution and a good representation of the physical processes there, but a lower resolution towards lower latitudes. Therefore eddies that are important for transporting waters from the West Greenland, East Greenland and Labrador Currents into the Labrador Sea are not resolved; although the effect of eddies is parameterised. In this model simulation, waters of polar origin are transported along the shelves of the Labrador Sea with

low mixing into the interior of the basin (Claudia Wekerle, Alfred Wegener Institute, Bremerhaven, pers. comm.). This might result in a higher than expected freshwater export to the subtropical North Atlantic via the extension of the Labrador Current. Moreover, the study by Müller et al. (2017) highlights the importance of eddies on the freshwater transport of the North Atlantic Current across 47 °N (close to the southern boundary of my study area). These eddies are also not resolved by the used model simulation. Since there are no transport observations at 45 °N to compare with, I calculated the freshwater content of the subtropical North Atlantic from 20 to 45 °N from the CORA salinity fields. The resulting values are very different from the simulated ones (Fig.5.11).

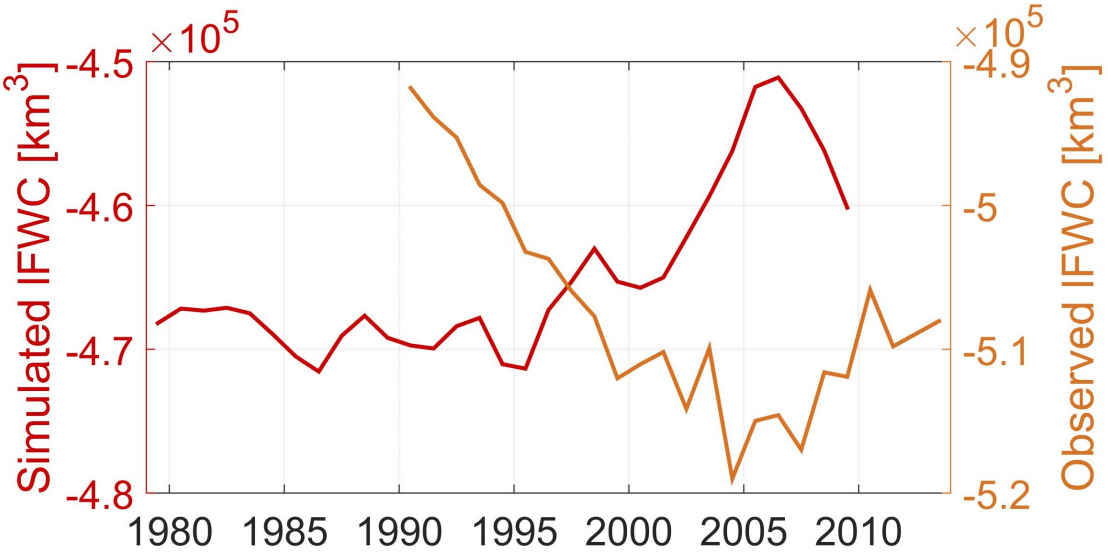


***Figure 5.11:*** *Comparison of the liquid freshwater content (lFWC) of the subtropical North Atlantic (20 45 °N) from observations (orange) and from the model simulation (red). Both time series have been calculated with the reference salinity* $S_{ref} = 35$.

Moreover, the simulated freshwater content of the SANA differs the most from the observations where anomalies of the net freshwater transport at the southern boundary are the highest (Fig. 4.10; Fig. 5.8b). Therefore I cannot conclude from the model simulation what effect the exchange with the subtropical North Atlantic has on the SANA freshwater content. However, the increased freshwater transport from the Arctic Ocean in the early 1980s and early 1990s that sum up to an addition of ∼8,000 km$^3$ to the SANA by the mid-1990s and the decreasing freshwater transport thereafter (Fig. 5.6b) agree well with the observed increase in the SANA liquid freshwater content in the 1990s and the decrease in the late 2000s (Fig. 4.10). Moreover, changing freshwater transports from the Arctic Ocean to the SANA could explain the observed anti-correlation of the upper Arctic Ocean total freshwater content and

the SANA liquid freshwater content (Fig. 4.14).

### 5.2.2 Salinity versus volume driven freshwater transport

In order to distinguish whether the freshwater transport variability is due to variations in the volume transport or due to variations in the salinity of the transported waters (or both), I display the salinity driven, volume driven and non-linear freshwater transports (for the calculation see Chap. 3.5) for the southward transport through the CAA and the Davis Strait (Fig. 5.12), for the southward transport through the FB (Fig. 5.13), and for the exchange with the subtropical North Atlantic (Fig. 5.14). This gives me first indications for the driver of the freshwater transport variability that I will further analyse in the next chapter.

In the CAA and the Davis Strait the southward freshwater transports are mainly driven by volume transport anomalies, which are highest in the mid-1980s to early 1990s and decrease towards the 2000s (blue lines in Fig. 5.12). However, in the Davis Strait there are two more peaks in the volume driven part of the freshwater transport in 1997 and 2003 (blue line in Fig. 5.12c). There are also smaller variations in the salinity driven freshwater transport through the Davis Strait ($\sigma$ ≈160 km$^3$/yr; purple line in Fig. 5.12c), which are less in the transport through the CAA (Entire Arctic Ocean: $\sigma$ ≈70 km$^3$/yr, Upper Arctic Ocean: $\sigma$ ≈60 km$^3$/yr; purple lines in Fig. 5.12a, b). The non-linear term is close to zero (green line in Fig. 5.12).

In the FB freshwater export all three components show high interannual and decadal variability (Fig. 5.13). The volume driven freshwater transport anomalies calculated for the SANA were mostly positive in the early 1980s, changed sign in the late 1980s/early 1990s followed by an increase until 2005 and a drop thereafter ($\sigma$ ≈220 km$^3$/yr; blue line in Fig. 5.13c). The volume driven component calculated for the upper Arctic Ocean shows similar variations (r=0.891) with smaller amplitudes ($\sigma$ ≈80 km$^3$/yr; blue line in Fig. 5.13b). The volume driven freshwater transport calculated for the entire Arctic Ocean also shows high interannual variability ($\sigma$ ≈200 km$^3$/yr; blue line in Fig. 5.13a), but differs significantly from the volume driven freshwater transport calculated for the SANA (r=0.353). The salinity driven freshwater transport was low in the 1980s and early 2000s and high in the 1990s and late 2000s (magenta lines in Fig. 5.13a-c). The non-linear term was low in the mid-1980s, around the year 2000 and in the late 2000s and high in the early 1980s, between the late 1980s and late 1990s and in the early/mid-2000s (green lines in Fig. 5.13a-c).

The southward freshwater transport across 45 °N is predominantly driven by variations in the volume transport ($\sigma$ ≈2,680 km$^3$/yr; blue line in Fig. 5.14a), but also

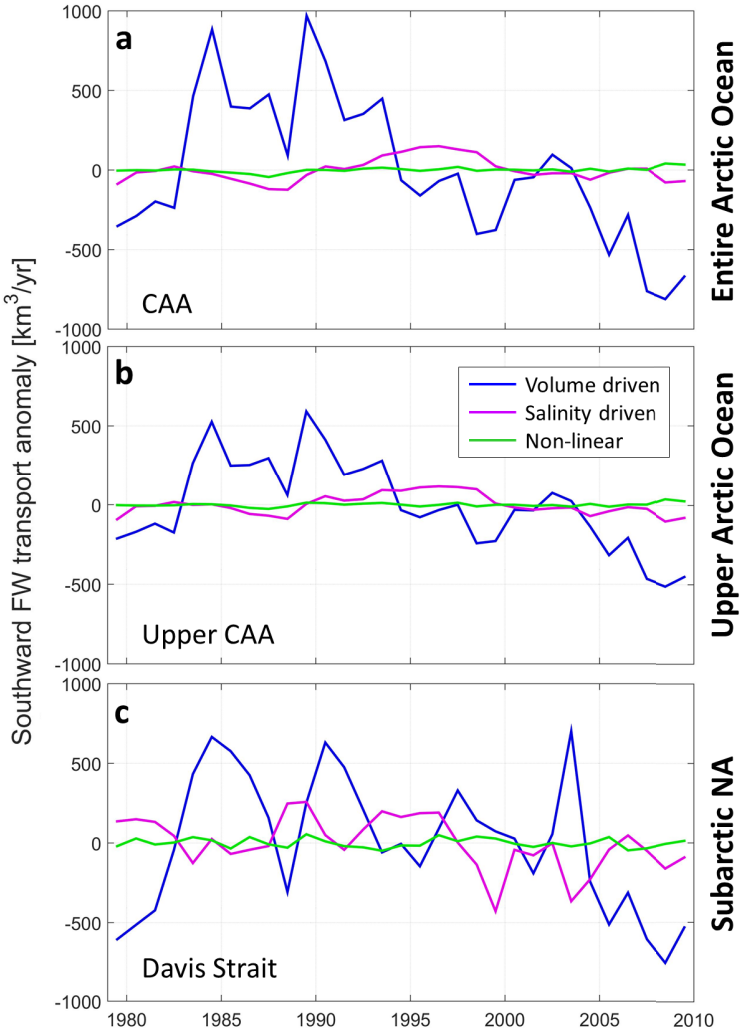


***Figure 5.12:*** *Salinity and volume driven Arctic freshwater export through the CAA and Davis Strait. Southward freshwater transport anomalies through the CAA (a, b) and the Davis Strait (c) (a: full water column, $S_{ref}$ = monthly mean salinity of the Arctic Ocean, b: surface to 34-isohaline, $S_{ref}$ = 34, c: full water columnm, $S_{ref}$ = monthly mean salinity of the SANA): volume driven component (blue), salinity driven component (magenta) and non-linear component (green). For the calculation of these components see Chap. 3.5.*

shows interannual to decadal variability in the non-linear term ($\sigma$ ≈1,990 km$^3$/yr; green line in Fig. 5.14a). The volume driven freshwater transport was increasing from the 1979 to the early/mid-2000s and then dropped in 2007 to 2009 (blue line in Fig. 5.14a). The non-linear transport anomalies were rather positive in the 1980s and 1990s followed by a sharp decrease to negative anomalies in the years after (green line in Fig. 5.14a). The variability of the salinity driven component is significantly smaller than the variability of the other components ($\sigma$ ≈420 km$^3$/yr; magenta line in Fig. 5.14a).

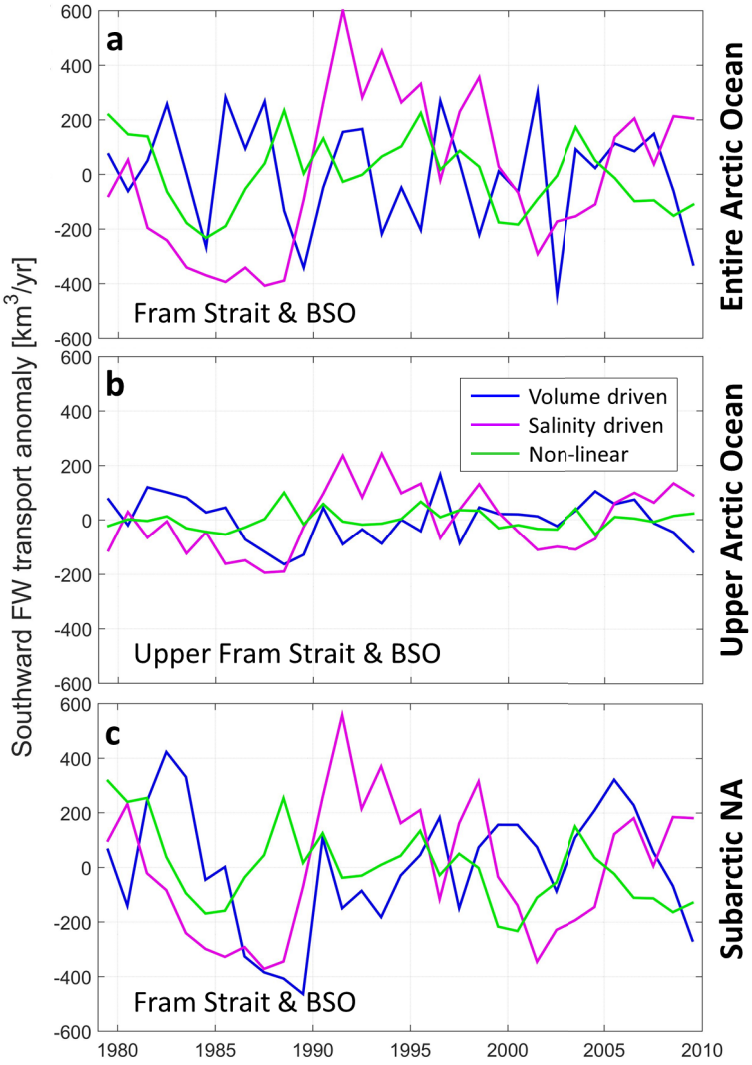


***Figure 5.13:*** *Salinity and volume driven Arctic freshwater export through FB. Southward freshwater transport anomalies through the FB (a: full water column, $S_{ref}$ = monthly mean salinity of the Arctic Ocean, b: surface to 34-isohaline, $S_{ref}$ = 34, c: full water column, $S_{ref}$ = monthly mean salinity of the SANA): volume driven component (blue), salinity driven component (magenta) and non-linear component (green). For the calculation of these components see Chap. 3.5.*

The northward freshwater transport across 45 °N is also predominantly driven by volume transport variations ($\sigma$ ≈3,040 km$^3$/yr; blue line in Fig. 5.14b) similar to those in the southward component (r=0.680; blue line in Fig. 5.14a), but with a more pronounced drop in 1995 to 1997. Both, the salinity driven ($\sigma$ ≈1,700 km$^3$/yr; magenta line in Fig. 5.14b) and the non-linear component ($\sigma$ ≈1,940 km$^3$/yr; green line in Fig. 5.14b) show a similar temporal evolution as the southward non-linear freshwater transport (r=0.885 and r=0.973, respectively; green line in Fig. 5.14a). For both directions the non-linear component of the freshwater transport is compa-

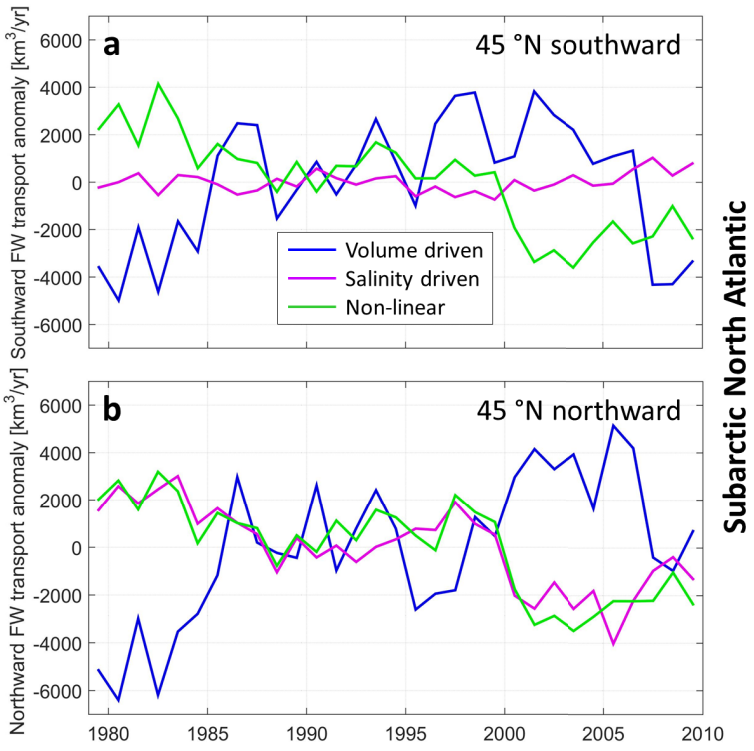


***Figure 5.14:*** *Salinity and volume driven subpolar – subtropical freshwater exchange. Southward (a) and northward (b) freshwater transport anomalies across 45 °N (full water column, $S_{ref}$ = monthly mean salinity of the SANA): volume driven component (blue), salinity driven component (magenta) and non-linear component (green). For the calculation of these components see Chap. 3.5.*

rably strong.

These findings allow answering my last research question concerning the freshwater flux variability in the following and will be used for the analyses of the driver of the observed freshwater content changes in the next chapter.

**Are the changes in the freshwater transport between the Arctic Ocean and the SANA rather driven by changes in volume flux or due to changes in the salinity of the transported water?**

The freshwater transport variability in the CAA, Davis Strait and across 45 °N is predominantly driven by changes in the volume transport (Fig. 5.12, Fig. 5.14). In contrast, the southward freshwater transport through the FB is driven by both, changes in the volume flux as well as changes in the salinity of the advected waters (Fig. 5.13). This is also supported by model results of Jahn et al. (2010a). Moreover, the non-linear term is comparably strong in the exchange with the subtropical North

Atlantic at 45 °N (Fig. 5.14) and in the southward freshwater transport through the FB (Fig. 5.13). This means that the volume transport and the salinity of the transported waters are partly covarying. At 45 °N this could be related to the strength of the the subpolar gyre and the related changes in the strength of the North Atlantic Current. When the volume transport of the North Atlantic Current increases, the effective salinity of the waters transported northwards across 45 °N will increase. The other way around, an increased volume transport of the Labrador Current would decrease the effective salinity of the waters transported southwards across 45 °N. In the Fram Strait an intensified transport in the fresh surface layer would increase the volume transport and at the same time decrease the effective salinity of transported waters. This is not the case in the CAA where the waters are more homogeneous throughout the water column and salinities are less variable (Fig. 5.12). The different driver of the volume and salinity variations in the transport from the Arctic Ocean to the SANA are analysed and discussed in the following chapter.

# Chapter 6

# Drivers of freshwater content variability

*In this chapter I present the results from the analysis of possible drivers for the freshwater variability in the Arctic Ocean and SANA. The chapter starts with a short literature review, introducing the research questions and showing long term means of sea level pressure, wind stress, sea surface height and upper ocean circulation of the northern high latitudes. I further compare the Arctic Ocean and SANA freshwater variability to fluctuations in the large-scale atmospheric oscillation indices (Chap. 6.1). This is followed by regression and correlation analyses to isolate possible atmospheric forcing patterns that drive the exchange between the two ocean basins (Chap. 6.2). Finally I present the atmospheric conditions during the time of freshwater content observations in both regions in order to find indications for the processes that have caused the rapid freshwater changes (Chap. 6.3). All results are discussed with regard to my research questions at the end of each section. The paragraphs marked with an asterisk (*) are taken from Campos and Horn (2018).*

---

As shown by the model results in the previous chapter, the freshwater content variability of the Arctic Ocean and SANA is mainly caused by variations in the oceanic transport. Thereby the exchange between the two ocean regions plays an important role for the freshwater content of both regions and can largely explain the observed anti-correlation. Many studies have investigated possible drivers of the freshwater transport on both sides of Greenland and proposed different chains of physical mechanisms. The latter are partly related to the prominent large-scale atmospheric oscillation patterns of the region, the AO and NAO (see Chap. 3.1.5), as follows.

The freshwater export from the Arctic Ocean through the various channels of the CAA was found to vary mainly due to volume flux anomalies (Fig. 5.12). The vari-

ations appear to be driven by variations in the large-scale atmospheric circulation (e.g., Jahn et al., 2010a,b; Peterson et al., 2012) which modulate the sea surface height gradient across the strait (e.g. McGeehan and Maslowski, 2012; Wekerle et al., 2013). Proshutinsky and Johnson (1997) identified two wind-driven circulation regimes in the Arctic Ocean that either accumulate fresh water in the western Arctic Ocean (anticyclonic) or release it to the North Atlantic (cyclonic). During anticyclonic circulation regimes fresh water accumulates in the Beaufort Gyre north of the CAA due to a wind-driven spin-up as a response to anomalously high sea level pressure over the Arctic (negative AO/NAO). During cyclonic regimes (positive AO/NAO) the Beaufort Gyre slows down due to cyclonic wind anomalies and releases the accumulated fresh water (Giles et al., 2012; Proshutinsky et al., 2002). This fresh water mainly exits the Arctic via the CAA and to a lesser extent via the Fram Strait. A tracer simulation study by Jahn et al. (2010b) showed that the main sources of the freshwater export through the CAA are PW and North American runoff. Although the Arctic Ocean circulation alternated between the cyclonic and anticyclonic pattern at 5 to 7 year intervals in the past, it has remained in an anticyclonic mode for 17 years since 1997 (Proshutinsky et al., 2015). Proshutinsky et al. (2015) speculated that freshwater fluxes from the Greenland Ice Sheet to the North Atlantic interrupted an ocean–atmosphere feedback loop that previously lead to an automatic decadal alternation between cyclonic and anti-cyclonic circulation regimes ("auto-oscillatory system").*

The variability of liquid freshwater export through Fram Strait was found to be driven by both, variations in the volume flux and changes in the salinity of the advected waters (Fig. 5.13; Jahn et al., 2010a). The salinity of the waters exported through Fram Strait depends on the source water which was found from a tracer simulation study to be mainly Eurasian runoff or PW (Jahn et al., 2010b). This study proposes that during years of an anticyclonic circulation anomaly (negative AO) Eurasian runoff is released from the Eurasian shelf (Jahn et al., 2010b). Morison et al. (2012) further suggest from their observational study that these shelf waters are directed towards Fram Strait by a strong Transpolar Drift. During a cyclonic circulation regime (positive AO) the Eurasian runoff is kept by a cyclonic circulation in the Eurasian basin (Morison et al., 2012). PW that is released from the Beaufort Gyre during positive AO periods is found to flow along the northern shelf of Greenland and to penetrate into Fram Strait (Jahn et al., 2010b). In agreement with this, Karcher et al. (2012) found, from iodine-129 observations and modeling, changing contributions of AW and PW in the Fram Strait outflow to result from changes in the Arctic Ocean circulation as a response to the large-scale atmospheric circulation. Ionita et al. (2016) related changes in the simulated Fram Strait sea ice export to atmospheric blocking events over Greenland during negative NAO phases,

which block the winds over the strait that mainly drive the southward sea ice transport. These Greenland blocking events are proposed to happen more frequently in recent years due to climate change (e.g., Hanna et al., 2016).*

To identify the key processes and physical mechanisms driving the freshwater content variability of the Arctic Ocean and SANA, I addressed the following questions:

- How do the freshwater content and transport variability compare to the large-scale atmospheric circulation variability?
- What drives the oceanic exchange between the Arctic Ocean and SANA in the model?
- What caused the observed rapid changes in the Arctic Ocean and SANA freshwater contents in 2002-2004 and after 2011?

In order to answer the first two questions, I used the CORE-II sea level pressure (see Chap. 3.1.3), wind stress fields which are used to force the FESOM simulation (see Chap. 3.2.1), and the simulated FESOM sea surface height and upper ocean circulation (surface to 200 m water depth). As the forcing dataset and the model simulation end in 2009, I used fields of sea level pressure and wind at 10 m above sea level from the NCEP/DOE Reanalysis 2 dataset (see Chap. 3.1.4) for answering my third research question.

For comparison with the pattern later described in this chapter, the long-term mean sea level pressure, wind stress, sea surface height and upper 200 m ocean circulation fields for the simulation period 1979-2009 are shown in Fig. 6.1. The high pressure system in the Canadian Arctic is the Beaufort High and the low pressure system next to Iceland is the Iceland Low. The difference to the higher pressure over Greenland on the one side and the higher pressure at lower latitudes on the other side drive intense southward winds along the East Greenland coast and the westward winds over the subpolar North Atlantic (Fig. 6.1a).

The sea surface height in the Canada Basin is elevated compared to that on the Arctic shelves and in the Eurasian Basin which is associated with the anticyclonic Beaufort Gyre circulation (Fig. 6.1b). The other way around, the sea surface height in the Irminger Sea, Labraor Sea and Newfoundland Basin is strongly lowered compared to that on the shelves of the western subpolar North Atlantic which is associated with the cyclonic Subpolar Gyre. Furthermore, the sea surface in the Nordic Seas deep basins is lower than on the shelves with related geostrophic southward flow along the western shelf (East Greenland Current) and northward flow along the eastern shelf (Norwegian Atlantic Current).

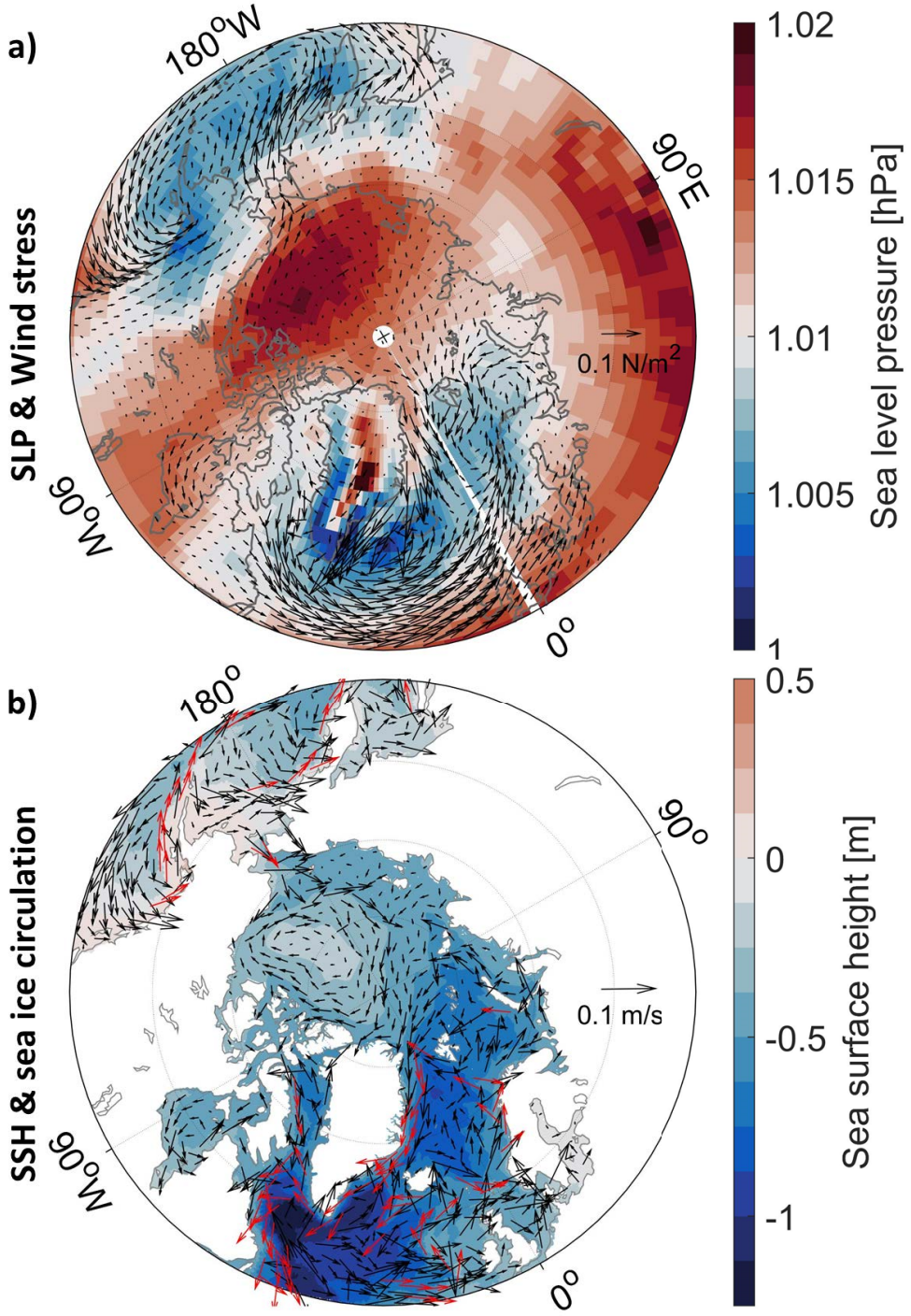


***Figure 6.1:*** *Long-term mean of CORE-II sea level pressure (SLP) and wind stress used as FESOM forcing (a), as well as sea surface height (SSH) and upper 200 m ocean circulation from the FESOM simulation (b) for the period 1979-2009. For the upper ocean circulation red arrows indicate velocities higher than 0.1 m/s and are set to a constant length (b).*

**General Remark**

For simplicity I use in the following the words export and import for the different directional transport components perpendicular to the sections in Fram Strait, Barents Sea Opening and the channels of the CAA. By export I mean the transport from the Arctic Ocean to the Baffin Bay and the Nordic Seas, respectively. Consequently the transport into the Arctic Ocean is referred to as import. Net transports are import minus export.

## 6.1 Relation of freshwater variations to atmospheric oscillation

Many of the processes described above are related to an anomalous amplitude of the AO and/or NAO. Variations of both atmospheric oscillation indices reflect variations of the large-scale atmospheric pressure patterns. These are associated with varying wind fields driving the upper ocean circulation and thus they can be expected to correlate with freshwater transport variations. To investigate a possible relationship of NAO and AO to the freshwater changes in the Arctic Ocean and SANA, I compared the simulated net freshwater transports of both regions to the oscillation indices (Fig. 6.2). Moreover, I calculated the correlation of the oscillation indices and the net freshwater transports as well as those freshwater transport components that show the highest variability (Tab. 6.1-6.3).

The simulated net freshwater transport of the entire Arctic Ocean and upper Arctic Ocean are higher correlated with the AO index than with the NAO index (Tab. 6.1-6.2). When considering the low-frequency variability (7 years running means) the correlation with the AO becomes statistically significant (95 % confidence) at a lag of 2 years. Moreover, all freshwater export components of the Arctic Ocean (trhough FB and CAA, solid and liquid) are significantly correlated with the AO when considering only the low-frequency variability (Tab. 6.1-6.2). Thereby the liquid and solid freshwater export through the CAA is positively correlated at zero lag, while the exports through the FB are lagging 2 to 4 years. Interestingly the liquid freshwater export through the FB is also significantly anti-correlated with the AO lagging 3 to 5 years (only given in the tables, when the anti-correlation was higher than the positive correlation).

Further the net freshwater transport of the SANA is significantly correlated with the AO at zero lag, but weakly correlated with the NAO (Tab. 6.3). However, in this case the correlation with the AO is only statistically significant within the 90 %

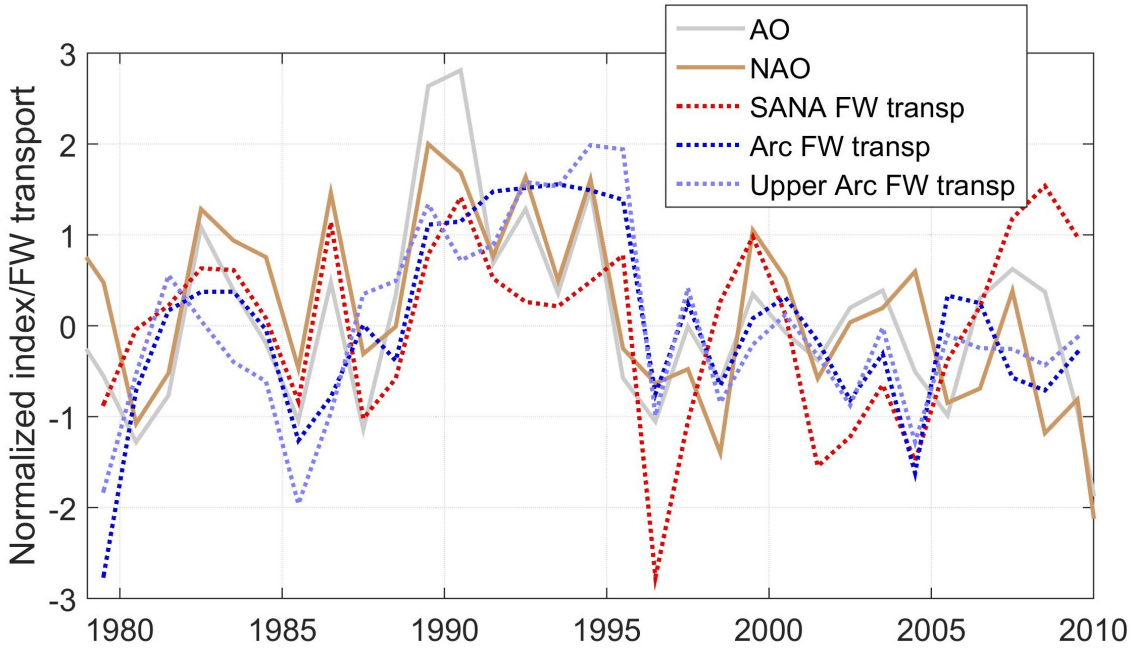


***Figure 6.2:*** *Annual means of simulated net total (solid +liquid) freshwater transport of the SANA (red dotted), the entire Arctic Ocean (inversed; dark blue dotted) and the upper Arctic Ocean (inversed; light blue dotted) compared to annual means of the AO index (grey solid) and the NAO index (brown solid). All time series have been demeaned, detrended and normalised by their standard deviation.*

confidence interval for the annual mean and not for the 7 year running mean. Looking at the freshwater transport components, again the FB liquid and solid freshwater export and the AO are significantly correlated at 2 to 4 years lag. Moreover, the AO and the liquid freshwater export through the FB are again significantly anti-correlated with the transport leading 4 to 5 years. For the Davis Strait freshwater export only the solid part shows significant correlation with the AO. The northward and southward freshwater transports across 45 °N are showing neither a significant correlation with the AO nor with the NAO (Tab. 6.3).

To find possible long-term connections between the observed freshwater content variations and atmospheric oscillations, I used the 50-year time series of the subpolar North Atlantic freshwater content derived from Mauritzen et al. (2012) for comparison with the AO and NAO index. Furthermore, I used the freshwater content time series from the model simulation for comparison. As the indices themselves are related to freshwater transports (Fig. 6.2) and the freshwater transports are related to the derivative of the freshwater content (Chap. 3.4), I used the cumulative atmospheric oscillation indices for comparison with the freshwater content. This comparison reveals a significantly positive correlation of the pentadal mean liquid freshwater content of the subpolar North Atlantic (Mauritzen et al., 2012) with the

pentadal means of both cumulative indices (Fig. 6.3), the AO index (r=0.91, at zero lag, N*=3.67, p=0.025) and the NAO index (r=0.95, at zero lag, N*=3.67, p=0.012). However, the annual mean simulated liquid freshwater content of the SANA is only weakly positive correlated with the cumulative AO index (r=0.20, at zero lag, N*=3.1, p=0.743) and cumulative NAO index (r=0.42, at -1 year lag, N*=3.1, p=0.474). Further the annual mean simulated total freshwater content of the upper Arctic Ocean is weakly negative correlated with the cumulative AO index (r=-0.37, at -1 year lag, N*=3.1, p=0.534) and the cumulative NAO index (r=-0.48, at zero lag, N*=3.1, p=0.409 ). The correlation coefficients more than double when comparing the AO with the low frequency variability (7 years running means) of the freshwater content of the SANA and the upper Arctic Ocean.

***Table 6.1:*** *Maximum correlations (for $|lag| <= 5$ years) of the AO/NAO and the freshwater transports for the entire Arctic Ocean (top to bottom, $S_ref$ = mean salinity of the Arctic Ocean). Lags are given in years and positive lags indicate the freshwater transport lagging the AO/NAO indices. Significant correlations at a 90 % confidence level are given in bold face. The correlation coefficient r, the effective degrees of freedom N* and the p-value are explained in Chap. 3.7.3.*

| ***Entire*** | AO | | | | NAO | | | |
|---|---|---|---|---|---|---|---|---|
| ***Arctic Ocean*** | r | lag | N* | p-value | r | lag | N* | p-value |
| *Net tfw transport* | | | | | | | | |
| annual mean | -0.528 | 0 | 4.43 | 0.2608 | -0.395 | 1 | 4.43 | 0.4167 |
| 7 year running mean | **-0.864** | **2** | **5.00** | **0.0122** | -0.710 | 3 | 3.57 | 0.1529 |
| *CAA lfw export* | | | | | | | | |
| annual mean | 0.455 | 0 | 6.20 | 0.2504 | 0.456 | 0 | 5.17 | 0.2966 |
| 7 year running mean | **0.753** | **0** | **5.00** | **0.0507** | 0.594 | 0 | 3.57 | 0.2573 |
| *CAA sfw export* | | | | | | | | |
| annual mean | 0.440 | 0 | 10.30 | 0.1464 | 0.402 | 0 | 5.17 | 0.3640 |
| 7 year running mean | **0.696** | **0** | **5.00** | **0.0824** | 0.545 | 0 | 3.57 | 0.3069 |
| *FB lfw export* | | | | | | | | |
| annual mean | 0.461 | 4 | 7.75 | 0.1914 | 0.411 | 4 | 5.17 | 0.3523 |
| 7 year running mean | **0.912** | **3** | **5.00** | **0.0042** | 0.740 | 4 | 3.57 | 0.1292 |
| *FB sfw export* | | | | | | | | |
| annual mean | 0.416 | 5 | 10.30 | 0.1722 | 0.333 | 5 | 5.17 | 0.4584 |
| 7 year running mean | **0.844** | **2** | **5.00** | **0.0169** | 0.721 | 3 | 3.57 | 0.1440 |

*Abbreviations: AO – Arctic Oscillation, CAA – Canadian Arctci Archipelago, FB – Fram Strait and Barents Sea Opening, lfw – liquid freshwater, NAO – North Atlantic Oscillation, sfw – solid freshwater, tfw – total freshwater*

***Table 6.2:*** *Maximum correlations (for $|lag| <= 5$ years) of the AO/NAO and the freshwater transports for the upper Arctic Ocean (surface to 34-isohaline, $S_ref = 34$). Lags are given in years and positive lags indicate the freshwater transport lagging the AO/NAO indices. Significant correlations at a 90 % confidence level are given in bold face. The correlation coefficient r, the effective degrees of freedom N* and the p-value are explained in Chap. 3.7.3.*

| ***Upper*** | A | | | | NAO | | | |
|---|---|---|---|---|---|---|---|---|
| ***Arctic Ocean*** | r | lag | N* | p-value | r | lag | N* | p-value |
| *Net tfw transport* | | | | | | | | |
| annual mean | -0.499 | 0 | 4.43 | 0.2922 | -0.364 | 0 | 4.43 | 0.4570 |
| 7 year running mean | **-0.864** | **2** | **5.00** | **0.0122** | -0.721 | 3 | 3.57 | 0.1440 |
| *CAA lfw export* | | | | | | | | |
| annual mean | 0.440 | 0 | 10.33 | 0.1464 | 0.402 | 0 | 5.17 | 0.3640 |
| 7 year running mean | **0.696** | **0** | **5.00** | **0.0824** | 0.545 | 0 | 3.57 | 0.3069 |
| *CAA sfw export* | | | | | | | | |
| annual mean | 0.440 | 0 | 10.30 | 0.1464 | 0.402 | 0 | 5.17 | 0.3640 |
| 7 year running mean | **0.696** | **0** | **5.00** | **0.0824** | 0.545 | 0 | 3.57 | 0.3069 |
| *FB lfw export* | | | | | | | | |
| annual mean | -0.477 | -3 | 7.75 | 0.1746 | -0.369 | -3 | 5.17 | 0.4081 |
| 7 year running mean | **0.860** | **4** | **5.00** | **0.0130** | 0.653 | 4 | 3.57 | 0.2018 |
| *FB sfw export* | | | | | | | | |
| annual mean | 0.416 | 5 | 10.30 | 0.1722 | 0.333 | 5 | 5.17 | 0.4584 |
| 7 year running mean | **0.844** | **2** | **5** | **0.0169** | 0.653 | 4 | 3.57 | 0.2018 |

*Abbreviations: AO – Arctic Oscillation, CAA – Canadian Arctci Archipelago, FB – Fram Strait and Barents Sea Opening, lfw – liquid freshwater, NAO – North Atlantic Oscillation, sfw – solid freshwater, tfw – total freshwater*

***Table 6.3:*** *Maximum correlations (for $|lag| <= 5$ years) of the AO/NAO and the freshwater transports for the SANA (top to bottom, $S_ref$ = mean salinity of the SANA). Lags are given in years and positive lags indicate the freshwater transport lagging the AO/NAO indices. Significant correlations at a 90 % confidence level are given in bold face. The correlation coefficient r, the effective degrees of freedom N* and the p-value are explained in Chap. 3.7.3.*

| ***SANA*** | AO | | | | NAO | | | |
|---|---|---|---|---|---|---|---|---|
| | r | lag | N* | p-value | r | lag | N* | p-value |
| *Net tfw transport* | | | | | | | | |
| annual mean | **0.510** | **0** | **10.30** | **0.0858** | 0.340 | 0 | 5.17 | 0.4485 |
| 7 year running mean | 0.666 | 0 | 5.00 | 0.1024 | 0.478 | -1 | 3.57 | 0.3795 |
| *DS lfw export* | | | | | | | | |
| annual mean | 0.431 | 0 | 7.75 | 0.2253 | 0.363 | 0 | 5.17 | 0.4162 |
| 7 year running mean | 0.634 | 0 | 4.17 | 0.1694 | 0.530 | 2 | 3.57 | 0.3227 |
| *DS sfw export* | | | | | | | | |
| annual mean | 0.471 | 1 | 7.75 | 0.1808 | 0.477 | 0 | 5.17 | 0.2720 |
| 7 year running mean | **0.869** | **0** | **5** | **0.0111** | 0.649 | 0 | 3.57 | 0.2054 |
| *FB lfw export* | | | | | | | | |
| annual mean | **-0.583** | **-5** | **7.75** | **0.0859** | -0.362 | -5 | 5.17 | 0.4177 |
| 7 year running mean | **0.751** | **4** | **5.00** | **0.0517** | 0.523 | 4 | 3.57 | 0.3302 |
| *FB sfw export* | | | | | | | | |
| annual mean | 0.416 | 5 | 10.30 | 0.1722 | 0.333 | 5 | 5.17 | 0.4584 |
| 7 year running mean | **0.844** | **2** | **5.00** | **0.0517** | 0.721 | 3 | 3.57 | 0.1440 |
| *45N lfw transport (sw)* | | | | | | | | |
| annual mean | 0.473 | 4 | 5.17 | 0.2766 | 0.364 | 4 | 5.17 | 0.4149 |
| 7 year running mean | 0.659 | 5 | 4.17 | 0.1481 | 0.659 | 5 | 3.57 | 0.1964 |
| *45N lfw transport (nw)* | | | | | | | | |
| annual mean | 0.418 | 4 | 10.30 | 0.1700 | 0.351 | 4 | 5.17 | 0.4330 |
| 7 year running mean | 0.641 | 5 | 5.00 | 0.1208 | 0.673 | 5 | 3.57 | 0.1841 |

*Abbreviations: AO – Arctic Oscillation, DS – Davis Strait, FB – Fram Strait and Barents Sea Opening, lfw – liquid freshwater, SANA – subarctic North Atlantic, NAO – North Atlantic Oscillation, nw – northward, sfw – solid freshwater, sw – southward, tfw – total freshwater*

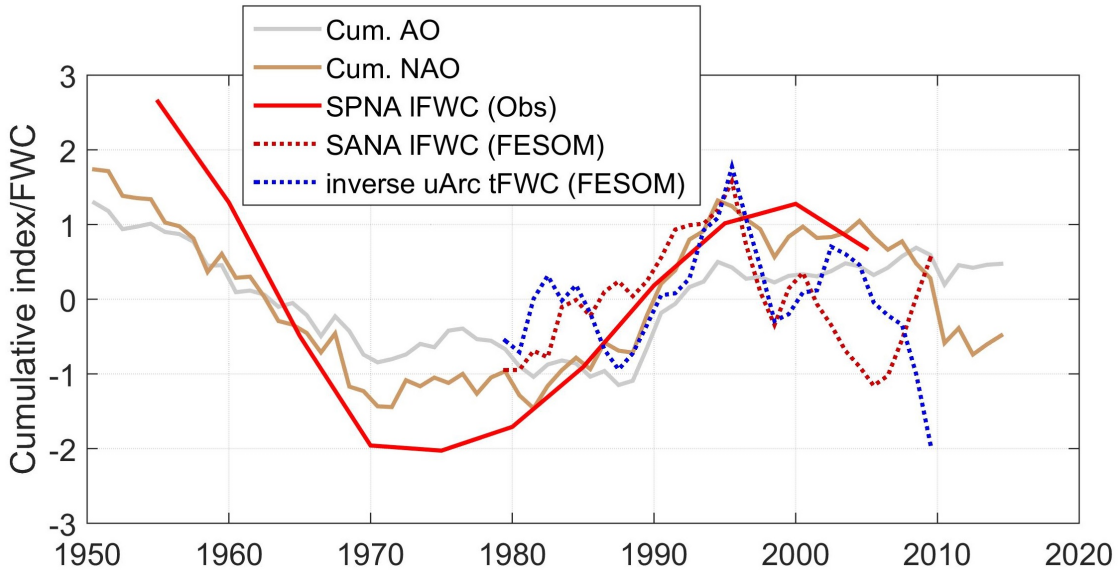


***Figure 6.3:*** *Comparison of the pentadal mean liquid freshwater content (lFWC) of the subpolar North Atlantic (SPNA) derived from Mauritzen et al. (2012) (red solid), the simulated lFWC of the SANA (red dotted), the simulated total freshwater content (tFWC) of the upper Arctic Ocean (inversed; blue dotted), the cumulative AO index (grey), and the cumulative NAO index (brown) based on annual means. All time series have been normalised by their standard deviation, detrended, and demeaned.*

For a better understanding of the underlying processes of the relationship between AO/NAO and the freshwater variations, I made composite maps of sea level pressure, wind stress, sea surface height and upper 200 m ocean circulation for a period of rather positive NAO and AO indices (1989-1995) and for a period of rather negative NAO and AO indices (2005-2009). The difference between the positive and the negative NAO/AO phases is shown in Fig. 6.4. In the positive phase the Arctic wind and ocean circulation is rather cyclonic with a weaker Beaufort High compared to the negative phase (Fig. 6.4a). Further, the sea surface height is lower in the Canada Basin and higher on the shelves than in the negative phase (Fig. 6.4b). The westerly winds over the subpolar North Atlantic are strengthened and wind anomalies over the Nordic Seas are directed towards Fram Strait (Fig. 6.4a). Moreover, the sea surface height in the western subpolar North Atlantic basins is lower and the Baffin Island Current, Labrador Current, and Irminger Current are stronger, while the East Greenland Current is weaker in the positive NAO/AO phase compared to the negative NAO/AO phase (Fig. 6.4b).These findings are discussed in the following.

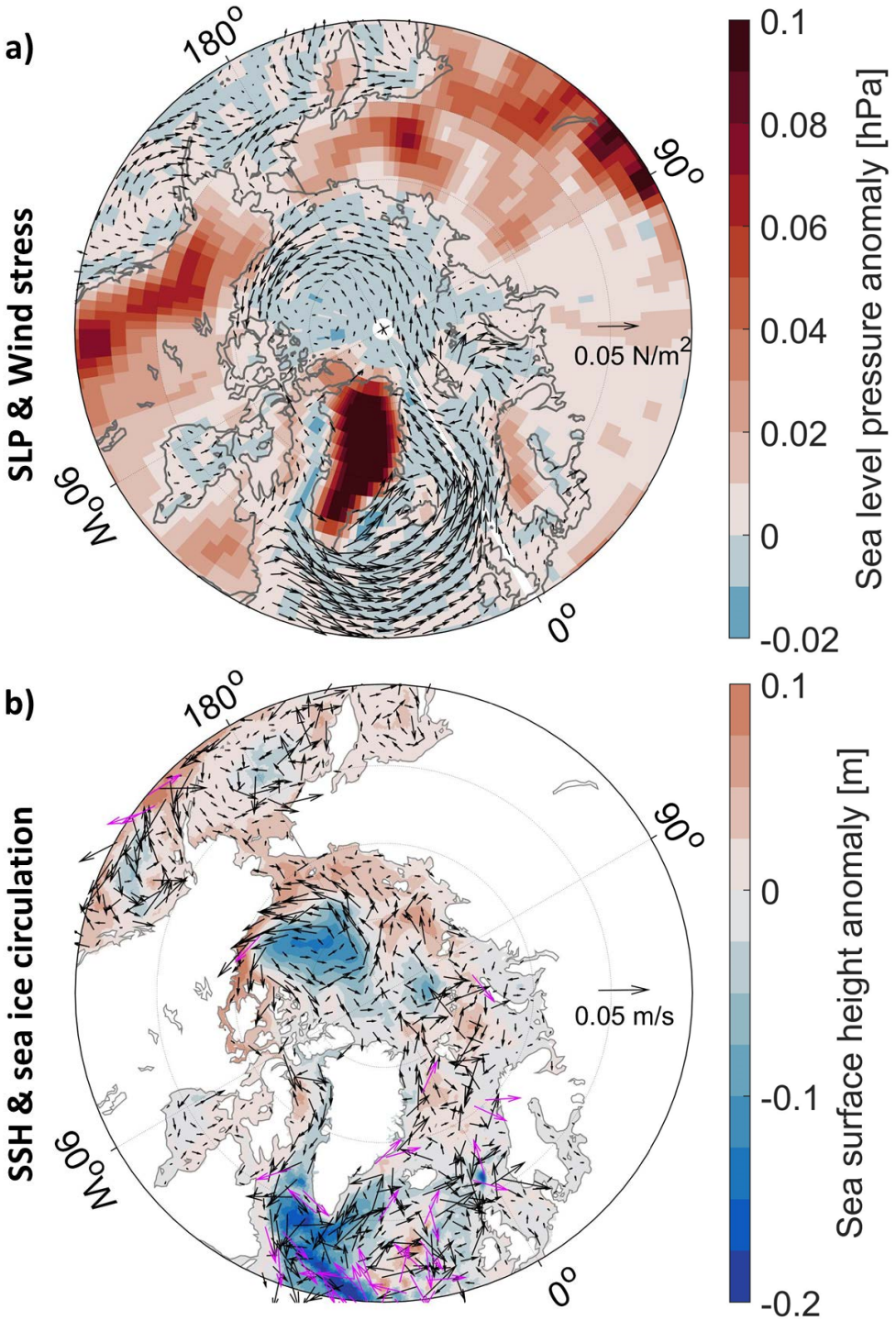


***Figure 6.4:*** *Difference between a rather positive NAO/AO phase (1989-1995) and a rather negative phase (2005-2009): CORE-II sea level pressure (SLP) and wind stress used as FESOM forcing (a), as well as sea surface height (SSH) and upper 200 m ocean circulation from the FESOM simulation (b). For the upper ocean circulation magenta arrows indicate velocity anomalies higher than 0.05 m/s and are set to a constant length (b).*

**How do the freshwater content and transport variability compare to the large-scale atmospheric circulation variability?**

I find positive correlations for the low-frequency variability (7 year running means) of the AO/NAO indices and of the Arctic freshwater export to the SANA (Fig. 6.2, Tab. 6.1-6.3) as well as for the pentadal means of the cumulative indices and the subpolar North Atlantic freshwater content (Fig. 6.3). Variations in the solid and liquid freshwater export through the CAA are in phase with the AO, while the solid and liquid freshwater export through the FB are lagging 2 and 3 to 5 years, respectively.

The comparison of the composite maps reveals that during a negative AO/NAO phase, meaning high pressure in the Arctic Ocean (strong Beaufort High), the anti-cyclonic winds over the Canada Basin are accelerated. By transferring momentum to the sea ice and upper ocean this leads to a strong Beaufort Gyre circulation, where fresh water can be accumulated in the interior of the gyre due to Ekman pumping (e.g., Proshutinsky et al., 2002, 2009, 2015; Dukhovskoy et al., 2006). The accumulation of fresh water leads to an elevated sea surface in the center of the gyre, which maintains the anti-cyclonic Beaufort Gyre circulation due to geostrophy. As fresh water is accumulated in the Beaufort Gyre, less fresh water is exported out of the Arctic Ocean resulting in a decrease in the SANA freshwater content. Due to the geographical distances a faster response of the CAA freshwater export than of the Fram Strait freshwater export would be expected and potentially explains the different lags in the maximum correlation. To estimate the propagation time from the Beaufort Gyre to Fram Strait a Lagrangian particle experiment as carried out by Hu and Myers (2013) would be a suitable tool. Hu and Myers (2013) investigated in their study the PW pathways in the Arctic Ocean. Their findings suggest that the PW needs 5 to 10 years from Bering Strait to Fram Strait. Thus a 3 to 5 year lagged response of the Fram Strait freshwater export to an accumulation of fresh water in the Beaufort Gyre or a freshwater release might be reasonable.

On the contrary, during a positive AO/NAO index, associated with low pressure over the Arctic Ocean, the anti-cyclonic winds over the Canada Basin are weaker (cyclonic wind anomalies; Fig. 6.4) also weakening the Beaufort Gyre circulation due to the reduction in momentum transfer from the atmosphere and sea ice to the ocean. As the gyre circulation slows down, the accumulated fresh water is released to the shelves and the sea surface height difference between the Canada Basin and the shelves is weakened. Thus also the geostrophic anti-cyclonic flow is decreased (cyclonic circulation anomalies; Fig. 6.4b). The release of fresh water from the Beaufort Gyre allows an increased freshwater export to the North Atlantic potentially resulting in an increase of SANA freshwater content and a decrease of

Arctic Ocean freshwater content.

Also the model study of Wekerle et al. (2013) showed higher transport through the CAA during positive NAO phases. They argued that this is due to (i) strong winds over the Labrador Sea cooling the upper ocean and (ii) low sea level pressure anomaly in the Arctic Ocean promoting cyclonic wind anomalies over the Canadian Basin. Both lead to a higher sea surface height gradient between the Arctic Ocean and the Labrador Sea leading to enhanced transports. Both signatures are represented in the composite maps of the positive and negative AO/NAO phases (Fig. 6.4).

The formation of the GSAs of the subpolar North Atlantic has also been related to changes from a negative to positive Winter NAO index, which led to an intensification of the northwesterlies and thereby enhanced freshwater export from the Arctic Ocean (e.g., Belkin, 2004). A model experiment by Condron et al. (2009) showed a clear response of the Arctic freshwater budget to extreme NAO wind forcing as described above. Moreover Ionita et al. (2016) found from model simulation a distinct link between Greenland atmospheric blocking events related to negative NAO index phases and the export of sea ice through the Fram Strait. My study also revealed intensified northwesterlies during the positive AO/NAO phase that I have chosen for the composite maps, but the Greenland atmospheric blocking signature in the sea level pressure fields is not observed (Fig. 6.4a). As Greenland blocking is a short-term phenomenon, its signature (high sea level pressure anomaly over Greenland and Iceland) might therefore not be resolved by the composite maps of annual mean sea level pressure. Only the Baffin Island current is stronger in the related ocean circulation composite indicating increased freshwater transport through the CAA, but the East Greenland Current exporting Arctic fresh water through the Fram Strait is weakened (Fig. 6.4b). However, the composite maps can only be used for analysing the instantaneous response to the atmospheric oscillation state, and the time series correlations suggest a delayed response of the freshwater export through the FB to the AO/NAO forcing.

The liquid freshwater export through the FB is significantly anti-correlated to the AO index with the export leading 3 to 5 years and positively correlated with a 3 to 5 years lag of the export. One possible explanation would be that both, the index and the export, go through cycles of 12 to 20 years with a phase shift of 3 to 5 years, so that a phase of increased FB export follows a positive AO phase due to a lagged response and is followed automatically by a negative AO phase. Or there is a feedback from the ocean to the atmosphere associated with the Fram Strait freshwater export that drives sea level pressure changes thereby influencing the AO, which is followed by a lagged response of the FB freshwater export to the change in the AO. Arzel et al. (2008) proposed a link between Fram Strait freshwater export

and decreasing convection in the Nordic Seas, leading to an increase in the northward heat transport to the Barents Sea and thereby in the surface air temperature over the Barents Sea. This is proposed to increase the sea level pressure over the Nordic Seas. However these mechanisms are related to projected conditions in the twenty-first century and cannot be tested with the FESOM model as it is only an ocean sea ice model with no atmospheric coupling.

The freshwater export variability through the CAA and through the FB seem to respond differently to fluctuations in the large-scale atmospheric circulation. Therefore I analysed which atmospheric and oceanic pressure and circulation pattern are related to an increased freshwater export through the CAA and which pattern are related to an increased freshwater export through the FB. The results are shown in the following section.

## 6.2 Drivers of the Arctic freshwater export

For finding atmospheric and oceanic patterns that are related to transport variations between the Arctic Ocean and the SANA, I analysed the cross-correlation and regression of the annual mean transport time series and fields of sea level pressure, wind stress, sea surface height and upper 200 m ocean or sea ice circulation. I only show regression coefficients for correlations with a correlation coefficient $|r| > 0.4$ at zero lag, which is for most correlations the 80 % confidence level. In order to be independent from reference salinities, I used volume transport instead of the volume-driven freshwater transport (see Chap. 3.5) and the effective salinity of the transport (see Chap. 3.6) instead of the salinity-driven freshwater transport (see Chap. 3.5).

As the liquid freshwater export through the CAA is largely volume-driven (Fig. 5.12), I show the cross-correlation and regression only for the southward volume transport (full water column). A high volume export is associated with a weak Beaufort High, anomalously low sea level pressure on the Greenland shelves, strong winds over the CAA and cyclonic wind anomalies over the Canada Basin (Fig. 6.5a). The associated ocean pattern is characterized by a low sea surface height in the Canada Basin, in the eastern CAA, on the Greenland shelves and in the Irminger and Labrador seas as well as a high sea surface height on the Canadian Arctic shelves and in the western CAA and Baffin Bay (Fig. 6.5b). The related upper ocean circulation pattern represents a weakened Beaufort Gyre, strengthened Baffin Island Current and Labrador Current and a weakened East Greenland Current (Fig. 6.5b).

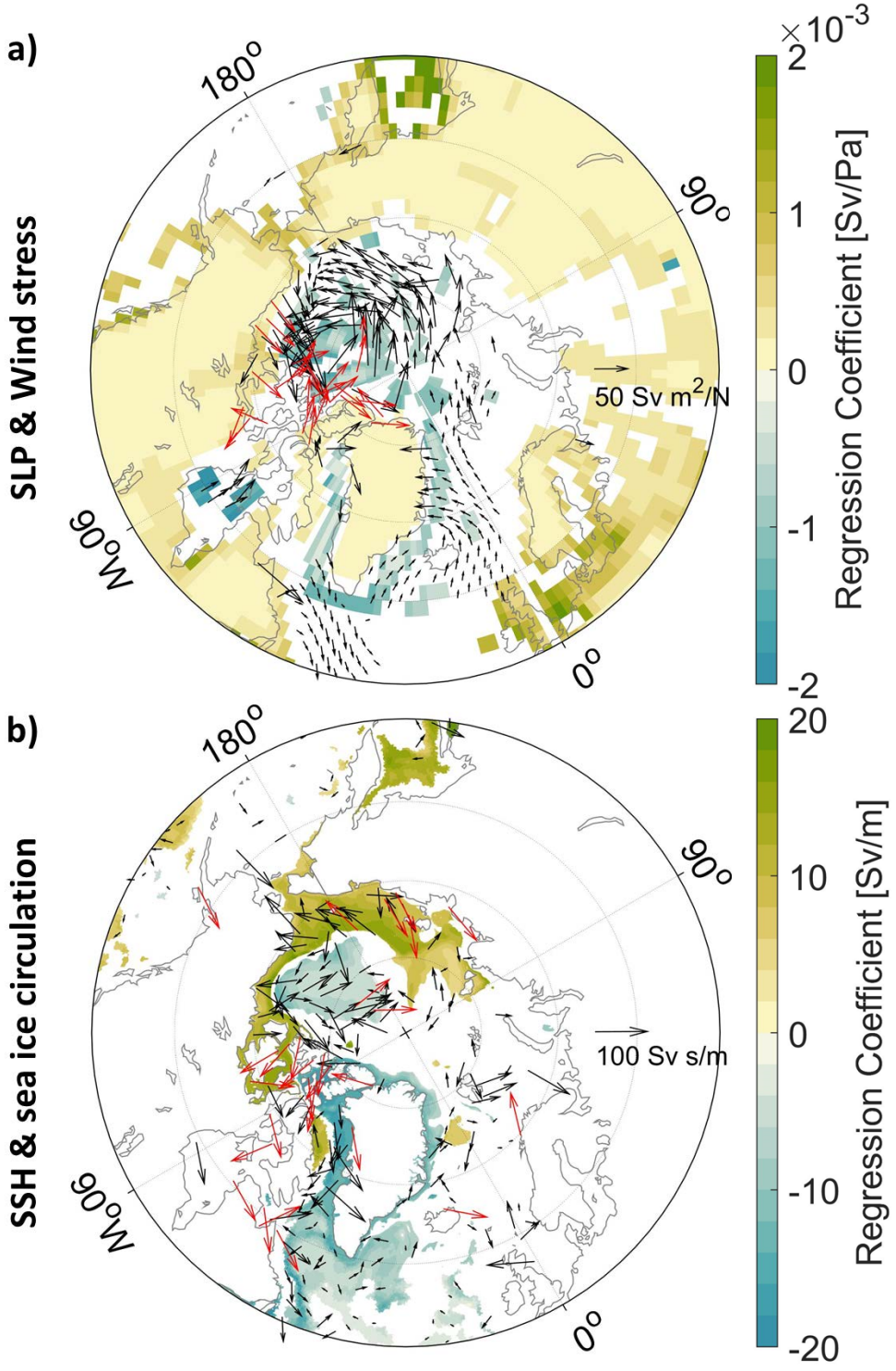


***Figure 6.5:*** *Regression analysis of simulated annual mean volume export through the CAA (full water column) and (a) CORE-II sea level pressure (SLP) and wind stress used as FESOM forcing and (b) sea surface height (SSH) and upper 200 m ocean circulation from the FESOM simulation. Only regression coefficients for correlations $|r| > 0.4$ are shown. For the wind stress regression coefficients with a magnitude higher than 100 Sv m$^2$/N are shown in red with a constant length (a). For the upper ocean circulation red arrows indicate regression coefficients with a magnitude higher than 100 Sv s/m and are set to a constant length (b).*

***Table 6.4:*** *Maximum correlations (for |lag| <=5 years) of the transport components analysed in this section. Lags are given in years and positive lags indicate the variable given in the first column lagging the variable given in the first row. Significant correlations at a 90 % confidence level are given in bold face. The upper FB volume export is calculated between the surface and the 34-isohaline. All other transports are calculated for the full water column. The correlation coefficient r, the effective degrees of freedom N* and the p-value are explained in Chap. 3.7.3.*

| | FB volume export | | | | FB volume import | | | | FB ice export | | | | FB $S_{eff}$ export | | | |
|---|---|---|---|---|---|---|---|---|---|---|---|---|---|---|---|---|
| | r | lag | N* | p-value | r | lag | N* | p-value | r | lag | N* | p-value | r | lag | N* | p-value |
| FB volume import | **0.945** | **0** | **10.33** | **0.000** | | | | | | | | | | | | |
| FB ice export | -0.363 | 2 | 7.75 | 0.314 | -0.336 | 2 | 7.75 | 0.354 | | | | | | | | |
| FB $S_{eff}$ export | -0.390 | -2 | 7.75 | 0.277 | -0.318 | -2 | 7.75 | 0.382 | 0.414 | -5 | 7.75 | 0.246 | | | | |
| CAA volume export | -0.441 | -1 | 3.88 | 0.405 | -0.267 | -2 | 3.88 | 0.623 | 0.433 | -5 | 3.88 | 0.414 | 0.474 | 1 | 3.88 | 0.367 |
| CAA ice export | -0.322 | 2 | 10.33 | 0.300 | -0.193 | 3 | 10.33 | 0.541 | 0.507 | 2 | 7.75 | 0.146 | 0.327 | 1 | 7.75 | 0.367 |
| Upper FB volume export | **0.635** | **0** | **7.75** | **0.056** | 0.486 | 0 | 7.75 | 0.166 | 0.290 | 0 | 7.75 | 0.427 | **-0.739** | **0** | **7.75** | **0.018** |

| | CAA volume export | | | | CAA ice export | | | |
|---|---|---|---|---|---|---|---|---|
| | r | lag | N* | p-value | r | lag | N* | p-value |
| CAA ice export | 0.726 | 0 | 3.88 | 0.129 | | | | |
| Upper FB volume export | -0.558 | 0 | 3.88 | 0.277 | -0.330 | 0 | 7.75 | 0.363 |

*Abbreviations: CAA - Canadian Arctic Archipelago, FB – Fram Strait and Barents Sea Opening*

As the variability of the sea ice export through the CAA is very similar to the variability of the liquid volume export through the CAA but with a much smaller amplitude (Fig. 5.7, Tab. 6.4), the associated patterns from the cross-correlation and regression analysis are very similar, too (not shown).

The liquid freshwater export through the FB is driven by both, variations in the volume transport as well as variations in the salinity of the transported waters (Fig. 5.13). Therefore I used the volume export (full water column) as well as the effective salinity of the exported waters (full water column) for the analysis of possible drivers.

The regression analysis of the volume export through the FB shows a pattern of low sea level pressure over the Nordic Seas and high sea level pressure over the Newfoundland Basin (Fig. 6.6a). This sea level pressure pattern fosters cyclonic winds over the Nordic Seas and eastern subpolar North Atlantic with especially strong southward winds along the east coast of Greenland from Fram Strait to Iceland. Furthermore, wind anomalies in the Barents Sea are directed towards Spitsbergen (Fig. 6.6a).

The sea surface height anomalies associated with an increased volume export through the FB are negative in the Nordic Seas deep basins (especially in the Greenland Sea) and in the western Baffin Bay, whereas the anomalies on the East Greenland shelf and around Spitsbergen are positive (Fig. 6.6b). The pattern in the upper ocean circulation shows an intensified East Greenland and West Greenland Current and an indicated cyclonic circulation anomaly in the central Arctic Ocean (Fig. 6.6b). As the volume import through the FB is highly correlated with the volume export (Tab. 6.4), the associated pattern of regression and correlation coefficients looks very similar (not shown). Further the full water column volume export through the FB is significantly correlated to the export above the 34-isohaline (Tab. 6.4). Thus a similar pattern from the regression and cross-correlation analysis of the upper ocean transport can be expected (not shown).

The analysis of the regression between sea level pressure and the effective salinity of the exported waters through the FB reveals a general pattern of high sea level pressure over the Arctic Ocean and Nordic Seas and low sea level pressure over the eastern subpolar North Atlantic (not shown). However, the absolute values of the correlation coefficients were all lower than 0.4 and therefore no regression coefficients for the sea level pressure are shown in Fig. 6.7a. Wind anomalies are westward on the East Greenland shlef, northward in Fram Strait and north-eastward in the Eurasian Arctic (Fig. 6.7a).

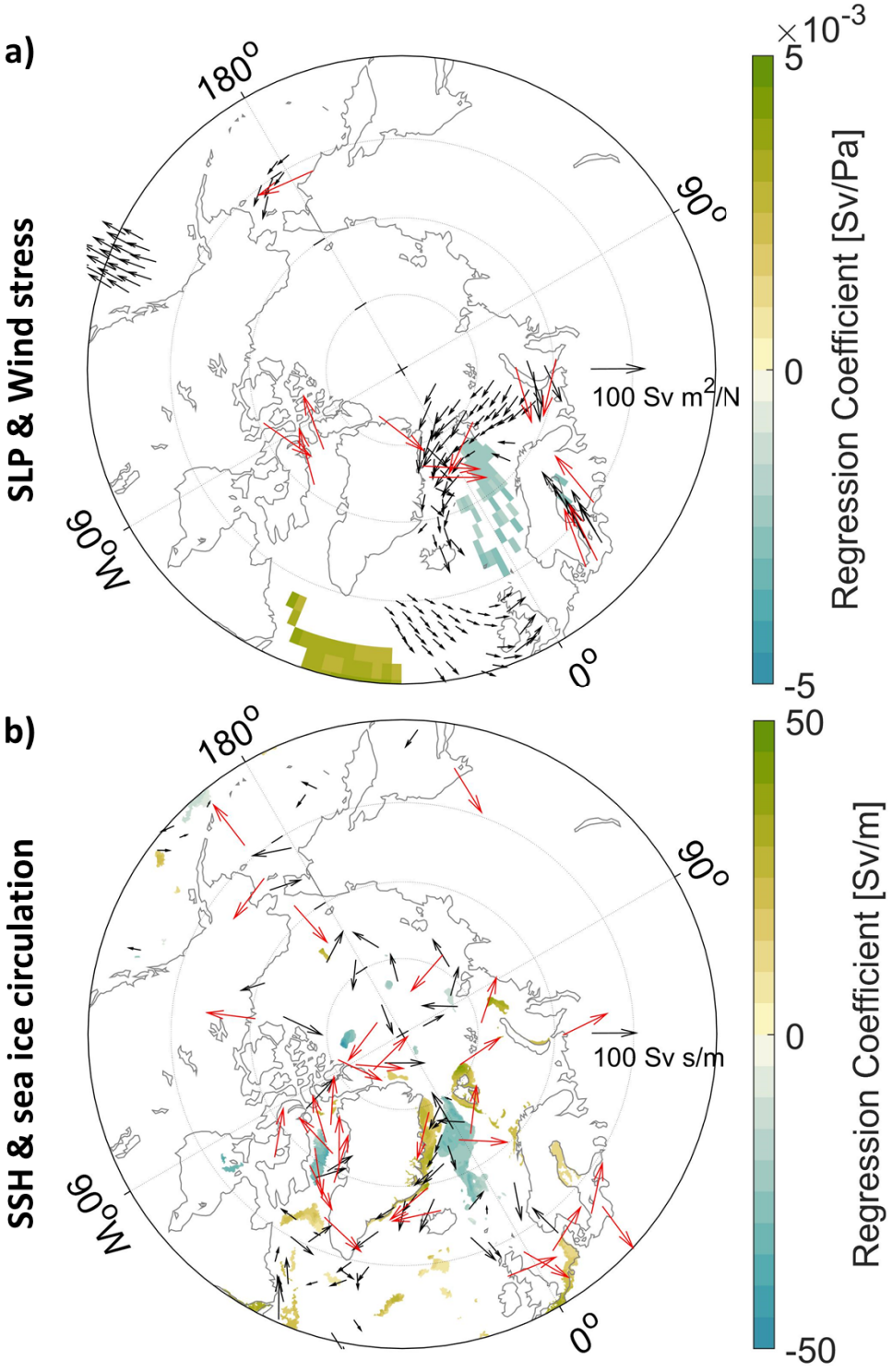


***Figure 6.6:*** *Regression analysis of simulated annual mean volume export through the FB (full water column) and a) CORE-II sea level pressure (SLP) and wind stress used as FESOM forcing and (b) sea surface height (SSH) and upper 200 m ocean circulation from the FESOM simulation. Only regression coefficients for correlations $|r| > 0.4$ are shown. For the wind stress regression coefficients with a magnitude higher than 100 Sv $m^2/N$ are shown in red with a constant length (a). For the upper ocean circulation red arrows indicate regression coefficients with a magnitude higher than 100 Sv s/m and are set to a constant length (b).*

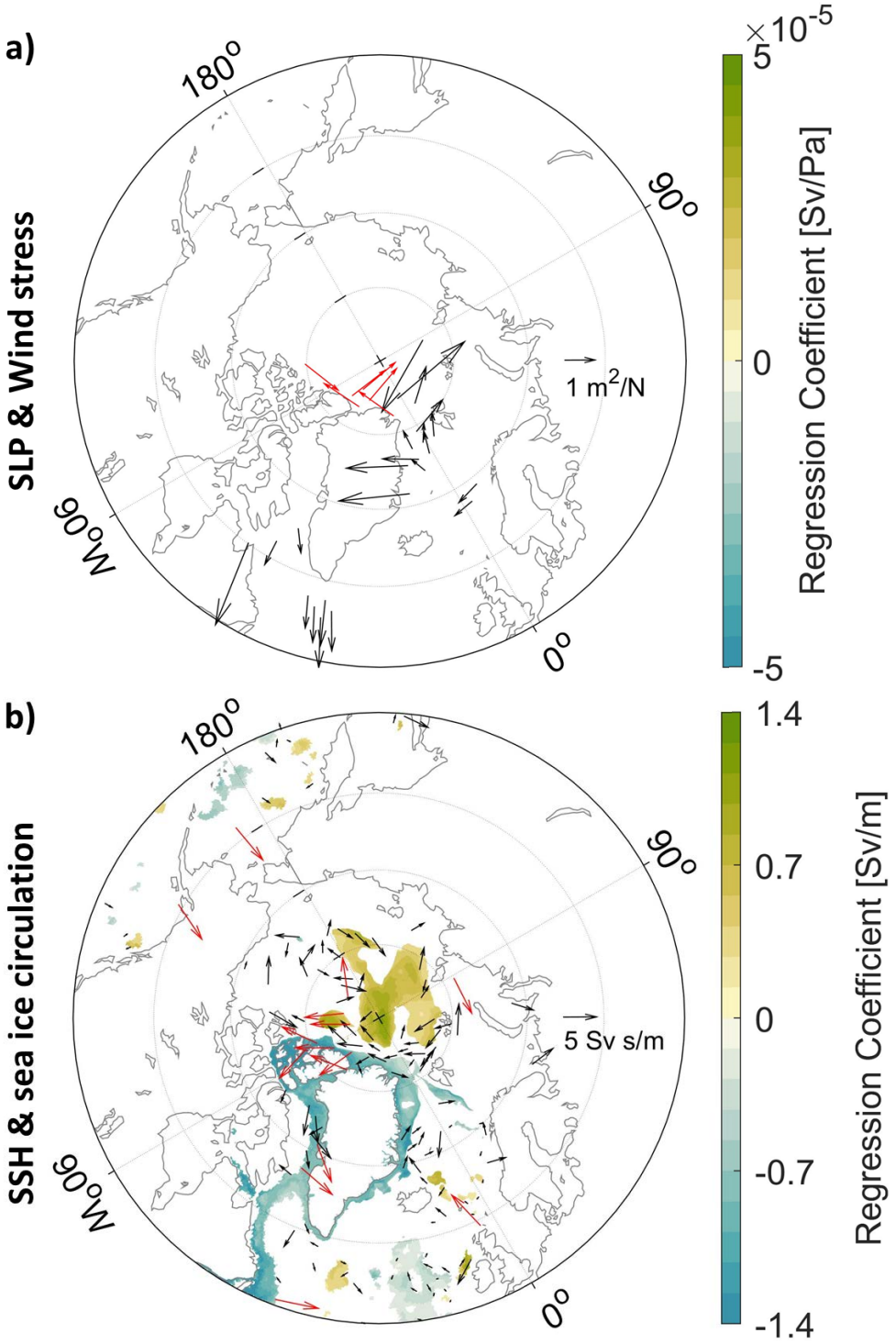


***Figure 6.7:*** *Regression analysis of simulated annual mean effective salinity of exported waters through the FB (full water column) and (a) sea level pressure (SLP) and wind stress and (b) sea surface height (SSH) and upper 200 m ocean circulation (b). Only regression coefficients for correlations $|r| > 0.4$ are shown. For the wind stress regression coefficients with a magnitude higher than 5 $m^2/N$ are shown in red with a constant length (a). For the upper ocean circulation red arrows indicate regression coefficients with a magnitude higher than 5 s/m and are set to a constant length (b).*

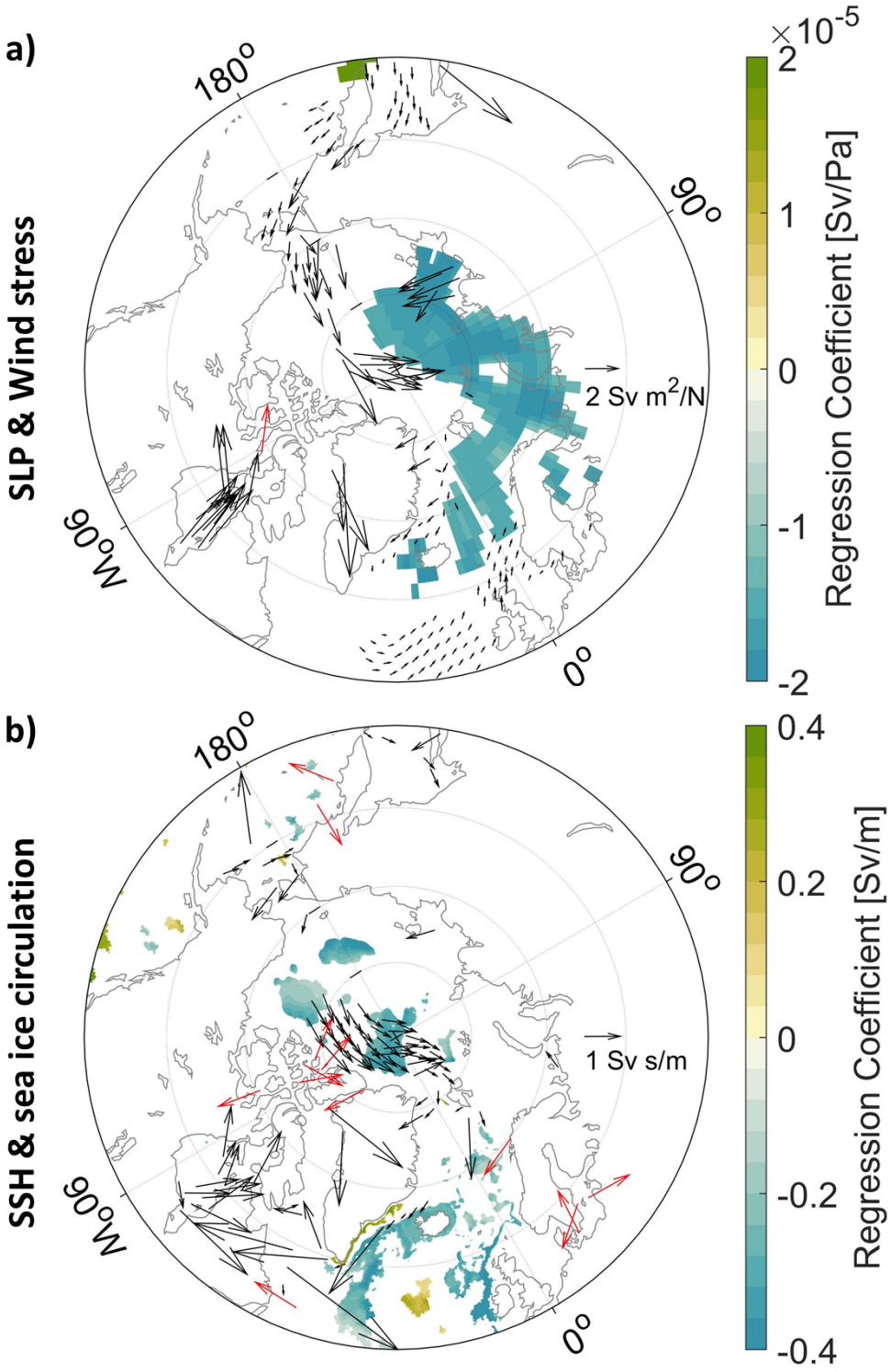


***Figure 6.8:*** *Regression analysis of simulated annual mean sea ice export through the FB and winter (DJF) mean (a) sea level pressure (SLP) and wind stress and (b) sea surface height (SSH) and sea ice circulation (b). Only regression coefficients for correlations $|r| > 0.4$ are shown. For the wind stress regression coefficients with a magnitude higher than 5 Sv $m^2/N$ are shown in red with a constant length (a). For the upper ocean circulation red arrows indicate regression coefficients with a magnitude higher than 5 Sv s/m and are set to a constant length (b).*

The sea surface height anomalies associated with an increased effective salinity of the exported waters through the FB are negative on the Greenland and Labrador shelves, in the eastern CAA and Baffin Bay as well as on the Barents Sea shelf south of Spitsbergen and are positive in the Eurasian Arctic Ocean (Fig. 6.7b). Furthermore, the East Greenland and West Greenland Currents are anomalously weak and the upper ocean circulation in the entire Arctic Ocean is rather anticyclonic. The effective salinity of the full water column volume export through the FB is significantly anti-correlated with the upper ocean volume export above the 34-isohaline (Tab. 6.4). This might explain the opposite sign in the regressed sea surface height on the Greenland shelf for the effective salinity (Fig. 6.7b) and for the volume export through FB (Fig. 6.6b) and the opposite direction of wind anomalies in Fram Strait and of the upper ocean circulation anomalies (Fig. 6.6, 6.7).

As sea ice has a strong seasonal cycle (Fig. 4.1), I used seasonal fields for the regression/correlation analysis of the sea ice export through the FB. Thereby I found the highest correlations and regressions for winter (DJF) conditions (Fig. 6.8). The sea ice export correlates with low sea level pressure over the Eurasian Arctic and Nordic Seas and wind anomalies from the Laptev Sea and Chukchi Sea along the northern coast of the CAA and Greenland towards the North Pole and Spitsbergen (Fig. 6.8a). The associated sea surface height anomalies are low in the Arctic Ocean and the sea ice circulation pattern is similar to the wind pattern with the ice drifting from the Canadian Arctic over the North Pole towards Spitsbergen (Fig. 6.8b).

### What drives the oceanic exchange between the Arctic Ocean and SANA in the model?

The southward volume and sea ice transport through the CAA is clearly driven by the strength of the Beaufort High and the associated anti-cyclonic wind and ocean circulation as well as the sea surface height difference between the Canada Basin and the shelves (Fig. 6.5 processes described above). Fresh water is accumulated in the Beaufort Gyre during anti-cyclonic circulation regimes and less volume, sea ice and fresh water is exported through the CAA. During cyclonic circulation regimes the accumulated fresh water is released and exported through the CAA (Fig. 6.9). These processes have also been described by a number of other studies (e.g., Proshutinsky et al., 2002, 2009, 2015; Dukhovskoy et al., 2006). Moreover, my regression analysis shows a clear sea surface height difference between the western and eastern CAA and Baffin Bay emphasizing a southward geostrophic flow through the Lancaster Sound and a strengthened Baffin Island Current.

So far the mechanisms driving the Fram Strait liquid freshwater export are poorly known (Haine et al., 2015). Jahn et al. (2010a) suggest from their model simula-

tion that variations in both, the volume-driven and the salinity-driven freshwater export through Fram Strait, result from the Beaufort Gyre circulation anomalies driven by the large-scale atmospheric circulation. They argue that a freshwater release from the Beaufort Gyre increases the freshwater content along the northern coast of Greenland, which increases the sea surface height north of Fram Strait and supplies fresher waters for the Fram Strait export. However, my study suggests that the volume import and export through the FB is not controlled by the Arctic upper ocean and wind circulation, but driven by the sea level pressure difference between the Nordic Seas and the western subpolar North Atlantic (Fig. 6.6). The negative pressure anomaly over the Nordic Seas and the positive pressure anomaly over the western subpolar North Atlantic supports a cyclonic wind circulation over the Nordic Seas with especially strong winds along the East Greenland coast driving the upper ocean. Thereby a sea surface height difference between the deep basins and the shelves is created due to Ekman transport which then drives the southward geostrophic flow along the western shelf and the northward geostrophic flow along

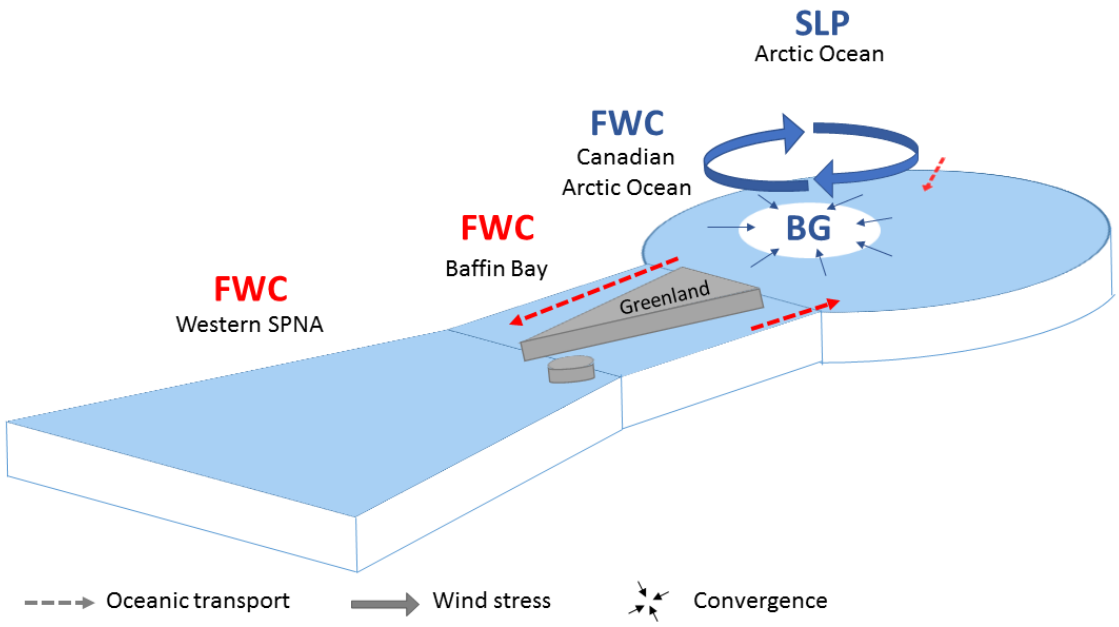


***Figure 6.9:*** *Schematic of suggested physical mechanisms driving increased volume and sea ice export through the CAA. Blue colour indicates a decrease/weakening and red colour indicates an increase/strengthening. When the sea level pressure (SLP) over the Arctic Ocean is decreased, the anticyclonic wind circulation and the Beaufort Gyre are weakened causing a release of the waters in the gyre due to decreased convergence. The export west of Greenland increases which is compensated by an increased volume import east of Greenland and from the Pacific Ocean. The increased CAA export results in a decreased freshwater content (FWC) in the Canadian Arctic Ocean and an increased FWC in the Baffin Bay and the western subpolar North Atlantic (SPNA).*

the eastern shelf of the Nordic Seas (Fig. 6.10). This way a strengthened cyclonic wind circulation over the Nordic Seas results in increased southward and northward volume transports through the FB.

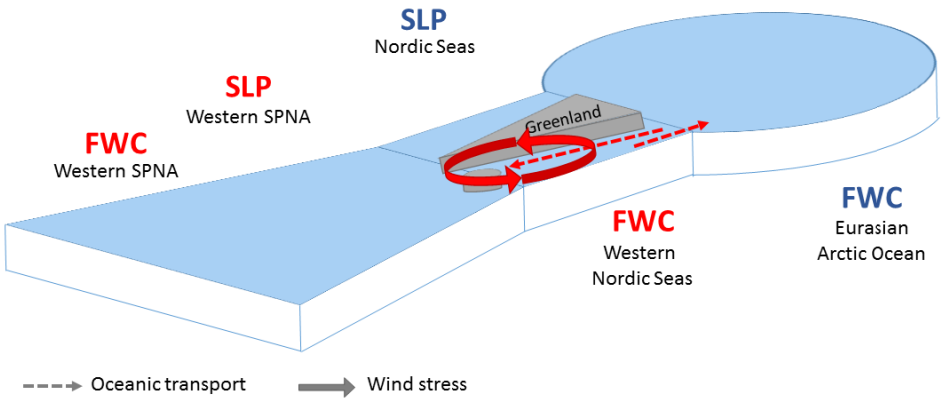


***Figure 6.10:*** *Schematic of suggested physical mechanisms driving increased volume export through FB. Blue colour indicates a decrease/weakening and red colour indicates an increase/strengthening. When the sea level pressure (SLP) is decreased over the Nordic Seas and increased over the western subpolar North Atlantic (SPNA), the cyclonic wind circulation over the Nordic Seas/ eastern SPNA is strengthened. The volume export through the FB increases compensated by an increased import. This results in a decreased freshwater content (FWC) in the Eurasian Arctic Ocean and an increased FWC in the western Nordic Seas and SPNA.*

The effective salinity of FB export is high, when the southward winds over the Fram Strait and the East Greenland Current are weak and when the upper Arctic Ocean circulation is rather anti-cyclonic (Fig. 6.7). The effective salinity is a transport-weighted salinity. In FB, it is therefore significantly anti-correlated with the upper ocean volume export that has a rather low salinity (Tab. 6.4). When the upper ocean volume transport increases, more fresh surface waters are transported and thereby the effective salinity of the transported waters decreases. This explains the pattern in the strength of the East Greenland Current and the winds along the East Greenland coast associated to the effective salinity of FB export (Fig. 6.7). The anti-cyclonic wind and upper ocean circulation anomalies in the Arctic Ocean suggest a state of freshwater accumulation in the Arctic Ocean, which may result in a more saline or less deep surface layer in the Fram Strait leading to an increased effective salinity of the transported waters.

From my results I propose that the sea ice export through FB is mainly driven by strong winds over the Arctic Ocean in winter-time pushing the sea ice from the Laptev and Chukchi Seas across the Arctic Ocean to Fram Strait and the Barents Sea (Fig. 6.8). These winds are associated with negative sea level pressure anomalies over the Eurasian Basin and the Nordic Seas. The anti-correlation between the annual sea ice export and the winter (DJF) sea level pressure between Iceland and Greenland (Fig. 6.8a) could indicate frequent or strong Greenland blocking events associated with decreased sea ice export as found by Ionita et al. (2016). This signature was not resolved in the composite maps of annual sea level pressure presented in the former section, but seems to be resolved by the seasonal regression analysis. Tsukernik et al. (2010) found from observational and reanalysis data that a dipole pattern of low pressure over the Barents Sea and high pressure over Greenland strengthens the meridional winds across Fram Strait, which drive the sea ice export. This pattern is the second empirical orthogonal function mode of daily sea level pressure. When using monthly sea level pressure for the analysis, only the low sea level pressure over the Barents Sea remains significant for the Fram Strait sea ice export. This agrees well with the findings of my study.

## 6.3 Causes of the recent freshwater content changes

Significant changes in the Arctic Ocean and SANA freshwater content have been observed (Fig. 4.14) between the time periods 1990-2002 (first phase), 2004-2010 (second phase) and after 2011 (third phase). To better understand which of the different processes driving the Arctic freshwater export was responsible for the observed changes, I looked at the sea level pressure and 10 m wind fields for these time periods. The liquid freshwater content of the SANA decreased from the first to the second phase while the total freshwater content of the Arctic Ocean increased (Fig. 4.14). From the second to the third phase the SANA liquid freshwater content increased again while the total freshwater content of the Arctic Ocean decreased (Fig. 4.14).

The Beaufort High and the associated anticyclonic wind circulation were stronger in the second phase than in the first phase (Fig. 6.11a). Moreover, the sea level pressure anomaly between Iceland and Greenland is positive with associated anticyclonic wind anomalies and strengthened southward winds in Fram Strait. Looking at the seasonal fields, there is a strong positive sea level pressure anomaly south of Iceland and over Siberia in winter time (DJF) with northward wind anomalies in Fram Strait and eastward wind anomalies along the Siberian coast Fig. 6.12a).

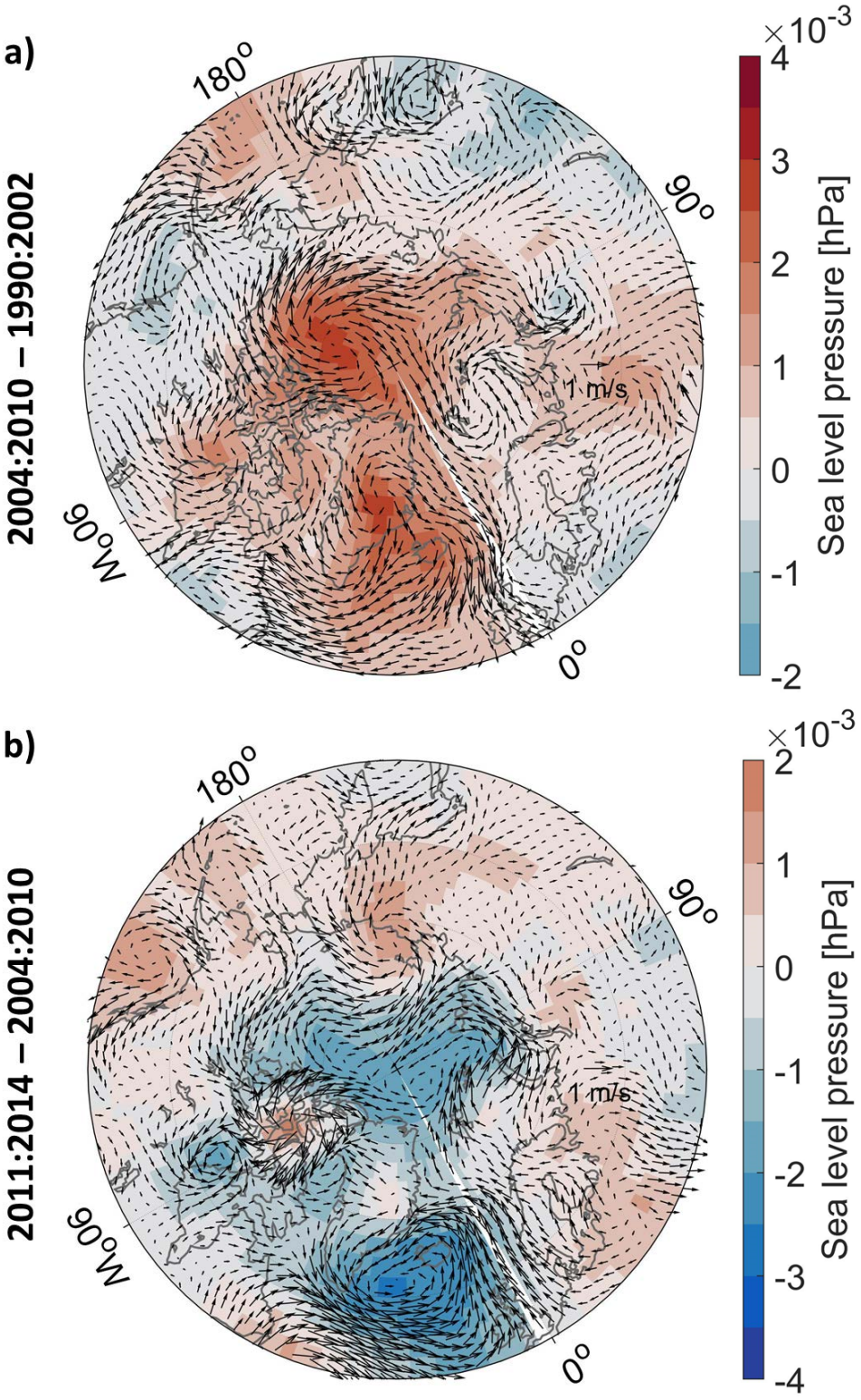


***Figure 6.11:*** *Difference of NCEP-DOE Reanalysis 2 sea level pressure and wind at 10 m height between the periods 1990-2002 and 2004-2010 (a), and between the periods 2004-2010 and 2011-2014 (b).*

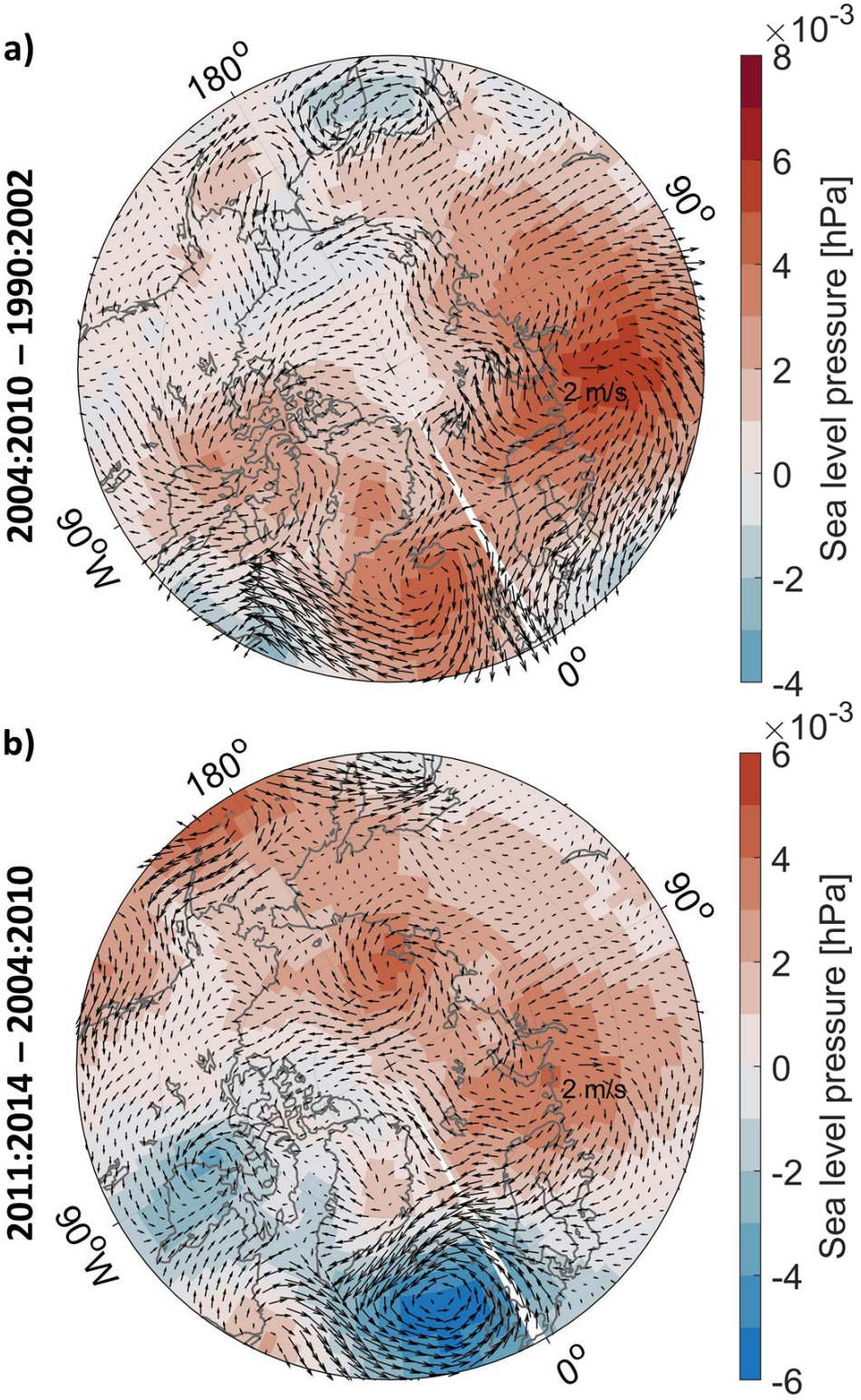


***Figure 6.12:*** *Difference of NCEP-DOE Reanalysis 2 winter (DJF) sea level pressure and wind at 10 m height between the periods 1990-2002 and 2004-2010 (a), and between the periods 2004-2010 and 2011-2014 (b).*

The difference in the atmospheric conditions between the second and third phase shows the opposite case: negative sea level pressure anomalies in the Arctic Ocean and southwest of Iceland as well as associated cyclonic wind anomalies and weakened southward winds in Fram Strait (Fig. 6.11b). However, the difference in the winter conditions between the second and third phase with an even lower sea surface anomaly and stronger cyclonic wind anomalies in the eastern subpolar North Atlantic still shows northward wind anomalies in Fram Strait (Fig. 6.12b). These results are discussed in the following.

### What caused the observed rapid changes in the Arctic Ocean and SANA freshwater contents in 2002-2004 and after 2011?

Between 2002 and 2004 the total freshwater content of the Arctic Ocean increased rapidly while the SANA liquid freshwater content decreased (Fig. 4.14). The sea level pressure and wind fields suggest a change to a rather anti-cyclonic circulation in the Arctic Ocean causing freshwater accumulation in the Beaufort Gyre (Fig. 6.11a). As shown in Fig. 6.5 the anti-cyclonic circulation regime is associated with a low volume/freshwater export through the CAA. Furthermore, I find indications for an increased effective salinity of the export through FB when the upper Arctic Ocean circulation is anti-cylonic (Fig. 6.7). Although the southward winds in Fram Strait are stronger in the second phase (2004-2010) than in the first phase (1990-2002), further south the winds are weaker (Fig. 6.11a). Moreover, the sea level pressure low close to Iceland creating the cyclonic wind circulation driving the liquid volume export through FB is weaker in the second phase, suggesting a decrease in the export east of Greenland. The winter signal shows indications for Greenland blocking associated with decreased sea ice export through FB (Fig. 6.12a; Ionita et al., 2016). All these together would sum up to a decreased freshwater export from the Arctic Ocean to the SANA possibly explaining the observed change in freshwater content. The suggested physical mechanisms described above are summarised in Fig. 6.13.

From the second (2004-2010) to the third phase (2011-2014) the SANA liquid freshwater content started to increase again while the total freshwater content of the Arctic Ocean decreased (Fig. 4.14). The sea level pressure and wind fields show the opposite change of the one in 2002-2004 described above. The Arctic wind circulation became more cyclonic again due to a weaker Beaufort High suggesting a release of the accumulated fresh water from the Beaufort Gyre and an increased liquid and solid freshwater export through the CAA (Fig. 6.11b). Furthermore, the Iceland Low became stronger which possibly strengthened the cyclonic wind circulation driving the volume export through the FB by creating a sea surface height gradient between the shelves and deep basins. However, the southward winds

in Fram Strait itself decreased in the period mean. The winter fields show strong negative sea level pressure anomalies between Iceland and Greenland suggesting the Greenland blocking events got less frequent or less strong (Fig. 6.12b). All together the atmospheric conditions suggest a decrease of the Arctic freshwater export from the second to the third phase possibly explaining the observed increase (decrease) in the SANA (Arctic Ocean) freshwater content.

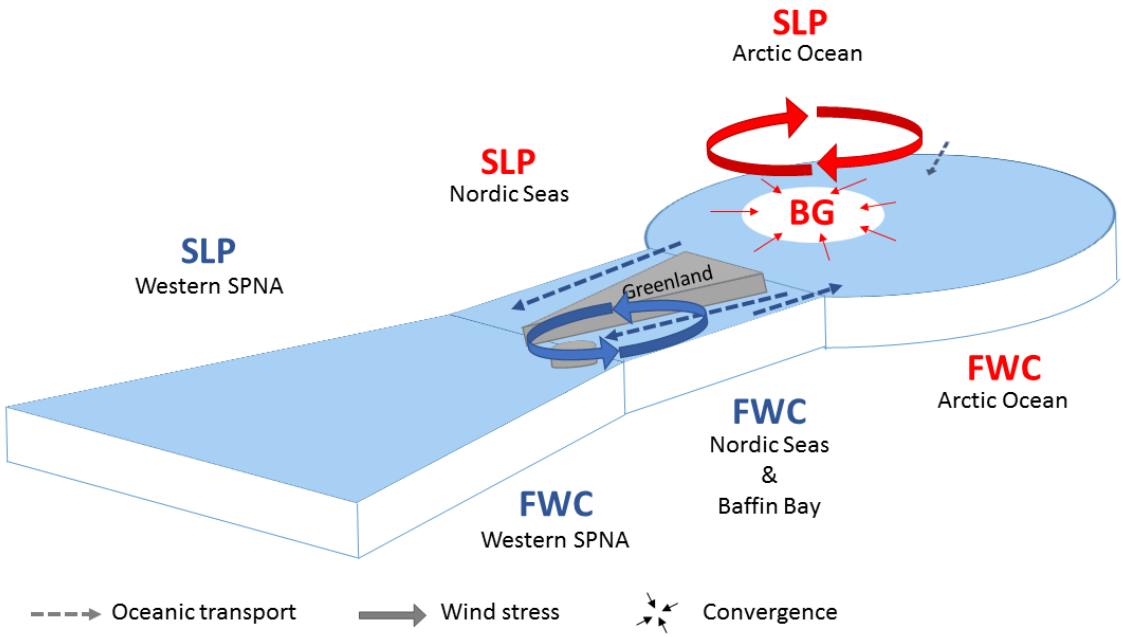


***Figure 6.13:*** *Schematic of suggested physical mechanisms responsible for the increase in Arctic Ocean freshwater content (FWC) and SANA FWC between the periods 1992-2002 and 2004-2010. Blue colour indicates a decrease/weakening and red colour indicates an increase/strengthening. An increased sea level pressure (SLP) over the Arctic Ocean and the Nordic Sea and a decreased SLP over the western subpolar North Atlantic (SPNA) support anticyclonic wind anomalies over the Arctic Ocean and the Nordic Seas/eastern SPNA. These wind regimes are proposed to be associated with a decreased export to the SANA on both sides of Greenland resulting in a freshwater accumulation in the Arctic Ocean and a deficit in the SANA freshwater content (FWC).*

From the difference in the composite maps I cannot quantify the relative contribution of the liquid and solid freshwater exports through the CAA and the Fram Strait to the observed freshwater content changes in the Arctic Ocean and SANA. However, I found from lag correlation analysis that the liquid volume export through the CAA is positively correlated to freshwater inventories in the western Baffin Bay and on the Labrador shelf and negatively correlated to the freshwater inventories of the Canada Basin (not shown). Moreover, the liquid volume export through the FB is positively correlated to the liquid freshwater inventories on the Greenland shelves and in the Irminger and Labrador Seas and negatively correlated to the Eurasian

Basin liquid freshwater inventories (not shown). As most of the increase in the liquid freshwater content of the Arctic Ocean from the first to the second phase was observed in the Canada Basin (Fig. 4.5), the export through the CAA seems to have been more important for the Arctic Ocean freshwater content increase than the export through the FB. In the SANA the liquid freshwater inventories decreased strongest along the Greenland and Labrador shelves (Fig. 4.12) highlighting the importance of the export through both pathways. For the freshwater content of the central Irminger and Labrador Seas, however, the export through the FB appears to be more important than the export through the CAA, which is supported by findings of the tracer simulation study by Myers (2005). They found that freshwater anomalies transported in the East and West Greenland Currents are mixed into the Irminger and Labrador Seas by eddies, while freshwater anomalies transported by the Labrador Current rather concentrate on the shelf.

I suggest that there are times when the freshwater export through the CAA and through the FB are out of phase and only lead to a regional redistribution of fresh water within th Arctic Ocean or the SANA, but the effect on the overall SANA and Arctic Ocean freshwater content of the freshwater exports is more or less balanced. And then there are times, where both freshwater exports are in phase and cause an amplified signal in the freshwater content of the Arctic Ocean and the SANA. Therefore I hypothesise that the observed rapid changes in the Arctic Ocean and SANA freshwater content result from an interplay of the atmospheric patterns driving the freshwater export through the CAA and the patterns driving the freshwater export through the FB leading to an increased or decreased freshwater export through both pathways.

# Chapter 7

# Discussion

In recent decades the freshwater content of the upper Arctic Ocean and the SANA varied in opposing sense but with the same amplitudes (Fig. 4.14). I show that neither atmospheric freshwater fluxes nor continental runoff could have caused these variations. However, in both regions variations in the simulated net oceanic transport approximately matches the observed rates of freshwater content changes in timing as well as in size. For the Arctic Ocean I find that the freshwater export towards the North Atlantic affects the freshwater storage of the Arctic Ocean the most, which agrees with findings of other studies (Proshutinsky et al., 2002; Jahn et al., 2010a; Giles et al., 2012; Stewart and Haine, 2013). Moreover, the simulated mean volume and freshwater transports through the Arctic gateways mostly compare well with observational transport time series and estimates from literature (Fig. B.2; Tab. B.1).

Different circulation modes observed in the Arctic Ocean can cause on the one hand an accumulation of the liquid fresh water and sea ice, mainly in the Beaufort Gyre and on the other hand a release of these fresh waters (e.g., Mauritzen, 2012) to the SANA. My results suggest that the cyclonic circulation mode causes an increased sea ice and volume-driven freshwater export through the CAA on the one hand, and supports an increased sea ice and salinity-driven freshwater export through the FB on the other hand. The volume-driven freshwater export through the FB seems to be controlled by cyclonic winds over the Nordic Seas/eastern subpolar North Atlantic. Some model studies found in their simulations that the volume/freshwater export through the CAA and the Fram Strait are out of phase (e.g., Lique et al., 2009; Steele et al., 1996). In the FESOM simulation the volume exports are also anti-correlated, but not statistically significant (Tab. 6.4). From the composite maps of the sea level pressure and wind field (Fig. 6.11) I hypothesise that the strong freshwater content changes observed in the upper Arctic Ocean and SANA in the past two decades result from an interplay of both driving atmsopheric pattern and

the assocaited physical mechanisms. When sea level pressure is anomalously high over the Arctic Ocean and the Nordic Seas and wind anomalies are anticyclonic, less Arctic fresh water is exported into the SANA. This results in an increased upper Arctic Ocean freshwater content and a decreased SANA freshwater content. In the opposite case the accumulated fresh water is released into the SANA resulting in an increasing SANA freshwater content and a decreasing freshwater content of the upper Arctic Ocean. This could explain the anti-correlation of the two freshwater content time series with amplitudes of the same magnitude.

As I find significant anti-correlations of the freshwater inventories in the western subpolar North Atlantic at zero-lag (Fig. 4.12), the exported fresh water needs to reach this region at time-scales shorter than a year. Waters in the East Greenland Current have a residence time of only three months (e.g., Dodd et al., 2012), which makes a quick response of the SANA freshwater content to variations in the Arctic freshwater export through Fram Strait possible. At the same time the fresh water exported through the complex channel system of the CAA needs to cross the Baffin Bay before reaching the SANA region defined in this study. However, the variability of the simulated freshwater content of the Baffin Bay is relatively low (compared to the variability in the SANA and the Arctic Ocean) suggesting a quick through flow of Arctic fresh water (Fig. 7.1). Moreover, the simulated freshwater export through the CAA and those through the Davis Strait show a strongly similar variability with no obvious lag (r = 0.925; Fig. 5.7-5.8).

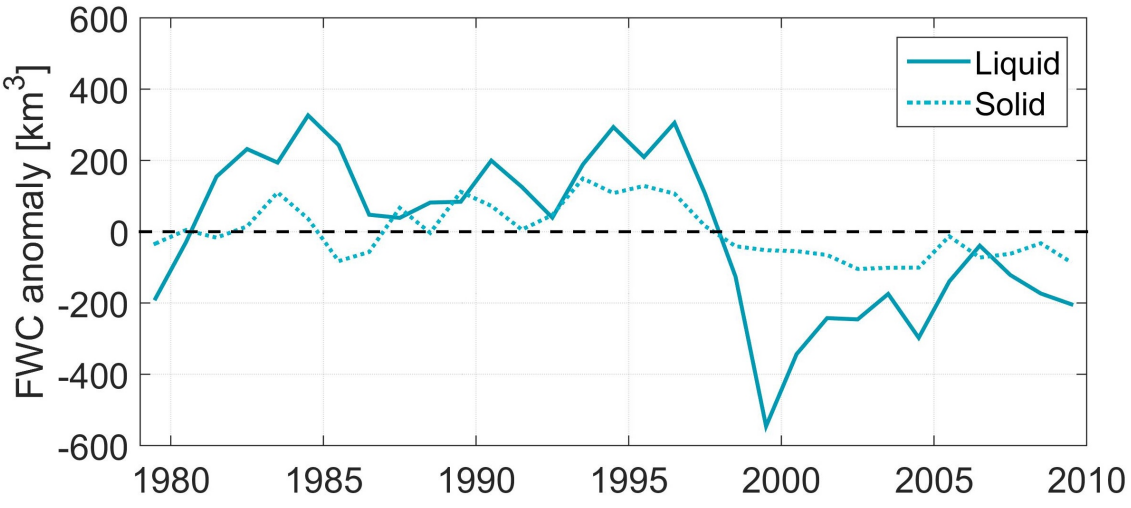


***Figure 7.1:*** *Anomalies of simulated liquid (solid line) and solid (dashed line) freshwater content (FWC) of the Baffin Bay (Davis Strait to sections of the CAA). Both time series have been calculated with the reference salinity 35.*

Still, the atmospherically driven variations in the Arctic freshwater export can neither explain the observed zero-lag anti-correlation of the total upper Arctic freshwater content with the freshwater inventories of the eastern SANA nor the positive correlation close to the Mid-Atlantic Ridge (Fig. 4.12). In the SANA the net precipitation from the CORE-II atmospheric forcing dataset shows a distinct positive linear trend over the northern Mid-Atlantic Ridge region whereas the trend is rather negative in most of the other parts of the SANA (not shown) possibly explaining the increased liquid freshwater inventories close to the Mid-Atlantic Ridge. Supporting this explanation, Josey and Marsh (2005) also related an increase of the freshwater content of this part of the SANA from the 1960s to the 1990s to an increased net precipitation due to a change in the local sea level pressure pattern.

Hátún et al. (2005) proposed that salinity changes in the eastern subpolar North Atlantic are related to throughput from the Subtropical Gyre. The latter is proposed to be controlled by the strength and size of the Subpolar Gyre represented by the Gyre Index, which is the principal component of the leading empirical orthogonal function of the North Atlantic sea surface height. However, Foukal and Lozier (2017) found, on the one hand, that the Gyre Index only represents a basin-wide sea level rise and is not related to the Subpolar Gyre strength and size. On the other hand, they did not find a relation between their measures of Subpolar Gyre strength and size and the salinity of the eastern subpolar North Atlantic. Further, they propose that the NAO dynamics, producing out-of-phase responses for the Subpolar Gyre and the Subtropical Gyre, control the intergyre throughput and thereby the eastern subpolar North Atlantic salinity. Comparing the annual NAO index with the mean salinity at the Iceland-Scotland Ridge from the FESOM simulation reveals, that positive (negative) NAO phases mostly coincide with a decreasing (increasing) mean salinity suggesting a decreased (increased) throughput of subtropical waters (Fig. 7.2). This mechanism might explain why freshwater inventory changes in the eastern SANA happen simultaneously to the changes in the upper Arctic Ocean and western SANA.

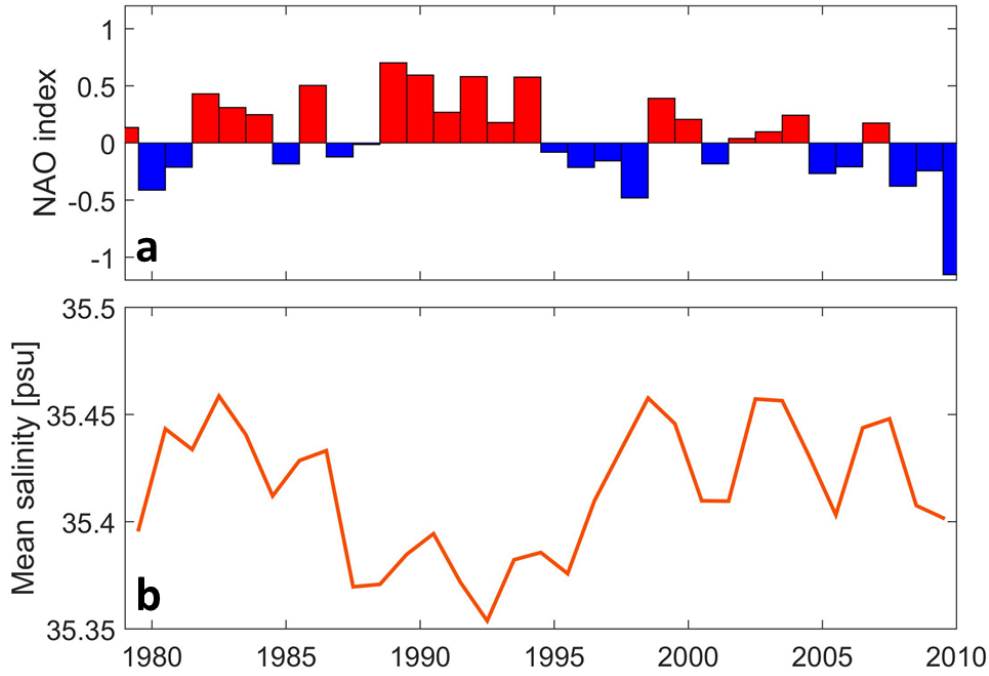


***Figure 7.2:*** *Annual mean NAO index (a) and the simulated mean salinity at the Iceland-Scotland Ridge section (b).*

Changes in the ocean circulation are not only driven by the atmosphere, but also have a feedback on the atmosphere and influence our climate. For the multidecadal timescales one example is the Atlantic Multidecadal Variability (AMV), which was initially called Atlantic Multidecadal Oscillation and first described by Schlesinger and Ramankutty (1994). The AMV is calculated by subtracting the global mean sea surface temperature anomalies from the North Atlantic sea surface temperature anomalies and is believed to be linked to internal ocean-atmosphere variability (e.g., Knudsen et al., 2011). The AMV is associated with a certain sea surface pressure pattern and a related wind field, which, amongst other effects, were found from climate reconstruction time series to affect the sea ice export through Fram Strait, the freshwater balance in the northern North Atlantic and the large-scale ocean circulation (Dima and Lohmann, 2007). As phases of high (low) AMV coincide with phases of low (high) freshwater content in the subpolar North Atlantic (on the basis of the pentadal means) with a lag of a five to ten years (Fig. 7.3), the decadal to multidecadal variability of both the Arctic Ocean freshwater content as well as the freshwater release to the SANA could also be part of the AMV.

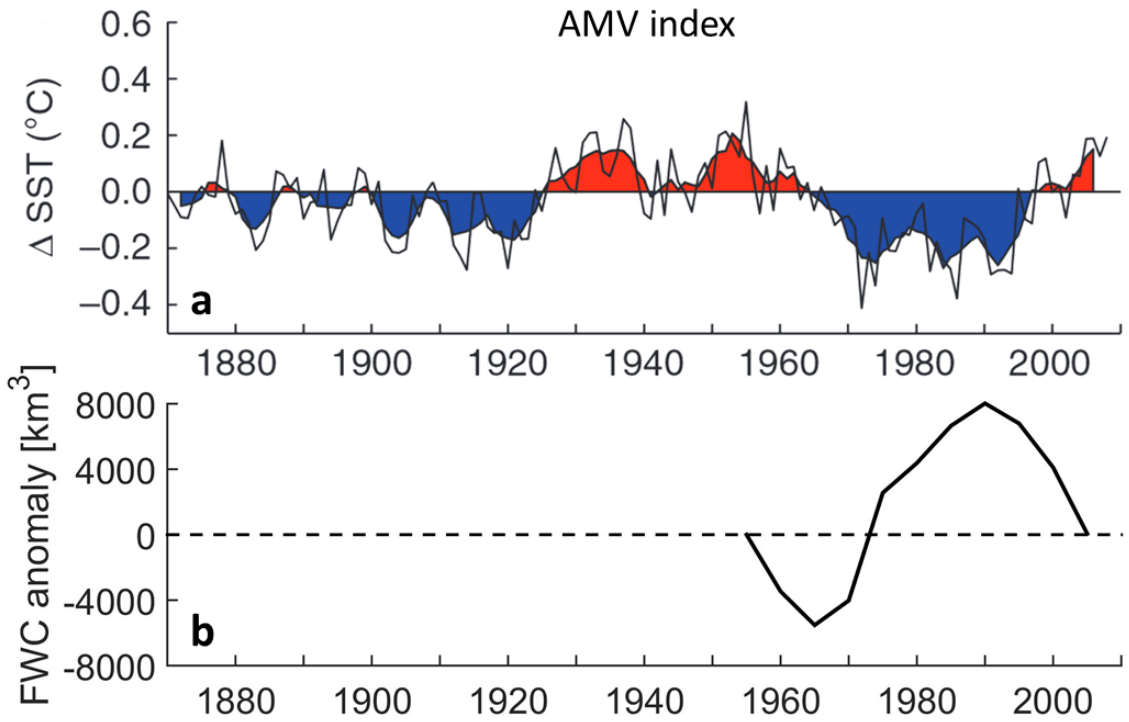


***Figure 7.3:*** *Atlantic Multidecal Variability (AMV) index (a; figure taken from Knudsen et al., 2011 with creative commons license: http://creativecommons.org/licenses/by-nc-nd/3.0/) compared to pentadal mean liquid freshwater content anomalies of the subpolar North Atlantic based on salt estimates from Mauritzen et al. (2012).*

# Chapter 8

# Conclusions and outlook

After having presented and discussed the results of my study in Chap. 4- 7, I draw the final conclusions and give a brief outlook in the following. Coming back to the objectives of my study, I will give the conclusions of my study and suggestions for further analyses by answering the main research questions introduced in the first chapter.

**Are the recent freshwater content changes in the upper Arctic Ocean and in the SANA linked?**

The liquid freshwater content of the SANA and the total freshwater content of the upper Arctic Ocean are significantly anti-correlated between 1992 and 2013 with anomalies of the same magnitude, and there are several physical mechanisms that could directly or indirectly link them. Therefore I conclude that the recent changes in the upper Arctic Ocean total freshwater content and in the SANA liquid freshwater content are strongly linked. I identified three phases: the freshwater content of the SANA (upper Arctic Ocean) was increased (decreased) between 1992 and 2002, decreased (increased) between 2004 and 2010 and increasing (decreasing) after 2011.

The anti-correlation of the upper Arctic Ocean total freshwater content and the SANA liquid freshwater inventories holds for most regions of the SANA despite a region close to the Mid Atlantic Ridge, where the liquid freshwater inventories are positively correlated to the upper Arctic Ocean total freshwater content. However, this positive correlation is statistically insignificant. I propose different processes to be responsible for the observed anti-correlations in the eastern and in the western SANA, which I will expand on when answering the third research question.

**What drives the freshwater variability of the two regions?**

From the results of the FESOM simulation I conclude that the total freshwater content variability of the upper Arctic Ocean is largely driven by variations in the freshwater export (solid and liquid) to the North Atlantic. The solid and liquid freshwater export through the CAA is increased when the Beaufort High and the associated anti-cyclonic wind circulation are weak, causing a release of fresh water from the Beaufort Gyre. The other way around, a strong Beaufort High leads to a spin-up of the Beaufort Gyre, an accumulation of fresh water in the interior of the gyre and decreased volume and freshwater exports through the CAA (see Chap. 6.2 for more details). These processes, mainly driving the freshwater content variability of the Canadian Arctic Ocean, the Baffin Bay and the Labrador shelf, are governed by variations in the large-scale atmospheric circulation: The anti-cyclonic circulation regime (strong Beaufort High) is associated with a negative AO and the cyclonic circulation regime (weak Beaufort High) with a positive AO.

The liquid freshwater export through the FB has a lagged correlation to the AO and its effective salinity shows positive regression with cyclonic ocean circulation anomalies in the upper Arctic Ocean. This points to a delayed response of the freshwater export through the FB to the freshwater release from the Beaufort Gyre. However, this hypothesis remains to be tested. A suitable tool would be a Lagrangian particle model experiment to trace pathways and propagation velocities of the fresh water released from the Beaufort Gyre during cyclonic circulation regimes.

I further conclude from the regression analysis that the volume-driven part of the liquid freshwater export through the FB is driven by a pattern of low sea level pressure over the Nordic Seas and high sea level pressure over the western subpolar North Atlantic. This sea level pressure pattern is associated with a cyclonic wind circulation over the Nordic Seas, which causes increased sea surface heights on the shelves of the Nordic Seas due to Ekman transport. The increased sea surface height gradient from the shelves to the basins leads to an increased southward geostrophic flow along the eastern shelf (East Greenland Current) and an increased northward geostrophic flow along the western shelf (Norwegian Atlantic Current; see Chap. 6.2 for more details). The liquid freshwater export through the FB is found to mainly influence the liquid freshwater content variability of the Eurasian Arctic Ocean, the Greenland shelf and the Irminger and Labrador Seas.

The variability of the sea ice export through the FB is largely influenced by variations in the sea level pressure over the Eurasian Arctic and the Nordic Seas. An anomalously low sea level pressure is associated with strengthened winds that push the sea ice from the Chukchi Sea towards Fram Strait and the Barents Sea, and drive the sea ice transport along the Greenland shelf. Positive sea level pressure

anomalies close to Greenland can block these winds (Greenland blocking events) and thereby reduce the sea ice export through FB.

Although I conclude from my results that the export of fresh surface waters has the largest effect on the variability of the upper Arctic Ocean freshwater content, I do not neglect the importance of the processes leading to diahaline mixing, such as entrainment, convection or brine rejection from sea ice formation. I estimated the freshwater flux across the 34-isohaline related to these processes (entrainment term) from the difference in the net freshwater flux (including net precipitation, river runoff, damping, and the oceanic liquid and solid freshwater transport above the 34-isohaline) and the freshwater storage above the 34-isohaline. As this entrainment term seems to compensate for the artifical fresh water flux induced by surface salinity restoring in the model, I suggest that the sea surface salinity restoring needs to be reduced or completely be omitted in order to get a better estimate of the entrainment term. A FESOM simulation without sea surface salinity restoring in the Arctic Ocean has just recently been performed (Wang et al., 2018a). Moreover, the net freshwater flux needs to further include the fluxes from eddy diffusion and numerical diffusion. Thus the uncertainty in the entrainment term is reduced to the interpolation errors of the gateway fluxes.

Moreover, I conclude from the analysis of freshwater fluxes in the FESOM simulation that the liquid freshwater content of the SANA is driven by both, the freshwater import from the Arctic Ocean and the freshwater exchange with the subtropical North Atlantic. The solid and liquid freshwater transport from the Arctic Ocean to the SANA mainly drives the freshwater inventory variability of the western SANA. The processes are described above. I expect the exchange with the subtropical North Atlantic to be the main driver of the freshwater inventory variability of the eastern SANA. However, a model simulation with an increased resolution in the North Atlantic is needed to draw concise conclusions to the effect of the freshwater exchange with the subtropical North Atlantic on the SANA liquid freshwater content.

**Which processes/physical mechanisms have led to the observed changes in the freshwater content?**

As mentioned above, I propose different drivers of the observed freshwater changes in the western SANA and in the eastern SANA. From the regression analysis and from the atmospheric conditions during the time of observations I conclude that the freshwater export from the Arctic Ocean to the SANA decreased from the period 1992-2002 to the period 2004-2010 due to a spin up of the Beaufort Gyre and blocked southward winds along the East Greenland coast. This caused a decrease in the liquid freshwater content of the western SANA and an increase of the total

freshwater content of the upper Arctic Ocean. Further I propose that the increasing SANA freshwater content and the decreasing upper Arctic Ocean freshwater content after 2011 resulted from an increased Arctic freshwater export due to a freshwater release from the Beaufort Gyre and strengthened cyclonic winds over the Nordic Seas/eastern subpolar North Atlantic.

I found implications for changes in the salinity of the AW entering the Nordic Seas at the Iceland Scotland Ridge. These changes are possibly caused by variations in the contribution of subpolar gyre and subtropical gyre waters driven by the large-scale atmospheric circulation. Phases of a positive (negative) NAO coincide with a decreasing (increasing) AW salinity at the Iceland Scotland Ridge. This relationship might explain the observed anti-correlation of the liquid freshwater inventories of the eastern SANA and the upper Arctic Ocean total freshwater content. This hypothesis could be tested with a FESOM simulation in a setup of increased resolution in the entire SANA region.

Since 2011 I see first indications for a freshwater decrease in the Arctic Ocean and an increase in the SANA. The CORA salinity dataset (Chap. 3.1.1), the objectively mapped liquid freshwater inventories of the upper Arctic Ocean (Chap. 3.1.2) and the PIOMAS sea ice volume estimates (Chap. 3.2.2) have been updated during my studies and now provide new data for 2014/15 (asterisks in Fig. 8.1). The additional data points in the time series show that the liquid freshwater content of the SANA increased even more after 2013 reaching values higher than the former maximum in 1996. The total freshwater content of the upper Arctic Ocean increased at the same time due to an increase in the solid freshwater content in 2013 and 2014. However, the PIOMAS sea ice volume estimates show a decrease again in 2016/17. Another update of the objectively mapped liquid freshwater inventories produced by Benjamin Rabe using the Unified Database for Arctic and Subarctic Hydrography (Behrendt et al., 2018) is already in the planning stages adding another year to the total freshwater content time series of the upper Arctic Ocean.

Following my argument, the increasing liquid freshwater content of the SANA could be the start of another phase of increased Arctic freshwater export to the SANA. The potential release of several thousand cubic kilometers of fresh water accumulated in the late 2000s in the Arctic Ocean into the North Atlantic could have an impact on the deep water formation in the North Atlantic in the following years. So far, however, an intensification of the deep convection in the Labrador Sea in the period 2012-2016 is recorded (Yashayaev and Loder, 2016), suggesting that the temperature forcing is still stronger than the salinity forcing. Furthermore, a reduction of fresh water in the Arctic near-surface layer would mean lower density stratification. This would allow easier release of heat and nutrients from the AW layer to the surface, which could accelerate sea-ice decrease, warming of the Arctic

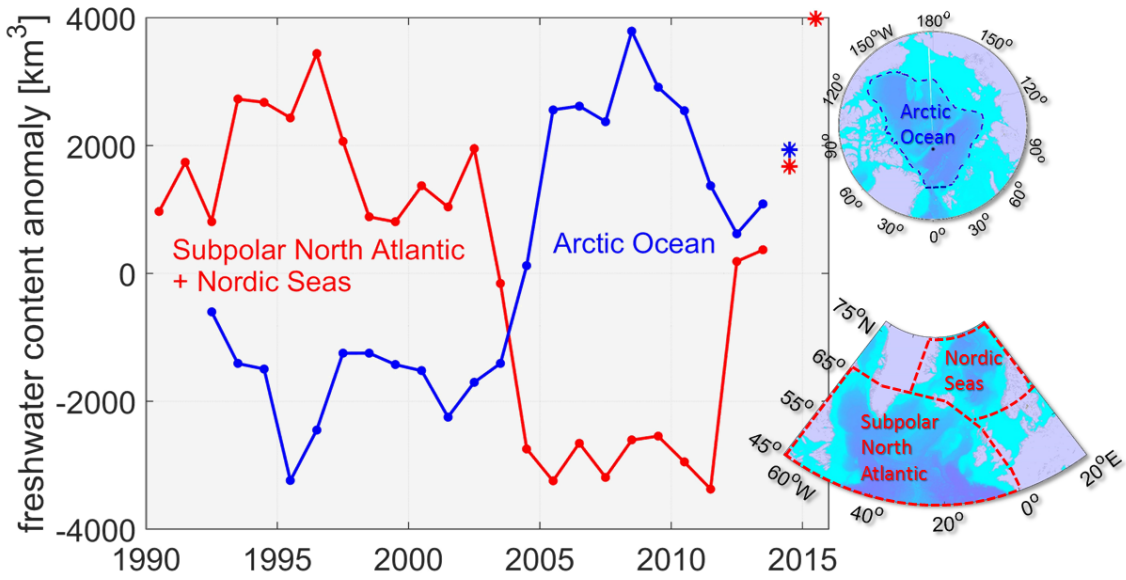


***Figure 8.1:*** *Freshwater content anomalies of the upper Arctic Ocean and the SANA (update of Fig. 4.14). Annually averaged liquid freshwater content anomaly (1990-2015) of the SANA in red and the total freshwater content anomaly (1992-2014) of the Arctic Ocean in blue. The freshwater contents were calculated with the reference salinity 35. Asterisks indicate new estimates from updated data sets.*

atmosphere (Arctic Amplification), and biological productivity.

A new forcing for FESOM just recently became available that additionally covers the time period 2010 to 2015 and includes freshwater fluxes from ice sheets and glaciers. This forcing could be used for a longer simulation that would allow studying more recent freshwater content changes and their potential impact on the stratification in the Arctic Ocean and at the deep convection sites. Peeking into output of an attempt to use this new forcing in a FESOM simulation reveals that the observed general freshwater content variability of the SANA and Arctic Ocean is well represented in the simulation in parts: the simulated anomalies vary in frequency and sign similar to the observations. However, the magnitude of the anomalies is significantly higher than the observed ones. This emphasises how difficult it is to simulate ocean dynamics realistically.

# Appendix A

# Abbreviations & symbols

***Table A.1:*** *Abbreviations*

| | |
|---|---|
| AO | Arctic Oscillation |
| AMV | Atlantic Multidecadal Variability |
| AW | Atlantic Water |
| CAA | Canadian Arctic Archipelago |
| CORA | COriolis Re-Analysis |
| CORE-II | Common Ocean-ice Reference Experiment version 2 |
| CTD | Conductivity Temperature Depth |
| DOE | Department of Energy |
| FB | Fram Strait and Barents Sea Opening |
| FESOM | Finite Element Sea ice Ocean Model |
| GSA | Great Salinity Anomaly |
| NAO | North Atlantic Oscillation |
| NCAR | National Centers for Atmospheric Research |
| NCEP | National Centers for Environmental Prediction |
| NOAA | National Oceanic and Atmospheric Administration |
| PHC3.0 | Polar science center Hydrographic global ocean Climatology version 3 |
| PIOMAS | Pan-arctic Ice Ocean Modeling and Assimilation |
| PW | Pacific Water |
| SANA | Subarctic North Atlantic, i.e. subpolar North Atlantic + Nordic Seas |

***Table A.2:*** *Symbols*

| | |
|---|---|
| $a$ | regression coefficient (slope of regression line) |
| $b$ | y-axis intercept of the regression line |
| $C_{fw}$ | freshwater content |
| $C_{fw,liq}$ | liquid freshwater content |
| $C_{sal}$ | salt content |
| $D_{eddy}$ | freshwater flux from eddy diffusion |
| $D_{num}$ | freshwater flux from numerical diffusion |
| $E$ | freshwater flux from Evaporation |
| $f$ | freshwater fraction |
| $T_{fw,liq}$ | liquid freshwater transport |
| $h$ | integration depth |
| $h_{fw}$ | liquid freshwater inventory |
| $I$ | freshwater flux from net sea ice melt |
| $M$ | freshwater flux from diahaline mixing (Entrainment term) |
| $N^*$ | Effective degrees of freedom |
| $P$ | freshwater flux from precipitation |
| $p$ | significance of correlation |
| $P_V$ | percentage variance |
| $r$ | correlation coefficient |
| $R$ | freshwater flux from river runoff |
| $S$ | salinity |
| $S_{eff}$ | effective salinity |
| $S_{mean}$ | mean salinity |
| $S_{ref}$ | reference salinity |
| $S_{rest}$ | freshwater flux from surface salinity restoring (Damping term) |
| $\sigma$ | standard deviation |
| $\sigma^2$ | variance |
| $\sigma_m$ | standard error of the mean |
| $T_{fw}$ | freshwater transport |
| $T_{fw,45N}$ | freshwater transport across the 45 °Nsection |
| $T_{fw,AO}$ | freshwater ftransport to the Arctic Ocean |
| $T_{fw,Beri}$ | freshwater transport through Bering Strait |
| $T_{fw,BSO}$ | freshwater transport through Barents Sea Opening |
| $T_{fw,CAA}$ | freshwater transport through Canadian Arctic Archipelago |
| $T_{fw,Davi}$ | freshwater transport through Davis Strait |
| $T_{fw,Fram}$ | freshwater transport through Fram Strait |
| $T_{fw,Huds}$ | freshwater transport through Hudson Strait |
| $T_{fw,liq}$ | liquid freshwater transport |

| | |
|---|---|
| $T_{fw,NS}$ | freshwater transport through the gateways of the North Sea |
| $T_{fw,SANA}$ | freshwater flux from net oceanic transport to the Subarctic North Atlantic |
| $T_{sal}$ | salt transport |
| $T_{vol}$ | volume transport |
| $V$ | ocean volume |
| $v_{\perp}$ | velocity perpendicular to cross-section |

# Appendix B

# Supplementary information

## B.1 Simulated volume and freshwater transports in comparison to observations

To review the performance of the model simulation in representing the ocean transports through the various gateways realistically, I compared the time averages of the simulated freshwater and volume transports to estimates from literature. Further I compared the simulated liquid freshwater transports through the Arctic gateways to observational time series provided by Takamasa Tsubouchi, University of Bergen, Norway. These comparisons are described in the following.

In the model simulation about 1 Sv is transported from the North Pacific into the Arctic Ocean through Bering Strait (Fig. B.1). The annual mean Bering Strait throughflow was estimated from mooring observations to be ∼0.8 Sv (Woodgate et al., 2010). However, Woodgate et al. (2012) observed an increase in volume transport from ∼0.7 Sv in 1991 to ∼1.1 Sv in 2011. The simulated mean freshwater and sea ice transport are slightly smaller than previous estimates (Tab. B.1). Still, the simulated freshwater transport compares well with the observational transport time series (updated from Tsubouchi et al., 2012) between 2004 and 2010 (Fig. B.2).

About 1.5 Sv exit the Arctic Ocean through the CAA in the model simulation (∼0.7 Sv through Lancaster Sound, ∼0.05 Sv through Hell Gate and ∼0.75 Sv through Nares Strait). The observational mean volume transports are estimated to 0.7 Sv through Lancaster Sound during 1998-2006 (Prinsenberg et al., 2009), 0.8 ± 0.3 Sv through Nares Strait between 2003 and 2006 (Münchow et al., 2006), and 0.3 Sv through Hell Gate in 2000-2002 (Melling et al., 2008).

In Fram Strait ∼6.9 Sv are transported northward and ∼9.3 Sv are transported southward in the FESOM simulation. Beszczynska-Möller et al. (2011) estimate the

long-term mean northward volume transport by the West Spitsbergen Current to 6.8 ± 0.5 Sv, which agrees well with the simulated transport. A mooring array in the western Fram Strait recorded an increase in the East Greenland Current volume transport from 3.7 ± 1.4 Sv in 2002 to 10 ± 3.8 Sv in 2007 (de Steur et al., 2009).

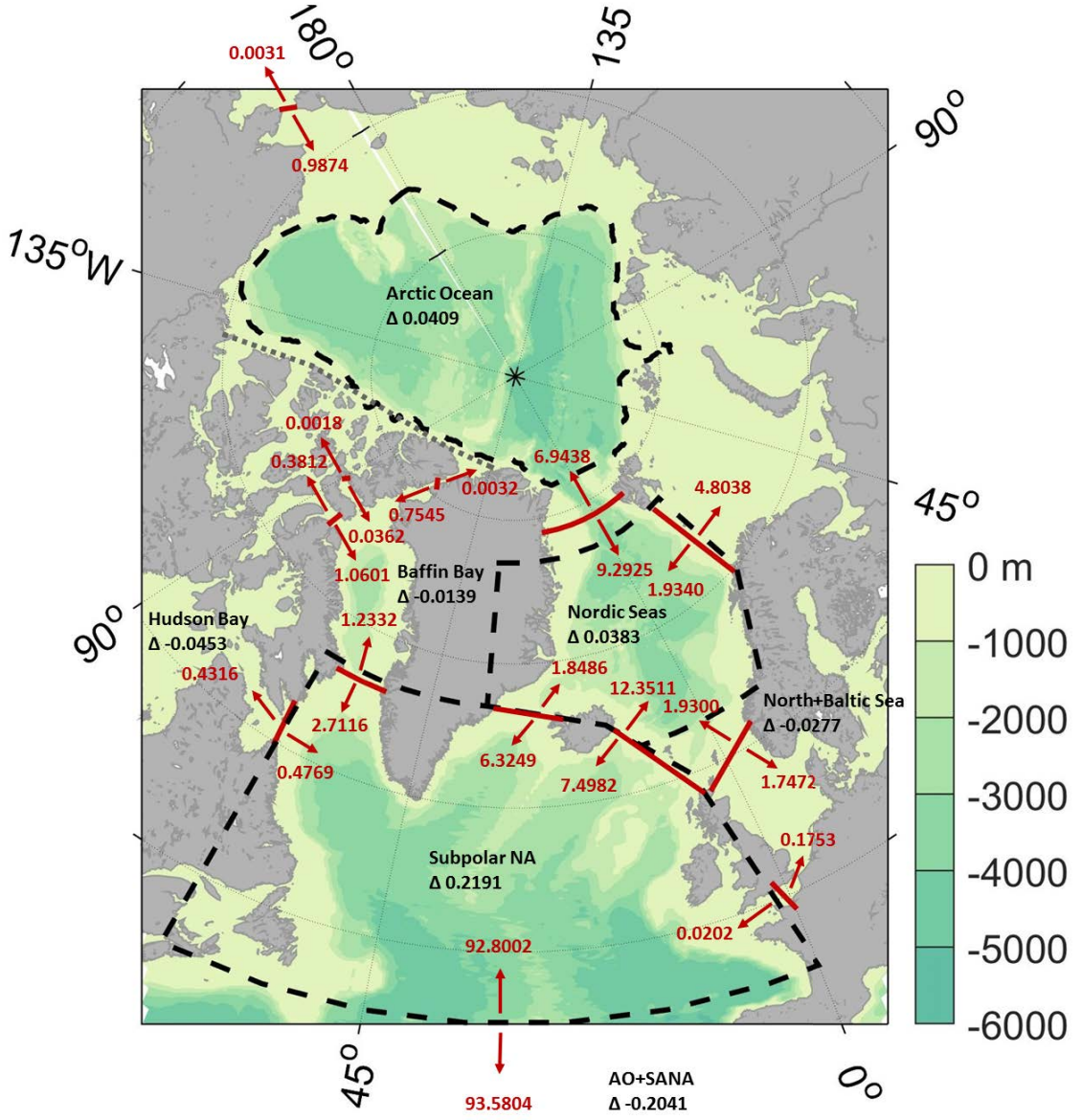


***Figure B.1:*** *Simulated volume budget of the Arctic Ocean (AO) and SANA. Time mean advective volume transports across the sections in both directions (red) and resulting imbalances for the different ocean regions (black) are given in Sverdrup.*

The net liquid freshwater transport through Fram Strait is on average significantly smaller than the observational estimates compiled by Haine et al. (2015) (Tab. B.1), yet, the transport time series of the last five years agrees well with observations (Fig. B.1). Furthermore, the mean solid freshwater transport is significantly higher in the model simulation than estimated from observations (Tab. B.1).

The simulated 4.8 Sv entering the Barents Sea from the Nordic Seas are 0.2 Sv higher than the observational estimates of 2 Sv volume transport (1979-2007) by the North Cape Current (Smedsrud et al., 2010) and 2.6 Sv volume transport by the Norwegian Coastal Current including AW and coastal water (Skagseth et al., 2011). Moreover, the simulated westward flow across the Barents Sea Opening of 1.9 Sv is 0.4 Sv larger than the transport found by Panteleev et al. (2006) from model data assimilation. Further, the simulated negative freshwater transport associated with the salty AW inflow to the Barents Sea is higher than observed (Tab. B.1; Fig. B.1).

The Hudson Bay outflow is estimated to 1-1.2 Sv mainly balanced by an inflow of ∼1 Sv and a net flow of ∼0.1 Sv across Hudson Strait resulting from net precipitation, river runoff and the advective transport from the CAA through the Fury and Hecla Strait into the Hudson Bay (Straneo and Saucier, 2008). In the model simulation however, the inflow and outflow should be balanced as there is no connection of the Hudson Bay to the CAA and as river runoff and net precipitation are only virtual salt fluxes without a numerical volume transport. Therefore the difference in the (higher than observed) transport components across Hudson Strait in the model simulation must be a result of interpolation errors (Sidorenko et al., 2009). The 45.3 mSv too high outflow from the Hudson Bay would translate into a 3 mSv (93.5 $km^3$/yr) too high freshwater input to the SANA (relative to the mean salinity of the SANA).

The simulated net volume flux across Davis Strait of ∼1.5 Sv is close to the observational estimate of 1.6 ± 0.5 Sv between 2004 and 2010 (Curry et al., 2014). However, the associated liquid freshwater transport is lower than observed, whereas the sea ice transport is too high in the model compared to observational estimates (Tab. B.1; Fig. B.2).

The East Greenland Current carries about 0.6 ± 0.1 Sv polar surface water and 2.8 ± 0.7 Sv intermediate waters through the Denmark Strait (Håvik et al., 2017). Together with the dense Denmark Strait overflow of 3.2 ± 0.5 Sv (Jochumsen et al., 2017) the observed southward flow is close to the simulated 6.3 Sv. Hansen and Østerhus (2000) estimate the AW inflow to the Nordic Sea to 1 Sv through Denmark Strait, 3.3 Sv between Iceland and Faroe Islands and 3.7 Sv between Faroe Islands and Scotland. The simulated volume transport is significantly higher, in particular, across the Iceland-Scotland Ridge (∼12.4 Sv). Moreover, the Iceland-

***Table B.1:*** *Comparison of mean freshwater sources and sinks of the entire Arctic Ocean from this study and literature. Time period average of freshwater transport plus/minus the standard deviation of annual mean values.*

| | **1979-2009**[a] | **1980-2000**[b] | **2000-2010**[b] |
|---|---|---|---|
| *Freshwater sources [$km^3$ $yr^{-1}$]* | *Freshwater transport, $S_{ref}$=34.8* | | |
| River runoff | 3,990 ± 160 | 3,900 ± 390 | 4,200 ± 420 |
| Net precipitation | 2,080 ± 150 | 2,000 ± 200 | 2,200 ± 220 |
| Bering Strait (liquid) | 2,290 ± 250 | 2,400? ± 300 | 2,500 ± 100 |
| Bering Strait (solid) | 70 ± 60 | 140 ± 40 | 140 ± 40 |
| **Total input** | **8,440 ± 340** | **8,800 ± 530?** | **9,400 ± 490** |
| *Freshwater sinks [$km^3$ $yr^{-1}$]* | *Freshwater transport, $S_{ref}$=34.8* | | |
| Fram Strait (liquid) | -1,830 ± 310 | -2,700 ± 530 | -2,800 ± 420 |
| Fram Strait (solid) | -2800 ± 480 | -2,300 ± 340 | -1,900 ± 280 |
| Davis Strait (liquid) | -2,360 ± 490 | -3,200 ± 320 | -2,900 ± 190 |
| Davis Strait (solid) | -530 ± 110 | -160 ± ? | -320 ± 45 |
| Barents Sea Opening | -870 ± 170 | -90 ± 90 | -90 ± 90 |
| **Total output** | **-8,390 ± 770** | **-8,700 ± 700** | **-8,250 ± 550** |
| **Residual** | **50 ± 890** | **100 ± 900?** | **1,200 ± 730** |

[a] *This study*
[b] *Haine et al. (2015)*

Scotland overflow was estimated to 2.7 Sv (Hansen and Østerhus, 2000), which again differs significantly from the simulated southward transport of ∼7.5 Sv. The inflow into the North Sea is ∼0.1 Sv through Dover Strait and more than 1 Sv across the norther boundary, while 1.3-1.8 Sv are transported out of the North Sea along the Norwegian Trench (Howarth, 2009). The simulated transports are a little higher with 0.15 Sv, ∼1.7 Sv and ∼1.9 Sv, respectively.

In the FESOM simulation a total of 92.8 Sv are transported northwards and 93.6 Sv are transported southward across 45 °N. Observations in the western subpolar North Atlantic at 47 °N deliver transport estimates of 30 Sv flowing south with the Deep Western Boundary Current, 110 Sv flowing north with the North Atlantic Current, and 80 Sv recirculating back south (Mertens et al., 2014). These three volume transport estimates observed in the western subpolar North Atlantic already exceed the simulated northward and southward volume transports calculated for a cross-section through the entire North Atlantic at 45 °N.

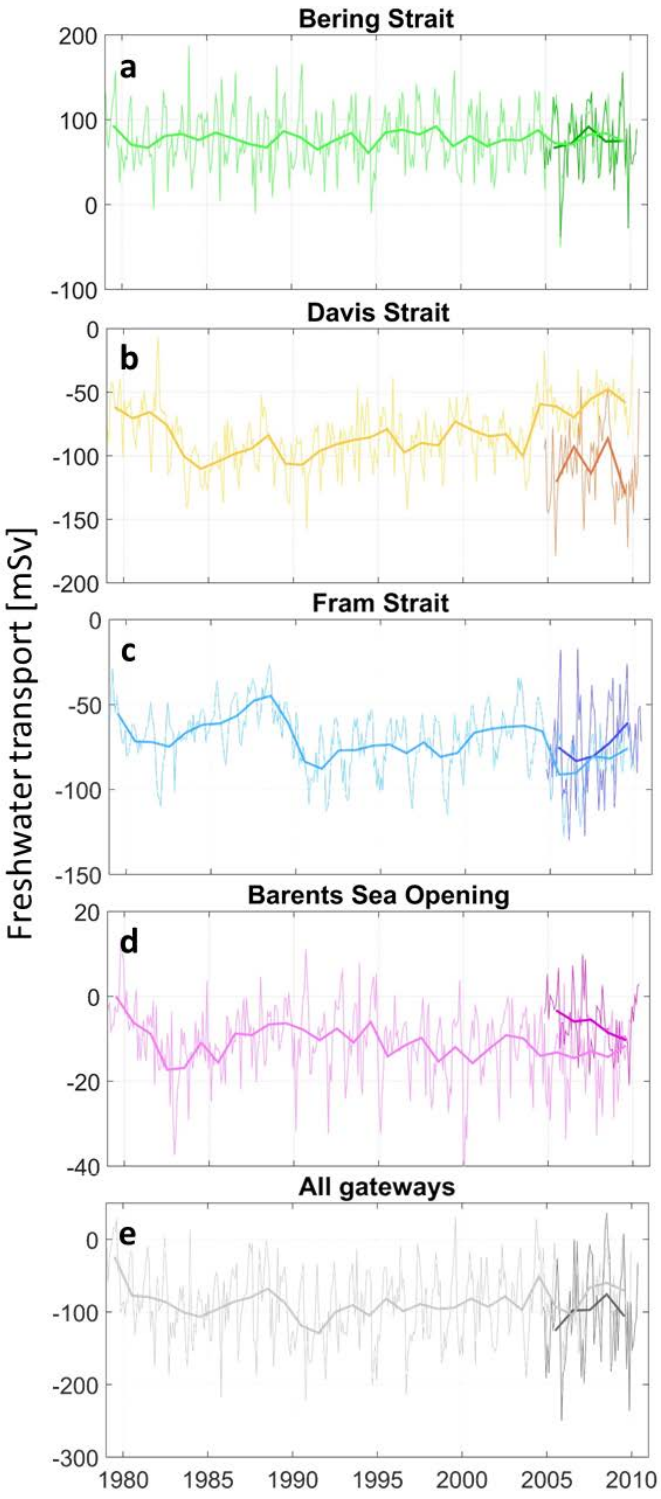


***Figure B.2:*** *Simulated net freshwater transports (1979-2009; lighter colours) through the Arctic gateways compared to observational transport time series (Oct. 2004 May 2010; darker colours) updated from Tsubouchi et al. (2012): Bering Strait (a), Davis Strait (b), Fram Strait (c), Barents Sea Opening (d) and all gateways (e). Monthly means re shown in thinner lines and annual means in thicker lines. The freshwater transports have been calculated with the reference salinity 35.*

## B.2 Simple box model to compare freshwater transports calculated with different reference salinities

As described in Chap. 3.5.1 the freshwater transports through single gateways are sensitive to the choice of reference salinity. However, the net freshwater transport across all gateways of one enclosed region is insignificantly sensitive to the choice of reference salinity, as the differences in the freshwater transports through the different gateways are largely balanced. So the challenge is to choose a reference salinity which delivers a freshwater transport that adequately represents the effect of the exchange through the gateway on the freshwater/salt content of the investigated region.

Therefore I use a simple box model of the Arctic Ocean and SANA with realistic ocean volume $V$, ocean mean salinity $S_{mean}$ and volume and salt fluxes. For orientation I use mean volume transports $T_{vol}$ and mean salinities $S$ close to the average from the model simulation (also considering sea ice transport) and adapt the volume transports to compensate the meteoric transports (closed volume budget).

For the ocean region the salt content

$$C_{sal} = V \cdot S_{mean}[kg] \tag{B.1}$$

and the freshwater content

$$C_{fw,S_{ref}} = V \, \frac{S_{ref} - S_{mean}}{S_{ref}}[km^3] \tag{B.2}$$

with three different reference salinities $S_{ref}$ following the concepts introduced in Chap. 3.5.1 (salinity of major salt source, mean ocean salinity, and boundary mean salinity) are calculated for times $t_0$ and $t_0 + 1\ month$.

For every flux component I calculate the salt transport

$$T_{sal} = T_{vol} \cdot S \ \ [kg/month], \tag{B.3}$$

the freshwater transport $T_{fw}$ for the three different reference salinities

$$T_{fw,S_{ref}} = T_{vol} \, \frac{S_{ref} - S}{S_{ref}} \ \ [km^3/month] \tag{B.4}$$

and the change this transport induces in the ocean salinity $\Delta\ S$ calculated for three different cases/assumptions:

Case 1: there is only this single inflow/outflow, which is not compensated by another outflow/inflow but increases/decreases the ocean volume.

$$\Delta S_v = \frac{C_{sal} + \Delta T_{sal}}{V + \Delta T_{vol}} \tag{B.5}$$

Case 2: the inflow/outflow is compensated by another outflow/inflow with the same volume and the mean salinity of the ocean region.

$$\Delta S_{c1} = \frac{C_{sal} + \Delta T_{sal} - T_{vol} \cdot S_{mean}}{V} \tag{B.6}$$

Case 3: the inflow/outflow is compensated by all other outflows/inflows with the same volume and the mean salinity of all these outflows/inflows (including meteoric waters).

$$\Delta S_{c2} = \frac{C_{sal} + \Delta T_{sal} - T_{vol} \cdot S_{in/out}}{V} \tag{B.7}$$

Further the net salt transport, freshwater transport and induced ocean salinity changes are calculated and compared to the differences in salt content and freshwater content between $t_0$ and $t_0$+1$month$. Moreover, the percentage of the induced salinity change and freshwater transport of each transport component from the net change and transport, respectively, is calculated and given in brackets (Fig. B.3-B.4).

For each flux component, the percentage of freshwater transport from the net freshwater transport relative to the mean ocean salinity and the percentage of induced ocean salinity change from the overall ocean salinity change for case 2 and for case 1 compare well (Fig. B.3-B.4). The relative salinity changes calculated for case 3 do not compare well with any of the three different freshwater transports calculated using the different reference salinities.

Although case 3 seems to be most realistic, the assumption here is that an inflow of e.g., 1 Sv to the Arctic Ocean via Bering Strait is compensated by 0.5 Sv through the CAA and 0.5 Sv through the FB. However, there is no certainty to what fraction the Bering Strait inflow is compensated by the FB outflow and by the CAA outflow, neither in terms of time variability nor in terms of the time mean. The freshwater transport calculated with the ocean mean salinity seems to best represent the ocean salinity changes when assuming either no other flux (and an adjustment of the ocean volume) or when assuming an homogenized ocean with a compensating flow having the same salinity as the entire ocean region. That I is why I use the current mean ocean salinity for each time step for calculating the freshwater transports of the entire Arctic Ocean and SANA in my study. Still, freshwater transports calculated against an artificial reference salinity needs to be interpreted with care.

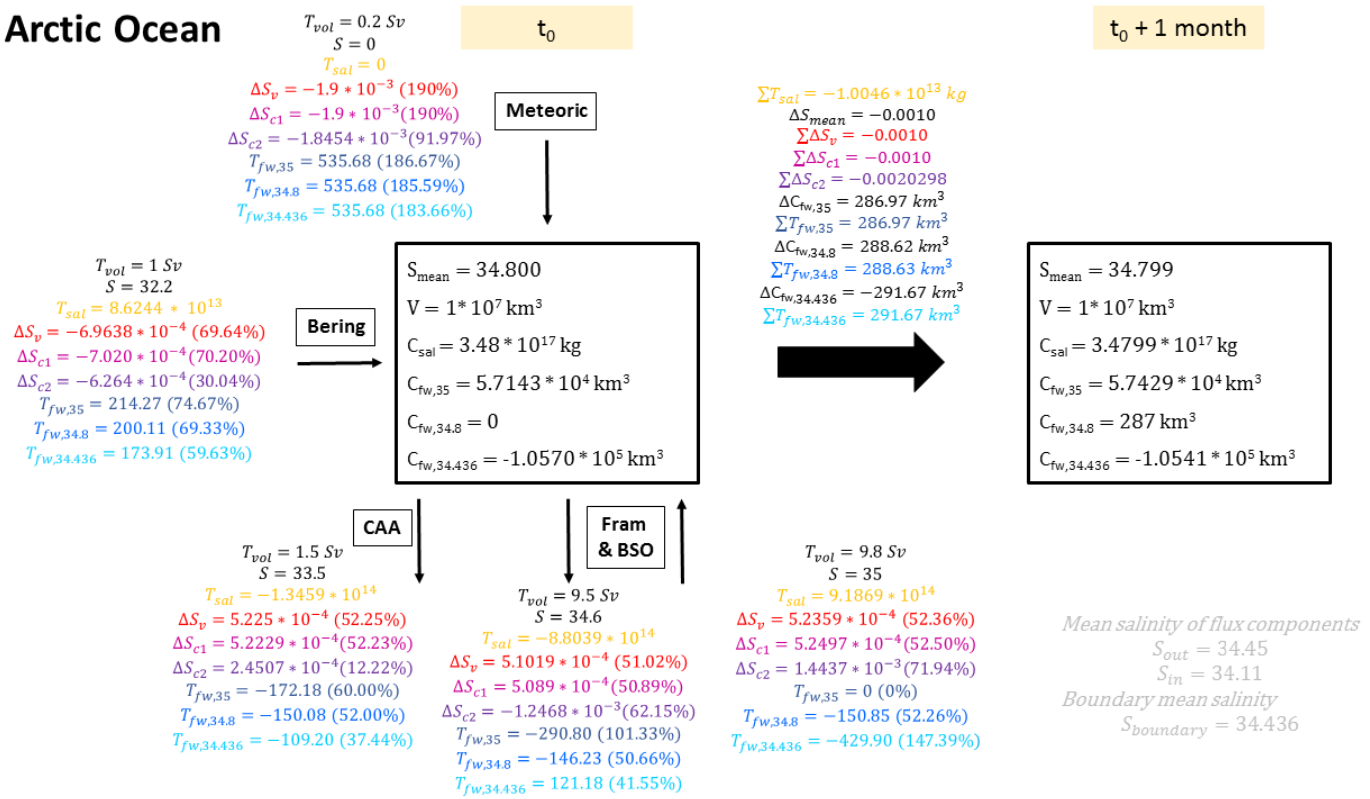


***Figure B.3:*** *Simple box model of the Arctic Ocean with meteoric flux, Bering Strait inflow, Canadian Arctic Archipelago (CAA) outflow and Fram Strait and Barents Sea Opening (BSO) inflow and outflow. Ocean mean salinity $S_{mean}$, ocean volume $V$, salt content $C_{sal}$ and freshwater content $C_{fw}$ are given for the moments $t_0$ and $t_0 + 1month$ (black boxes). For each flux component the volume transport $T_{vol}$ [Sv] and the mean salinity $S$ (black font), the salt transport $T_{sal}$ [kg/month] (yellow font), the induced ocean salinity change without compensation flux $\Delta\ S_v$ (red font) and with compensation flux $\Delta\ S_c$ (magenta font: mean ocean salinity, purple font: mean salinity of flux component), and the freshwater transport $T_{fw}$ [$km^3$/month] calculated with different reference salinities (dark blue font: salinity of salt source, lighter blue font: mean ocean salinity, turquoise font: boundary mean salinity) are given. The boundary mean salinity $S_{boundary}$ and the mean salinity of all influxes $S_{in}$ and of all outflows $S_o ut$ are given in the lower right corner (grey font). The net salinity changes and freshwater changes are given at the large black arrow between the states of $t_0$ and $t_0 + 1month$.*

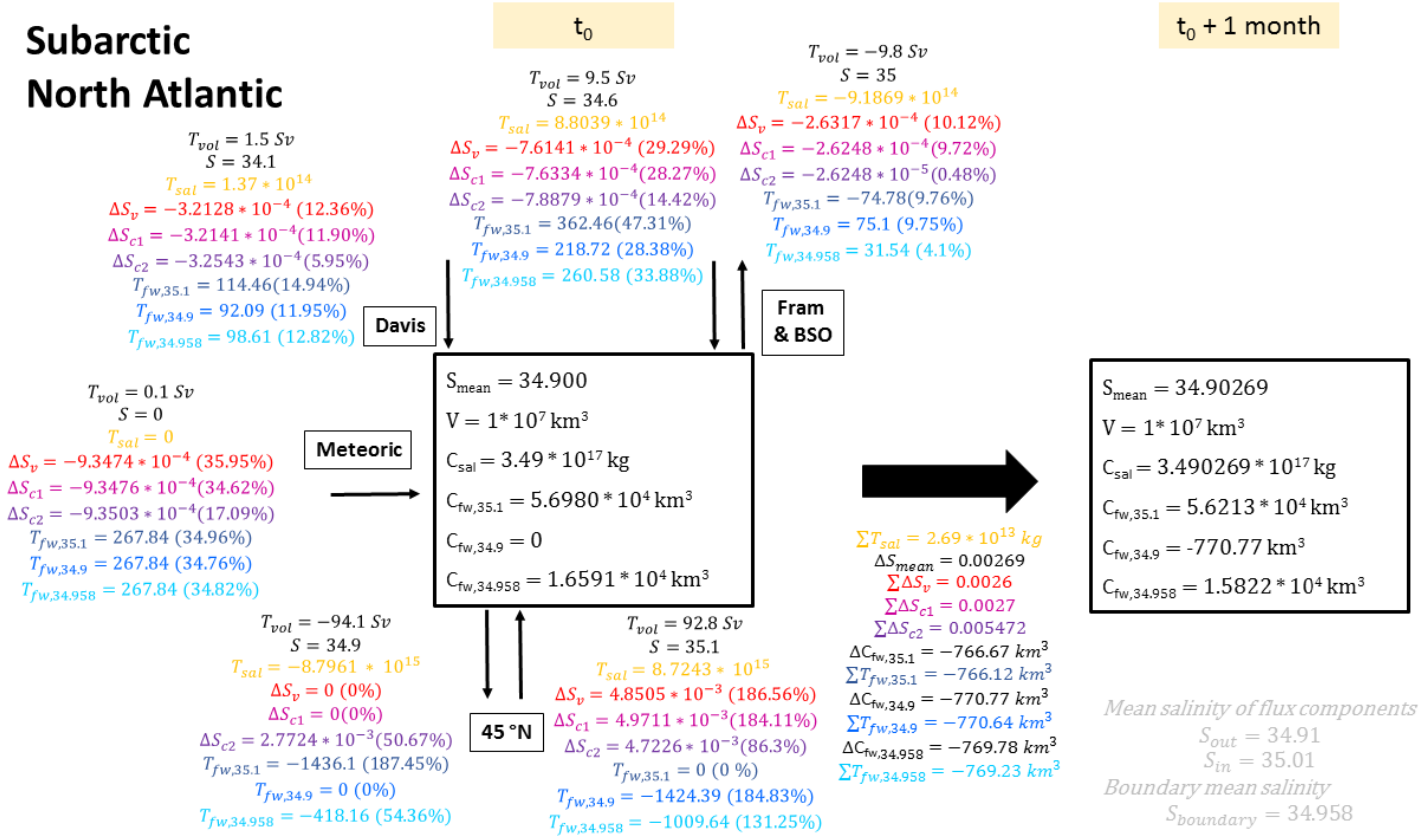


***Figure B.4:*** *Simple box model of the SANA with meteoric flux, Davis Strait inflow, Fram Strait and Barents Sea Opening (BSO) inflow and outflow and the inflow and outflow across 45 °N. The layout is the same as in Fig. B.3.*

# Bibliography


Aagaard, Knut and Eddy C. Carmack (1989), "The role of sea ice and other fresh water in the Arctic circulation." *Journal of Geophysical Research*, 94, 14,414–485,498.

Arzel, Olivier, Thierry Fichefet, Hugues Goosse, and Jean Louis Dufresne (2008), "Causes and impacts of changes in the Arctic freshwater budget during the twentieth and twenty-first centuries in an AOGCM." *Climate Dynamics*, 30, 37–58.

Bacon, Sheldon, Yevgeny Aksenov, Stephen Fawcett, and Gurvan Madec (2015), "Arctic mass, freshwater and heat fluxes: methods and modelled seasonal variability." *Philosophical Transactions of the Royal Society A: Mathematical, Physical and Engineering Sciences*, 373, 20140169.

Bamber, Jonathan, Michiel Van Den Broeke, Janneke Ettema, Jan Lenaerts, and Eric Rignot (2012), "Recent large increases in freshwater fluxes from Greenland into the North Atlantic." *Geophysical Research Letters*, 39, 8–11.

Bamber, Jonathan L., A. J. Tedstone, M. D. King, I. M. Howat, E. M. Enderlin, M. R. van den Broeke, and B. Noel (2018), "Land ice freshwater budget of the Arctic and North Atlantic Oceans: 1. Data, methods, and results." *Journal of Geophysical Research: Oceans*, 1–11.

Behrendt, Axel, Hiroshi Sumata, Benjamin Rabe, and Ursula Schauer (2018), "UDASH Unified Database for Arctic and Subarctic Hydrography." *Earth System Science Data*, 10, 1119–1138.

Belkin, Igor M. (2004), "Propagation of the "Great Salinity Anomaly" of the 1990s around the northern North Atlantic." *Geophysical Research Letters*, 31, 4–7.

Belkin, Igor M., S. Levitus, John Antonov, and S.-A. Malmberg (1998), ""Great Salinity Anomalies" in the North Atlantic." *Progress in Oceanography*, 41, 1–68.

Beszczynska-Möller, Agnieszka, Rebecca A. Woodgate, Craig Lee, Humfrey Melling, and Michael Karcher (2011), "A synthesis of exchanges through the main oceanic gateways to the Arctic Ocean." *Oceanography*, 24, 76–93.

Böning, Claus W., M. Scheinert, J. Dengg, Arne Biastoch, and A. Funk (2006), "Decadal variability of subpolar gyre transport and its reverberation in the North Atlantic overturning." *Geophysical Research Letters*, 33, 1–5.

Bönisch, Gerhard and Peter Schlosser (1995), "Deep water formation and exchange rates in the Greenland/Norwegian Seas and the Eurasian Basin of the Arctic Ocean derived from tracer balances." *Progress in Oceanography*, 35, 29–52.

Bourgain, P., J. C. Gascard, J. Shi, and J. Zhao (2013), "Large-scale temperature and salinity changes in the upper Canadian Basin of the Arctic Ocean at a time of a drastic Arctic Oscillation inversion." *Ocean Science*, 9, 447–460.

Boyer, Tim, Syd Levitus, John Antonov, Ricardo Locarnini, Alexey Mishonov, Hernan Garcia, and Simon A. Josey (2007), "Changes in freshwater content in the North Atlantic Ocean 1955-2006." *Geophysical Research Letters*, 34, 1–5.

Cabanes, C., A. Grouazel, K. von Schuckmann, M. Hamon, V. Turpin, C. Coatanoan, F. Paris, S. Guinehut, C. Boone, Nicolas Ferry, C. de Boyer Montégut, T. Carval, G. Reverdin, Sylvie Pouliquen, and Pierre Yves Le Traon (2013), "The CORA dataset: validation and diagnostics of in-situ ocean temperature and salinity measurements." *Ocean Science*, 9, 1–18.

Campos, Camila and Myriel Horn (2018), "The physical system of the arctic ocean and subarctic seas in a changing climate." In *YOUMARES 8–Oceans Across Boundaries: Learning from each other*, 25–40, Springer.

Carmack, Eddy, Igor V. Polyakov, L. Padman, I. Fer, E. Hunke, J. Hutchings, J. Jackson, D. Kelley, Ron Kwok, C. Layton, H. Melling, D. Perovich, O. Persson, B. Ruddick, Mary Louise Timmermans, John M. Toole, T. Ross, S. Vavrus, and P. Winsor (2015), "The increaing role of oceanic heat in sea ice loss in the new Arctic." *American Meteorological Society*, 2079–2106.

Carmack, Eddy C., M. Yamamoto-Kawai, Thomas W. N. Haine, Sheldon Bacon, B. A. Bluhm, Camille Lique, H. Melling, Igor V. Polyakov, Fiamma Straneo, Mary Louise Timmermans, and W. J. Williams (2016), "Freshwater and its role in the Arctic marine system: Sources, disposition, storage, export, and physical and biogeochemical consequences in the Arctic and global oceans." *Journal of Geophysical Research G: Biogeosciences*, 121.

Comiso, Josefino C., Claire L. Parkinson, Robert Gersten, and Larry Stock (2008), "Accelerated decline in the Arctic sea ice cover." *Geophysical Research Letters*, 35, 1–6.

Condron, Alan, Peter Winsor, Chris Hill, and Dimitris Menemenlis (2009), "Simulated response of the Arctic freshwater budget to extreme NAO wind forcing." *Journal of Climate*, 22, 2422–2437.

Curry, Beth, Craig M. Lee, B. Petrie, R. E. Moritz, and Ron Kwok (2014), "Multiyear volume, liquid freshwater, and sea ice transports through Davis Strait, 2004-10." *Journal of Physical Oceanography*, 44, 1244–1266.

Curry, Ruth, Bob Dickson, and Igor Yashayaev (2003), "A change in the freshwater balance of the Atlantic Ocean over the past four decades." *Nature*, 426, 826–829.

Curry, Ruth and Cecilie Mauritzen (2005), "Dilution of the northern North Atlantic Ocean in recent decades." *Science*, 308, 1772–1774.

Curry, Ruth G. and M. S. McCartney (2001), "Ocean gyre circulation changes associated with the North Atlantic Oscillation." *Journal of Physical Oceanography*, 31, 3374–3400.

Dai, Aiguo, Taotao Qian, Kevin E. Trenberth, and John D. Milliman (2009), "Changes in continental freshwater discharge from 1948 to 2004." *Journal of Climate*, 22, 2773–2792.

Danilov, S., Q. Wang, R. Timmermann, N. Iakovlev, D. Sidorenko, M. Kimmritz, T. Jung, and J. Schröter (2015), "Finite-Element Sea Ice Model (FESIM), version 2." *Geoscientific Model Development*, 8, 1747–1761.

Danilov, Sergey, Gennady Kivman, and Jens Schröter (2004), "A finite-element ocean model: Principles and evaluation." *Ocean Modelling*, 6, 125–150.

de Steur, Laura, Edmond Hansen, Rüdiger Gerdes, Michael Karcher, Eberhard Fahrbach, and J. Holfort (2009), "Freshwater fluxes in the East Greenland Current: A decade of observations." *Geophysical Research Letters*, 36, L23611.

Déry, Stephen J. and E. F. Wood (2005), "Decreasing river discharge in northern Canada." *Geophysical Research Letters*, 32, 1–4.

Dickson, Robert R., Jens Meincke, Svend-Aage Malmberg, and Arthur J. Lee (1988), "The "Great Salinity Animaly" in the northern North Atlantic 1968-1982." *Progress in Oceanography*, 20, 103–151.

Dima, Mihai and Gerrit Lohmann (2007), "A hemispheric mechanism for the Atlantic Multidecadal Oscillation." *Journal of Climate*, 20, 2706–2719.

Dodd, Paul A, Benjamin Rabe, Edmond Hansen, Eva Falck, Andreas Mackensen, Eelco Rohling, Colin Stedmon, and Svein Kristiansen (2012), "The freshwater composition of the Fram Strait outflow derived from a decade of tracer measurements." *Journal of Geophysical Research*, 117, 1–26.

Dukhovskoy, Dmitry, Mark Johnson, and Andrey Proshutinsky (2006), "Arctic decadal variability from an idealized atmosphere-ice-ocean model: 2. Simulation of decadal oscillations." *Journal of Geophysical Research: Oceans*, 111, 1–17.

Dutton, A., A.E. Carlson, A.J. Long, G.A. Milne, P.U. Clark, R. DeConto, B.P. Horton, Stefan Rahmstorf, and M.E. Raymo (2015), "Sea-level rise due to polar ice-sheet mass loss during past warm periods." *Science*, 349, aaa4019.

Fischer, Jürgen and Friedrich A. Schott (2002), "Labrador Sea water tracked by profiling floats - From the boundary current into the open North Atlantic." *Journal of Physical Oceanography*, 32, 573–584.

Foukal, Nicholas P. and M. Susan Lozier (2017), "Assessing variability in the size and strength of the North Atlantic subpolar gyre." *Journal of Geophysical Research: Oceans*, 122, 6295–6308.

Giles, Katharine A., Seymour W. Laxon, Andy L. Ridout, Duncan J. Wingham, and Sheldon Bacon (2012), "Western Arctic Ocean freshwater storage increased by wind-driven spin-up of the Beaufort Gyre." *Nature Geoscience*, 5, 194–197.

Glessmer, Mirjam Sophia, Tor Eldevik, Kjetil Våge, Jan Even Øie Nilsen, and Erik Behrens (2014), "Atlantic origin of observed and modelled freshwater anomalies in the Nordic Seas." *Nature Geoscience*, 7, 801–805.

Haak, H., Johann Jungclaus, U. Mikolajevicz, and Mojib Latif (2003), "Formation and propagation of great salinity anomalies." *Geophysical Research Letters*, 30, 1473.

Haine, Thomas W. N., Beth Curry, Rüdiger Gerdes, Edmond Hansen, Michael Karcher, Craig Lee, Bert Rudels, Gunnar Spreen, Laura de Steur, Kial D. Stewart, and Rebecca Woodgate (2015), "Arctic freshwater export: Status, mechanisms, and prospects." *Global and Planetary Change*, 125, 13–35.

Häkkinen, Sirpa (1999), "A simulation of thermohaline effects of a Great Salinity Anomaly." *Journal of Climate*, 12, 1781–1795.

Häkkinen, Sirpa (2002), "Freshening of the Labrador Sea surface waters in the 1990s: Another great salinity anomaly?" *Geophysical Research Letters*, 29, 85–1–85–4.

Hamon, M., Gilles Reverdin, and Pierre-Yves Le Traon (2012), "Empirical correction of XBT data." *Journal of Atmospheric and oceanic technology*, 29, 960–973.

Hanna, Edward, Thomas E. Cropper, Richard J. Hall, and John Cappelen (2016), "Greenland Blocking Index 1851-2015: a regional climate change signal." *International Journal of Climatology*, 36, 4847–4861.

Hansen, Bogi and Svein Østerhus (2000), "North Atlantic – Nordic Seas exchanges." *Progress in Oceanography*, 45, 109–208.

Hattermann, Tore, Pål Erik Isachsen, Wilken-Jon von Appen, Jon Albretsen, and Arild Sundfjord (2016), "Eddy-driven recirculation of Atlantic Water in Fram Strait." *Geophysical Research Letters*, 43, 3406–3414.

Hátún, Hjálmar, Anne Britt Sandø, Helge Drange, Bogi Hansen, and Hedinn Valdimarsson (2005), "Influence of the Atlantic subpolar gyre on the thermohaline circulation." *Science*, 309, 1841–1844.

Håvik, L., R. S. Pickart, Kjetil Våge, D. Torres, A. M. Thurnherr, Agnieszka Beszczynska-Möller, W. Walczowski, and Wilken-Jon von Appen (2017), "Evolution of the East Greenland Current from Fram Strait to Denmark Strait: Synoptic measurements from summer 2012." *Journal of Geophysical Research: Oceans*, 122, 2017–2033.

Holland, Paul R., Adrian Jenkins, and David M. Holland (2008), "The response of ice shelf basal melting to variations in ocean temperature." *Journal of Climate*, 21, 2558–2572.

Holliday, N. Penny, S. L. Hughes, S. Bacon, and B. Hansen (2008), "Reversal of the 1960s to 1990s freshening trend in the northeast North Atlantic and Nordic Seas." *Geophysical Research Letters*, 35, 1–5.

Howarth, M. J. (2009), "North Sea Circulation." In *Ocean Currents: A derivative of the Encyclopedia of Ocean Sciences* (John H. Stelle, Steve A. Thorpe, and Karl K. Turekian, eds.), Academic Press.

Hu, Xianmin and Paul G. Myers (2013), "A Lagrangian view of Pacific water inflow pathways in the Arctic Ocean during model spin-up." *Ocean Modelling*, 71, 66–80.

Hunke, Elizabeth C. and John K. Dukowicz (2002), "The elastic-viscous-plastic sea ice dynamics model in general orthogonal curvilinear coordinates on a sphere–incorporation of metric terms." *Monthly Weather Review*, 130, 1848–1865.

Huntington, Thomas G. (2006), "Evidence for intensification of the global water cycle: Review and synthesis." *Journal of Hydrology*, 319, 83–95.

Ionita, Monica, Patrick Scholz, Gerrit Lohmann, Mihai Dima, and Matthias Prange (2016), "Linkages between atmospheric blocking, sea ice export through Fram Strait and the Atlantic Meridional Overturning Circulation." *Scientific Reports*, 6, 32881.

IPCC (2014), "Climate Change 2014: Synthesis Report. Contribution of Working Groups I, II and III to the Fifth Assessment Report of the intergovernmental panel on Climate Change." *Core Writing Team, R. K. Pachauri and L.A. Meyer, IPCC, Geneva, Switzerland*, 151pp.

Jahn, Alexandra and Marika M. Holland (2013), "Implications of Arctic sea ice changes for North Atlantic deep convection and the meridional overturning circulation in CCSM4-CMIP5 simulations." *Geophysical Research Letters*, 40, 1–6.

Jahn, Alexandra, Bruno Tremblay, Lawrence A. Mysak, and Robert Newton (2010a), "Effect of the large-scale atmospheric circulation on the variability of the Arctic Ocean freshwater export." *Climate Dynamics*, 34, 201–222.

Jahn, Alexandra, L. Bruno Tremblay, Robert Newton, Marika M. Holland, Lawrence A. Mysak, and Igor A. Dmitrenko (2010b), "A tracer study of the Arctic Ocean's liquid freshwater export variability." *Journal of Geophysical Research: Oceans*, 115, C07015.

Jochumsen, Kerstin, Martin Moritz, Nuno Nunes, Detlef Quadfasel, Karin M. H. Larsen, Bogi Hansen, Hedinn Valdimarsson, and Steingrimur Jonsson (2017), "Revised transport estimates of the Denmark Strait overflow." *Journal of Geophysical Research: Oceans*, 122, 3434–3450.

Josey, Simon A. and Robert Marsh (2005), "Surface freshwater flux variability and recent freshening of the North Atlantic in the eastern subpolar gyre." *Journal of Geophysical Research C: Oceans*, 110, 1–17.

Jungclaus, Johann, H. Haak, Mojib Latif, and U. Mikolajevicz (2005), "Arctic North Atlantic interactions and multidecadal variability of the meridional overturning circulation." *Journal of Climate*, 4013–4031.

Kalnay, Eugenia, Masao Kanamitsu, Robert Kistler, William Collins, Dennis Deaven, Lev Gandin, Mark Iredell, Suranjana Saha, Glenn White, John Woollen, et al. (1996), "The ncep/ncar 40-year reanalysis project." *Bulletin of the American meteorological Society*, 77, 437–471.

Kanamitsu, Masao, Wesley Ebisuzaki, Jack Woollen, Shi-Keng Yang, J. J. Hnilo, M. Fiorino, and G. L. Potter (2002), "NCEP-DOE AMIP-II reanalysis (R-2)." *Bulletin of the American Meteorological Society*, 83, 1631–1643.

Karcher, Michael, Rüdiger Gerdes, Frank Kauker, Cornelia Köberle, and Igor Yashayaev (2005), "Arctic Ocean change heralds North Atlantic freshening." *Geophysical Research Letters*, 32, 1–5.

Karcher, Michael, John N. Smith, Frank Kauker, Rüdiger Gerdes, and William M. Smethie (2012), "Recent changes in Arctic Ocean circulation revealed by iodine-129 observations and modeling." *Journal of Geophysical Research: Oceans*, 117, 1–17.

Kieke, Dagmar, Monika Rhein, Lothar Stramma, William M. Smethie, John L. Bullister, and Deborah A. LeBel (2007), "Changes in the pool of Labrador Sea Water in the subpolar North Atlantic." *Geophysical Research Letters*, 34, 1–5.

Knudsen, Mads Faurschou, Marit-Solveig Seidenkrantz, Bo Holm Jacobsen, and Antoon Kuijpers (2011), "Tracking the Atlantic Multidecadal Oscillation through the last 8,000 years." *Nature communications*, 2, 178.

Köberle, Cornelia and Rüdiger Gerdes (2006), "Simulated variability of the Arctic Ocean freshwater balance 1948 - 2001." *Journal of Physical Oceaonography*, 1628–1644.

Koenigk, Torben, Uwe Mikolajewicz, Helmuth Haak, and Johann Jungclaus (2007), "Arctic freshwater export in the 20th and 21st centuries." *Journal of Geophysical Research*, 112.

Kuhlbrodt, T. and J. M. Gregory (2012), "Ocean heat uptake and its consequences for the magnitude of sea level rise and climate change." *Geophysical Research Letters*, 39.

Large, W. G. and S. G. Yeager (2009), "The global climatology of an interannually varying air  sea flux data set." *Climate Dynamics*, 33, 341–364.

Latarius, Katrin and Detlef Quadfasel (2016), "Water mass transformation in the deep basins of the Nordic Seas: Analyses of heat and freshwater budgets." *Deep-Sea Research I*, 114, 23–42.

Levitus, S., John I. Antonov, T. P. Boyer, O. K. Baranova, H. E. Garcia, R. A. Locarnini, A. V. Mishonov, J. R. Reagan, D. Seidov, E. S. Yarosh, and M. M. Zweng (2012), "World ocean heat content and thermosteric sea level change (0 2000 m), 1955  2010." *Geophysical Research Letters*, 39, 1–5.

Lindsay, R. and A. Schweiger (2015), "Arctic sea ice thickness loss determined using subsurface, aircraft, and satellite observations." *Cryosphere*, 9, 269–283.

Lique, Camille, Anne Marie Treguier, Markus Scheinert, and Thierry Penduff (2009), "A model-based study of ice and freshwater transport variability along both sides of Greenland." *Climate Dynamics*, 33, 685–705.

Marshall, David P. and Laure Zanna (2014), "A conceptual model of ocean heat uptake under climate change." *Journal of Climate*, 27, 8444–8465.

Maslanik, James A., C. Fowler, J. Stroeve, S. Drobot, J. Zwally, D. Yi, and W. Emery (2007), "A younger, thinner Arctic ice cover: Increased potential for rapid, extensive sea-ice loss." *Geophysical Research Letters*, 34, 2004–2008.

Mauritzen, Cecilie (2012), "Arctic freshwater." *Nature Geoscience*, 5, 162–164.

Mauritzen, Cecilie, A. Melsom, and R.T. Sutton (2012), "Importance of density-compensated temperature change for deep North Atlantic Ocean heat uptake." *Nature Geoscience*, 5, 905–910.

McClelland, James W., Stephen J. Déry, Bruce J. Peterson, Robert M. Holmes, and Eric F. Wood (2006), "A pan-arctic evaluation of changes in river discharge during the latter half of the 20th century." *Geophysical Research Letters*, 33, 2–5.

McGeehan, Timothy and Wieslaw Maslowski (2012), "Evaluation and control mechanisms of volume and freshwater export through the Canadian Arctic Archipelago in a high-resolution pan-Arctic ice-ocean model." *Journal of Geophysical Research: Oceans*, 117, 1–25.

McPhee, M. G., A. Proshutinsky, J. H. Morison, M. Steele, and Matt B. Alkire (2009), "Rapid change in freshwater content of the Arctic Ocean." *Geophysical Research Letters*, 36, 1–6.

Melling, Humfrey, Tom A. Agnew, Kelly K. Falkner, David A. Greenberg, Craig M. Lee, Andreas Münchow, Brian Petrie, Simon J. Prinsenberg, Roger M. Samelson, and Rebecca A. Woodgate (2008), "Fresh-water fluxes via Pacific and Arctic outflows across the Canadian polar shelf." In *Arctic-Subarctic Ocean Fluxes*, chapter 9, 193–247, Springer Netherlands.

Mertens, Christian, Monika Rhein, Maren Walter, Claus W. Böning, Erik Behrens, Dagmar Kieke, Reiner Steinfeldt, and Uwe Stöber (2014), "Circulation and transports in the Newfoundland Basin, western subpolar North Atlantic." *Journal of Geophysical Research: Oceans*, 7772–7793.

Miller, Gifford H., Richard B. Alley, Julie Brigham-Grette, Joan J. Fitzpatrick, Leonid Polyak, Mark C. Serreze, and James W. C. White (2010), "Arctic ampli-

fication: Can the past constrain the future?" *Quaternary Science Reviews*, 29, 1779–1790.

Morison, James, Ron Kwok, Cecilia Peralta-Ferriz, Matt B. Alkire, Ignatius Rigor, Roger Andersen, and Mike Steele (2012), "Changing Arctic Ocean freshwater pathways." *Nature*, 481, 66–70.

Müller, Vasco, Dagmar Kieke, Paul G. Myers, Clark Pennelly, and Christian Mertens (2017), "Temperature flux carried by individual eddies across 47N in the Atlantic Ocean." *Journal of Geophysical Research: Oceans*.

Münchow, Andreas, Humfrey Melling, and Kelly K. Falkner (2006), "An observational estimate of volume and freshwater flux leaving the Arctic Ocean through Nares Strait." *Journal of Physical Oceanography*, 36, 2025–2041.

Myers, Paul G. (2005), "Impact of freshwater from the Canadian Arctic Archipelago on Labrador Sea Water formation." *Geophysical Research Letters*, 32, 1–4.

Niederdrenk, Anne Laura, Dmitry V. Sein, and Uwe Mikolajewicz (2016), "Interannual variability of the Arctic freshwater cycle in the second half of the twentieth century in a regionally coupled climate model." *Climate Dynamics*, 47, 3883–3900.

Overeem, Irina and James P. M. Syvitski (2010), "Shifting discharge peaks in arctic rivers, 1977 - 2007." *Geogr. Ann.*, 92 A, 285–296.

Overland, James E. and Muyin Wang (2013), "When will the summer Arctic be nearly sea ice free?" *Geophysical Research Letters*, 40, 2097–2101.

Panteleev, G. G., D. A. Nechaev, and M. Ikeda (2006), "Reconstruction of summer Barents Sea circulation from climatological data." *Atmosphere-Ocean*, 44, 111–132.

Parkinson, Claire L. and Warren M. Washington (1979), "A large-scale numerical model of sea ice." *Journal of Geophysical Research*, 84.

Peterson, Bruce J., Robert M. Holmes, James W. Mcclelland, Charles J. Vo, Richard B. Lammers, Alexander I. Shiklomanov, Igor A. Shiklomanov, and Stefan Rahmstorf (2002), "Increasing river discharge to the Arctic Ocean." *Science*, 298, 2171–2173.

Peterson, Bruce J., James Mcclelland, Ruth Curry, Robert M. Holmes, John E. Walsh, and Knut Aagaard (2006), "Trajectory shifts in the Arctic and subarctic freshwater cycle." *Science*, 313, 1061–1066.

Peterson, Ingrid, James Hamilton, Simon Prinsenberg, and Roger Pettipas (2012), "Wind-forcing of volume transport through Lancaster Sound." *Journal of Geophysical Research*, 117, 1–17.

Pistone, Kristina, Ian Eisenman, and V Ramanathan (2014), "Observational determination of albedo decrease caused by vanishing Arctic sea ice." *PNAS*, 111, 3322–3326.

Pouliquen, Sylvie and A. Grouazel (2013), "Product user manual for global delayed mode insitu dataset INSITU_GLO_TS_REP_OBSERVATIONS_013_001_b called CORA." Technical report.

Prinsenberg, Simon, Jim Hamilton, Ingrid Peterson, and Roger Pettipas (2009), "Observing and interpreting the seasonal variability of the oceanographic fluxes passing through Lancaster Sound of the Canadian Arctic Archipelago." In *Influence of climate change on the changing arctic and sub-arctic conditions*, 125–143, Springer, Dordrecht.

Proshutinsky, A. Y. and M. A. Johnson (1997), "Two circulation regimes of the wind-driven Arctic Ocean between anticyclonic Gudkovich and Nikiforov with a wind-driven hydraulic." *Journal of Geophysical Research*, 102, 493–514.

Proshutinsky, Andrey, R. H. Bourke, and F. A. Mclaughlin (2002), "The role of the Beaufort Gyre in Arctic climate variability: Seasonal to decadal climate scales." *Geophysical Reserach Letters*, 29, 1–4.

Proshutinsky, Andrey, Dmitry Dukhovskoy, Mary-Louise Timmermans, Richard Krishfield, Jonathan L Bamber, and Andrey Proshutinsky (2015), "Arctic circulation regimes." *Philosophical Transactions of the Royal Society A: Mathematical, Physical and Engineering Sciences*, 373.

Proshutinsky, Andrey, Richard Krishfield, Mary-Louise Timmermans, John Toole, Eddy Carmack, Fiona Mclaughlin, William J. Williams, Sarah Zimmermann, Motoyo Itoh, and Koji Shimada (2009), "Beaufort Gyre freshwater reservoir: State and variability from observations." *Journal of Geophysical Research*, 114, 1–25.

Prowse, T., A. Bring, J. Mård, E. Carmack, M. Holland, A. Instanes, T. Vihma, and F. J. Wrona (2015), "Arctic freshwater synthesis: Summary of key emerging issues." *Journal of Geophysical Research G: Biogeosciences*, 120, 1887–1893.

Rabe, Benjamin, Michael Karcher, Frank Kauker, Ursula Schauer, John M. Toole, Richard A. Krishfield, Sergey Pisarev, Takashi Kikuchi, and Jie Su (2014), "Arctic Ocean basin liquid freshwater storage trend 1992 - 2012." *Geophysical Research Letters*, 41, 961–968.

Rabe, Benjamin, Michael Karcher, Ursula Schauer, John M. Toole, Richard A. Krishfield, Sergey Pisarev, Frank Kauker, Rüdiger Gerdes, and Takashi Kikuchi (2011), "An assessment of Arctic Ocean freshwater content changes from the 1990s to the 2006-2008 period." *Deep-Sea Research Part I: Oceanographic Research Papers*, 58, 173–185.

Rabe, Benjamin, Michael J Karcher, Frank Kauker, Ursula Schauer, John M. Toole, Richard A. Krishfield, Sergey Pisarev, Takashi Kikuchi, and Jie Su (2014), "(Table 1) Physical oceanography from several POLARSTERN cruises to the Arctic Ocean, 1993 - 2012." URL `https://doi.org/10.1594/PANGAEA.815756`. Supplement to: Rabe, B et al. (2014): Arctic Ocean basin liquid freshwater storage trend 1992 - 2012. Geophysical Research Letters, 41(3), 961-968, https://doi.org/10.1002/2013GL058121.

Rahmstorf, Stefan (1996), "On the freshwater forcing and transport of the Atlantic thermohaline circulation." *Climate Dynamics*, 12, 799–811.

Rahmstorf, Stefan (2007), "A semi-empirical approach to projecting future sea-level rise." *Science*, 315, 368–371.

Rennermalm, Asa K., Eric F. Wood, Andrew J. Weaver, Michael Eby, and Stephen J. Déry (2007), "Relative sensitivity of the Atlantic meridional overturning circulation to river discharge into Hudson Bay and the Arctic Ocean." *Journal of Geophysical Research*, 112.

Rhein, Monika, Dagmar Kieke, Sabine Hüttl-Kabus, Achim Roessler, Christian Mertens, Robert Meissner, Birgit Klein, Claus W. Böning, and Igor Yashayaev (2011), "Deep water formation, the subpolar gyre, and the meridional overturning circulation in the subpolar North Atlantic." *Deep-Sea Research Part II: Topical Studies in Oceanography*, 58, 1819–1832.

Roloff, Albrecht, Benjamin Rabe, Takashi Kikuchi, and Andreas Wisotzki (2015), "Physical oceanography from 49 XCTD stations during POLARSTERN cruise PS87 (ARK-XXVIII/4)." URL `https://doi.org/10.1594/PANGAEA.853770`.

Rothrock, D. A., D. B. Percival, and M. Wensnahan (2008), "The decline in arctic sea-ice thickness: Separating the spatial, annual, and interannual variability in a quarter century of submarine data." *Journal of Geophysical Research*, 113, 1–9.

Rudels, Bert (2009), "Arctic ocean circulation." In *Encyclopedia of Ocean Sciences* (J. H. Steele, K. K. Turekian, and S. A. Thorpe, eds.), 2nd edition, 211–225, Academic Press, San Diego.

Schlesinger, Michael E. and Navin Ramankutty (1994), "An oscillation in the global climate system of period 65-70 years." *Nature*, 367, 723–726.

Schweiger, Axel, Ron Lindsay, Jinlun Zhang, Mike Steele, Harry Stern, and Ron Kwok (2011), "Uncertainty in modeled Arctic sea ice volume." *Journal of Geophysical Research*, 116, 1–21.

Screen, James A and Ian Simmonds (2010), "The central role of diminishing sea ice in recent Arctic temperature amplification." *Nature*, 464, 1334–1337.

Serreze, Mark C., Andrew P. Barrett, Andrew G. Slater, Rebecca A. Woodgate, Knut Aagaard, Richard B. Lammers, Michael Steele, Richard Moritz, Michael Meredith, and Craig M. Lee (2006), "The large-scale freshwater cycle of the Arctic." *Journal of Geophysical Research: Oceans*, 111, 1–19.

Serreze, Mark C. and Roger G. Barry (2011), "Processes and impacts of Arctic amplification: A research synthesis." *Global and Planetary Change*, 77, 85–96.

Serreze, Mark C. and Jennifer A. Francis (2006), "The arctic amplification debate." *Climatic Change*, 76, 241–264.

Sidorenko, D., S. Danilov, Q. Wang, A. Huerta-Casas, and J. Schröter (2009), "On computing transports in finite-element models." *Ocean Modelling*, 28, 60–65.

Skagseth, Øystein, Kenneth F. Drinkwater, and Emanuele Terrile (2011), "Wind- and buoyancy-induced transport of the Norwegian Coastal Current in the Barents Sea." *Journal of Geophysical Research*, 116, C08007.

Smedsrud, L. H., Randi Ingvaldsen, Nansen Environmental, and Remote Sensing Centre (2010), "Heat in the Barents Sea: transport, storage, and surface fluxes." *Ocean Science*, 6, 219–234.

Smedsrud, Lars H., Mari H. Halvorsen, Julienne C. Stroeve, Rong Zhang, and Kjell Kloster (2017), "Fram Strait sea ice export variability and September Arctic sea ice extent over the last 80 years." *The Cryosphere*, 11, 65–79.

Steele, Michael, Rebecca Morley, and Wendy Ermold (2001), "PHC: A global ocean hydrography with a high-quality Arctic Ocean." *Journal of Climate*, 14, 2079–2087.

Steele, Michael, Don Thomas, Drew Rothrock, and Seelye Martin (1996), "A simple model study of the Arctic Ocean freshwater balance, 1979-1985." *Journal of Geophysical Research*, 101, 20,833–20,848.

Stewart, K. D. and T. W N Haine (2013), "Wind-driven Arctic freshwater anomalies." *Geophysical Research Letters*, 40, 6196–6201.

Stramma, Lothar, Dagmar Kieke, Monika Rhein, Friedrich Schott, Igor Yashayaev, and Klaus Peter Koltermann (2004), "Deep water changes at the western boundary of the subpolar North Atlantic during 1996 to 2001." *Deep-Sea Research Part I: Oceanographic Research Papers*, 51, 1033–1056.

Straneo, Fiammetta and Patrick Heimbach (2013), "North Atlantic warming and the retreat of Greenland's outlet glaciers." *Nature*, 504, 36–43.

Straneo, Fiammetta and Francois Saucier (2008), "The outflow from Hudson Strait and its contribution to the Labrador Current." *Deep-Sea Research I*, 55, 926–946.

Talley, Lynne D., George L. Pickard, William J. Emery, and James H. Swift (2011), *Descriptive Physical Oceanography: An Introduction*, 6 edition. Elsevier, Amsterdam, Boston, Heidelberg, London, New York, Oxford, Paris, San Diego, San Francisco, Singapore, Sydney, Tokyo.

Thompson, David W. J. and John M. Wallace (1998), "The Arctic Oscillation signature in the wintertime geopotential height and temperature fields." *Geophysical Research Letters*, 25, 1297–1300.

Timmermann, Ralph, Sergey Danilov, Jens Schröter, Carmen Böning, Dmitry Sidorenko, and Katja Rollenhagen (2009), "Ocean circulation and sea ice distribution in a finite element global sea iceocean model." *Ocean Modelling*, 27, 114–129.

Timmermans, Mary-Louise (2015), "The impact of stored solar heat on Arctic sea ice growth." *Geophysical Research Letters*, 42, 6399–6406.

Tomczak, Matthias and J. Stuard Godfrey (1994), *Regional Oceanography: An Introduction*, 1st edition. Elsevier Science ltd.

Toole, John M., Mary-Louise Timmermans, Don K. Perovich, Richard Krishfield, Andrey Proshutinsky, and J. A. Richter-Menge (2010), "Influences of the ocean surface mixed layer and thermohaline stratification on Arctic Sea ice in the central Canada Basin." *Journal of Geophysical Research*, 115, C10018.

Tsubouchi, Takamasa, Sheldon Bacon, A. C. Naveira Garabato, Yevgeny Aksenov, S. W. Laxon, Eberhardt Fahrbach, Agnieszka Beszczynska-Möller, E. Hansen, Craig M. Lee, and Randi B. Ingvaldsen (2012), "The Arctic Ocean in summer: A quasi-synoptic inverse estimate of boundary fluxes and water mass transformation." *Journal of Geophysical Research: Oceans*, 117, 1–28.

Tsukernik, Maria, Clara Deser, Michael Alexander, and Robert Tomas (2010), "Atmospheric forcing of Fram Strait sea ice export: A closer look." *Climate Dynamics*, 35, 1349–1360.

Velicogna, I. (2009), "Increasing rates of ice mass loss from the Greenland and Antarctic ice sheets revealed by GRACE." *Geophysical Research Letters*, 36, 5–8.

Vogt, Martin, Benjamin Rabe, Takashi Kikuchi, and Andreas Wisotzki (2015), "Physical oceanography from 15 XCTD stations during POLARSTERN cruise PS86 (ARK-XXVIII/3 AURORA)." URL `https://doi.org/10.1594/PANGAEA.853768`.

Wang, Qiang, Sergey Danilov, Dmitry Sidorenko, Ralph Timmermann, Claudia Wekerle, Xuezhu Wang, Thomas Jung, and Jens Schröter (2014), "The Finite Element Sea Ice-Ocean Model (FESOM) v.1.4: Formulation of an ocean general circulation model." *Geoscientific Model Development*, 7, 663–693.

Wang, Qiang, Claudia Wekerle, Sergey Danilov, Dmitry Sidorenko, Dmitry Sein, Benjamin Rabe, and Nikolay Koldunov (2018a), "Arctic sea ice decline significantly contributed to the unprecedented liquid freshwater accumulation in the Beaufort Gyre of the Arctic Ocean." *Geophysical Research Letters*, 45, 4956–4964.

Wang, Qiang, Claudia Wekerle, Sergey Danilov, Xuezhu Wang, and Thomas Jung (2018b), "A 4.5 km resolution Arctic Ocean simulation with the global multi-resolution model FESOM 1.4." *Geoscientific Model Development*, 1229–1255.

Wekerle, C. (2013), *Dynamics of the Canadian Arctic Archipelago throughflow: A numerical study with a finite element sea ice and ocean model*. Ph.D. thesis, University of Bremen.

Wekerle, Claudia, Qiang Wang, Sergey Danilov, Thomas Jung, and Jens Schröter (2013), "The Canadian Arctic Archipelago throughflow in a multiresolution global model: Model assessment and the driving mechanism of interannual variability." *Journal of Geophysical Research: Oceans*, 118, 4525–4541.

Wekerle, Claudia, Qiang Wang, Sergey Danilov, Vibe Schourup-Kristensen, Wilken-Jon von Appen, and Thomas Jung (2017), "Atlantic Water in the Nordic Seas: Locally eddy-permitting ocean simulation in a global setup." *Journal of Geophysical Research: Oceans*, 122, 914–940.

Winton, Michael (2008), "Sea ice – albedo feedback and nonlinear Arctic climate change." *Arctic Sea Ice Decline: Observations, Projections, Mechanisms, and Implications*, 111–132.

Wong, Annie, Robert Keeley, Thierry Carval, and And the Argo Data Management Team (2012), "Argo quality control manual, Version 2.7." URL `http://www.argodatamgt.org/content/download/341/{%}0A2650/file/argo-quality-control-manual-V2.7.pdf`.

Woodgate, Rebecca A., Thomas J. Weingartner, and Ron Lindsay (2012), "Observed increases in Bering Strait oceanic fluxes from the Pacific to the Arctic from 2001 to 2011 and their impacts on the Arctic Ocean water column." *Geophysical Research Letters*, 39, 2–7.

Woodgate, Rebecca A., Tom Weingartner, and Ron Lindsay (2010), "The 2007 Bering Strait oceanic heat flux and anomalous Arctic sea-ice retreat." *Geophysical Research Letters*, 37, 1–5.

Xu, X., H. E. Hurlburt, W. J. Schmitz, R. Zantopp, J. Fischer, and P. J. Hogan (2013), "On the currents and transports connected with the atlantic meridional overturning circulation in the subpolar North Atlantic." *Journal of Geophysical Research: Oceans*, 118, 502–516.

Yamamoto-Kawai, M., F. A. McLaughlin, Eddy C. Carmack, S. Nishino, and K. Shimada (2008), "Freshwater budget of the Canada Basin, Arctic Ocean, from salinity, d18O, and nutrients." *Journal of Geophysical Research: Oceans*, 113, 1–12.

Yang, Qian, Timothy H. Dixon, Paul G. Myers, Jennifer Bonin, Don Chambers, and M. R. van den Broeke (2016), "Recent increases in Arctic freshwater flux affects Labrador Sea convection and Atlantic overturning circulation." *Nature Communications*, 7, 10525.

Yashayaev, Igor and John W. Loder (2016), "Further intensification of deep convection in the Labrador Sea in 2016." *Geophysical Research Letters*, 44, 1429–1438.

Yashayaev, Igor, Dan Seidov, and Entcho Demirov (2015), "A new collective view of oceanography of the Arctic and North Atlantic basins." *Progress in Oceanography*, 132, 1–21.

Zhang, Jinlun and D A Rothrock (2003), "Modeling global sea ice with a thickness and enthalpy distribution model in generalized curvilinear coordinates." *Monthly Weather Review*, 131, 845–861.

# Acknowledgements

First of all, special thanks to Benjamin Rabe and Ursula Schauer for the supervision and support during my studies. Ben was always available when I had questions and took the time for discussions. Ursel helped me improving my scientific skills with her critical view and infected me with her enthusiam about the topic. Many thanks to both of you for all the advices and encouragement.

I further thank Torsten Kanzow for giving me the opportunity to write my PhD thesis in his research group, for the discussions during the committee meetings and for the evaluation of this work. Thank you to Maren Walter for the spontaneous commitment to evaluate my thesis.

The regular comittee meetings with Torsten, Ben, Ursel, Michael Karcher and Dagmar Kieke helped me a lot in reviewing my results, getting new ideas and finding my way. Thanks for all the intense discussions and for sharing your experiences.

Claudia Wekerle shared the data of her FESOM simulation with me and helped me a lot with teaching me how to handle the data. She was always available when I needed advice and gave me a pleasant start at AWI when we shared an office in the first year of my studies. My warmest thanks for your support and the nice chats during lunch and tea breaks.

Thanks to Takamasa Tsubouchi for providing the observational freshwater transport time series of the Arctic gateways for comparison. And thanks to Ben for providing the objectively mapped freshwater inventories for the upper Arctic Ocean.

Furthermore I thank all the people that supported me with proof-reading of my thesis: Ben, Ursel, Dagmar, Torsten, Claudia and Axel Behrendt. Your comments were invaluable for me.

It was a great experience to be part of ArcTrain, which gave me the opportunity to attend various seminars, workshops, retreats and annual meetings. Furthermore, I met a lot of people from Germany and Canada through ArcTrain and got an insight to research outside of my own field. I am thankful for these oppurtunities and for the shared experiences.

Thanks a lot to the colleagues from the oceanography, climate dynamics and sea ice physics sections for the comfortable working atmosphere, the nice chats during lunch break and for helping me with scientific and technical problems. Especially I thank the PhD students of the oceanography group for the mental support and encouragement.

Finally, special thanks to my fiancé who supported me in every possible way and to my family and friends for listening to my problems and for the pleasant distractions. You greatly supported me.

This work was supported by the German BMBF (Bundesministerium fr Bildung und Forschung) through the project Regional Atlantic Circulation and global ChangE (RACE and RACE II, #03F0651E and #03F0729E).